cyan_magenta_giallo_nero

Risk Mitigation for Earthquakes and Landslides

LESSLOSS Report - 2007/08

The report is intended to make earthquake engineers familiar with the main methods and computational tools needed for developing scenarios of earthquake ground motions and of ensuing damage to representative urban Infrastructure Systems (IS), as well as with illustrative examples of application to cities in Europe and neighbouring countries. The material illustrated is the outcome of the work carried out in LESSLOSS Sub-Project SP11, devoted to the title subject. Of main concern are the water and natural gas distribution networks and the sewage networks, because these are, with the transportation network, by far the most extensive IS in cities and, especially the first one, often the most vulnerable. Also, emphasis is placed more on the tools for achieving a scenario and on their application, rather than on the economic loss evaluation. As a partial justification of the belated development and interest in seismic IS damage, it is recalled that destructive earthquakes of recent decades in Europe did not cause large scale damage to IS.

In addition to describing tools for the practical construction of damage scenarios for IS, the report also highlights some innovative research trends in the field, especially the methods leading to the estimation of pipeline damage on the basis of the peak ground strains generated by the propagation of seismic waves, which in turn needs the support of advanced 2D or 3D wave propagation modelling.

The main sections of the report are devoted to:

- Calculation of seismic ground motions in an area, both of advanced and simplified engineering level, with applications for Thessaloniki and Düzce (Sect 2);
- Outline of the buried pipelines response during earthquakes, illustrating the chief elements at play on the side of the seismic loading effects and typical damage (Sect. 3);
- Vulnerability representations for IS components, mostly those consisting of buried pipelines (Sect. 4);
- Typical features of IS inventories, with examples (Sect 5);
- Damage evaluation tools at urban scenario and single pipeline level (Sect. 6);
- Damage scenario applications for Thessaloniki and Düzce (Sect 7);
- Conclusions.

ISBN 978-88-6198-012-9

Prediction of Ground Motion and Loss Scenarios for Selected Infrastructure Systems in European Urban Environments

LESSLOSS Report - 2007/08

EDITOR: E. FACCIOLI

Prediction of Ground Motion and Loss Scenarios for Selected Infrastructure Systems in European Urban Environments

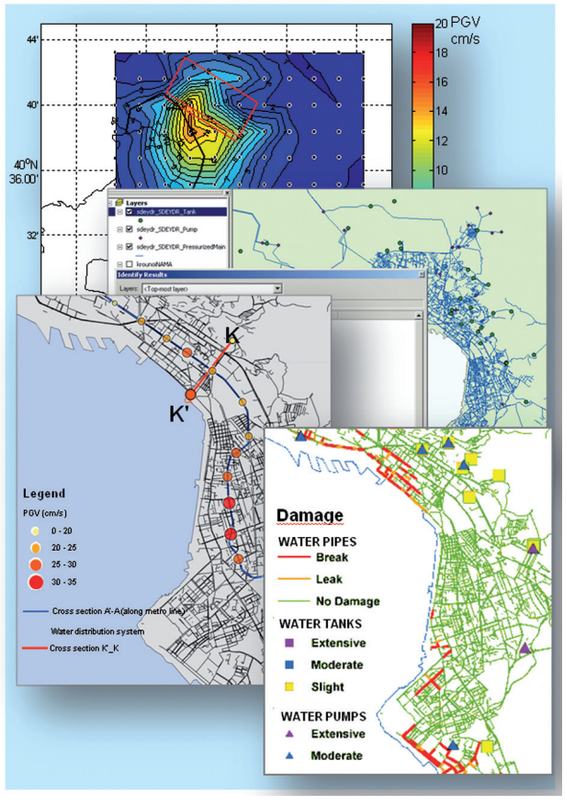

IUSS Press
Istituto Universitario di Studi Superiori di Pavia

LESSLOSS – RISK MITIGATION FOR EARTHQUAKES AND LANDSLIDES

LESSLOSS Report No. 2007/08

Prediction of Ground Motion and Loss Scenarios for Selected Infrastructure Systems in European Urban Environments

Editor

Ezio Faccioli

Reviewer

Rui Pinho

July, 2007

prodotto e distribuito da:
produced and distributed by:

IUSS Press
Via Ferrata 1 - 27100 Pavia, Italy
Tel.: (+39) 0382.516911 - fax: (+39) 0382.529131
Email: info@iusspress.it - web: www.iusspress.it

ISBN: 978-88-6198-012-9

FOREWORD

Earthquake and landslide risk is a public safety issue that requires appropriate mitigation measures and means to protect citizens, property, infrastructure and the built cultural heritage. Mitigating this risk requires integrated and coordinated action that embraces a wide range of organisations and disciplines. For this reason, the LESSLOSS Integrated Project, funded by the European Commission under the auspices of its Sixth Framework Programme, is formulated by a large number of European Centres of excellence in earthquake and geotechnical engineering integrating in the traditional fields of engineers and earth scientists some expertise of social scientists, economists, urban planners and information technologists.

The LESSLOSS project addresses natural disasters, risk and impact assessment, natural hazard monitoring, mapping and management strategies, improved disaster preparedness and mitigation, development of advanced methods for risk assessment, methods of appraising environmental quality and relevant pre-normative research.

A major objective of the project is to describe current best practice and advance knowledge in each area investigated. Thus, LESSLOSS has produced, under the coordination of the Joint Research Centre, a series of Technical reports addressed to technical and scientific communities, national, regional and local public administrations, design offices, and civil protection agencies with the following titles:

Lessloss-2007/01: Landslides: Mapping, Monitoring, Modelling and Stabilization

Lessloss-2007/02: European Manual for in-situ Assessment of Important Existing Structures

Lessloss-2007/03: Innovative Anti-Seismic Systems Users Manual

Lessloss-2007/04: Guidelines for Seismic Vulnerability Reduction in the Urban Environment

Lessloss-2007/05: Guidelines for Displacement-based Design of Buildings and Bridges

Lessloss-2007/06: Probabilistic Methods to Seismic Assessment of Existing Structures

Lessloss-2007/07: Earthquake Disaster Scenario Predictions and Loss Modelling for Urban Areas

Lessloss-2007/08: Prediction of Ground Motion and Loss Scenarios for Selected Infrastructure Systems in European Urban Environments

LIST OF LESSLOSS-2007/08 CONTRIBUTORS

Name:	Institution
Faccioli, E. (Editor and SP11 co-ordinator), Callerio A.	Studio Geotecnico Italiano srl, Milan, Italy; EF also Politecnico di Milano
Pitilakis, K., Kakderi, K., Alexoudi, M. Kim Stron	Aristotile University of Thessaloniki, Greece
Ameri, G., Akinci, A., Cocco, M., Cultrera, G., Franceschina, G., Pacor, F., Pessina, V., Lombardi, A.M., Zonno, G.	Istituto Nazionale di Geofisica e Vulcanologia, Rome and Milan, Italy
Ansal, A., Erdik, M., Tönük, G., Demircioglu, M.	Kandili Observatory and Earthquake Research Institute, Istanbul, Turkey
Paolucci, R., Scandella, L.	Politecnico di Milano, Italy

ABSTRACT

The report is intended to make earthquake engineers familiar with the main methods and computational tools needed for developing scenarios of earthquake ground motions and of ensuing damage to representative urban Infrastructure Systems (IS), as well as with illustrative examples of application to cities in Europe and neighbouring countries. The material illustrated is the outcome of the work carried out in LESSLOSS Sub-Project SP11, devoted to the title subject. Of main concern are the water and natural gas distribution networks and the sewage networks, because these are, with the transportation network, by far the most extensive IS in cities and, especially the first one, often the most vulnerable. Also, emphasis is placed more on the tools for achieving a scenario and on their application, rather than on the economic loss evaluation. As a partial justification of the belated development and interest in seismic IS damage, it is recalled that destructive earthquakes of recent decades in Europe did not cause large scale damage to IS.

In addition to describing tools for the practical construction of damage scenarios for IS, the report also highlights some innovative research trends in the field, especially the methods leading to the estimation of pipeline damage on the basis of the peak ground strains generated by the propagation of seismic waves, which in turn needs the support of advanced 2D or 3D wave propagation modelling.

The main sections of the report are devoted to:

- Calculation of seismic ground motions in an area, both of advanced and simplified engineering level, with applications for Thessaloniki and Düzce (Sect 2);
- Outline of the buried pipelines response during earthquakes, illustrating the chief elements at play on the side of the seismic loading effects and typical damage (Sect. 3);
- Vulnerability representations for IS components, mostly those consisting of buried pipelines (Sect. 4);
- Typical features of IS inventories, with examples (Sect 5);
- Damage evaluation tools at urban scenario and single pipeline level (Sect. 6);
- Damage scenario applications for Thessaloniki and Düzce (Sect 7);
- Conclusions.

TABLE OF CONTENTS

1. INTRODUCTION AND SCOPE

This report is intended to make earthquake engineers familiar with the main methods and computational tools needed for developing scenarios of earthquake ground motions and of ensuing damage to representative urban Infrastructure Systems (IS, "lifelines" in USA), as well as with illustrative examples of application to cities in Europe and neighbouring countries. The material illustrated is the outcome of the work carried out in Lessloss SubProject SP11, devoted to the title subject. Of main concern among the IS are here the water and natural gas distribution networks and the sewage netowrks, but the seimic vulnerability of other infrastructural components such as shallow tunnels and waterfront structures (various types of quaywalls) is also dealt with.

The approach presented herein shares the basic ground motion scenario treatment with Lessloss Report n°7, which is devoted to scenario predictions and loss modelling for urban areas, and is mainly focussed on the prediction of building damage and on the effectiveness of vulnerability reduction measures. Important differences between the Reports nos. 7 and 8 arise because the European experience and research on seismic vulnerability and damage scenarios of IS are at a less developed stage than in the case of building damage analyses and scenarios. This can explain why the emphasis in this report is placed more on the tools for achieving the different steps of a scenario and on their application, rather than on the (economic) loss evaluation, and on the impact of the loss of function of nevralgic IS on economic and social activities in the immediate post-disaster emergency.

As a partial justification of the belated development and interest in seismic IS damage, one may recall that destructive earthquakes of recent decades in Europe did not cause large scale damage to IS. This was most likely because the magnitude of such events has rarely exceeded 7.0, and IS damage is strongly driven by localised permanent ground deformations (e. g. caused by soil liquefaction, landsliding, surface faulting) which in turn depend on the source energy and the shaking duration. As long as the latter remain limited, IS damage will on average also be modest. On the other hand, the two devastating Turkey earthquakes of August and November 1999 did cause significant damage to IS, for the reasons just mentioned, but their magnitudes (Mw) were 7.4 and 7.2, respectively.

Apart from the latter events, the historical record of earthquake damage to IS in urban

environments in Europe and nearby regions is very limited, and well documented case histories are indeed scarce. Among the few published observations one can recall damage to some quaywalls at Ulcinj harbour during the destructive 1979 Montenegro event, ruptures to the Apulian aqueduct main tunnel in the 1980 Irpinia (Italy) earthquake and some damage to the water and sewage distribution systems in the city of Lefkas (Greece) during the damaging 2003 Lefkas earthquake, as described in Sect. 2 of this report.

The case of the Apulian acqueduct tunnel "Pavoncelli" provides a significant example of the complexity of the task of seismic damage assessment and interpretation for an important IS [Cotecchia, 1986]. Figure 1.1 illustrates the location of the "Pavoncelli" tunnel, while Figure 1.2 depicts the damaged sections observed along the tunnel together with the geology. No immediate correlation could be observed between the damage observed after the Irpinia earthquake (1980) and the geological and geomorphological characteristics, with the exception perhaps of the ruptures located at a 4.5 km at the interface between the units 2 and 5 (which however do not substantially differ, at this scale, in terms of average mechanical properties). In Figure 1.3 some pictures show clearly the effects of the Irpinia earthquake on the tunnel mansonry arch and inverted arch.

It is also appropriate to recall that, among EC research projects of the most recent framework programmes, only one has dealt in some extension with the seismic vulnerability and damage to IS, that is Risk-UE (2001). Specifically, this project produced a methodological handbook on the vulnerability assessment of lifelines and essential facilities [Monge et al., 2004].

Emphasis in the scenario applications has been placed on water and gas distribution systems because these are, with the transportation network, by far the most extensive IS in cities and, especially the first one, often the most vulnerable, due to age of its components and degradation of materials (at least in several European cities). Moreover, the loss of function of such systems has the greatest impact on the population, not to mention, in the case of natural gas, the collateral fire hazard.
While the overall aim of this report is to describe the tools available for the practical construction of damage scenario for IS, the material presented also highlights some recent and innovative research trends in the field. Among these are the advanced source and wave propagation modelling that can be employed for simulating the surface ground motions in the city area of interest, and especially the use of methods leading to the estimation of pipeline damage on the basis of the peak ground strains generated by the propagation of seismic waves. This in turn needs the support of advanced 2D or 3D wave propagation modelling, extensively documented in the sequel, that has not been commonly used in the context of lifeline earthquake engineering.

As regards the contents, Sect. 2 describes the methods available for computing seismic ground motions in an area, as a consequence of selecting a given fault as the scenario source, both at the advanced and the simplified engineering level, and it includes examples of application for the cities of Thessaloniki (Greece) and Düzce (Turkey).
Sect. 3 provides a brief outline of the buried pipelines response during earthquakes, aimed at bringing out the chief elements at play on the side of the seismic loading effects, and on that of the typical damage, as well as of some key concepts concerning the seismic verification of the buried pipelines taken from Eurocode 8. Next, Sect. 4 is devoted to vulnerability representations for IS components, mostly those consisting of buried pipelines, while Sect. 5 illustrates typical features of IS inventories, with examples. Damage evaluation tools at urban scenario and single pipeline level in Sect. 6, while Sect. 7 illustrates applications to Thessaloniki and Düzce. Conclusions are summarised in Sect. 8.

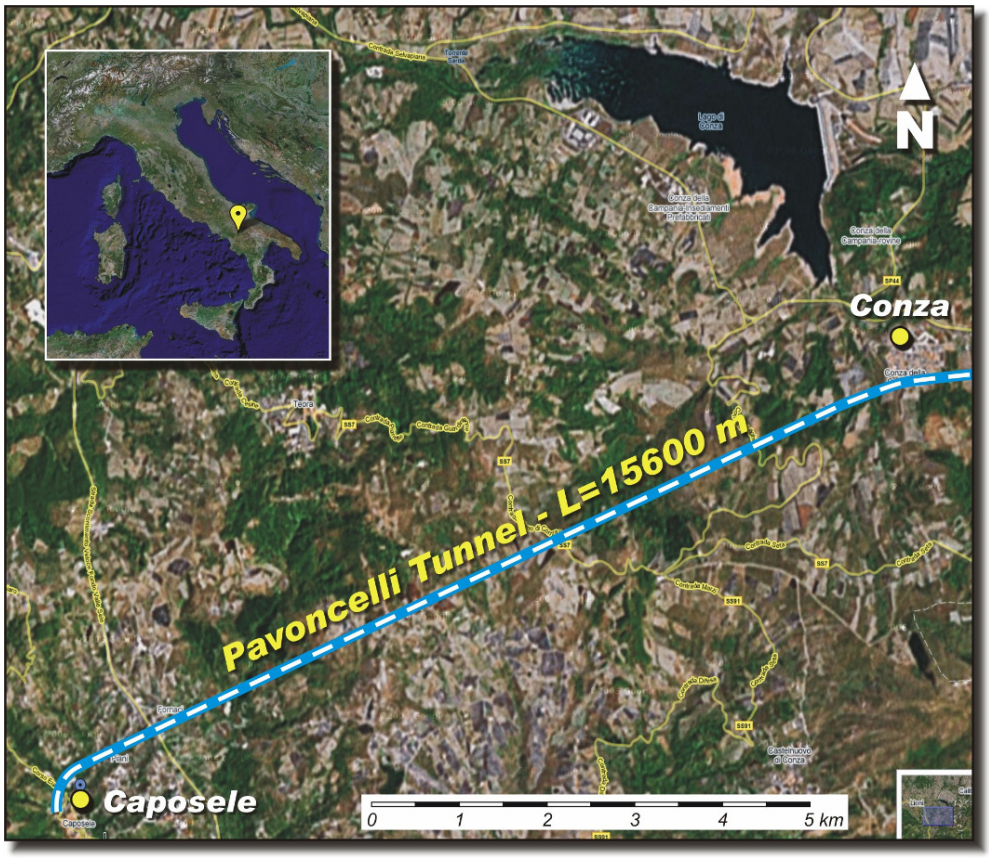

Figure 1.1: location of the Apulian water supply Tunnel "Pavoncelli", in the Southern Appennines, Italy.

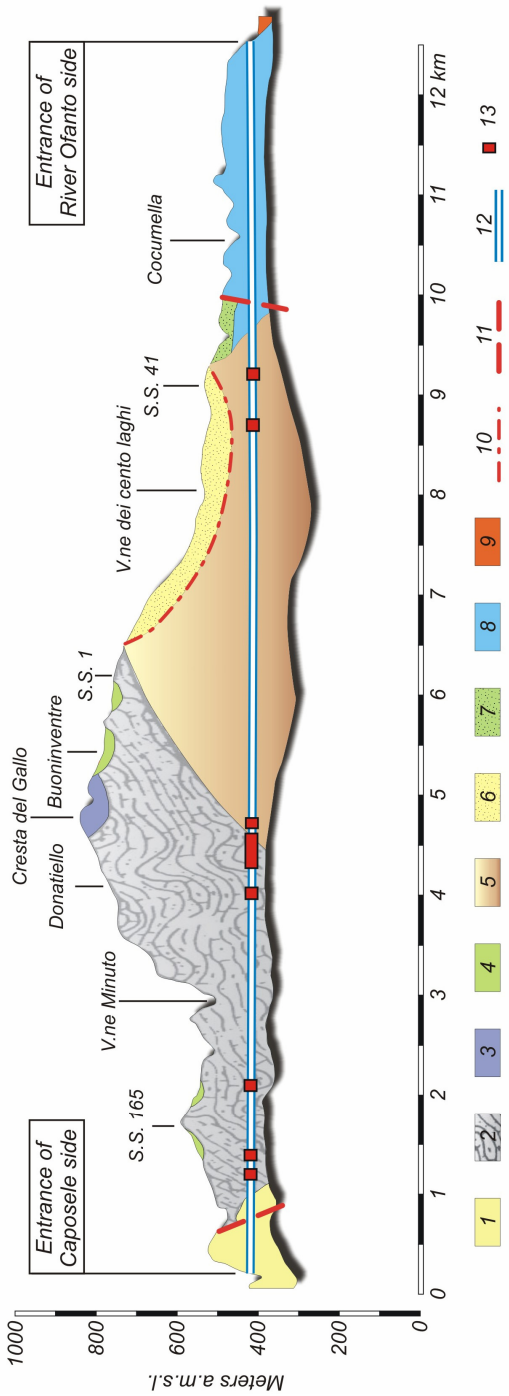

Figure 1.2: Geological cross section along the Pavoncelli tunnel and location of the most important damage (red dots) induced by the November 23, 1980 earthquake (from Cotecchia et al., 1980). 1: Limestones and Carbonatic Breccias (Cretaceus-Upper Paleocene); 2: Marls and Marly Limestones (Oligocene -- Miocene); 3: Calcarenites and Carbonatic Breccias (Upper Oligocene -- Lower Miocene); 4: Debris; 5: Shales, Marly Limestones and Jaspers, Varicoloured Clays Formation At. (Upper Cretaceus -- Oligocene) ; 6: Landslide debris; 7: Sands and Conglomerates of the Ofanto River Basin (Upper --Middle Pliocene) ; 8: Blue-Grey Calys of the Ofanto River Basin (Middle Pliocene); 9: Alluvium deposits of the Ofanto River (Holocene); 10: Slide surface; 11: Fault; 12: Tunnel; 13: Damaged sections. After [Cotecchia,1986]

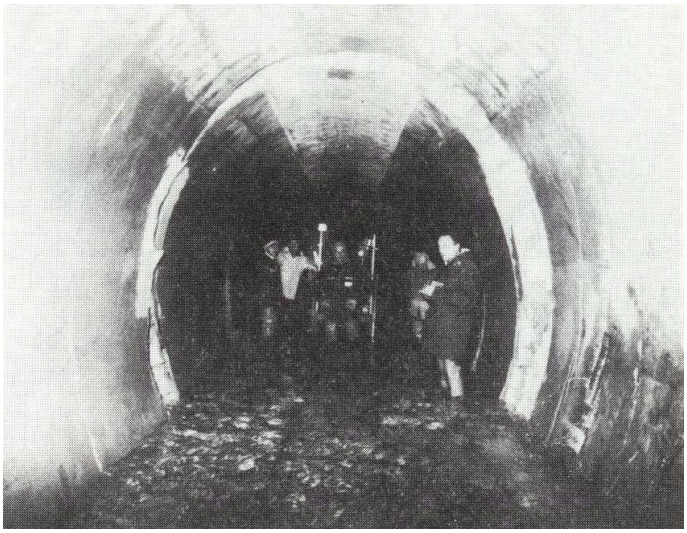

(a)

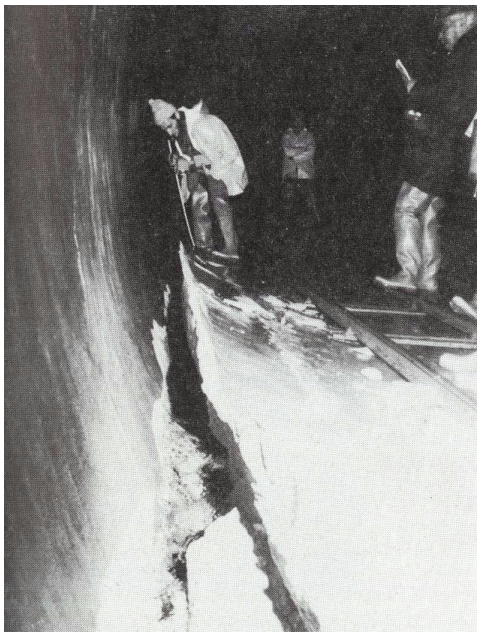

(b)

(c)

Figure 1.3: Pavoncelli acqueduct tunnel (Southern Italy). Damage observed after the Irpinia 1980 earthquake [Cotecchia, 1986]: (a) Fracture through the tunnel section with transversal and longitudinal shift; (b) rupture of the tunnel inverted arch; (c) Vertical failure.

2.CREATION OF EARTHQUAKE GROUND MOTION SCENARIOS

2.1 NUMERICAL SIMULATION OF EARTHQUAKE GENERATED SURFACE GROUND MOTIONS AND OF TRANSIENT GROUND STRAINS

Since a single, well defined earthquake provides a direct and natural reference, a predominantly deterministic viewpoint has been adopted throughout this report. In the present Section, the extensively used term *scenario,* or *earthquake ground motion scenario*, denotes both the particular choice of earthquake source, and associated fault rupture parameters (when needed), and the ensuing ground motion field calculated by an appropriate numerical tool, or empirically estimated, at a set of selected points within the urban area of interest.

Underground IS consist essentially of flexible buried pipes and these tend to follow the displacement and deformation patterns of the surrounding ground excited by the passage of seismic waves. Such elements tend to be more sensitive to ground motion wavelengths from several tens to few hundreds of m, which we indicatively take to correspond to frequencies ≤ 2 Hz, or periods ≥ 0.5 s. In LessLoss Report n° 7 [2007], dealing with scenarios related to building damage, the characterisation of ground motion, while stemming from the same seismotectonic assumptions and computational tools as the present one, is focussed towards a higher frequency range, from, say, 1.0 Hz to 4-5 Hz, appropriate for the evaluation of damage to the vast majority of ordinary buildings.

Recent studies on the large Denali, Alaska, earthquake (M=7.9) of 2002 [Ellsworth et al. 2004; Kayen et al., 2004] showed that the damage to pipeline systems is strongly related to the static offset of the ground occurring in the vicinity of the earthquake source. This makes the ability to compute permanent ground displacement in the near field of a rupturing fault an important additional requirement for computational tools adopted in creating seismic scenarios aimed at damage evaluation of infrastructural systems. Equally important, and also requiring quantitative estimation, are other effects induced by strong shaking, such as ground settlements due to soil liquefaction or large permanent displacements caused by earthquake-triggered landslides, already discussed in Sect. 1.

2.1.1 General approaches available

This sub-section describes the general approaches and the numerical tools available either for computing "synthetic" strong ground motions, i. e. time series of acceleration,

velocity or displacements, or single ground motion parameters, at pre-selected points in an area of interest. Illustrated first is the simulation of seismic motions on exposed rock (§ 2.1.1.1), while the effects of local soil conditions are treated successively (§ 2.1.1.2). The application to specific cities, i.e. Thessaloniki and Düzce, is presented in sub-sect.2.2; in particular, the former, together with Istanbul, had been targeted in Lessloss as representative for both SP10 and SP11.

The first important distinction among recommended approaches for creating ground shaking scenarios is between simplified and advanced methods. Simplified methods, directly applied in a GIS environment, make use of attenuation relations of ground motion parameters and of a local geological (or geotechnical) map for the urban area of interest; they were investigated in detail and extensively applied in the previous EC Project Risk_UE (see [Faccioli E., 2006]), aimed at the elaboration of damage scenarios for European cities. Some features of the simplified methods are described in the sequel (§ 2.1.2).

Advanced methods, extensively applied in Lessloss, are presented herein with greater emphasis because of their capability of physically representing the ground motion including very low frequency components, which most empirical attenuation relationships cannot do. In particular, the cited static offset that may occur in the source region is handled (in the adopted discrete wavenumber/finite element technique) by analytically computing the complete Green's functions from zero up to a few Hz, so that the synthetic seismograms reproduce both the transient and the static ground displacement.

On the other hand, the ability of the advanced methods to cope with the complexity of the shaking phenomena needs to be independently checked for applicative purposes. Thus, it is necessary to compare the results of advanced simulations with alternative representations, such as those yielded by empirical predictive relationships, at least in the range of validity of the latter. Moreover, engineers usually base their selection of design or verification earthquake motions on their return period (T_R). For this purpose, response spectra calculated from the synthetic seismograms at specific locations should be compared with uniform hazard (UH) spectra provided by independent probabilistic analyses, in order to associate a plausible estimate of T_R to a chosen reference scenario, whenever its selection was not driven by a specific deaggregation analysis.

It is realised that advanced simulation methods, unlike the simplified ones, may not be easily available for practical engineering applications. Such methods are illustrated herein for the crucial purpose of better quantifying the variability of the ground motion scenarios: depending on the magnitude of the earthquake and the location of the generating faults, the predicted ground shaking values may well exceed the standard error ($m \pm \sigma$) bands associated with the mean empirical predictions, even neglecting local soil effects.

2.1.1.1 *Advanced methods for the numerical simulation of ground motions on exposed bedrock*

To enhance their engineering applicability, the numerically generated ground motions in the region of interest should be "broadband" (BB), i. e. they should consist of signals encompassing approximately the 0 – 10 Hz frequency band. The general approach adopted carries out separately the low frequency band (0.0-1.0Hz) and high frequency (1.0-10 Hz) calculations, and then combines them with an appropriate summing criterion at each location (station) of interest. The low-frequency calculations were performed using a Discrete-Wave number/Finite-Element method, called COMPSYN [Spudich and Xu, 2002; LessLoss Deliverable D83], while for the high frequency range of strong ground motion generated by an extended fault a hybrid stochastic-deterministic approach, or DSM-Deterministic-Stochastic Method [Pacor et al., 2005], has been adopted.
The ground motion signals generated by this approach on exposed bedrock are to be successively used as an input to local soil amplification analyses.

Discrete-Wave number/Finite-Element technique (COMPSYN) for a low frequency motions

Physically based computations of earthquake ground motion time series can be divided into two parts, the first being the determination of what happens at the earthquake source to generate seismic waves, and the second the description of how those waves are altered by the geologic structures encountered as they propagate away from the source. The most general deterministic techniques for simulating ground motion rest on the solution of the elastodynamic equations. They adopt the finite element (FE) and finite difference (FD) methods which accommodate arbitrary 3-dimensional (3D) Earth crust profiles. These methods converge to the exact solution at wavelengths longer than the associated numerical grid dimensions, but suffer from heavy computational loads when source and observer are separated by more than a few wavelengths [Day, 1977]. More economical solutions are obtained by modelling the Earth with layers of constant elastic parameters. The COMPSYN code uses FE and FD numerical methods to calculate synthetic ground motion seismograms for hypothetical ruptures occurring on faults of finite spatial extent. The flowchart of COMPSYN is illustrated in Figure 2.1.

COMPSYN uses the numerical techniques of [Spudich and Archuleta, 1987] to evaluate the representation theorem integrals on a fault surface. The kinematics description of the fault rupture consists of specifying parameters such as the rupture velocity, the rise time, the slip model and the seismic moment on the rupturing fault. The slip distribution on the fault, i. e. the distribution of relative displacement across the fault at each point, has been computed with the k^2 method [Herrero and Bernard, 1994; Gallovic and Brokešová, 2007], because it is considered more realistic with respect to a homogeneous distribution.

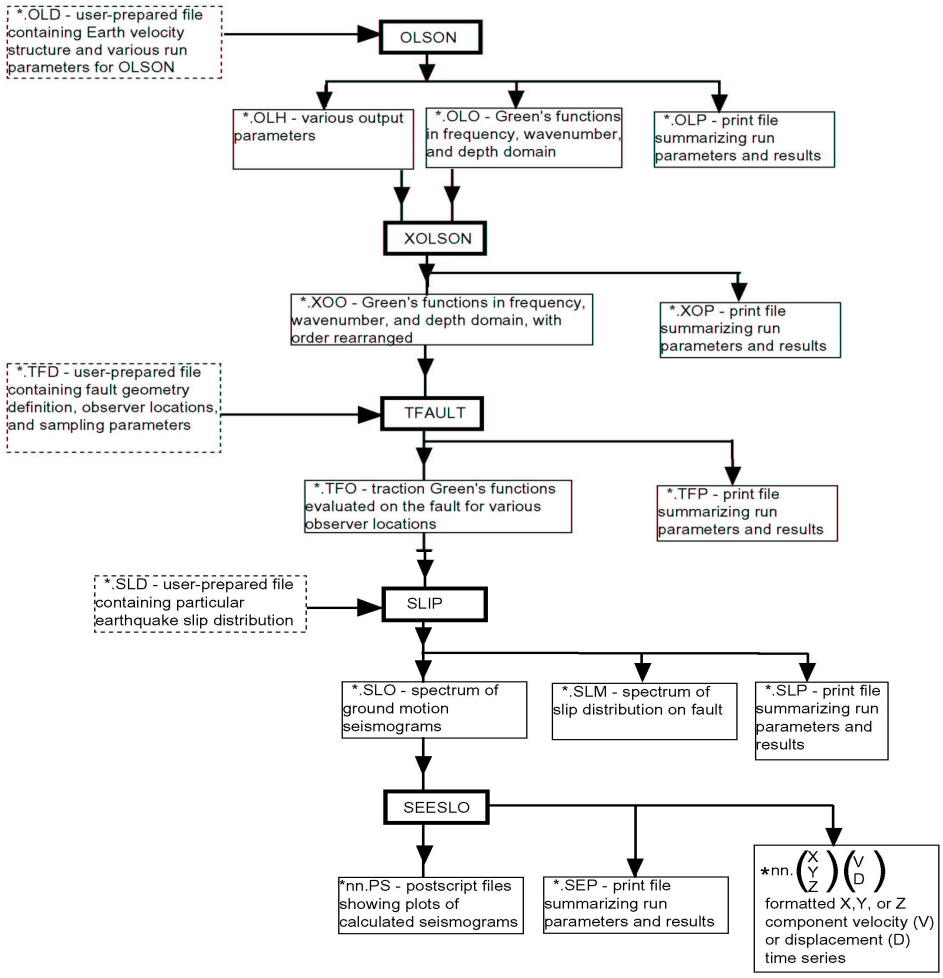

Figure 2.1: **Flow chart of COMPSYN code (Spudich and Xu, 2002)**

As already mentioned, the Green's functions, which describe the wave propagation through the adopted Earth crust model, were calculated using the hybrid Discrete Wavenumber / FE (DWFE) method of [Olson et al., 1984]. This assumes that the crustal model consists of a 1D layered elastic medium, in which anelastic attenuation is neglected. The method allows to calculate the complete response of an arbitrarily complicated Earth structure, so that all P and S waves, surface wave, etc., and near-field terms are included in the calculated seismograms. Although faster than other comparable FE methods, the cost of computation increases as the cube of the number of wavelength separating source and observer, making DWFE a low-frequency method. Once the Green's functions for one selected crustal velocity profile have been calculated, the code allows the simulation of many hypothetical rupture models in a relatively minimal time.

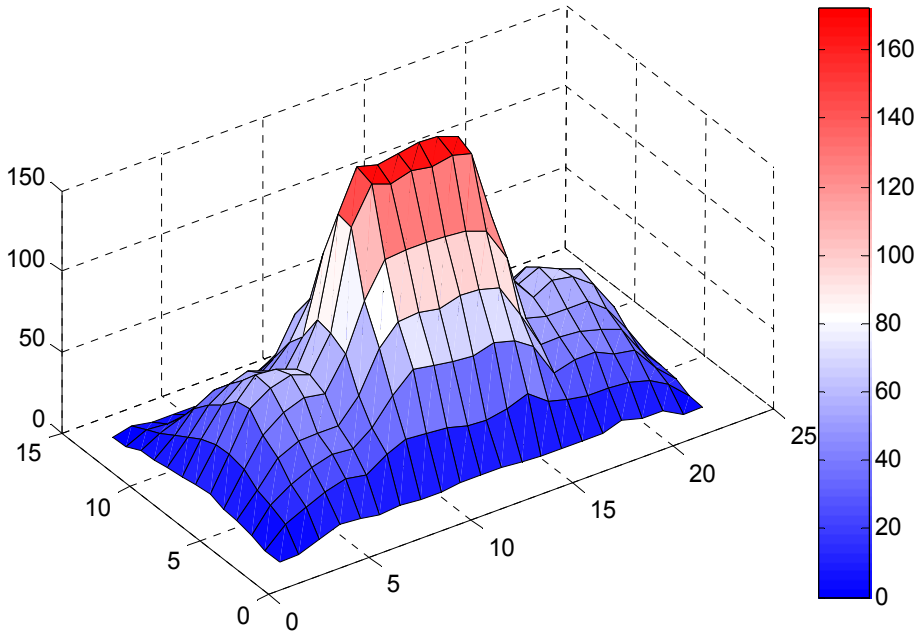

Figure 2.2: **Example of k^2 slip distribution.**

DSM (Deterministic Stochastic Method) technique for high frequency motions

A hybrid stochastic-deterministic approach, or DSM [Pacor et al., 2005], was used for the prediction of high-frequency strong ground motion generated by extended faults: the method allows the computation of synthetic time series for direct S-wave field at exposed bedrock sites. Different rupture models on the selected faults can be considered and the complexity of near-source ground motion can be retained even when the input data regarding earthquake source, propagation medium, and site characteristics are roughly estimated. The synthetic time series are calculated in the frequency band of engineering interest (from 0.5-1Hz to 10 or more Hz) and the results are independent from the velocity profile of the propagating medium. Although this technique is approximated, it is suitable to generate shaking scenarios near an extended fault using different source models, whereby the direct *S* wave-field is generally dominant in amplitude.

DSM is based on a modification of the stochastic approach of [Boore, 2003] (Point-Source-Stochastic-Method – PSSM), to predict strong ground motion close to the seismic source. Briefly, the calculation of any ground motion time series is carried out by the following four-step procedure:

i) an acceleration envelope radiated from an extended fault is computed by a simplified solution [Bernard and Madariaga, 1984; Spudich and Frazer, 1984] for a defined

kinematic fault rupture process; the Green functions are computed as asymptotic solution of the elastodynamic equation (ray theory) in a flat-layered velocity model;

ii) a time series of Gaussian white noise is windowed with the deterministic envelope, which is smoothed and normalized so that the integral of the squared envelope is unity;

iii) the windowed-noise time series is transformed into the frequency domain and multiplied with a point-source-like amplitude spectrum. The parameters of the reference spectrum (i.e., corner frequency, distance from the fault, and radiation pattern) are evaluated through the kinematic model to capture the finite-fault effects;

iv) the result of the previous step is back transformed to the time domain.

The approach follows the PSSM procedure except for two important modifications. First, the envelope does not have a predetermined functional form; rather, it is calculated deterministically based on a plausible rupture model on extended fault (step 1 in Figure 2.3). The rupture scenario is described by specifying a nucleation point on a rectangular fault plane, from which the rupture propagates radially outward with a prescribed velocity. A slip distribution over the fault may also be assigned to complete the kinematic source description.
Second, the various parameters of the point-source ground motion spectrum were generalised so as to account for the extended fault model (step 3 in Figure 2.3). The spectrum is thus also modified by directivity effects, as observed in the near-field ground motion. Fault distance *R* and radiation pattern are defined as a spatial average over the fault weighted by the envelope function itself. The guiding principle in all these modifications has been to develop a robust methodology capable of capturing the complexity of near-source ground motion, even when the input data regarding earthquake source, propagation medium, and site characteristics are roughly guessed.

In a typical application of this modelling technique, a large number of synthetic time series are generated such that, on average, the spectral properties of the time series mimic those of real earthquake ground motion.

Broad band (BB) synthesis

To generate the BB strong motion seismograms a combination is carried out, in the frequency domain, of the deterministic low-frequency waveforms (COMPSYN method) with the stochastic high-frequency synthetics seismograms computed with the DSM method (see previous paragraphs). This approach yields seismograms that cover the entire frequency range of engineering interest. The BB signal contains exact low-frequency near-field terms and approximate high-frequency contributions. The amplitude spectra of accelerograms calculated by the two techniques are combined together at

intermediate frequencies, where their domain of validity overlaps, by using the following expression in the frequency domain:

$$BB(f) = W_l LF(f) + W_h HF(f) . \tag{2.1}$$

In the previous expression, in terms of Fourier spectra, BB is the broad band signal, LF and HF are the synthetics in low and high frequency, respectively. The weighting functions W_l and W_f are defined as illustrated in Figure 2.5a. The frequencies f_a and f_b identify the transition band where the low and high frequency seismograms are combined: for $f < f_a$ the contribution to the broad band signal is completely given by the low frequency part; while for $f > f_b$, the broad band signal coincides with the high frequency seismogram. In the transition band the two signals are weighted so that their sum is unity at each frequency (Figure 2.5b). The inverse Fourier transform of *BB(f)* yields the final composite broadband time series (Figure 2.5c).

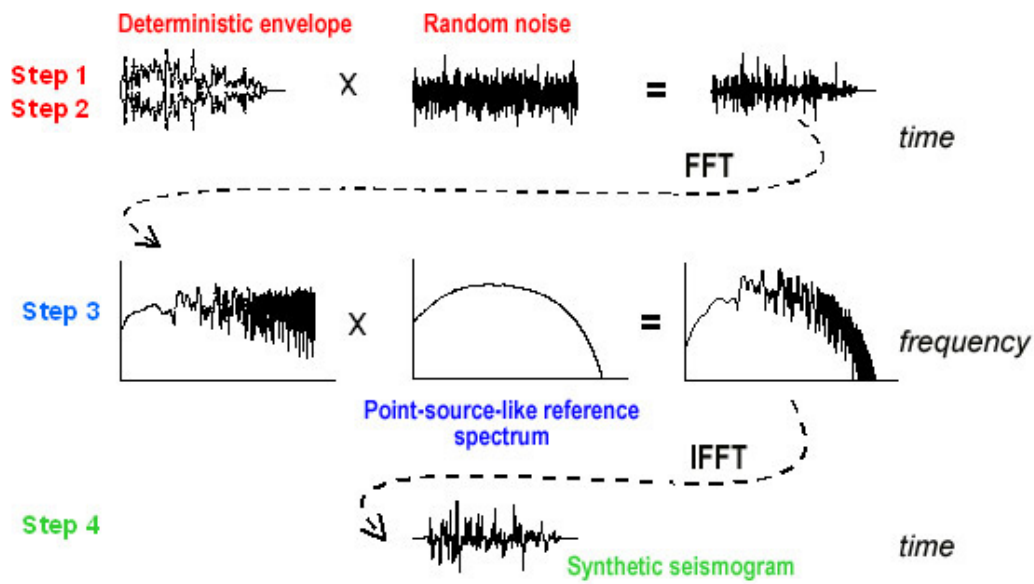

Figure 2.3: Outline of DSM method: white noise windowed with the deterministic envelope (steps 1 and 2); FFT multiplied by a point-source-like amplitude spectrum (step 3); inverse FFT (step 4).

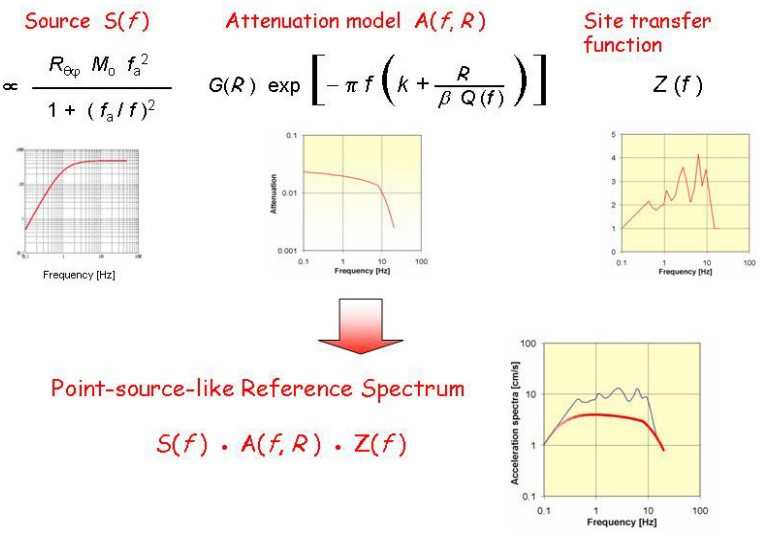

Figure 2.4: Point-source-like amplitude spectrum. The parameters of reference spectrum (i.e., corner frequency, distance from the fault, and radiation pattern) are evaluated through the kinematic model to capture the finite-fault effects. The other parameters, such as seismic moment M_0, spectral decay parameter k, quality factor Q, transfer function Z(f)) should be known.

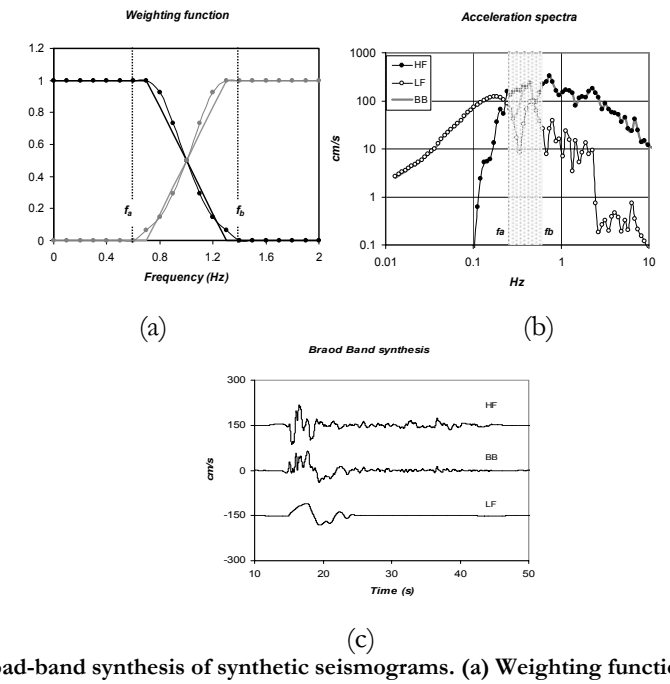

Figure 2.5: Broad-band synthesis of synthetic seismograms. (a) Weighting functions used to combine the high and low frequency signals; (b) Fourier amplitude spectra of low frequency, high frequency and composite signals (f_a and f_b delimit the transition band); (c) High frequency (HF), low frequency (LF) and broad band (BB) seismograms of ground velocity.

2.1.1.2 *From bedrock ground motions to the surface response of local soil*

It has been well established that local geology and near-surface soil deposits significantly modify strong ground motion and may even control the irregular distribution of damage observed during large earthquakes. Hence, the wave propagation phenomena in near-surface geological configurations (including topographic relief), going under the general denomination of *site effects*, are among the main causes of earthquake damage. Such effects, controlled by the stiffness and internal dissipation characteristics of the ground materials, may also entail a certain degree of nonlinearity, introduced by the inelastic material behaviour of the sediments, and depending on the amplitude of the exciting motion. Nonlinearity arises because soils become less stiff and more energy absorbing with increased levels of strain. However, interpretation of several observations from a number of recent destructive earthquakes (e.g. Kobe 1995), indicates that – aside from the case of very soft sediments - manifestations of nonlinear ground response (permanent settlements, cracking etc.) in water saturated materials tend to appear for maximum accelerations exceeding 0.4g or more.

Among the additional factors affecting the seismic surface response, the finite lateral extent of soil layers can generate surface waves at the edges of alluvial valleys, which in turn may increase the amplitude and duration of ground motion. They may also contribute to the spatial variability of ground motion, which could have major significance in the seismic response of long structures such as dams, bridges or lifeline systems.

A "methodological" classification can be made for the estimation of site effects, including experimental, attenuation (with statistical analysis of existing strong motion data), and numerical methods, [Bard, 1999; Pitilakis, 2004]. Experimental approaches may be based on different kinds of data: macroseismic observations, microtremor measurements, weak seismicity surveys or strong motion accelerograms. Attenuation models take a purely empirical approach that simply identifies different site categories and model coefficients for each site category. When the geotechnical characteristics of the site or of the area are known, site effects can be estimated through numerical analysis, using simple or more sophisticated approaches. Amongst the simpler analytical methods that allow computation of the seismic response of a given site, the most widely used employ the multiple reflection theory of S waves in horizontally layered deposits, often referred to as "1D analysis of soil profiles (columns)". Advanced methods can be classified into analytical methods, ray methods, boundary based techniques and domain based techniques. Complex phenomena controlling site effects can be identified, such as the nature of the incident wave field (1-D, 2-D or 3-D), geological structure geometries, or different mechanical behaviour of earth material. Finally, several empirical relations exist between surface geology and various measures of strong earthquake motion.

In the current engineering practice the site specific response of soil deposits to strong ground motions is often estimated by taking a set of time histories compatible with the specified response spectra on rock as control (or input) motions, rather than using the scenario bedrock motions generated by the previously described methods. The compatibility of the input motions with reference response spectra, although a generally good criterion, is a less stringent requirement for IS than for buildings, because the seismic response of the former tends to be controlled by the deformation of the surrounding soil rather than by inertial effects. The selected input motions are then used to drive a computation propagating the motions through the soil profile. The main steps to be followed to modify the bedrock earthquake motions to account for the effects of soil local soil response may be summarised as:

- *Site Characterisation:* Based on available geotechnical, geological and geophysical data, idealised soil profiles and full geotechnical cross-sections (or even 3D models) are selected and worked out for the zone of interest. Complete dynamic site characterisation includes the shear wave velocity (V_s) profile, representing the dynamic shear modulus at low strain, and – depending on the severity of expected motions - the relationships describing the variation of shear modulus and damping ratio with shear strain (modulus reduction curve and damping ratio curve, respectively).
- *Selection of input motions:* Within the framework established in Lessloss SP11, and for the reasons already discussed, input motions for the soil response analyses should preferably be those resulting from the scenario studies for bedrock motions previously illustrated. As an alternative, recorded motions can be selected, in the form of a set of time histories with suitable characteristics (e.g. peak values, duration of strong shaking), generally similar to those of available design rock motions, e. g. for 100 or 475 return periods, and to the scenario results. The reference rock spectrum fit may be improved by scaling natural time histories by a factor not exceeding about 2. Preferably, rock motions are assigned at hypothetical rock outcrops, rather than directly at the base of the soil profiles because the motions at the base of the soil profile will differ from those of the outcrop. Most commonly used computer codes (e.g. EERA) allow the rock motion to be assigned as an outcropping motion.
- *Ground response analyses:* Motions at the ground surface should preferably be computed (especially in 1D analyses) by using the best-estimate (average), upper-bound and lower-bound soil properties to incorporate uncertainties parametrically. The calculated histories of ground surface motions for the various analyses made can then be statistically analyzed to develop the response quantities of direct relevance for the seismic response, typically maximum ground velocity or displacement and longitudinal, near surface ground (shear) strain in appropriate directions.

Depending on the geometry, the loading conditions, and the configurations of ISs of interest, the surface response of local soil deposits will be evaluated using one or multi-dimensional wave propagation. Following are a few comments on this aspect:

- *One-dimensional (1D) wave propagation analyses:* these are widely used for site response, as they are – sometimes erroneously - believed to provide conservative results. Several commercial, or freely distributed codes, with different soil models are available for use on PCs. 1D analysis are time tested, i.e. most design projects in the past using this methodology seem to have survived the earthquakes. The main assumptions are:
  i) The soil layers are horizontal and extend to infinity.
  ii) The ground surface is level.
  iii) The incident earthquake motions are spatially-uniform, horizontally-polarized shear waves, and propagate vertically.
  iv) The lateral heterogeneities are taken into account by adoption of different soil profiles

- *Two (2D) or three-dimensional (3D) wave propagation analyses:* these require considerably more computation time, due to the increased complexity in the model, compared to their 1D counterparts. Dynamic finite-element (FE) or spectral element (SE, illustrated in more detail in the sequel) analyses may be used to compute the responses, as well as the finite difference method (see Moczo et al. [1996]). Irregular soil layering, and inclined material boundaries can be taken into account in multidimensional analyses. The 2D analyses are commonly used for geotechnical structures that can be idealized as plane strain problems, e.g. retaining walls, earth dams, tunnels and, moreover, nonlinear analyses can be carried out to estimate permanent displacements as well as dynamic ground motions, and can be extended to evaluate soil-structure interaction problems. 3D analyses are useful when the boundary conditions of the problem or the motions vary significantly in three dimensions.

Numerical tools for 1D Approaches

In general, seismic response analysis is performed via computer codes, such as SHAKE [Schnabel *et al.*, 1972] and its more recent spreadsheet versions EERA (Equivalent-linear Earthquake Response Analysis) and NERA (Nonlinear Earthquake Response Analysis) [Bardet *et al.*, 2000; Bardet and Tobita, 2001], CYBERQUAKE Version 2.0 [2000], Cyclic 1D [Elgamal *at al.*, 2002], and DEEPSOIL [Hashash and Park, 2005], to quote a few.

Equivalent linear analysis

The equivalent linear approach consists of modifying a linear viscoelastic constitutive soil model, such as Kelvin – Voigt (where the shear stress τ depends on the shear strain γ and its rate), to account for some types of soil non-linearities. The approach is implemented e.g. in the EERA and CYBERQUAKE [BRGM, 1998-2000] codes. The equivalent linear shear modulus, G, is taken as the secant shear modulus G_s, which depends on the shear strain amplitude, γ.

$$G_s = \tau_c / \gamma_c \tag{2.2}$$

where: τ_c and γ_c are the shear stress and strain amplitudes, respectively. The equivalent linear damping ratio, D_s is the damping ratio that produces the same energy loss in a single cycle as the hysteresis stress – strain loop of the irreversible soil behavior. In site response analysis, the material behavior is generally specified by two experimental curve families: G/G_o versus γ and D_s versus γ. The real behavior of the soil under dynamic-cyclic loading, where the shear modulus G and the damping ratio D constitute functions of the imposed shear strain amplitude γ, is considered through an iterative approach: the used values of G and D parameters are successively altered until they become compatible with the values of shear strains γ obtained from the analysis.

Elastoplastic analysis

In order to account for the effect of cyclic pore-water increase due to the seismic loading, elastoplastic analyses of 1D soil profiles can be performed, typically by using a discrete model such as finite element and lumped mass models, and performing time domain step-by-step integration of the equation of motion. A truly nonlinear approach requires the specification of the shapes of hysteresis loops and their cyclic dependence through an increased number of material parameters. Various constitutive soil models are used for this purpose, which differ in terms of stress-strain relationships, pore-pressure generation, and/or cyclic modulus degradation. Because they may be formulated in terms of effective stresses, nonlinear models can account for the build up of pore water pressure that is critical in liquefaction hazard analysis. The wave equation solution can be combined with the numerical solution of the diffusion equation to compute the redistribution and dissipation of excess pore water pressures. Also, permanent displacements and deformations can be predicted since the strain does not return to zero following cyclic loading; this feature may be of substantial value in analysing the seismic response of IS, because it is the source of localized offsets in the ground profile configuration. The constitutive soil model determines the accuracy of a nonlinear site response analysis and the accuracy increases with increasing number of constitutive parameters. However, the amount of effort required to develop the required parameters for accurate models often

limits their practical applicability. Nonlinear models are justified where large soil strains or displacements are expected.

The NERA computer programme is the non linear version of EERA. DEEPSOIL is a 1D programme, developed by [Hashash and Park, 2005] at University of Illinois at Urbana-Champaign, that can perform both nonlinear and equivalent linear analyses, and features an intuitive graphical user interface. It incorporates an extended hyperbolic model as constitutive description.

CYCLIC 1D-Beta Version, developed by [Elgamal et al., 2002], is a nonlinear FE programme for executing site amplification and liquefaction simulations (for level as well as mildly inclined sites), where the cyclic soil behavior is simulated within an incremental plasticity coupled solid-fluid (u-p) formulation.

To illustrate the application of some of the 1D computational tools, seismic response analyses were conducted at several sites in the city of Lefkas (Greece), for the August, 2003 earthquake (Ms=6.4), using geotechnical data mostly obtained afterwards. An accelerograph record of the mainshock (PGA=0.43g) along with additional records from aftershocks are available. Of particular interest is the circumstance that appreciable damage to some IS components was caused by the 2003 earthquake, as documented in a later section of this report.

The near surface formations in Lefkas consist of recent deposits, down to maximum depths varying from 10.6 to 16.0m, overlying a stiff to hard marl layer extending to the bedrock. The site response was calculated using 32 simplified 1D profiles, distributed over a 150m grid, that were validated using additional data from aftershock records at multiple sites within the examined area. Figure 2.6 shows the location of the available soil profiles and recording stations along with the 1D profiles used for ground motion analysis. Moreover, the estimation of permanent ground displacements due to liquefaction was conducted based on the results of previous 1D-EQL analyses, resulting in good agreement with in situ measurements of permanent ground displacements performed after the earthquake.

In addition, several elastoplastic analyses using the mentioned 1D-CYCLIC programme were performed for selected profiles along the coastal zone and the marina area, where liquefaction induced phenomena had been observed. The nonlinear analyses were conducted using the same input motions as the equivalent linear analyses, and resulted in lower values of surface ground accelerations and velocities (60% for maximum acceleration (PGA) and 30% for maximum velocity (PGV) values), that can be attributed to the energy dissipation of the liquefied soils along with the different simulation techniques. Greater reduction in PGA and PGV values was observed in areas where total

liquefaction was produced during the elastoplastic analysis, and in soil layers where liquefaction has occurred (elastoplastic analysis); also, shear strains have significantly higher values compared to the EQL analysis. Finally, normalised response spectra at the surface were calculated yielding higher values for the elastoplastic analysis compared to 1D-EQL analysis, regardless of the occurrence of liquefaction. Figure 2.7 shows comparative results for the response spectra of the analyses performed for soil profile 9.

Figure 2.6: Location of the soil profiles and recording stations in Lefkas city [Tow, Das, Mar, Hosp (record of the main shock)], and of 1D profiles used for ground motion analysis (green dots)

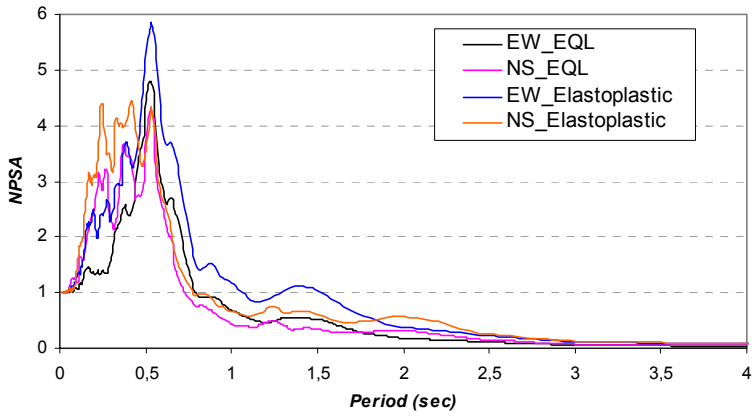

Figure 2.7: Normalised response spectra calculated at profile site 9 in Lefkas, for the 14/08/2003 earthquake scenario (EW, NS components): EQL and elastoplastic analysis.

2.1.1.3 *Modelling 2D-3D seismic wave propagation as a key to the computation of ground strains*

In the absence of earthquake induced permanent displacement and deformations, the seismic response of buried pipes is controlled by the amplitude of transient strain, induced in the ground by seismic wave propagation. The need of modelling seismic wave propagation in order to compute strains and curvatures is explicitely stated in Eurocode 8, Part 4 [cit.], as follows (Par. 6.3.3):

"A model for the seismic waves shall be established, from which soil strains and curvatures affecting the pipeline can be derived (NOTE: Informative Annex B provides methods for the calculation of strains and curvatures in the pipeline for some cases, under certain simplifying assumptions).

Ground vibrations in earthquakes are caused by a mixture of shear, dilatational, Love and Rayleigh waves. Wave velocities are a function of their travel path through lower and higher velocity material. Different particle motions associated with these wave types make the strain and curvature in the pipeline also depend upon the angle of incidence of the waves. A general rule is to assume that sites located in the proximity of the epicentre of the earthquake are more affected by shear and dilatational waves (body waves), while for sites at a larger distance, Love and Rayleigh waves (surface waves) tend to be more significant.

The selection of the waves to be taken into account and of the corresponding wave propagation velocities shall be based on geophysical considerations."

Transient strains and curvatures are induced in buried pipes also as a result of incoherent, or out of phase ground motion along their length. These effects are significant because of the length of underground pipes and justify the fact that pipelines oriented parallel to a radial line extending away from an earthquake source tend to suffer more damage than pipelines which are perpendicular to the wave passage. In other words, longitudinal deformations dominate under seismic action rather than shear strains.

If the seismic excitation at the surface is treated as a simple travelling wave of constant shape, the peak horizontal soil strain can be related to the peak horizontal particle velocity V_p, both in the direction of propagation, by the relationship:

$$\varepsilon_p = \frac{V_p}{C} \tag{2.3}$$

where C is the apparent propagation velocity of the waves with respect to the ground surface [Newmark, 1967]. For body waves, S-waves only are considered, since they carry more energy and tend to generate larger ground motion than P-waves; for surface waves, the most significant motions are those caused by Rayleigh waves. The apparent propagation velocities are given in the following equations:

$$C = C_S = \frac{V_S}{\sin \gamma_S} \qquad \textit{for S-waves} \tag{2.4}$$

where V_S is the shear wave velocity of soil and γ_S is the incidence angle of S-waves with respect to the vertical;

$$C = C_R = C_{pb} = \lambda f \qquad \textit{for R-waves} \tag{2.5}$$

where C_{pb} is the phase velocity, λ the wavelength and f the frequency.

Solutions for free field ground strains and curvatures caused by P-, S-, and R-waves, neglecting the pipe-ground interaction, were developed using Newmark's approach [St John and Zahrah, 1987]. For P-waves and R-waves the maximum longitudinal strain occurs when the direction of propagation is parallel to the pipe axis, for S-waves, when propagation is oblique to the pipeline axis (45°), as shown in the following Table 2.1.
Since longitudinal ground deformations tend to exert the primary influence on pipe response under seismic action, 2D or 3D analyses are necessary to reproduce the wave propagation along the pipe longitudinal axis. It must be stressed that 2D or 3D analyses can generate longitudinal strains, while 1D simulations can reproduce only shear strains, which do not cause significant effects on pipes. For this reason, a sufficiently general, flexible and accurate tool of numerical analysis is required to carry out multi-dimensional wave propagation, allowing also – if required – to introduce structural pipe elements into the model. Such a method is illustrated in the following paragraph.

Table 2.1 Ground strains induced by seismic waves propagating along a pipeline [St. John and Zahrah, 1987]. V_{pP}, V_{pS}, V_{pR} are the peak particle velocity caused by P-, S-, and R-waves, respectively (equivalent to PGV); c_P, c_S, c_R are the corresponding apparent propagation velocities. ϕ is the angle of incidence of the waves with respect to the pipeline axis; it is measured in the horizontal plane in the case of R-waves and in the vertical plane in the case of body waves.

Wave type	Longitudinal strain	Maximum longitudinal strain
P-wave	$\varepsilon = \frac{V_{pP}}{c_P}\cos^2\phi$	$\varepsilon = \frac{V_{pP}}{c_P}$ *for* $\phi = 0^\circ$
S-wave	$\varepsilon = \frac{V_{pS}}{c_S}\sin\phi\cos\phi$	$\varepsilon = \frac{V_{pS}}{2c_S}$ *for* $\phi = 45°$
R-wave (compressional component)	$\varepsilon = \frac{V_{pR}}{c_R}\cos^2\phi$	$\varepsilon = \frac{V_{pR}}{c_R}$ *for* $\phi = 0^\circ$

Numerical methods for 2D/3D seismic wave propagation and dynamic soil structure interaction

The use of the elastodynamics equations in numerical simulations of seismic wave propagation and dynamic soil-structure interaction has been intensively investigated in recent years. The challenge is to develop high-performance numerical methods that are capable of solving the equations accurately, and that allow to deal with large and complex computational domains as encountered in realistic 3D applications. The development of such methods for elastic wave propagation is witnessed by the rapid growth, over the past 10 years, of physically based 3D models for simulating earthquake ground motion and soil-structure interaction effects.

The Finite Difference Method (FDM), previously mentioned, has been widely implemented with a varying degree of sophistication. For classical second-order centered FDMs, at least 15 point must be used for the wavelength corresponding to the upper half power frequency [Kelly et al., 1976]. An interesting overview focused on the stability condition and grid dispersion of the 3D fourth-order FDs was provided by Moczo [Moczo et al., 2000]. Another difficulty with FDs is their inability to implement free-surface conditions with the same accuracy as in the interior regions of the model and their lack of geometrical flexibility. Even though some techniques have incorporated surface topography using methods based on grid deformation or vacuum-to-solid taper [Ohminato and Chouet, 1997] combined with the staggered grid formulation, they often remain limited to simple geometrical transformations and may affect the stability criterion or may require up to 15 grid points per shortest wavelength in the case of vacuum-to-solid techniques, which puts some limitations for narrow free-surface structures. Anyway, FDMs remain nowadays perhaps the most used methods in numerical wave propagation.

Finite-element methods (FEM) are better suited than FDM for problems that involve realistic soil models, highly heterogeneous materials, and interaction with structural elements. In recent years

Bielak and his co-workers [Bielak et al., 2003] extended in a 3D FE formulation a powerful method, called "domain reduction method" (DRM), that can efficiently propagate 3D wave fields from an arbitrary earthquake source into heterogeneous geological domains with large localized impedance contrasts and allow introducing structural elements in the "reduced" model region.

Spectral methods, introduced in fluid dynamics around 20 years ago, have also been formulated for elastodynamics [Gazdag, 1981; Kosloff and Baysal, 1982]. To deal with general boundary conditions, a set of algebraic polynomials in space (Chebischev or Legendre) replaces the original set of truncated Fourier series. The so-called global pseudo-spectral method [Kosloff et al., 1990] became one of the leading numerical techniques in the 1980s in view of its accuracy, in terms of the minimum number of grid

points needed to represent the Nyquist wavelength for nondispersive propagation. In this method, the numerical solution is derived so as to satisfy the wave equation in differential form at some suitably chosen collocation points. Unfortunately, global spectral methods suffer from severe limitations: nonuniform spacing of the collocation points for algebraic polynomials puts stringent constraint on the time step that cannot be easily removed; complex geometries and heterogeneous material properties cannot be handled easily nor, when the method is based on a strong formulation of the differential equations, realistic free-surface boundary conditions.

The spectral element methods (SEM) have been proposed for wave propagation recently by [Priolo et al., 1994] and [Faccioli et al. 1996]. The version developed by [Faccioli et al. 1997; see also Komatitsch and Vilotte, 1998] has been implemented in the numerical codes ELSE and GEO-ELSE (GEO-ELasticity by Spectral Elements), developed at the Dipartimento di Ingegneria Strutturale (DIS) of the Politecnico di Milano in cooperation with the CSR4 of Cagliari. In GEO-ELSE the typical seismic excitations include: incident plane wave, seismic moment for single point and for extended fault.
Using SEM it is possible to analyse a complex propagation problem (see Figure 2.8), including the entire domain from the seismic source to the Earth surface; in particular, one can evaluate the significant contribution of surface waves to pipelines deformation.
A major asset of the SEM is the flexibility in addressing both applications with complex geometries and large scale problems, thanks to the capability of playing indifferently on the mesh refinement or on polynomial order to increase the accuracy of the numerical solution. Furthermore, the parallel version of the code coupled with state-of-the-art algebraic solvers and pre-conditioners aims at improving the capabilities of the sequential code. The analytical basis of the SEM are briefly illustrated in Appendix A.

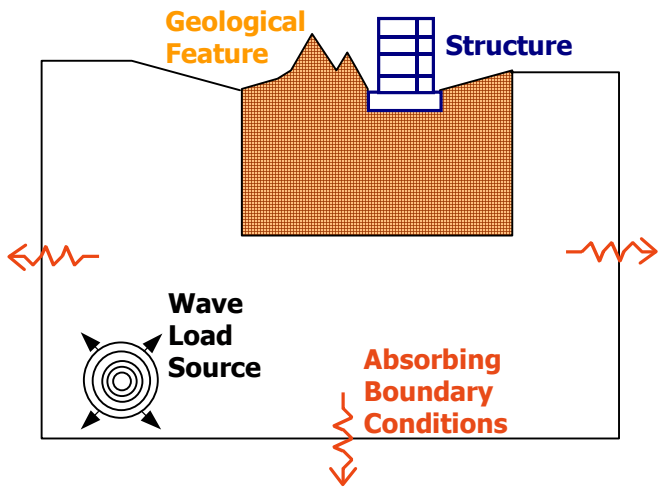

Figure 2.8: Model of a complex problem of propagation.

Domain reduction method (DRM)

The so-called Domain Reduction Method (DRM) provides an efficient way for reducing the computational effort required by large-scale numerical wave propagation from a half-space that contains the seismic source, into a localized region including site effects or structure interaction.
Numerical wave propagation from the earthquake source onto a localized region (some distance away from the seismic source), containing strong geological or topographical irregularities, requires a very large computational effort, especially in 3D analysis, because of the exceedingly large problem size. An effective tool for tackling this problem implies some kind of substructuring of the problem at study. The Domain Reduction Method [Loukakis, 1988] is one of the substructuring methods, whereby the analysis of the source and wave propagation in the half-space is separated from that of the irregular region, including site effects or structure interaction. The main challenge of this approach is the coupling of the solutions typically obtained by different methods in two different domains.
The analytical bases of the DRM are also illustrated in the Appendix A.

2.1.2 Simplified engineering approaches

2.1.2.1 *Spatial distribution of peak ground motion parameters*

In a seismic scenario context, much simpler tools than those illustrated in the previous subsections are also available for producing map representations of the earthquake ground-shaking in an urban area, suitable as a basic input for developing relatively detailed earthquake damage scenarios. Within the EC project Risk_UE [see Faccioli, 2006)] homogeneous criteria in the construction of ground shaking scenarios were defined and tested in different European cities, emphasising a common treatment of the regional seismotectonic setting and of the geological (or geotechnical) zonation at the urban scale. On the basis of this and of similar experiences, a deterministic ground-shaking representation at city scale can be produced with a GIS (Geographic Information System) tool by combining:

(i) the location and geometry of the scenario "reference earthquake" source, typically a fault, with assigned magnitude,
(ii) an appropriate attenuation relation for the selected ground motion descriptor(s),
(iii) a "seismically oriented" geological/geotechnical zonation of the urban area of interest.

The identification of the reference earthquake (i) is a common step to both the numerical (advanced) and the empirical simulations. Seismically active faults are identified and

described in databases such as FAUST [European Catalogue of Seismogenic Sources, see http://faust.ingv.it/], at the European scale, or – at the scale of a single country – such as DISS (Database of Individual Seismonic Sources in Italy). Otherwise, detailed seismotectonic studies are available in the literature for many active fault systems in different regions. A geographic de-aggregation of composite seismic hazard (PSHA) calculations could guide the selection of the reference earthquake(s) sources. In addition to the examples of Thessaloniki described in the following, the case of Istanbul will also be briefly illustrated, as one in which the identification of the reference earthquake was supported not only by seismotectonic considerations, but also by PSHA analysis.
Attenuation relations of strong motion parameters constitute the key tool for the generation of deterministic, or probabilistic, scenarios. A number of such relations have been tested for constructing ground motion maps for city areas, see e.g. [Pessina, 1999 and Faccioli, 2006]. Also in the present work different attenuation relationships have been used, the choice of which depends on the period range of interest in the simulations, the seismotectonic setting and the parameters that have to be estimated, as outlined in Table 2.2.

Table 2.2 Main features of selected attenuation relations of ground motion parameters

Parameter predicted	Attenuation relation(s)
a_{max}(≡PGA), *SA*	AMB05 [Ambraseys et al., 2005], developed for maximum ground acceleration (a_{max}) and response spectral acceleration (SA) for crustal earthquakes with $M_W \geq 5$ and distance to the surface projection of the fault less than 100 km. It is appropriate for Europe because its dataset (595 strong-motion records) comes from earthquakes occurring in Europe and the Middle East. Local site effects and fault mechanism are accounted for.
a_{max} v_{max} d_{max}	TB02 [Tromans and Bommer, 2002] predicts peak ground motion values (acceleration, velocity and displacement), and is calibrated on a European database, that includes significant crustal earthquakes. The total database consists of 249 strong-motion records of 51 European events with $5.5 \leq M_S \leq 7.9$.

Table 3.2 (cont): Main features of selected attenuation relations of ground motion parameters

Parameter predicted	Attenuation relation(s)
a_{max} v_{max}(≡PGV) d_{max}	SK03 [Skarlatoudis et al, 2003] also predicts peak ground motion values (acceleration, velocity and displacement) for shallow earthquakes in Greece with $4.5 \leq M \leq 7.0$ and epicentral distance ≤ 160 km. The relations are: $\text{Log PGA} = 0.86 + 0.45M - 1.27 \log(R^2 + h^2)^{1/2} \pm 0.286$ $\text{Log PGV} = -1.47 + 0.52M - 0.93 \log(R^2 + h^2)^{1/2} \pm 0.303$ $\text{Log } d_{max} = -4.08 + 0.88M - 1.27 \log(R^2 + h^2)^{1/2} \pm 0.424$ where *M* is magnitude, *R* epicentral distance and *h* focal depth.
PSA **(*a_{max}*)**	AK06 [Akinci et al., 2006]: predictive relationships for the ground motion in the Marmara region (NW Turkey) parametrized after regressing three-component waveforms from regional earthquakes, in the frequency range 0.4–15.0 Hz, and in the distance range 10–200 km. The data set consists of 2400 three-component recordings from 462 earthquakes, mostly weak motion events, recorded at 53 stations, with Mw between 2.5 and 7.2.
SA	**ABR97** [Abrahamson and Silva, 1997]: response spectral attenuation for the average horizontal and vertical component from shallow earthquakes in active tectonic regions. Calibrated on 655 records of 58 earthquakes, it considers style of falting, hanging wall and site reponse effects, and it predicts SA values for up to 5 s period.
a_{max} ***PSV***	SEA99 [Spudich et al, 1999] predicts geometric mean horizontal peak acceleration and 5%-damped pseudo-velocity response spectrum ordinates in extensional tectonic regimes. Valid up to 100 km, for $M \geq 5$ and $T \leq 2$ s.
SD	FA07 [Faccioli et al., 2007] predicts the displacement response spectrum (SD) ordinates (geometric mean of horizontal components) for $T \leq 15$ s. It accounts for local ground conditions and uses the focal distance.

In the simplified engineering approach, local soil amplification may be accounted for in the scenario ground shaking directly through the site factors of the attenuation relations: all recent relations use a ground condition classification consistent with those adopted in the main seismic codes, either in Europe or the US, e.g. Eurocode 8 – Part 1. (CEN, 2004), based on V_{S30}. Incorporating item (iii) in the prediction will be the most expensive part of the process if at least a geological map, indicatively at the 1:10 000 scale, is not

available for the city of interest. Estimating the influence of the soil profile on the ground motion parameters is likely to introduce significant uncertainties, especially for the softer materials (ground class D), due to the difficulty of carrying out a proper geotechnical characterisation of the ground in densely populated urban areas, and because the depth of the deposits is only loosely accounted considered in most attenuation relations. For this reason, parametric 1D numerical simulations of the local ground response should in most cases be employed in sections of urban areas susceptible to high soil amplification.

It is worth noting that attenuation relationships for long period spectral response (i. e periods larger than, say, 3 or 4 s) are still scarce, and that quantification of the effects of the local soil profile on the amplification of shaking are also under rapid evolution, due to the fast increase in number and quality of strong motion data.

2.1.2.2 *Simplified formulas for ground strains*

Since strong lateral ground discontinuities may significantly affect the seismic response of buried pipelines due to localised peaks of ground strain, it is necessary to evaluate how impedance contrasts and geometric parameters, which may characterize a geological configuration, influence the ground strain estimate.

For this purpose a set of parametric 2D analyses on the geometric models shown in Figure 2.9 has been performed. Theoretical analyses, based on simple closed-form solutions for wave propagation in a dipping layer, were likewise performed for the wedge (a) and the wall-layer geometries (b). Numerical simulations were performed with the already described spectral element code GEO-ELSE for the wedge-layer system (c) and the dipping rock-soil interface model (d).

As shown in Figure 2.10, it is useful to represent the longitudinal Peak Ground Strains (PGS) as a function of the normalized distance x/L, the meaning of L being explained in Figure 2.9c. Figure 2.10 suggests that the calculated spatial variation of PGS peaks at x/L=p, where the variation of p with the dipping angle α can be estimated by the following formula:

$$p(\alpha) = -0.58 \sin \alpha + 0.76. \tag{2.6}$$

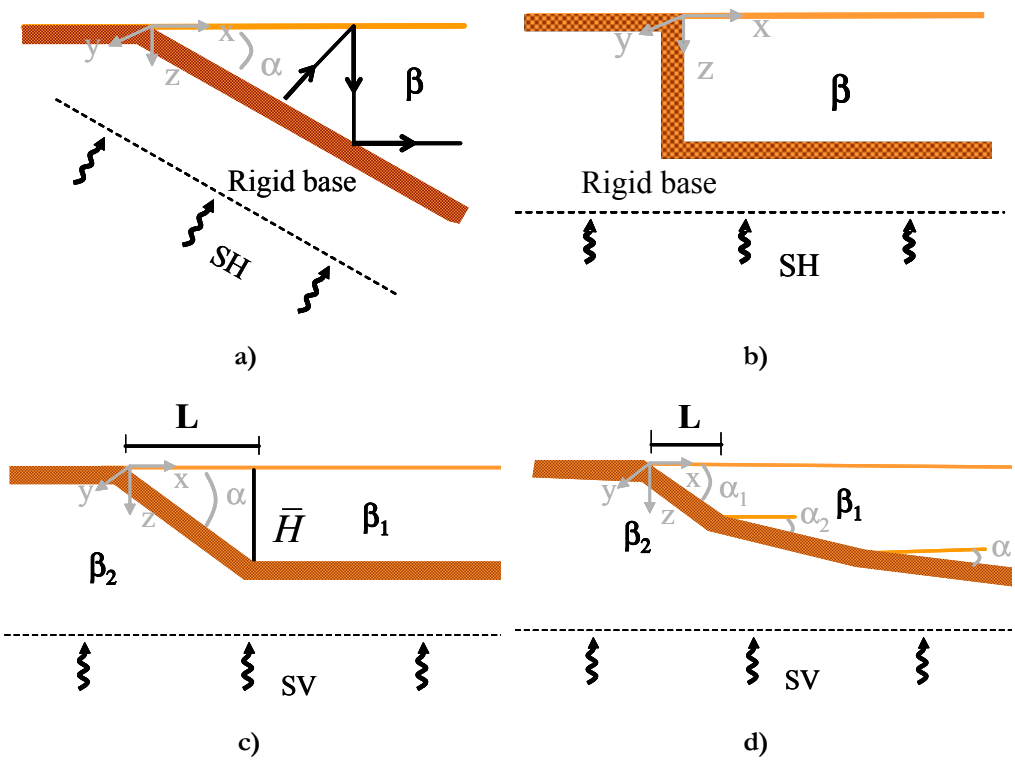

Figure 2.9: Geometrical models used for parametric 2D analyses: a) wedge; b) wall-layer system; c) wedge-layer system; d) dipping soil interface. Analyses of models a) and b) were performed using theoretical closed-form solutions [Sanchez Sesma, 1999]; numerical simulations for models c) and d) were performed with the spectral element code GEO-ELSE.

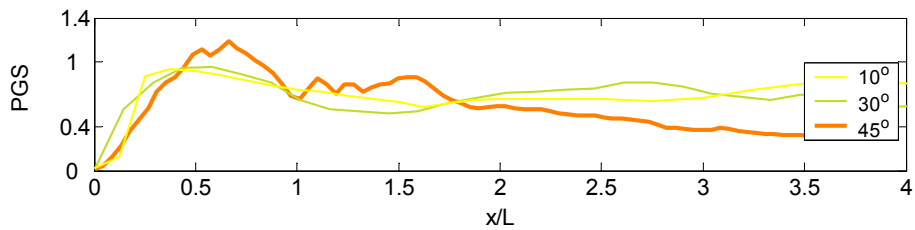

Figure 2.10: Spatial variation of PGS as a function of x/L for the model c) in Figure 2.9 for various dipping angles α, $\bar{H} = 40$ m, $\beta_1 = 200$ m/s, $\beta_2 = 1000$ m/s, $\rho_1 = 1500$ Kg/m², $\rho_2 = 2000$ Kg/m². The excitation is the Gilroy array 1 N-S record of the 1989 Loma Prieta earthquake.

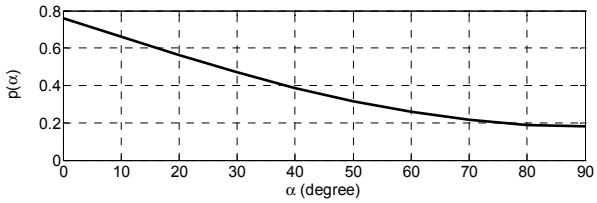

Figure 2.11: Function $p(\alpha)$ which defines the position of the maxima of PGS as a function of x/L, versus the dip angle α.

A semi-empirical relationship between PGS and the maximum surface ground velocity PGV is now introduced as follows.

$$PGS = r\frac{PGV}{\beta}\left[F_1(x/L,\alpha)+F_2(x/\bar{H},\alpha)\right]. \tag{2.7}$$

In analogy with (2.6), the basis of equation (2.7) remains the ratio between PGV and the shear wave velocity β. The other terms on the right hand side of (2.7) have the following meaning:

$$r = \frac{1-\eta}{1+\eta} \tag{2.8}$$

is the reflection coefficient, where

$$\eta = \frac{\rho_{soil}\beta_{soil}}{\rho_{rock}\beta_{rock}} \tag{2.9}$$

is the soil-bedrock impedance ratio (η<1). r increases as η decreases and vanishes when η=1, as it is physically expected, since for vertically propagating S-waves in a homogeneous medium the longitudinal strains vanish.

The two functions F_1 and F_2 between square brackets in (2.7) depend on the geometric parameters: the dip angle α, the normalized position x/L of the site with respect to the soil-bedrock contact, while the geometrical meaning of L and $\bar{H} = L\tan\alpha$ is clear from Figure 2.9c and Figure 2.9d. These functions were determined to be of the form:

$$\begin{cases} F_1(x/L,\alpha) = A(\alpha)\dfrac{x}{L}e^{-\gamma_1(\alpha)\left(\frac{x}{L}\right)^{1/3}} \\ F_2(x/\bar{H},\alpha) = B(\alpha)\dfrac{x}{\bar{H}}e^{-\gamma_2(\alpha)\left(\frac{x}{\bar{H}}\right)^{1/5}} \end{cases} \tag{2.10}$$

where $A(\alpha)$ and $B(\alpha)$ govern the amplitudes of longitudinal strains, while γ_1 and γ_2 are selected in such a way that the peak value of PGS occurs at the location $p(\alpha)$ defined by (2.6), see Figure 3.12, so that

$$\begin{cases} A(\alpha) = -0.0013\alpha^2 + 0.25\alpha + 7.8 \\ B(\alpha) = 0.11\alpha^2 - 1.8\alpha + 6.2 \end{cases} \qquad \begin{cases} \gamma_1(\alpha) = 3 \big/ p(\alpha)^{1/3} \\ \gamma_2(\alpha) = 5 \big/ p(\alpha)^{1/5} \end{cases} . \tag{2.11}$$

As shown in Figure 2.13 the contribution of F_1 decreases as the dip angle increases and vanishes for $\alpha = 90^o$, while the contribution of function F_2 increases as the dip angle increases and tends to vanish for small angles (less than 10°). In fact F_1 takes into account the amplification factors due to the wedge configuration near the soil-rock contact, while F_2 takes into account the propagation effects on a "wall-layer" like configuration (see Figure 2.9).

Apart from the reflection coefficient *r*, the function $F = F_1 + F_2$ has the role of modifying the shear wave velocity into an apparent wave velocity $c_a = \beta / F$. The most favourable case turns out to be the one with low dip angles, for which the geological configuration resembles the 1D case of a horizontal layer. In this limiting case, with vertical wave propagation, longitudinal strains should theoretically vanish.

Finally, the previous parametric analyses, on which (2.7) has been based, were performed under the assumption of vertically incident shear wave propagation. Therefore the proposed formula may not apply when Rayleigh waves are predominant.

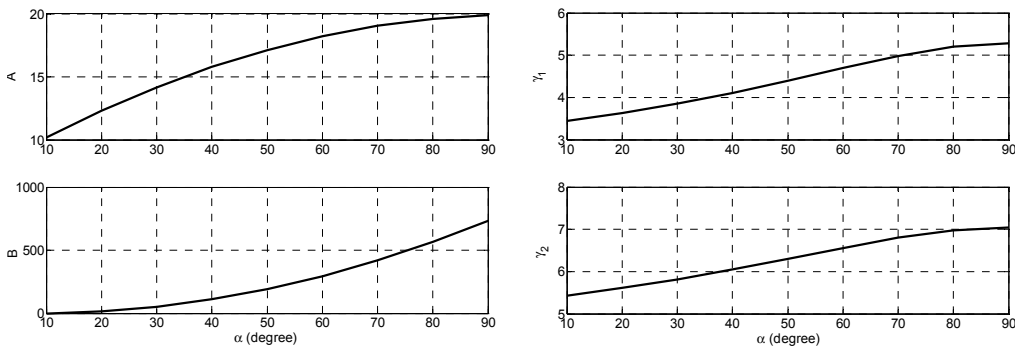

Figure 2.12: Left: functions $A(\alpha)$, $B(\alpha)$ which govern the amplitude of longitudinal strains; right: functions $\gamma_1(\alpha)$, $\gamma_2(\alpha)$ which govern the peak position of strains.

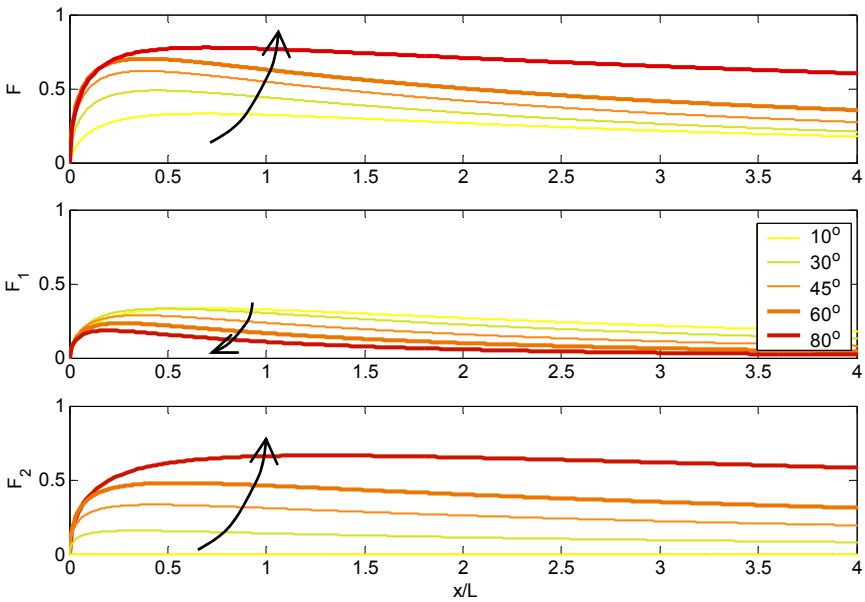

Figure 2.13: Functions $F = F_1 + F_2$, F_1, F_2 for various dipping angles vs. the non-dimensional distance x / L.

2.1.3 Methods to determine permanent ground displacements due to liquefaction, landslides and fault rupture

This sub-section contains a summary of different methods for the determination of permanent ground displacements due to liquefaction, landslides and fault rupture, in most real cases the leading causes of damage to buried pipeline components of IS.

Ground failures in engineering practice are normally quantified by permanent ground displacements, and they can be caused by:

i) Liquefaction (lateral spreads and settlements)

ii) Landsliding

iii) Surface fault rupture.

Table 2.3: Summary of the methods for estimating displacements due to liquefaction induced lateral spreads

Reference	Relationship	Description of Parameters	Model	Comments
[Hamada et al. 1986]	$D(m)=0.75H^{1/2}\theta^{1/3}$	- D, permanent horizontal ground displacement (m) - H, thickness of the liquefied layer (m) - θ, larger of the ground surface slope or the slope of the lower boundary of the liquefied zone in percent	Empirical model based on observations in uniform sands of medium grain size in: 1964 Niigata, M=7.5 1971 San Fernando, M=7.1 1983 Nihonkai-Chubu, M=7.7	Simple equation, not directly related to earthquake characteristics
[Youd and Perkins, 1987] **(Liquefaction Severity Index)**	$\log(LSI) = -4.49 - 4.86\log R + 0.98Mw \leq 100$	- LSI, Liquefaction Severity Index - R , horizontal distance from the seismic energy source in kilometers - M_W the moment magnitude	Empirical model based on observed lateral displacements from a number of case histories in Western U.S. The LSI represents a conservative estimate of ground displacement in a given area; failures with smaller displacement would also be expected in the area	older relation, mostly for US

Table 2.3 (cont.): Summary of the methods for estimating displacements due to liquefaction induced lateral spreads

Reference	Relationship	Description of Parameters	Model	Comments
[Byrne, 1991]	$\frac{D^3}{3(\gamma_{lim}T_L)^2} - D\tau_{st} - \frac{1}{2}mv_o^2 = 0 \quad D < \gamma_{lim}T_L$ $D = \frac{3mv_o^2 + 4S_r\gamma_{lim}T_L}{6(S_r - \tau_{st})} \quad D \geq \gamma_{lim}T_L$	- D, estimated lateral ground displacement - Sr, residual strength of the liquefied soil, - γlim, limiting shear strain, - TL thickness of the liquefied layer, - τst, average shear stress required for static equilibrium (on a failure surface passing through the middepth of the liquefied layer), - m, mass of the soil above the failure surface, - vo, velocity of the mass at the instant of liquefaction	Analytical, developed by modelling a slope as a crust of intact soil resting on a layer of liquefied soil. Elastic-perfectly plastic model.	A relevant, but difficult to use (complicated application) approach for cartographic applications in a wide area
[Baziar et al. 1992]	$D = N\frac{v_{max}^2}{a_{max}} f\left(\frac{a_y}{a_{max}}\right)$	- D, estimated lateral ground displacement - N, equivalent number of cycles of harmonic loading, - v_{max}, peak horizontal velocity, - a_{max}, peak horizontal acceleration - a_y, yield acceleration.	Analytical, developed using a sliding block analysis (assuming harmonic accelerations)	simple but not suitable for cartographic assessment

Table 2.3 (cont.): Summary of the methods for estimating displacements due to liquefaction induced lateral spreads

Reference	Relationship	Description of Parameters	Model	Comments
[Bartlett and Youd, 1995]	Free face model: logDH= -16.366+4.178MW-0.927logR -0.013R+0.657logW+0.348logT15 +4.527log(100-F15)-0.922(D50)15 Sloping ground model: logDH= -15.787+4.178MW-0.927logR -0.013R+0.429logS+0.348logT15 +4.527log(100-F15)-0.922(D50)15	- DH, estimated lateral ground displacement (m), - MW, moment magnitude, - R, horizontal distance from the seismic energy source (km), - W, ratio of the height of the free face to the horizontal distance between the base of the free face and the point of interest, - T15 , cumulative thickness (m) of saturated granular layers with (N1)60<15, - F15 , average fines content for the granular layers comprising T15 (%), - (D50)15 , average mean grain size for the granular layers comprising T15, (mm) - S, ground slope (%).	Empirical model based on observations from Western U.S and Japan Free face model: (for sites near steep banks) Sloping ground model: (for gently sloping sites)	some parameters are difficult to be estimated, uncertainties inserted

Table 2.3 (cont.): Summary of the methods for estimating displacements due to liquefaction induced lateral spreads

Reference	Relationship	Description of Parameters	Model	Comments
[Youd et al., 1999]	Free face model: logDH= -18.084+4.581MW-4.518logR* -0.011R+0.551logW +0.547logT15 +4.976log(100-F15) - 0.923log((D50)15+0.1mm) Sloping ground model: logDH= -17.614+4.581MW-4.518logR* -0.011R+0.343logS +0.547logT15 +4.976log(100-F15) - 0.923log((D50)15+0.1mm)	- Same as above - R*=R+Ro and Ro=10(0.89M-5.64)	Improvement of the previous model	
[Youd et al., 2002]	Free face model: logDH= -16.713 + 4.532MW - 4.406log R* - 0.012R + 0.592logW + 0.540logT15 + 4.413log(100-F15) - 0.795log((D50)15+0.1mm) Sloping ground model: logDH= -16.213 + 4.532MW - 4.406logR* - 0.012R + 0.338logS+ 0.540logT15 + 4.413log(100-F15) - 0.795log((D50)15+0.1mm)	Same as above	- additional data, - further statistical analyses	

Table 2.3 (cont.): Summary of the methods for estimating displacements due to liquefaction induced lateral spreads

Reference	Relationship	Description of Parameters	Model	Comments
[Bardet et al., 2002]	Free face & Sloping ground model: log(D+0.01) = bo + boff + b1MW + b2Log10R + b3R + b4Log10W + b5Log10S + b6LogTL	- D, estimated lateral ground displacement (m); - MW, moment magnitude; - R, horizontal distance from the seismic energy source (km); - S, ground slope (%); - TL, the thickness of liquefiable layer (m)	- based on the database by Bartlett and Youd - the data are divided in two data sets: (A) complete data for all ranges of displacement amplitude, (B) data limited to displacement amplitudes smaller than 2 m	Simple equation, the most critical parameters are taken into account
[HAZUS 1999, 2004]	$E\left[PGD_{SC}\right] = K_{\Delta} \cdot E\left[PGD \middle\vert \left(PGA/PL_{SC}\right) = a\right]$	- $E\left[PGD \middle\vert \left(PGA/PL_{SC}\right) = a\right]$ is the expected permanent ground displacement PGD for a given susceptibility category SC under a specified level of normalized ground shaking (PGA/PGA(t)) PGA(t), threshold ground acceleration necessary to induce liquefaction - KΔ, displacement correction for magnitudes other than 7.5	The relationship for lateral spreading was developed by combining the Liquefaction Severity Index (LSI) by Youd and Perkins (1987) with the ground motion attenuation relationship by Sadigh, et. al. (1986) as presented in Joyner and Boore (1988)	simple, more suitable for a first estimation in a wide area

Table 2.4: Summary of the methods for estimating displacements due to ground settlements in saturated and unsaturated soils

Reference	Relationship	Description of Parameters	Model	Comments
Tokimatsu and Seed (1987)	Dry sands: A plot for determination of induced cyclic shear strain. A plot relating volumetric strain εc,M=7.5, cyclic shear strain and N1 or relative density. Saturated sands: A chart for estimation of volumetric strain from CSRM=7.5 and standard penetration test.	- N1=SPT values, Dr= relative density - τav= average cyclic shear stress induced by the earthquake (depending on αmax) - Gmax= maximum shear modulus - γcyc=cyclic shear strain - CSRM=7.5=cyclic stress ratio - (N1)60=corrected SPT values	Based on laboratory tests and previous studies on natural deposits of sands	difficult application, requires the use of charts, good knowledge of ground conditions
Pradel (1998)	$\gamma = \left(\frac{1+\alpha \cdot e^{b \frac{\tau_{av}}{G_{max}}}}{1+\alpha} \right)$ $\varepsilon_{15} = \gamma \cdot \left(\frac{N_1}{20} \right)^{-1.2}$ and $\varepsilon_{Nc} = \varepsilon_{15} \cdot \left(\frac{N_c}{15} \right)^{0.45}$	- γ =shear strain - τ_{av}= average cyclic shear stress induced by - the earthquake (depending on αmax) - Gmax= maximum shear modulus - ε_{15}=volumetric strain after 15 cycles - ε_{Nc}=volumetric strain after N cycles - N_1= (SPT) values - N_c=number of cycles	Analytical method based on Tokimatsu and Seed's (1987) procedure, including a simple set of equations is proposed for estimating Gmax, cyclic shear strain γ, and volumetric strain	easier application, use o equations instead of charts, good knowledge of ground conditions

Table 2.4 (cont): Summary of the methods for estimating displacements due to ground settlements in saturated and unsaturated soils

Reference	Relationship	Description of Parameters	Model	Comments
Takada and Tanabe (1988)	for embankment : $PGD = 0.11 \cdot \frac{H_1 \cdot H_2 \cdot PGA}{N} + 0.2$ for plain site: $PGD = 0.3 \cdot \frac{H_1 \cdot PGA}{N} + 0.02$	- PGD, permanent ground deformation - H1, thickness of liquefied layer (m); - H2, height of embankment (m); - PGA, Peak Ground Acceleration (m/s²); - N, SPT value in the sandy layer	Empirical equations based on observations from Japanese earthquakes	simple, bulk estimation?
HAZUS 1999, 2004	The expected settlement, is the product of the probability of liquefaction for a given ground motion level and the characteristic settlement amplitude appropriate to the susceptibility category.	Susceptibility category (low, moderate, high, very high)	Ground settlement associated with liquefaction is assumed to be related to the susceptibility category assigned to an area	quite simplified

Table 2.5: Summary of the methods for estimating displacements due to landslide induced movements

Reference	Relationship	Description of Parameters	Model	Comments
Travasarou et al., (2004)	$\ln(D) = -1.64 - 3.57 \cdot \ln(k_y) - 0.478 \cdot (\ln(k_y))^2 + 0.825 \cdot \ln(k_y) \cdot \ln(SA(1.5T_s)) + 3.75 \cdot \ln(SA(1.5T_s)) - 0.33 \cdot (\ln(SA(1.5T_s)))^2 + 0.872 \cdot T_s - 0.082 \cdot T_s^2 + 0.3 \cdot (M - 6.7) + \varepsilon$	D, seismic displacement in cm, Ky, yield coefficient of the slope, Ts, initial fundamental period of the slope, SA(4.5Ts), spectral acceleration at a degraded period of the slope (4.5Ts), M, magnitude of the modal event controlling the hazard for the specified level of the spectral acceleration, ε, normally-distributed random variable with zero mean and standard deviation σ=0.77	- probabilistic methodology - based on an analytical "idealized" slope model - the predictive equation has two branches separately computing the probability of "zero" displacement occurring from the distribution of "nonzero" displacement	the fundamental period of the slope and spectral acceleration values are required

The amount and type of ground deformation is a function of geological and geotechnical factors. In recent years a number of researchers have developed methods to estimate permanent ground displacements produced by ground failure. Because of the complexity of the mechanisms that produce ground failures, procedures for prediction of the resulting deformations are largely empirical or semi-analytical in nature. For brevity, most of the different methods and procedures are synthetically described in three summary tables, namely Table 2.3 for permanent horizontal ground displacements caused by lateral spreads, Table 2.4 for those caused by settlements in saturated and unsaturated soils, and Table 2.5 for displacements related to landsliding.
Regarding the methods for estimating fault-induced permanent ground displacements, Wells and Coppersmith (1994) used a worldwide database of source parameters to develop a series of empirical relationships among moment magnitude (M) and maximum and average expected relative surface displacement (in m) across a fault according to fault type. Table 2.6 shows the proposed relationships.

The present summary review is based on previous work conducted within the EC RISK-UE project (2001-2004), with additional data-validations and properly improved with some new formulas and methods.

Table 2.6: Fault-induced relative Permanent Ground Displacement (PGD), in m, as a function of earthquake moment magnitude M [from Wells and Coppersmith, 1994].

Fault type	Fault induced Permanent Ground Displacements	
Strike slip	Average	log(PGD) = -6.32+0.90·M
	Maximum	log(PGD) = -7.03+4.03·M
Reverse	Average	log(PGD) = -0.74+0.08·M
	Maximum	log(PGD) = -4.84+0.29·M
Normal	Average	log(PGD) = -4.45+0.63·M
	Maximum	log(PGD) = -5.90+0.89·M
All	Average	log(PGD) = -4.80+0.69·M
	Maximum	log(PGD) = -5.46+0.82·M

2.2 APPLICATIONS: GROUND MOTION SCENARIOS FOR SELECTED CITIES

Illustrated in this sub-section are the salient features and results of the application of the previously described approaches to the creation of ground motion scenarios, including bedrock and surface soil motions, transient ground strain, and permanent ground deformations, to the urban areas of Thessaloniki and Düzce. The results are displayed in terms of time histories and response spectra at selected sites, time sections of ground strain, and also maps of peak values and permanent ground displacements.

2.2.1 Ground motion scenarios for Thessaloniki, Greece: seismotectonic context and definition of the reference earthquakes

As regards the seismo-tectonic context, Thessaloniki is located in Central Macedonia, Northern Greece, in an area characterized by NE-SW and NS extensional stress field driven by the Hellenic subduction zone in the Aegean Sea. High-angle normal faults bound continental-type basins and grabens which are W-SE and EW trending [Tranos et al., 2003; McClusky, S. et al., 2000; Goldsworthy et al, 2002; Ambraseys and Jackson, 1998]. Between such faults, the Mygdonian graben is the largest basin in the area. Its southern edge is bounded by an EW fault system of 65 km length that extends from Strymonikos gulf to the East to Thessaloniki to the West, called Thessaloniki-Rendina Fault System (TRFS) in [Tranos et al., 2003]. The general trend of TRFS is compatible with the current regional N–S extensional stress field, characterised by a slip rate of 0.4 mm/y. Part of this fault system is the Gerakarou-Stivos fault, associated to the damaging 1978 Thessaloniki earthquake [Stiros and Drakos, 2000]. The TRFS continues westwards towards the city through a large number of sub-parallel small fractures and large faults with E-W strike and North dipping [Tranos et al., 2003], forming a complicate fault zone named Thessaloniki-Gerakarou Fault Zone (TGFZ). To the East, the TRFS is characterized by the Nea Apollonia, Kokalou-Nea Madyotos and Rendina faults, which have almost identical geometries to the TGFZ and the Gerakarou-Stivos fault.
The study area is characterised by intense seismic activity with strong historical earthquakes of magnitude > 6.0 [Papazachos and Papazachou, 1997], the most recent of which occurred in the broader Thessaloniki area on the Gerakarou-Stivos fault, along the Mygdonian graben, on June 20, 1978, with M = 6.5. The mainshock caused extensive damage and loss of life in the metropolitan area and the surrounding villages. In 1999 a seismic sequence with the largest event of M 3.7 occurred near the city in the central part of Mt. Chortiatis. The earthquakes were felt throughout the whole Thessaloniki area [Papazachos et al., 2000]. According to Tranos et al. [2003], a major threat for Thessaloniki would be the possible reactivation of the western part of the TRFS. These authors suggested that the occurrence of the 1978 mainshock brought the adjacent fault segments closer to failure. On the basis of the previous considerations, the rupture of four segments along the TGFZ was assumed in order to compute the ground shaking scenario for Thessaloniki. To simulate the long-period ($f \leq 2.0$ Hz) motions in terms of velocity/displacement time histories, the already described, COMPSYN-based approach was used, and the corresponding computer codes (Spudich and Xu, 2002). The wave field generated by the 1978 earthquake was reproduced first with the aim of calibrating the source parameters and the propagation model for the scenario. The rupture of the four fault segments along the TGFZ was associated to magnitudes from 5.9 to 6.5, see Table 2.7 and Figure 2.15. For each fault, two models with the same rupture velocity but different nucleation points were assumed and the low-frequency technique was used to compute velocity and displacement ground motions at a grid of sites in the city of

Thessaloniki.

For comparison, in the scenario study for the Istanbul metropolitan area, not documented here, dedicated PSHA calculations were performed in the phase of identification of the scenario earthquake source. In other words, unlike the case of Thessaloniki, such sources were not defined on the base of seismotectonic studies only, mainly because they were better known in location and capability. The probabilistic analysis were developed for both 10% and 50% probability of exceedance (PE) in 50 years using the standard time-independent Poisson model and a time-dependent (lognormal) model. A geographic de-aggregation of composite PSHA calculations was then performed in order to identify the location sources most probably contributing to hazard at the city (Figure 2.16). As a matter of fact, deaggreagtion analysis allows to pick a *"governing"* earthquake, in terms of magnitude *M* and source-to site distance *R*, and identifies the location of the most probable source contributing to hazard at a well-defined site. The major contribution for PGA (47%) with 475 yrs recurrence time comes from the Central Marmara Fault, CMF, with a magnitude around M 7.4, denoted as "Scenario I", while 30% of the total hazard for 70 yrs recurrence time comes from the so-called North Boundary Fault, NBF, with a magnitude around M=6.9, denoted as "Scenario II".

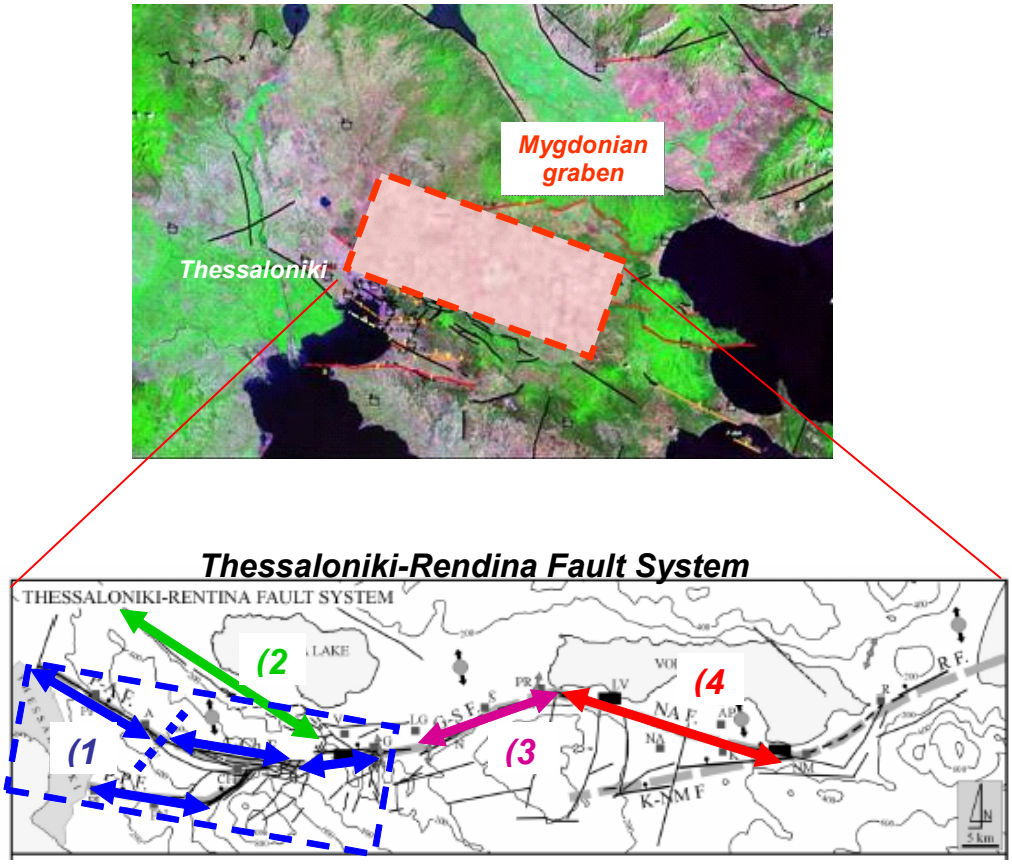

Figure 2.14: Top panel: map of Central Macedonia (Chalkidiki peninsula) with tectonic features indicated by red and black lines [redrawn from Pavlides 2004] ; the dashed box indicates the Mygdonian basin area. Bottom panel: Thessaloniki-Rendina Fault Sistem with the Thessaloniki-Gerakarou Fault Zone (1) in the blue box, Lagina-Ag.Vasilios fault (2), Gerakarou-Stivos fault (3) and Nea Apollonia fault (4). [from Tranos et al., 2003].

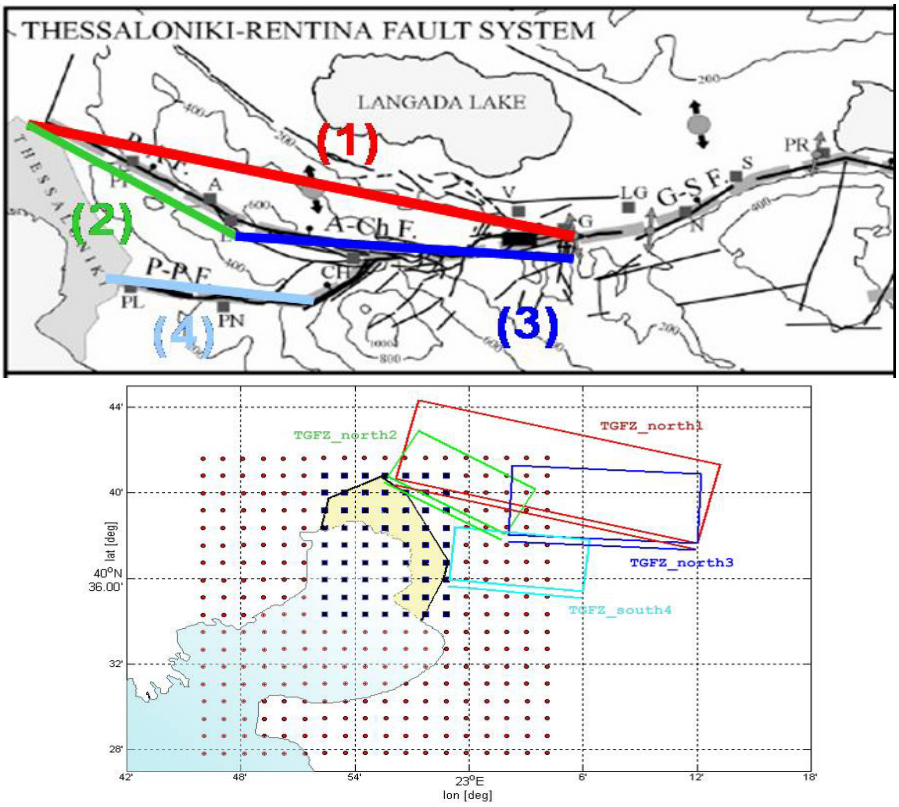

Figure 2.15: **Top: fault traces of the four hypothesized seismic sources [from Tranos et al. 2003]. Bottom: surface projection of the faults used in the simulations and grid of receivers: the blue squares indicate COMPSYN stations, in yellow the Thessaloniki urban area.**

Table 2.7 - Fault parameters (rise time = 0.7 s, rupture velocity = 2.8 km/s and rake angle = -90° are the same for all shaking scenarios)

Fault	*M*	*Mo (dyne.cm)*	*L xW (km^2)*	*<Δu> (cm)*	*Strike (deg)*	*Dip (deg)*	*Ztop* (km)*
1978 mainshock	6.5	6.3×10^{25}	22 x 14	59	288	51	1.1
North 1	6.5	6.3×10^{25}	23 x 14	57	284	60	1.0
North 2	5.9	0.8×10^{25}	10 x 9	26	300	60	1.0
North 3	6.2	2.2×10^{25}	14 x 12	39	273	60	1.0
South 4	5.9	0.8×10^{25}	10 x 9	26	276	60	1.0

*Ztop = depth of top of fault

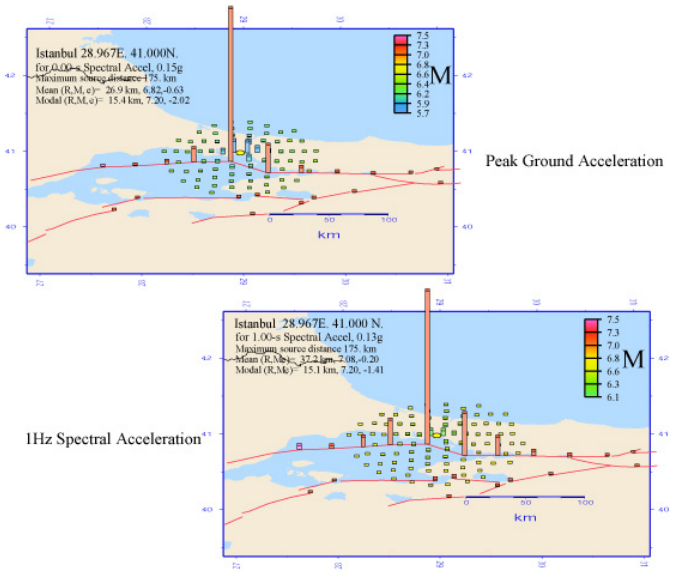

Figure 2.16: **Geographic Deaggregation of seismic hazard at Istanbul site 50% probability of exceedance in 50 years. Poisson model**

2.2.1.1 *The 1978 Thessaloniki earthquake*

The 1978 earthquake was simulated to test the source parameters and to calibrate the crustal velocity model to be used for the shaking scenarios. The 1978 mainshock (M 6.5) was a double event on an oblique-to-normal blind fault at the SW margin of Mygdonian basin, as shown in Figure 2.17 [Stiros and Drakos, 2000]. The epicentre was located about 25km NE of the city, and the earthquake was recorded by one accelerograph station (THE) located in the basement of an eight-story building (City Hotel) at the shore line of the city. The PGA value was relatively low (~0.15g), possibly due to non linear soil response [Pitilakis et al., 2004].

The mainshock simulation was performed using the fault model from [Stiros and Drakos, 2000], illustrated in Figure 2.18, with the main parameters listed in Table 2.7.

A normal fault mechanism was assumed with bilateral rupture starting from the hypocenter location (rupture velocity of 2.7 km/s and uniform slip distribution). The 1D crustal model for S-wave velocity was inferred from the 3D tomographic image of the crust-uppermost mantle in the Aegean area using the group velocities of Rayleigh wave fundamental mode [Karagianni et al. 2005]; P-velocities and density are from [Papazachos and Nolet, 1997] (Table 2.8). Anelastic attenuation was not included in the model and ground motions were simulated up to 3 Hz, taking into account the site effects throughout the 1D transfer function of [Klimis et al., 1999].

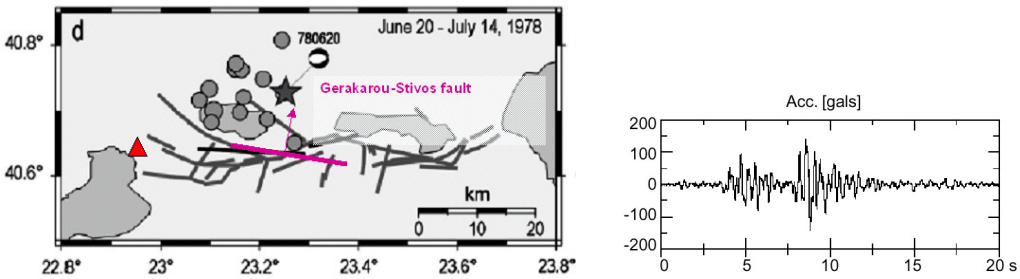

Figure 2.17: **Left: epicentral distribution of the 1978 seismic sequence with M≥4.3 occurred from June 20 to July 14, 1978 [redrawn from Tranos et al., 2003]. The fault trace of the Gerakarou-Stivos fault, which ruptured during the 1978 Thessaloniki earthquake, is inferred by [Stiros and Drakos, 2000]. Right: the accelerogram recorded at the City Hotel station in downtown Thessaloniki shows the double event of June 20, 1978, earthquake (M=6.5).**

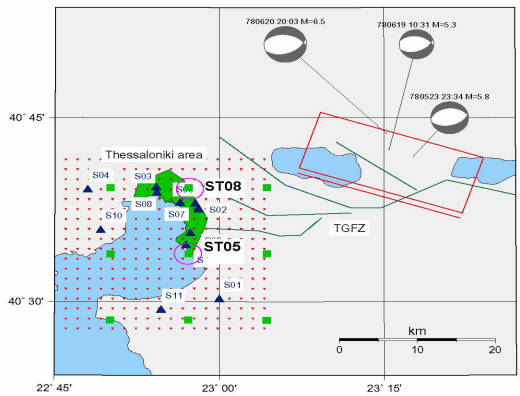

Figure 2.18: **Position and dimension of the 1978 source fault. The focal mechanisms of 1978 earthquake and of the two main aftershocks are also reported. ST07 corresponds to THE accelerometric station.**

The computed velocity waveforms, lowpass filtered at 1 Hz, and their Fourier spectra are compared in Figure 2.19 with the data recorded at the the accelerograph station. The synthetic seismograms fit reasonably the observations of the M 6.5 mainshock [Margaris and Boore,1998] both in waveform and in amplitude values (Figure 2.19). The similarity in duration indicates that both the first seismic phases and the successive ones, dependent on the propagation model, are correctly computed. However, the complexity of recorded signal can not be reproduced using a purely deterministic source model without stochastic components. The comparison suggests that the Compsyn simulation should be considered reliable up to about 1 Hz.

Table 2.8 - 1D crustal model for the studied area

Depth (km)	Vp (km/s)	Vs (km/s)	Rho (g/cm³)
0	4.5	2	2.4
1	6.06	3.44	2.7
5	6.07	3.46	2.8
11	6.37	3.64	2.9
21	6.96	3.98	3
31	7.64	4.36	3.2

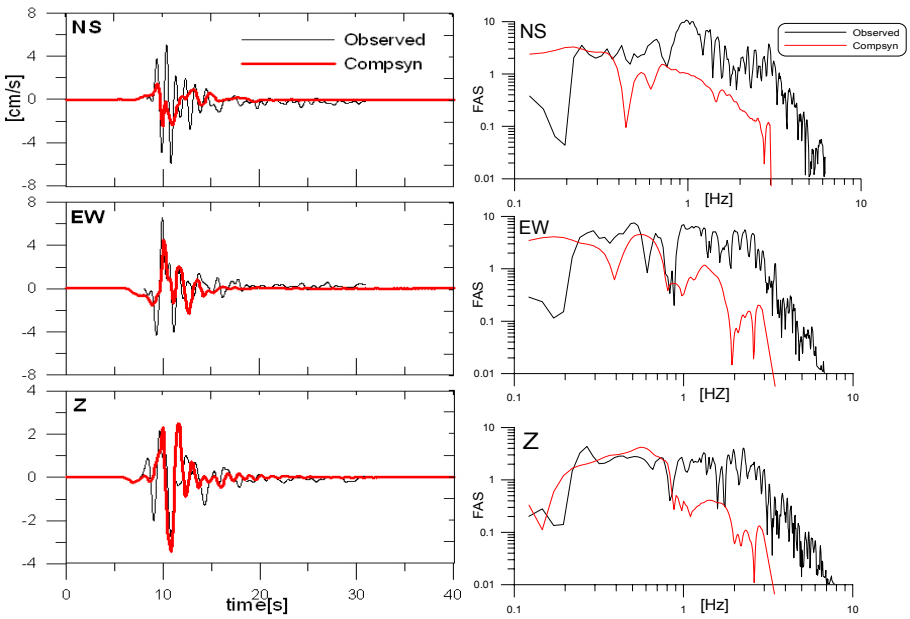

Figure 2.19: Comparison between simulated and recorded waveforms at the City-Hotel accelerograph station in Thessaloniki, 1978. Velocity time series lowpass filtered at to 1 Hz (left panel) and velocity Fourier spectra (right panel) are shown. Black line = observations; red line = synthetic data.

2.2.1.2 *Assumptions for the ground shaking scenarios*

As already stated, ground shaking scenarios for Thessaloniki were calculated for 4 sources of magnitudes 5.9 to 6.5, rupturing the TGFZ (Table 2.7 and Figure 2.15**).**

Ground velocity and displacement time series were calculated at 63 hypothetical rock sites in the urban area (see locations in Figure 2.15), considering 2 nucleation points for each fault, thus giving a total of 8 scenarios. Two different locations of the hypocenter

have been adopted: one nucleation point lies at the center of the fault and produces a bilateral rupture; the other lies on the right side of the fault and generates a unilateral rupture directed towards the Thessaloniki urban area. The latter scenario is expected to be the worst for the city, due to the source directivity effects. As for the 1978 earthquake, the TGFZ faults were assumed to have normal mechanism, with dip towards the North, and to be blind, i.e. not intersecting the surface. The fault length L is inferred from [Tranos et al., 2003], the width W from the seismogenic depth, and the magnitude from the correlation between fault area and magnitude of [Wells and Coppersmith, 1994].

2.2.1.3 *Maps of ground shaking on rock*

Based on seismotectonic considerations and on the comparison with probabilistic seismic hazard analysis, the North1 (M6.5) fault was assumed to be capable of generating the maximum credible earthquake (with an associated indicative T_r = 500 yrs); while the North2 and South faults were considered capable of generating a smaller, and more frequent event (T_r = 50 yrs), having the same magnitude (M5.9) and similar geometry, but with different position respect to the city. The North3 fault is not of concern because it is farther away from the city and included in the previous cases.

Examples of the results obtained are mapped in Figure 2.20 to Figure 2.22.. Figure 2.20 shows the Peak Ground Displacement values generated from the North1 and South sources, plotted separately for the horizontal components of motion, in the case of bilateral nucleation of fault rupture. As expected, the largest ground motion is generated by the North1 fault (the North2 source produces maps with similar trends but lower amplitudes). The South fault gives a peculiar distribution of peak ground displacement. Comparing the shaking maps of South and North2 sources (Figure 2.21) shows that the simulated PGV values from South scenarios (Figure 2.21, top) are systematically lower in the metropolitan area than those from North2 scenarios (bottom), although the two faults generate the same magnitude (5.9) and are at similar distances from the sites. This is because in the South scenarios most of sites are located in a nodal plane area so that the combination of source-site geometry and focal mechanism produces minimum peak values in the Thessaloniki urban area.

Figure 2.22 displays examples of maps of permanent ground offset generated by the N1 and South faults, in terms of horizontal (vector sum) and vertical displacement components. Again, the dependence of the low frequency ground motion on the radiation pattern of the source is clearly visible.

2.2.1.4 *Uncertainties in the scenario predictions: numerically simulated vs. empirically predicted peak motion values*

It was found in the work carried out in SP10 on Thessaloniki, by comparing the synthetic peak ground motion values to those predicted by different attenuation relations, that for all scenarios the variability of the former was comparable to the standard error ($m \pm 1\sigma$) band of the latter and that, in all cases, the quasi-unilateral rupture propagation produced

the highest dispersion. However, as shown in Figure 2.23, the comparison does not allow a clear identification of the most representative scenario for M 5.9 magnitude, since both North2 and South options match the variability of the empirical predictions.
The simulated Peak Velocity and Displacement values are compared to the empirical predictions in Figure 2.24 and Figure 2.25.
For all faults, the simulated PGVs fit better the regional Greek attenuation relation (SK03) and lie inside its standard error band (Figure 2.24), while the simulated displacements are in better agreement with the European based TB02 relation, and still fall inside its m $\pm$ σ, band (Figure 2.25). At a given distance the simulated data exhibit a variability of up to a factor of 2, depending on the position of the nucleation point. Note that for the low frequency peak velocity and displacement parameters the comparison may rest on less firm ground than for PGA (used in SP10): indeed, the empirically predicted velocities and displacements are more uncertain, due to the long period noise that affects the analogue record processing and double integration.

2.2.1.1 *Numerically simulated vs. empirically predicted response spectra at selected "test" sites*

The 5% damped Pseudo Velocity (PSV) and Displacement (SD) response spectra calculated from the simulated time histories at selected "test" sites (6 and 11 in Figure 2.18) were compared with empirically predicted response spectra, with the aim to assess the engineering applicability of the scenarios.
Empirical PSV spectra were computed using Sea99 (see Table 2.2); in order to cover a larger period range (up to 5 s), the Abr97 attenuation relation was also used, although it was derived for SA values. Finally, the displacement spectral response SD was empirically predicted by the recent relation Fa07, that covers the whole range of periods up to 10 s and is calibrated on a very extensive set of digitally recorded accelerograms.
Figure 2.26 illustrates the comparison between the mean horizontal PSV, at 5% damping, computed from the time series generated with Compsyn from the North1 scenario and the empirical velocity response spectra (Sea99 and Abr97). Although the simulated data are nominally generated for periods as low as 0.3 s, we consider them representative only for period larger than 1 s: the trend of the spectral values is generally comparable to the empirical ones for T $\geq$ 2.5 s. To allow for detailed site response analysis at selected locations, BB time series of ground motion were also generated in addition to the band limited, low frequency synthetics, for the North1 bilateral scenarios. The intermediate frequency band, where the high and low frequency seismograms were "pasted" together, was selected by visual analysis, identifying the overlapping frequency range. On average, the transition band is from 0.5 – 1.0 Hz for the EW component and 1 – 2 Hz for the NS component. Figure 2.27 shows an example of BB synthesis for site 10.
Figure 2.28 and Figure 2.29 display the 5% damped acceleration and displacement response spectra from BB signals for North1 scenario at sites 07 and 10, and compare them with the empirical predictions yielded by the attenuation relations AMB05 and

Fa07. The simulated response spectra are contained in the standard error band of the empirical predictions but lie mostly in the band between m and m-1σ.

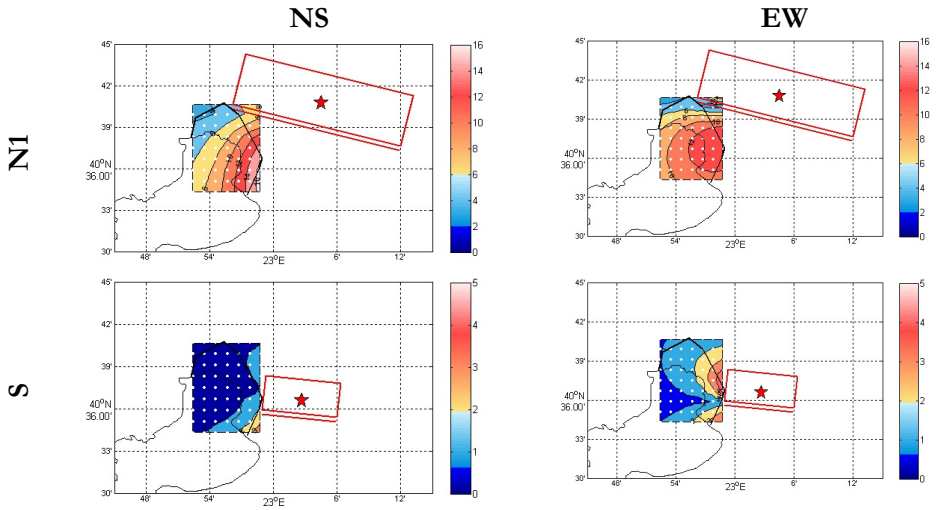

Figure 2.20: **PGD maps at bedrock obtained for the North 1 scenarios (top panel) and South1 (bottom panel) with bilateral nucleation for NS (left panels) and EW component (right panels).**

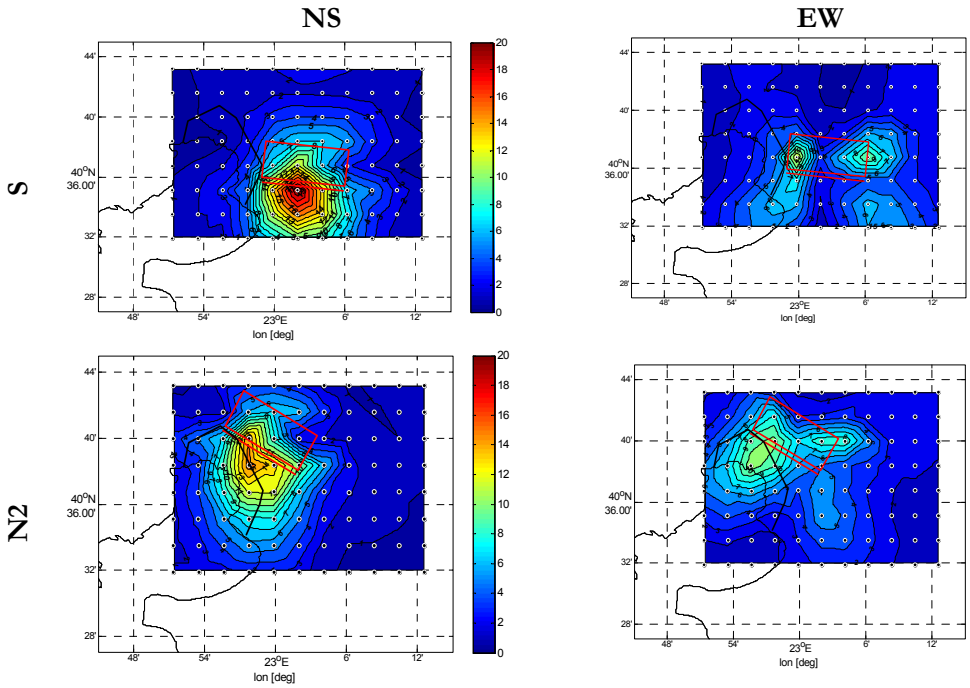

Figure 2.21: **PGV maps (cm/s) NS and EW components: South bilateral scenario (top) and North 2 bilateral scenario (bottom)**

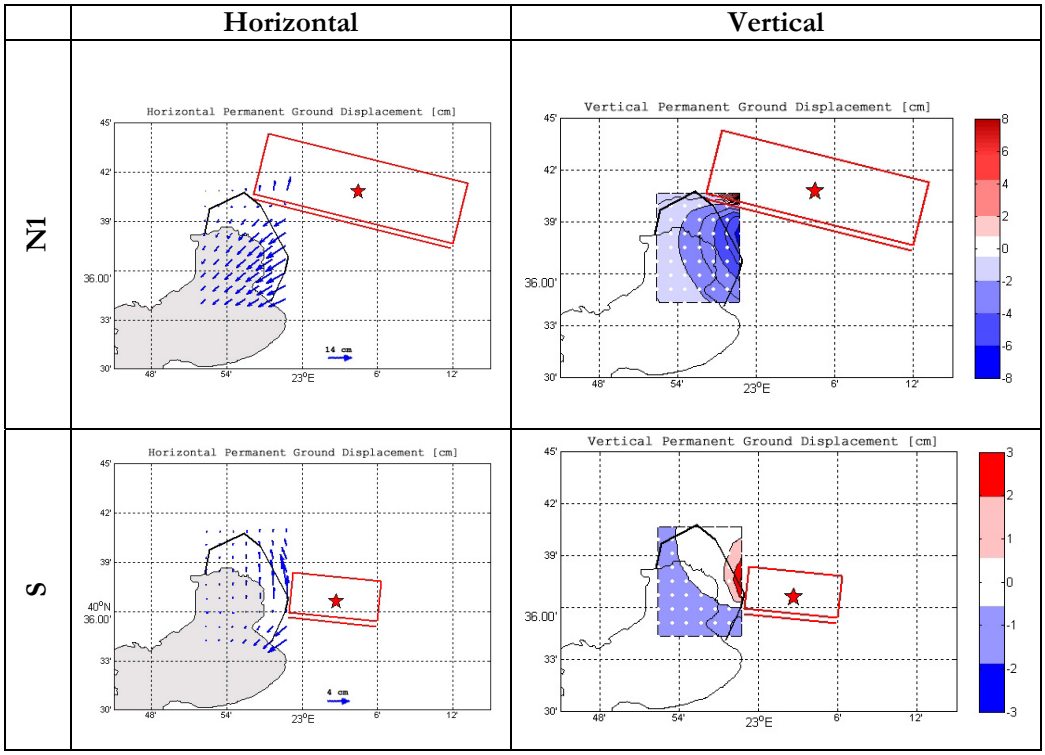

Figure 2.22: **Permanent displacements at the bedrock surface obtained for the North 1 scenarios (top panels) and South (lower panels) with bilateral nucleation, showing the vector sum of horizontal components (left panels) and vertical component (right panels). The epicenter, the fault surface projection, and the urban area of Thessaloniki are also shown.**

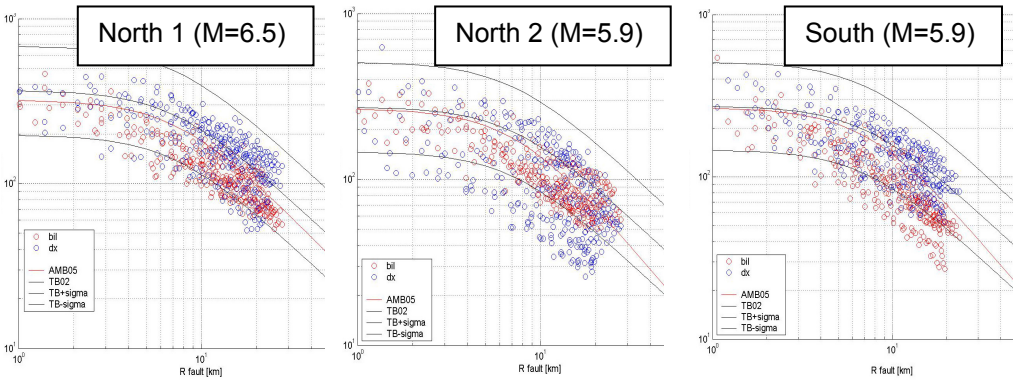

Figure 2.23: **PGA empirical attenuation equations (black lines: Tromans and Bommer [2002]; red lines: Ambraseys et al., [2005]), vs. simulated peak values of level I (M 6.5) and II (M 5.9) scenarios. Red and blue symbols correspond to bilateral and quasi-unilateral scenarios, respectively.**

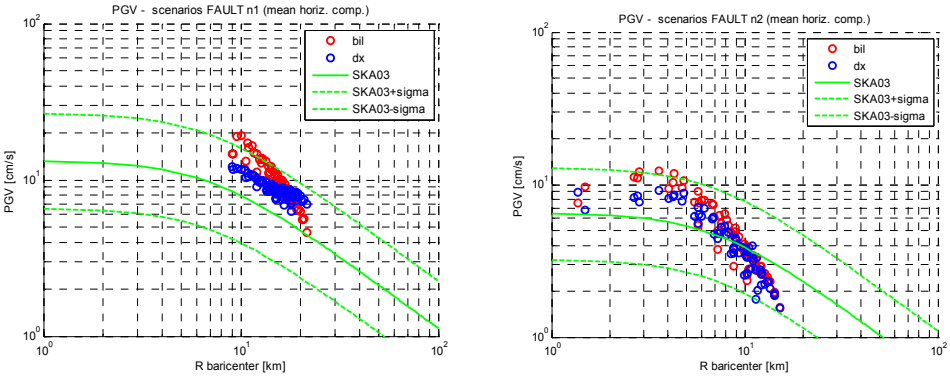

Figure 2.24: **PGV values from the simulated North1 and North2 scenarios, compared with those derived from the SK03 (Table 2.2) predictive equation. Red dots: bilateral rupture; blue dots: left lateral rupture**

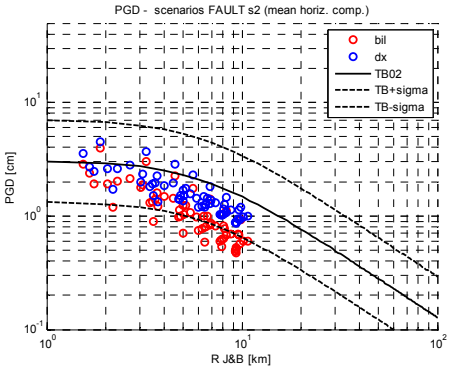

Figure 2.25: **Peak Ground Displacement (cms) values from the simulated South scenario, compared with those derived from the TB02 predictive equation. Red dots: bilateral rupture; blue dots: left lateral rupture.**

2.2.1.2 *On the choice and characterisation of reference scenarios; results of simplified engineering approach*

The comparisons with both the peak and the response spectral values suggest that all the considered scenario earthquake sources (North1, North2 and South) would be suitable for loss estimation analysis. Peak ground velocities and displacements from the simulations are summarised in Table 2.9. On the other hand, the dependence of the low frequency ground motion on the radiation pattern of the seismic source cannot be identified by comparing only the peak values, while it is clearly visible in the maps of Figure 2.20 and Figure 2.21.

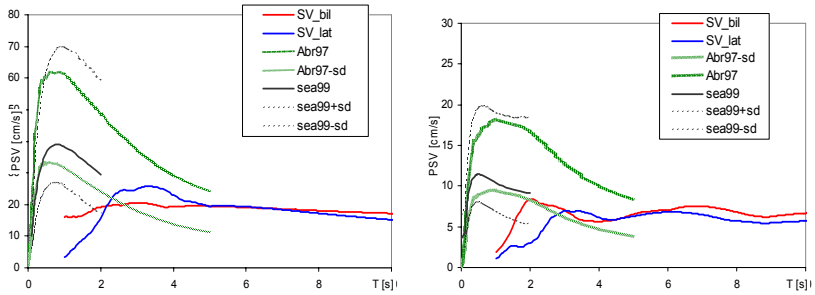

Figure 2.26: **Pseudo Velocity Spectra for North1 scenarios, at test site 6 (left) and 11 (rigth). Bilateral simulation (red line) and unilateral one (blue) are compared with Sea99 (mean value m and m ± σ) and Abr97 (mean values and m - σ)**

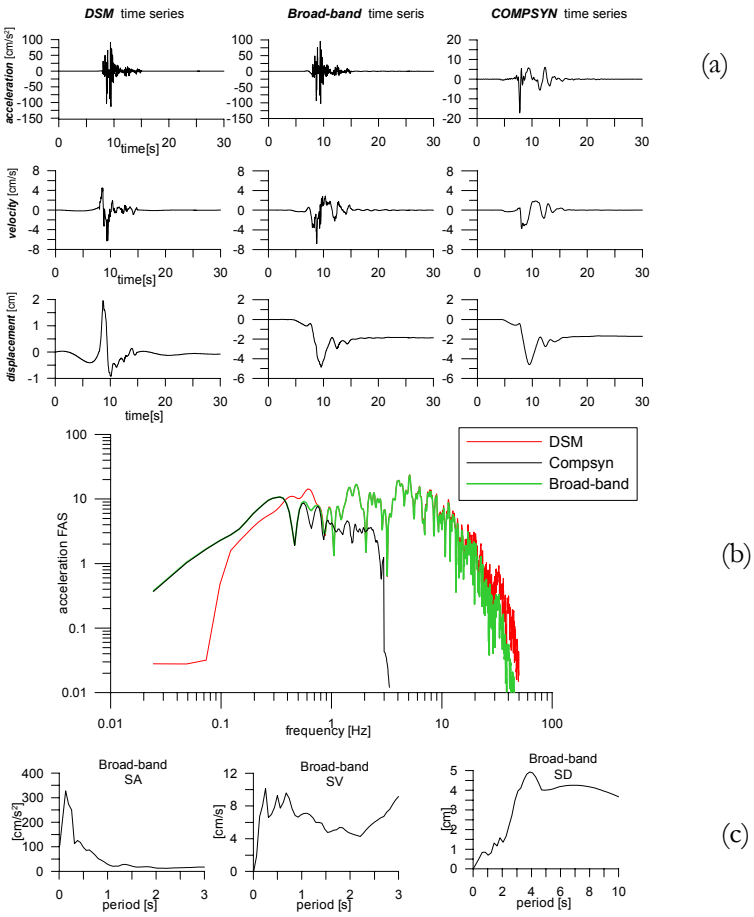

Figure 2.27: **BB synthesis for scenario North1 (bilateral model) at site 10: (a) acceleration, velocity and displacement time series from DSM, broad band and COMPSYN methods; (b) Acceleration Fourier spectra: from DSM (red line), Broad band (green line) and COMPSYN (grey line); (c) BB acceleration, velocity and displacement response spectra for 5% damping.**

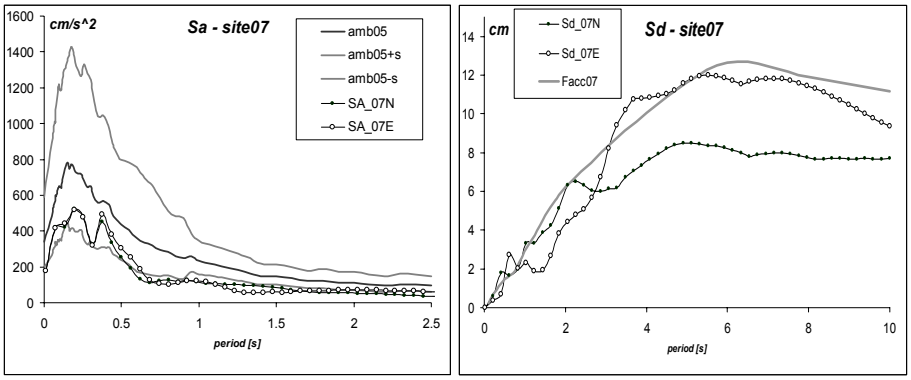

Figure 2.28: **Site 07: NS and EW BB acceleration (left) and displacement (right) response spectra compared with the mean (m) and m ± σ empirical predictions from the AMB05 and Fa07 attenuation relationships. The site is located at 13 km from the fault.**

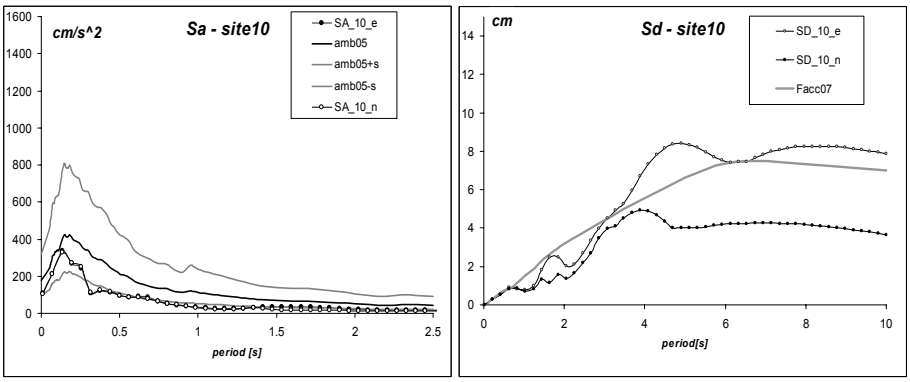

Figure 2.29: **Site 10: NS and EW BB acceleration (left) and displacement (right) response spectra compared with the mean (m) and m ± σ empirical predictions from the AMB05 and Fa07 attenuation relationships. The site is located at 24 km from the fault.**

Table 2.9: **Peak ground motion parameters on exposed rock for three fault rupture assumptions. Min, Max and Mean values are computed from 63 sites in the Thessaloniki urban area.**

	VELOCITY (cm/s)			***DISPLACEMENT(cm)***		
	Min	***Max***	***Mean***	***Min***	***Max***	***Mean***
TGFZ_South Bilateral	0.7	6.2	2	0.5	4.0	1.3
TGFZ_South Unilateral	1.4	6.0	2.7	0.9	4.5	1.7
TGFZ_North2 Bilateral	1.6	12.3	5.3	1.3	6.5	3.9
TGFZ_North2 Unilateral	1.5	9.1	4.6	1.6	6.5	3.9
TGFZ_North1 Bilateral	4.6	19.2	10.4	2.9	15.0	9.0
TGFZ_North1 Unilateral	6.3	12.1	8.8	4.6	15.6	9.9

The summary values of Table 2.9 indicate scenario ground motion of moderate severity, except perhaps for the North 1 fault ruptures.
In order to better understand the spatial distribution of ground motions, a comparison has been made between the maps obtained by the advanced simulations and by the simplified engineering approach.
Examples of maps calculated with the simple engineering approach are illustrated in Figure 2.30 for both the M5.9 scenario events (North1 and South). The expected maximum ground displacement (well approximated by D10, the SD response at 10 s period, according to Fa07) ranges between 3 and 3.7 cm, in the whole city, but depends on the location of the source: the South faults affect the Eastern part of the city while the North2 scenarios produce larger values in the Northern sections.

Further, Figure 2.31 depicts the values of peak displacement calculated with Compsyn (on the top of the Figure, unilateral and quasi-unilateral rupture, respectively) and the empirical ones (TB02) assumed as reference. This allows to identify a section of the city where the simulated values are larger than the m + 1 σ values estimated with the empirical attenuation TB02. The same check was performed also for PGA and PGV, but it did not disclose values of numerical simulations exceeding the m+1 σ empirical values.

A final comparison was made between the response spectra of the advanced simulation scenarios and the Uniform Hazard (UH) spectra [1], in order to define the most representative scenarios for return periods of 50 and 500 yr. This comparison led to grouping the results into level I scenarios, generated by strong seismic sources (M6.5), and level II scenarios, generated by moderate sources (M5.9). The first group includes the N1 bilateral and quasi-unilateral cases, while level II scenarios group the N2 and S sources, with the two different assumptions on rupture nucleation.
As an example Figure 2.32 compares the deterministic and UH probabilistic response spectra at site S07, in the city of Thessaloniki, for level I (left panel) and level II scenarios (right panel). At this site, the level I scenarios result in good agreement between deterministic (N1) and UH spectra for 500 yr RP, while all of the level II scenario spectra range between the UH spectra for 50 and 200 yr RP. Thus, the comparisons provide useful constraints as to the exceedance probabilities of the ground motions generated by the advanced methods.

[1] Computed with the CRISIS2003 code, developed by M. Ordaz and co-workers of Instituto de Ingenieria of National Autonomous University of Mexico, and based on the approach described in [Ordaz et al 1991]

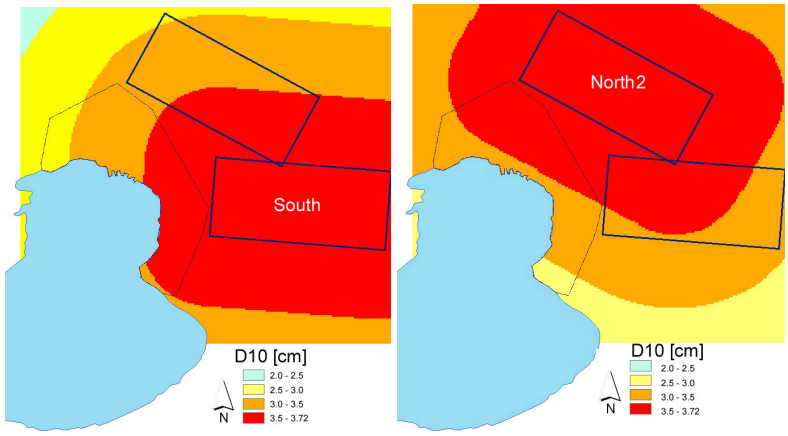

Figure 2.30: Displacement spectral response at T=10 s in Thessaloniki, calculated with Fa07 and the simplified engineering method, for South and North2 scenarios.

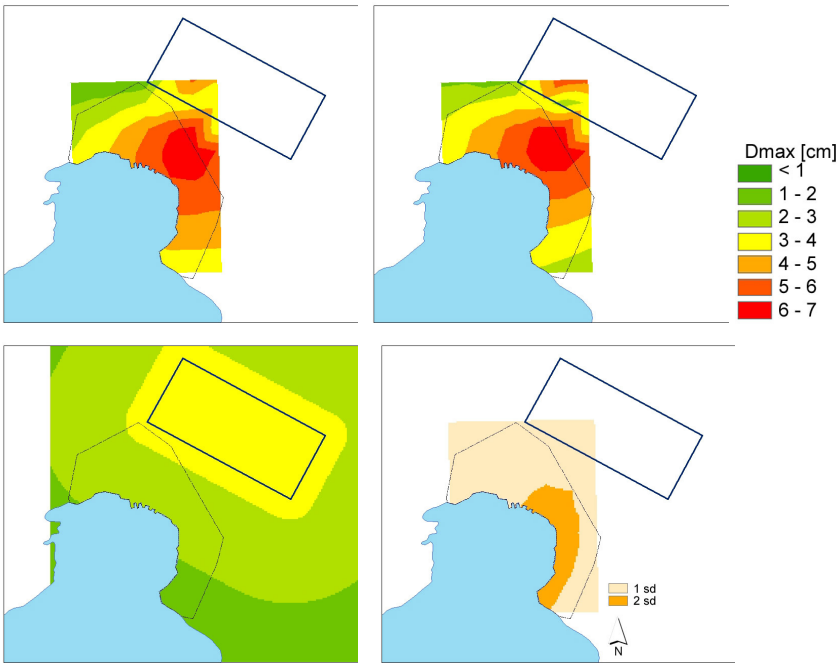

Figure 2.31: Comparison between spatial distributions of peak ground displacement (D_{max}) from the advanced simulations (top) and the empirical ones carried out with the simplified method (bottom, left). In some sections of the city, the simulated level I values could be larger than the m + 1 σ (sd) estimates calculated by TB02, as shown in bottom right panel.

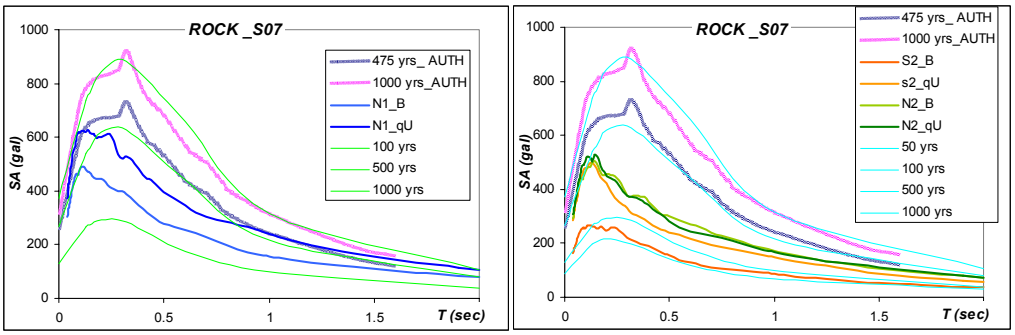

Figure 2.32: Comparison at site S07 between UH, probabilistic acceleration response spectra and deterministic simulations obtained with North1 scenarios (left panel), and with North2 and South scenarios (right panel). Comparisons were made for both bilateral and unilateral rupture propagation. Response spectra computed by CRISIS2003 are plotted with thin lines, and 475 and 1000 yr RP response spectra computed by AUTH (Aristostle University of Thessaloniki) are also plotted for comparison

In the case of Istanbul, the deterministic scenarios show a large spatial variability, more complex than in the Thessaloniki case because of the extension of the considered area and the relative location of the faults with respect to the city. For example, the PGA spatial distribution shows that the largest fault segment (scenario I earthquake) generates a strong directivity effect in the city and the expected PGA can exceed 1g. This variability corresponds to more than 1 s. d. of the attenuation relationships applicable for the region. Scenario I earthquakes generate peak velocities in Istanbul up to about 45 cm/s at a fault distance of 14 km, and peak displacements up to 97 cm at 15 km. The acceleration and velocity response spectra of the simulated ground motions agree with the empirical relationships predicted by AMB05, BOM98, TB02 and AK06. For the CMF case, all the simulated ground velocities are in good agreement with TB02 relationships (inside the mean ± 1 s.d. band) in the distance range 10-80 km.

2.2.1.3 *Surface soil response in selected areas: 1D equivalent site response analyses*

Sensitivity of surface response to the excitation

Rather than performing the response calculation of the near-surface soil deposits at all the sites where the previous scenario bedrock motions had been obtained, use was made of the results of a previous microzonation study performed in the metropolitan area of Thessaloniki, as follows. The output ground motion from a few 1D equivalent site response analyses using for seismic excitation the broad band (BB) time histories previously illustrated at selected sites in the city (see locations in Figures 2.18 and 2.33), were compared with those of the cited microzonation study. The comparison has been

conveniently performed on the response spectra at each site, although the latter are not the optimal ground motion measure used for evaluating the seismic damage to IS.

The microzonation study relied on the results of a recent probabilistic seismic hazard analysis performed in the area, in which recent empirical relations for the attenuation of ground motion parameters had been used. The results of such study were associated to return periods of 100, 475 and 1000 years respectively. Five appropriately selected real accelerograms (Table 2.10) scaled to the PGA values obtained from the microzonation study for the 3 return periods at 4 selected sites (named 5, 7, 10 and 11 – see Figure 2.33 and Table 2.11), were used for the analyses assuming exposed bedrock conditions. The normalized acceleration response spectra of the 5 accelerograms are compared to those of the previously described BB synthetics in Figure 2.34a and Figure 2.34b, respectively.

To evaluate the sensitivity of the surface ground response to the bedrock input, 1D site response analyses were performed at the previous 4 sites (Figure 2.33), which have a detailed soil profile classification. The results obtained from the analyses are shown in Figures 2.35-2.38 in terms of spectral accelerations, with comparison between the deterministic scenario (BB input) spectra and those calibrated on the probabilistic evaluation of seismic excitation (microzonation study).

Despite the fact that several differences exist between the two different groups of input motions, both in terms of peak and spectral values and of duration and frequency content, the results derived from the 1D analyses using the deterministic scenarios tend to lie in the lower portion of the standard error band (represented by a shaded area in the figures) of the microzonation study spectra for 475yr. Actually, in a number of cases the spectra from the deterministic BB simulations lie between the 100 and 475 mean spectra from the Microzonation study. The 475 yr spectrum is generally rather close to the spectra for 1000 years return period, not shown in the figures. In conclusion, the comparison indicates that seismic damage estimations to the Tessaloniki IS based on the results of the microzonation study will be conservative with respect to those observed from the deterministic scenarios, other conditions being equal.

Ground motion scenarios

Using the linear equivalent 1D method for calculating the site-specific soil response on a dense grid of regularly spaced points, several maps (PGA, PGV etc) were produced, providing the input required for estimating seismic damage to the water distribution system and other ISs. Figures 2.39 and 2.40 illustrate the computed distributions of PGA, PGV and PGD (permanent ground displacements e.g. settlements and lateral spreading) values, obtained in the Microzonation study for 100 and 475 year return periods.

Table 2.10 - Microzonation Study of Thessaloniki: Selected Acceleration Time Histories.

Acc. n	1	2	3	4	5
Code	855-Y	MONT_T	WWT180	Koz95-T	Thes78_Dec
Earthquake	Umbria-Marche	Montenegro	N.Palm Springs	Κοζάνη	Θεσσαλονίκη
Country	Italy	Yugoslavia	USA	Greece	Greece
Date	05/04/1998	15/04/1979	08/07/1986	13/05/1995	20/06/1978
Time	15.52.20	6.19.41	9.20.00	8.47.15	20.03.22
Latitude	43.19	41.98	33.99	40.18	40.73
Longitude	12.72	18.98	-116.6	21.66	23.25
Depth (Km)	10	12	11	14	6
Mw	4.8	6.9	6.2	6.5	6.2
Mechanism	Normal	Thrust	Reverse-oblique	Normal	Normal
Site	Gubbio-Piana	Hercegnovi Novi-O.S.D. Pav.Sch	5072 Whitewater Trout Farm	Kozani-Prefecture	THE_6-City Hotel
Building type	free-field	free-field	free-field	free-field	free-field
Geology	Rock	Rock	Rock	Rock	Rock
Epicentral Distance R (km)	18	65	6	17	29
PGA (g)	0.235	0.256	0.492	0.142	0,074 (0,143)

Table 2.11 - Microzonation Study of Thessaloniki results in terms of PGA values at selected sites.

	Return Period (yrs)		
	100	475	1000
Site	PGA (g)		
5	0.14	0.28	0.32
7	0.12	0.20	0.28
10	0.12	0.20	0.22
11	0.12	0.24	0.32

Figure 2.33: Sites (11) at the Thessaloniki broader area where specific response analyses were performed. Additional response analyses using broadband synthetics were performed at sites 5, 7, 10 and 11 (within a circle).

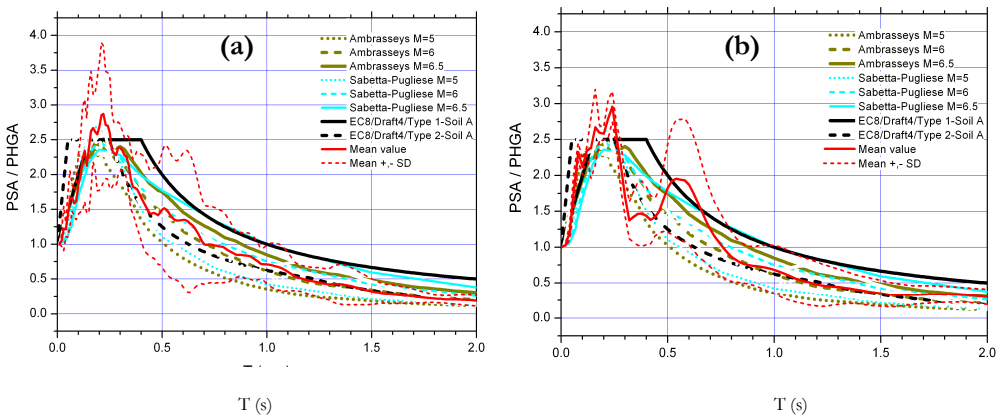

Figure 2.34: Normalized acceleration response spectra of input motion on rock compared with mean values of the PSH analyses: (a) Microzonation study of Thessaloniki, mean spectra of 5 accelerograms (in red), (b) "Broadband synthetics" at sites 5, 7, 10 and 11 for the N1 fault with bilateral rupture (in red).

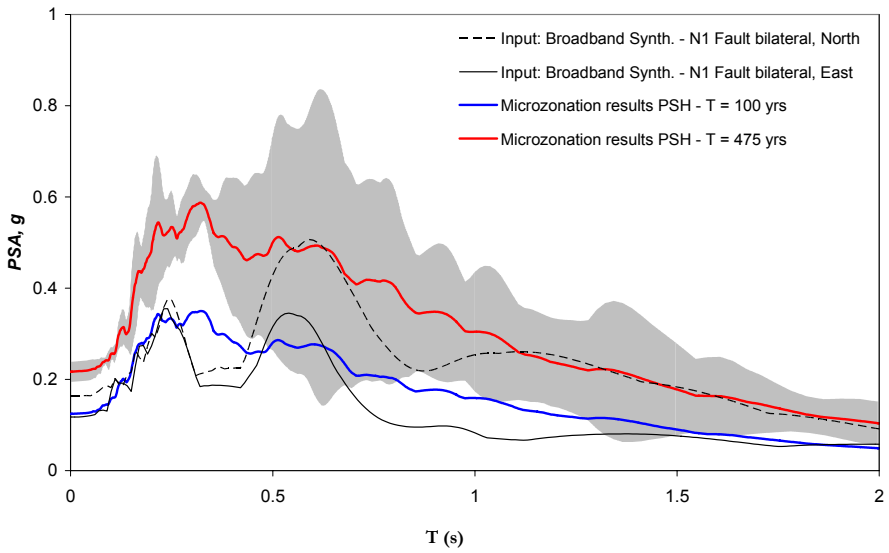

Figure 2.35: Results of 1D - EQL analyses at Site S05 in terms of PSA: the spectra obtained using as seismic excitation one deterministic bedrock scenario (Broadband synthetics, Thessaloniki-Gerakarou N1 fault – bilateral rapture) are compared with those derived from the microzonation study for T = 100 yrs (average) and T = 475 yrs (average ± 1 σ shaded area).

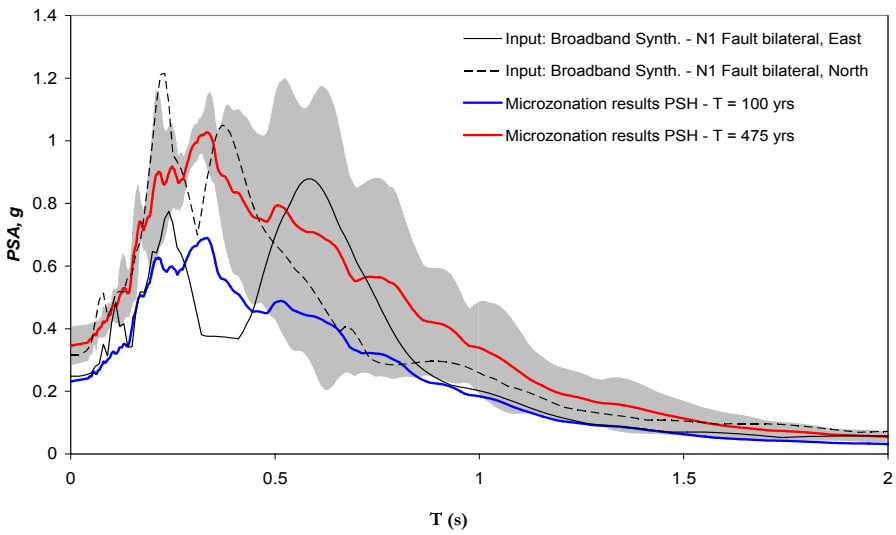

Figure 2.36: Results of 1D - EQL analyses results at Site S07 in terms of PSA: the spectra obtained using as seismic excitation one deterministic bedrock scenario (Broadband synthetics, Thessaloniki-Gerakarou N1 fault – bilateral rapture) are compared with those derived from the microzonation study for T = 100 yrs (average) and T = 475 yrs (average ± 1 σ shaded area).

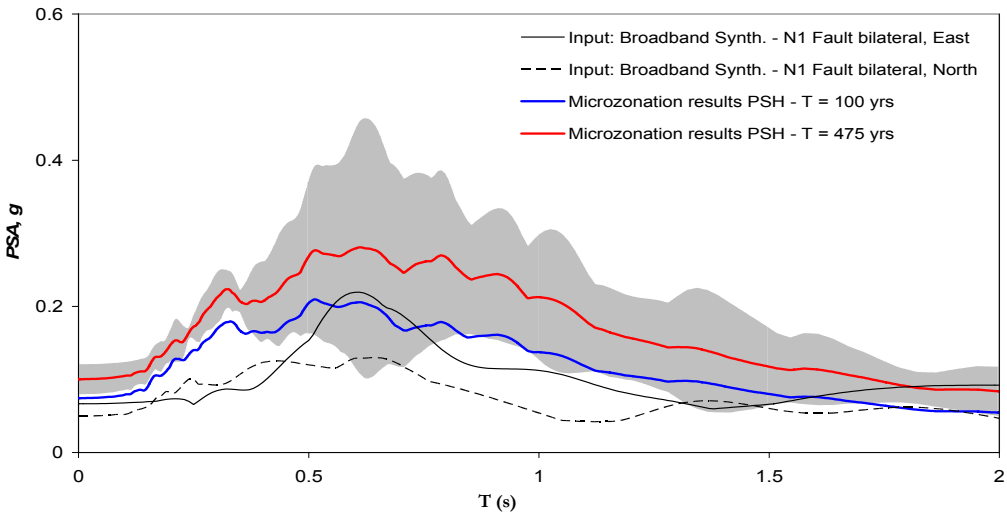

Figure 2.37: Results of 1D - EQL analyses at Site S10 in terms of PSA: spectra obtained using as excitation one deterministic bedrock scenario (Broadband synthetics, Thessaloniki-Gerakarou N1 fault – bilateral rapture) are compared with those derived from the microzonation study for T = 100 yrs (mean) and T = 475 yrs (mean ± 1 σ shaded band).

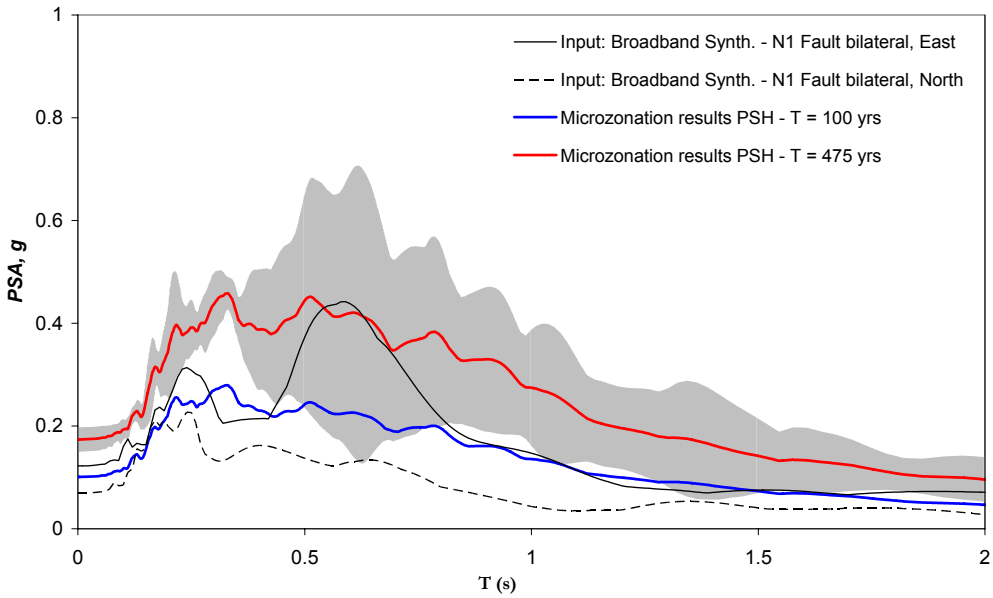

Figure 2.38: Results of 1D - EQL analyses at Site S11 in terms of PSA: the spectra obtained using as seismic excitation one deterministic bedrock scenario (Broadband synthetics, Thessaloniki-Gerakarou N1 fault – bilateral rapture) are compared with those derived from the microzonation study for T = 100 yrs (average) and T = 475 yrs (average ± 1 σ shaded area).

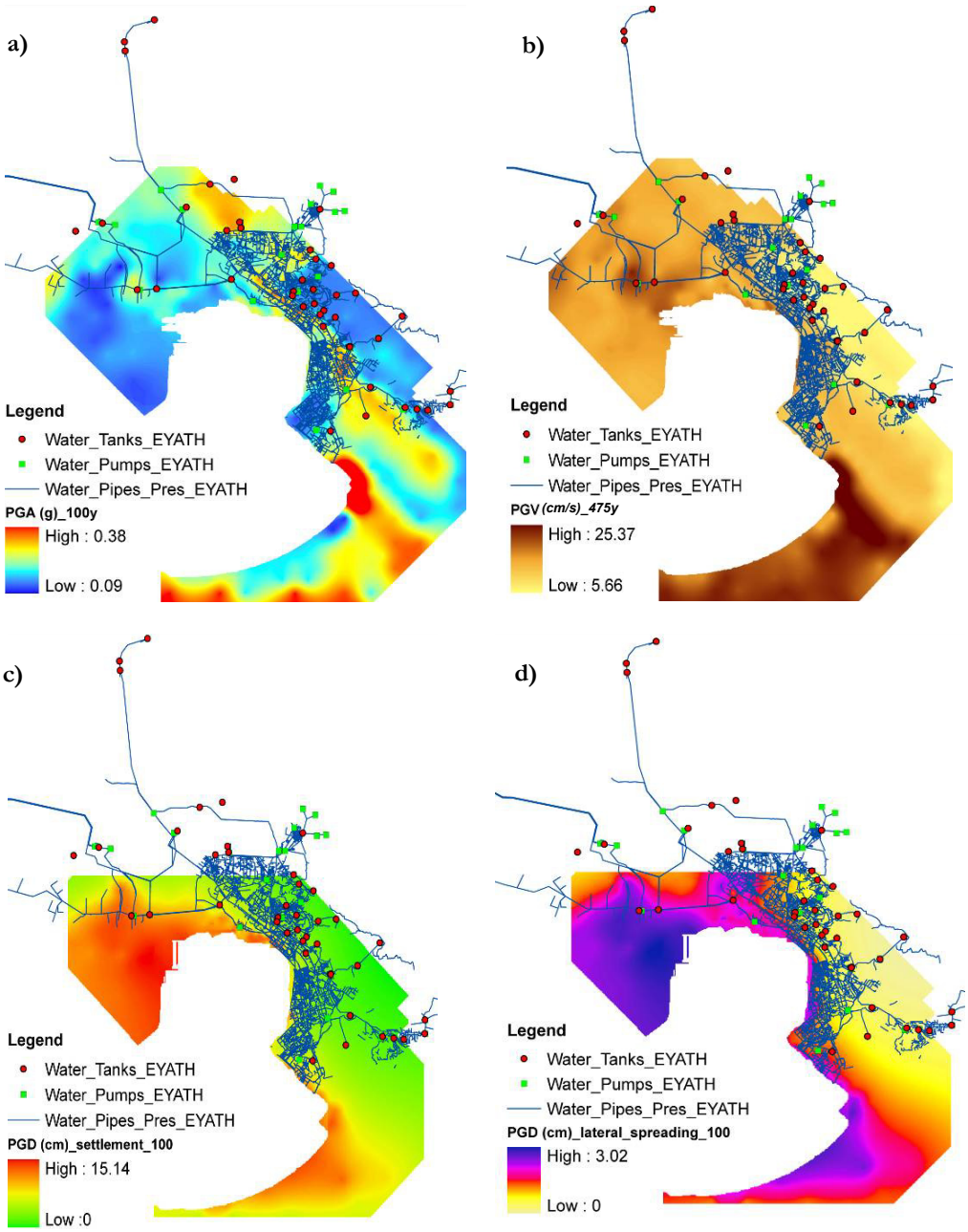

Figure 2.39: Spatial distribution of a) PGA (g), b) PGV (cm/s), c) PGD (m)- settlements and d) PGD (m)-lateral spreading from the microzonation in Thessaloniki (based on probabilistic input for 100 year return period)

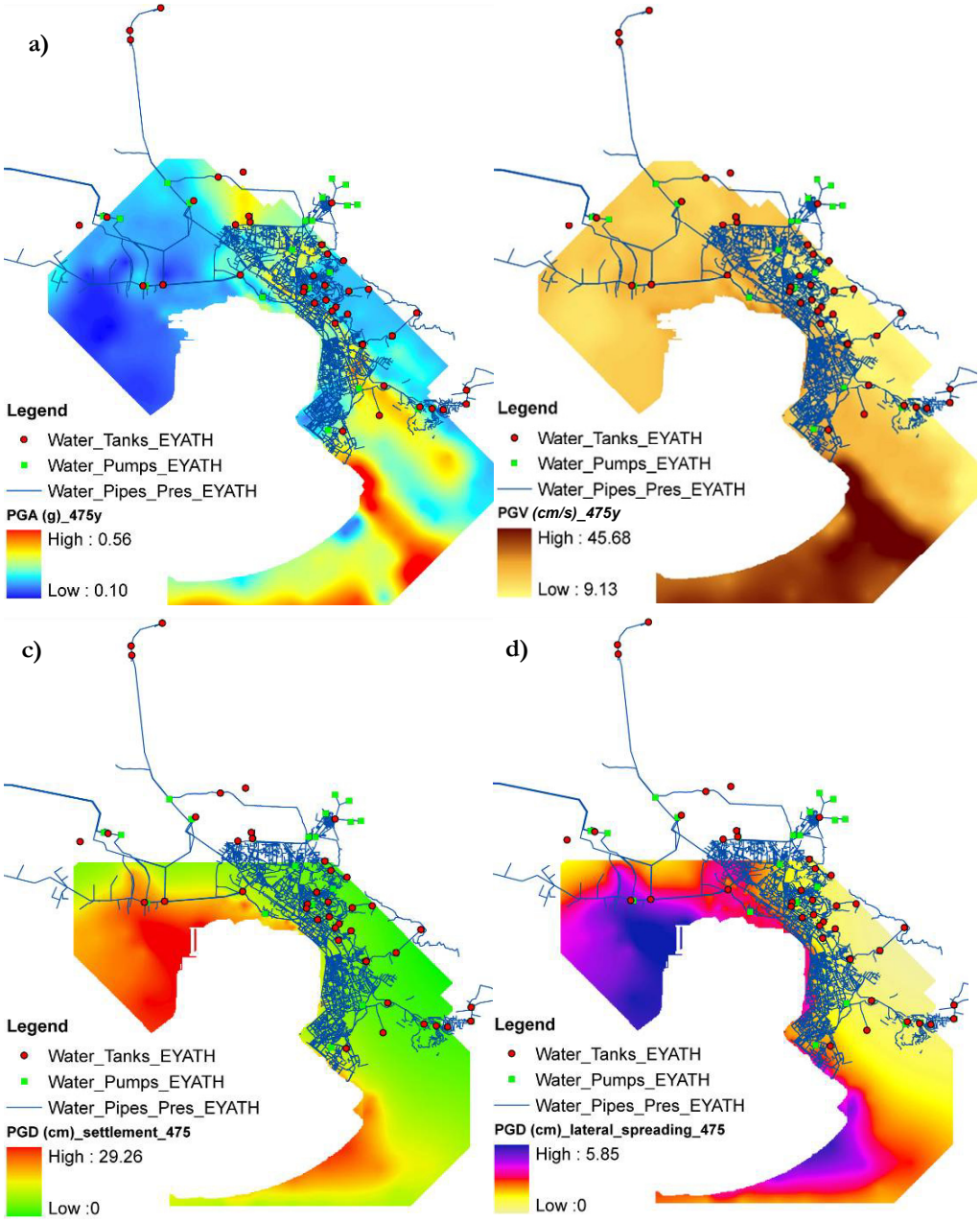

Figure 2.40: Spatial distribution of a) PGA (g), b) PGV (cm/sec), c) PGD (m)- settlements and d) PGD (m)-lateral spreading from the microzonation study in Thessaloniki (based on probabilistic input for 475 year return period)

2.2.1.4 *Soil response in selected areas: 2D analyses on representative cross-sections*

Two detailed geological and geotechnical cross-sections, representative of the Thessaloniki city, have been defined, denoted as K-K' and A-A' in Figure 2.41; locations of geotechnical and geophysical field tests (including cross-hole, down-hole, sampling borehole/SPT, soil mechanic and laboratory tests) on which the soil characterization is based are also shown.

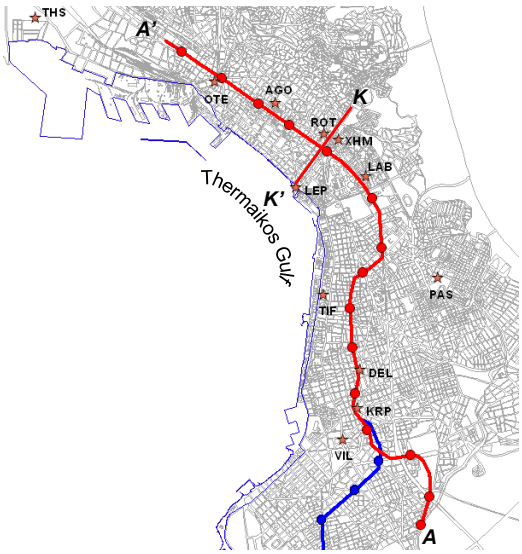

Figure 2.41: Location of the K-K' "White Tower- Evangelistria" and A-A' "Metro" cross-sections. The circles represent the metro station locations; the stars denote the location of tests where samples of the main soil formations were selected for the soil model characterization (from Anastasiadis, 2006).

The K-K' cross-section is also called "White Tower- Evangelistria" since the edge K' coincides with the White Tower monument on the water front, and the axis crosses the Evangelistria area to NE. The A-A' cross-section is named "Metro", since it follows the Metro line, whose main stations are shown in Figure 2.41.

The K-K' cross-section is the shortest one joining the coastline and the boundary between sediments and bedrock in the SSW-NNE direction. Its length is about 2 km and the depth of the bedrock-sediments interface varies from 0 to 180-200 m, while the shear wave velocity VS ranges from 200 m/s at the surface to 850 m/s in depth (Figure 2.42). The dynamic soil properties of the soil formations are listed in Table 2.12. The cross-section is characterized by a strong lateral discontinuity from low to higher velocity values between the centre and the NE end (K), a potentially unfavourable situation in terms of ground strain amplification and, as a consequence, in terms of underground lifeline damage.

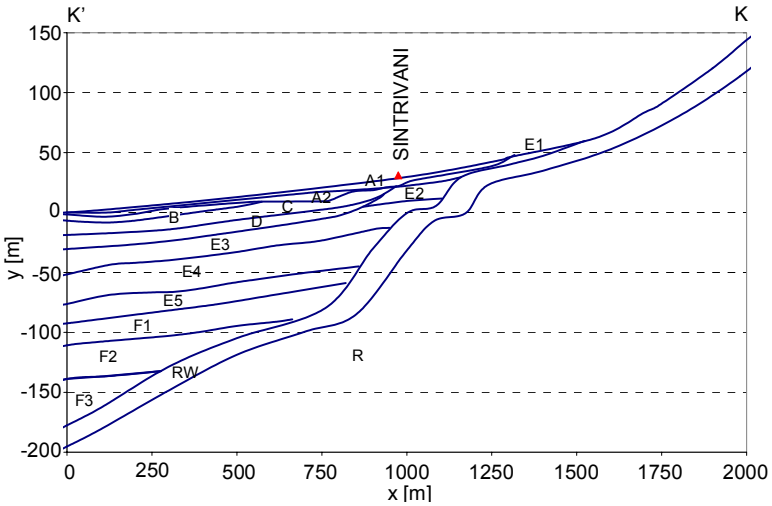

Figure 2.42: Soil layering in the K-K' "White Tower-Evagelistria" cross-section (K-K') in the centre of Thessaloniki, with the comarked nearby the Sintrivani metro station.

Table 2.12 - Geotechnical parameters which characterize ground materials in the K'-K "White Tower- Evangelistria" cross-section in the centre of the Thessaloniki city as shown in Figure 2.42 (from Anastasiadis, 2006)

Formation	*Vs* (m/s)	*Vp* (m/s)	ρ (KN/m3)	*Qs*
A	250	400	18.14	20
A1	250	1700	19.12	20
B	200	1800	17.65	25
C	350	1900	19.12	20
D	280	1800	1961	20
E1	350	1900	20.10	8
E2	400	1950	20.10	8
E3	500	2000	20.10	15
E4	600	2050	20.59	30
E5	700	2100	20.59	30
F1	750	3100	21.09	60
F2	800	3200	21.57	60
F3	850	3300	21.57	60
RW	1200	5000	24.52	120
R	2500	5000	24.52	200

The A-A' geological cross-section, shown in Figure 2.43, has been derived projecting the soil formations encountered along the metro line (Table 2.13) on a single plane, so as to obtain a single representative cross-section. The tunnel develops at 10÷15 m depth within an irregular soil structure, which results in complex site effects, and it extends for about 9 km of length.

2D Spectral Element analyses of wave propagation, as described in Section 2.1.1.3, have been performed on the previous cross-sections using vertically propagating shear waves as input motions. In particular the broad band (BB) synthetic signals evaluated at one rock site (S07 in Figure 2.18), rotated along the cross section directions, have been used (N24^o and N114^o for K-K' and A-A' cross sections, respectively). Since only the wave propagation effects have been studied, the accelograms were deprived of the static offset components by a high pass filter with a cut-off frequency at 0.08 Hz. The following Figures 2.44 and 2.45 show the ground response profiles obtained along the cross-sections.

The two cross-sections intersect in the proximity of the Sintrivani station, at x ≈ 950 m on the K'-K cross-section and x ≈ 3000 m on A'-A, as shown in Figures 2.42 and 2.43. Although the motions in different directions of propagation are simulated, the peak displacement, velocity and acceleration at the intersection zone are in agreement, as it may be seen by comparing Figure 2.44 (x= 3000 m) and Figure 2.45 (x= 1000 m).

It is interesting to compare the ground response at the metro tunnel depth with that evaluated at the average buried pipeline depth of 3 m from the surface (Figure 2.44). While horizontal displacements, velocities and strains are slightly de-amplified at the tunnel depth, shear strains, negligible in the proximity of the surface, are strongly amplified at depth reaching and exceeding the longitudinal deformations. As expected, in the proximity of the surface the response is amplified due to site effects, most of all in terms of PGA. While horizontal peak ground strains PGS_{xx} are highest between x = 4500 m and x =7500 m, due the basin-shaped soil profile configuration, shear strains PGS_{xy} exhibit a prominent peak, some 6 times or more higher than PGS_{xx} values, in correspondence of the strongest lateral discontinuity between the soft layers and the outcropping bedrock, at around x = 5000 m. These results highlight how shear strains may play a significant role at depth.

While shear strains are mostly of interest for seismic design of tunnels in a transversal cross-section, seismic design of pipelines is mainly governed by longitudinal strains. As shown in Figure 2.46 (lhs), at around 3 m depth, where most pipelines are embedded, the ratio between PGS_{xy} and PGS_{xx} ranges between about 1 and 4, with a mean value around 1.75. At larger depths, as shown in Figure 2.46 (rhs) for a representative depth of 15 m, this ratio is even higher, as expected for incidence of S waves. Although further studies are recommended to assess a general relationship between PGS_{xy} and PGS_{xx} as a function of depth, earthquake magnitude and site characteristics, the results shown in Figure 2.46 allow to estimate shear strains from longitudinal strains or viceversa, at least as a first approximation, at shallow depths (< 5 m).

To compare ground motion scenarios obtained with 2D and 1D equivalent analyses, illustrated in the previous paragraph (2.2.1.3), the 2D peak ground velocity values PGV along the metro line are highlighted in Figure 2.47.

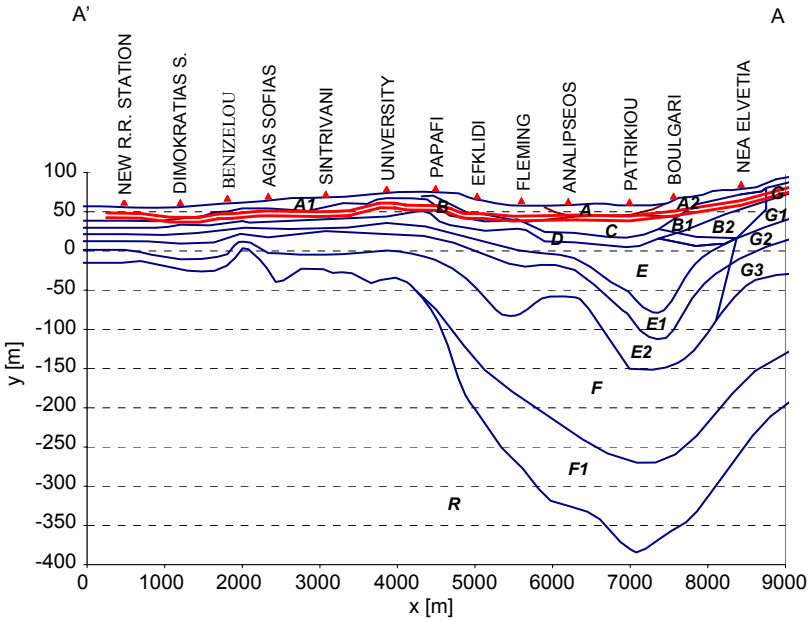

Figure 2.43: Soil structure of the A-A' "Metro" cross-section in the Thessaloniki urban area with the corresponding formations listed in Table 2.13. The buried metro line is highlighted (red lines), with the stations at the surface.

Table 2.13 - Geotechnical parameters which characterize the ground materials in the A-A' "Metro" cross-section in the centre of the Thessaloniki city (from Anastasiadis, 2006)

Formation	*Vs* (m/s)	*Vp* (m/s)	ρ (KN/m3)	*Qs*
A	225	400	1850	20
A1	300	600	1850	20
A2	300	1700	1850	20
B	280	1700	1850	30
B1	380	1800	1900	30
B2	475	1900	1950	40
C	350	1900	1950	20
D	400	1950	2050	10
D1	475	1950	2050	15
G	380	700	1900	40
G1	475	1900	1950	50
G2	550	2000	2050	60
G3	625	2000	2050	60
E	475	1950	2050	15
E1	550	2000	2050	15
E2	625	2050	2100	30
F	800	3200	2190	60
F1	1025	3600	2300	60
R	2200	4000	2400	200

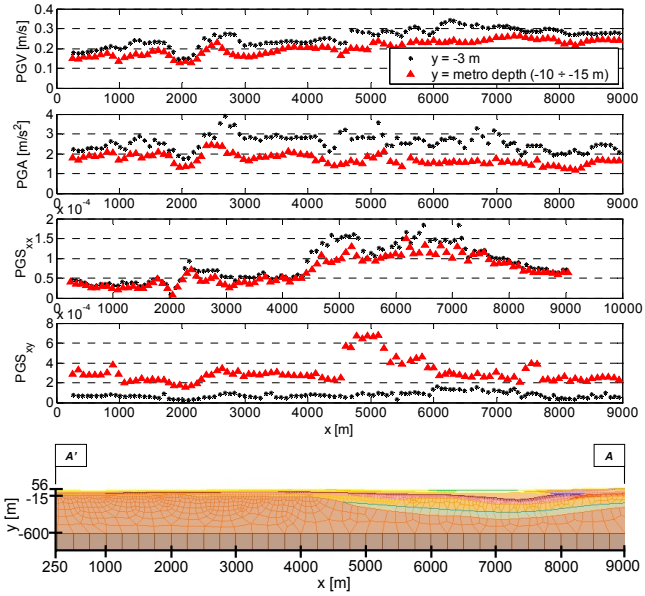

Figure 2.44: Seismic response profiles due to the Mw 6.5 scenario event (see par. 2.2.1.3) along the A-A' cross-sections at 3 m depth and at the metro line depth (10÷15 m). Peak horizontal ground velocity (PGV), acceleration (PGA), longitudinal strain (PGSxx) and peak shear ground strain (PGSxy) are shown.

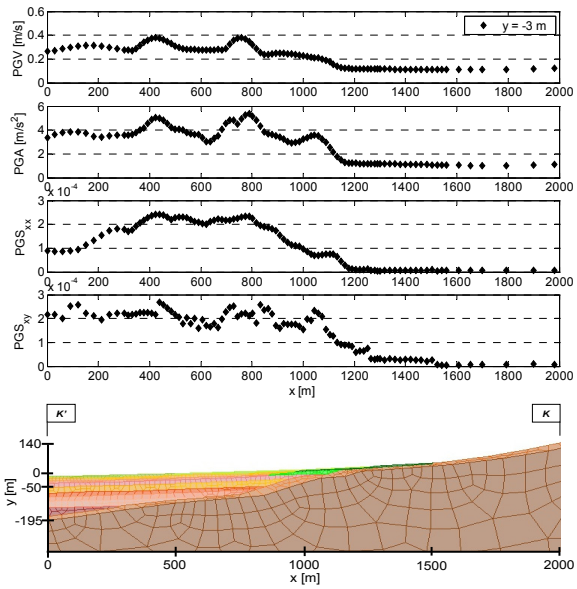

Figure 2.45: Seismic response profiles due to the Mw 6.5 scenario event (see par. 2.2.1.3) along the K'-K cross-section, at 3 m of depth. Peak horizontal ground velocity (PGV), acceleration (PGA), longitudinal strain strain (PGSxx) and peak shear ground strain (PGSxy).

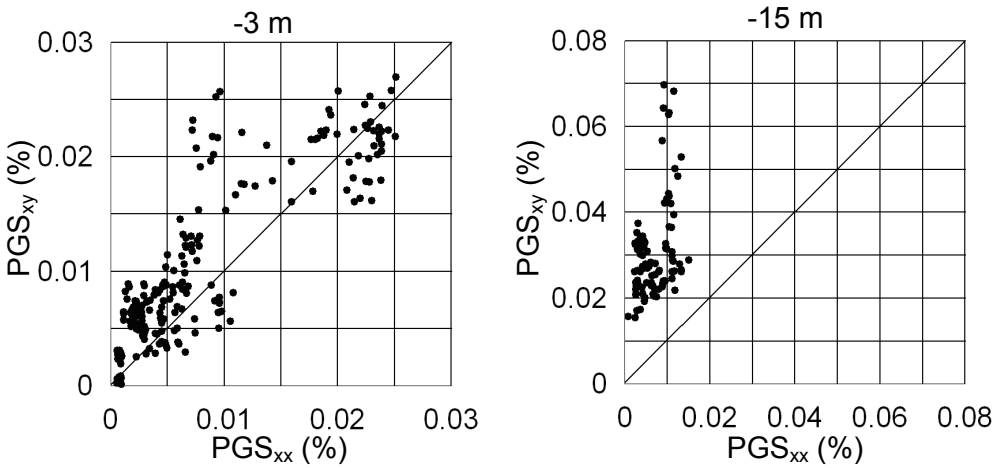

Figure 2.46: Peak values of shear strain vs. the corresponding longitudinal (horizontal) strain at 3 m (left) and 15 m (right) depth obtained by 2D numerical simulations of two geological cross-sections in Thessaloniki, subject to in-plane vertical incidence of S-waves. The Mw 6.5 scenario earthquake motion (see par. 2.2.1.3) was considered.

Comparison of 1D and 2D results

Since the input motion for the 2D ground response analyses (Par. 2.2.1.4) has been associated to an indicative return period of 500 years (Par. 2.2.1.3), the 2D seismic response in the proximity of the surface (3 m depth) can be compared with the surface 1D seismic scenario for 475 in terms of PGV. From Figure 2.47 and Figure 2.40b, relative to 2D and 1D analyses respectively, it can be pointed out that, while 1D results yield to a range of PGV values from 20 to 30 cm/s along the metro line, the 2D analyses allow to better highlight the critical areas where the largest seismic response is expected. The southern part of the line is subjected to a higher ground amplification (with PGV reaching 30-35 cm/s[2]) due to the strong lateral heterogeneity between the soft layers and the outcropping bedrock, at around x=5000 m, corresponding to the Efklidi metro station (see Figure 2.43). Obviously, 1D simulations neglect the effects of lateral variation of soil properties and the contribution of surface wave as well. The K'-K cross-section is also characterized by a strong lateral contrast, as shown in Figure 2.42. The higher amplification of soft soil on the sea cost is captured by the 1D analyses as shown in Figure 2.40b, but, as expected, the 2D simulations provide a more accurate evaluation of site effects.

[2] But it should be recalled that the input for the 2D analyses is less severe than that used for the 1D analyses.

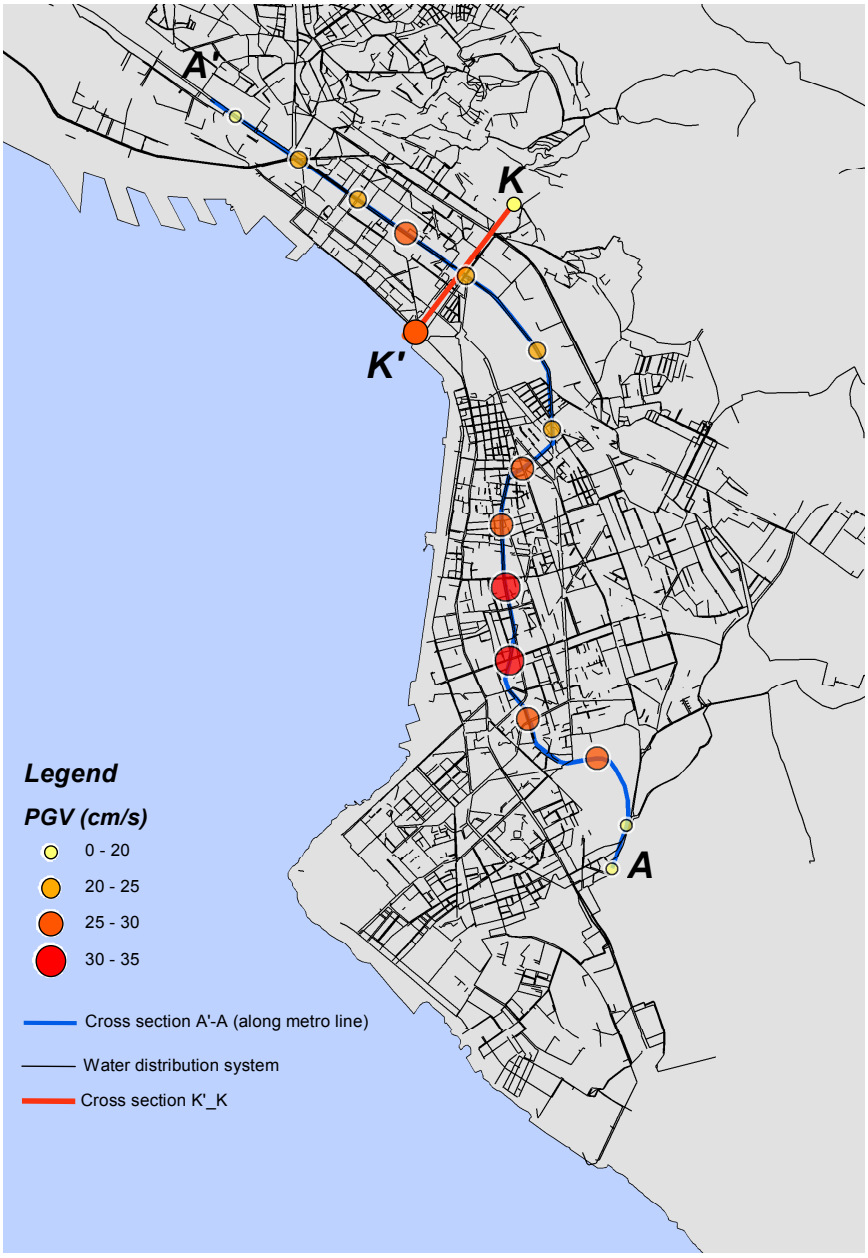

Figure 2.47: Peak ground velocity values obtained from the 2D numerical wave propagation analyses (see Figure 2.44) at different locations along the Metro line and along the K-K' cross-section at 3 m depth. The layout of the water distribution system is also shown.

2.2.2 Ground motion scenario for the Düzce, Turkey, urban area, by means of 2D ground response analysis

2.2.2.1 *Introduction*

The damage to the underground ISs caused in the city of Düzce (Turkey) by the destructive Mw 7.1 shock of November 12, 1999 provided an important case history to SP11 (see Deliverable D116). For this reason, some simulation studies carried out in 2D to obtain the ground displacements and the seismically induced ground strains in the Düzce urban area are illustrated here. In particular a North-South geological cross-section has been analysed by means of an approach that takes into account the simultaneous effects of the seismic source, the propagation path, complex geological site conditions and topographic amplification. To reduce the computational effort required by such a large scale numerical problem the Domain Reduction Method (DRM) described at the end of paragraph 2.1.1.3, has been applied.

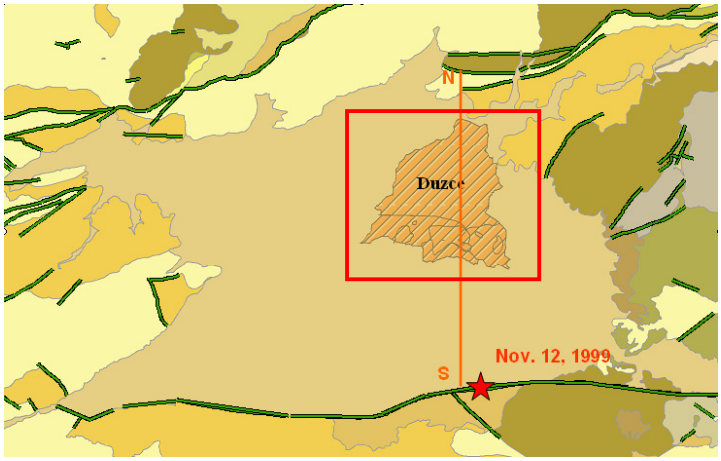

Figure 2.48: Düzce basin with the Düzce city. The solid line represents the location of the analysed NS cross-section and the star the epicentre of the November 12, 1999 earthquake (The red squared area is zoomed in detail in Figure 2.50)

Moreover, the shaking scenario has been evaluated not only for ground displacement but also for strains, as in the Thessaloniki case. Due to the nature of the numerical models adopted, involving 2D in plane wave propagation, attention was focused on the longitudinal ground strains, which are the largest component close to the surface. In particular, peak ground strains at shallow depth have been related to peak ground velocity, in order to check the available relations used in the engineering practice, see par. 2.1.1.3, as well as the simplified formula illustrated in par. 2.1.2.2.

2.2.2.2 *Method adopted*

The Domain Reduction Method has been applied to study the seismic response of the Düzce basin during the November, 1999 earthquake.Recall that the main feature of DRM is the ability to couple solutions typically obtained by different methods in two different domains. Figure 2.49 shows the adopted scheme.

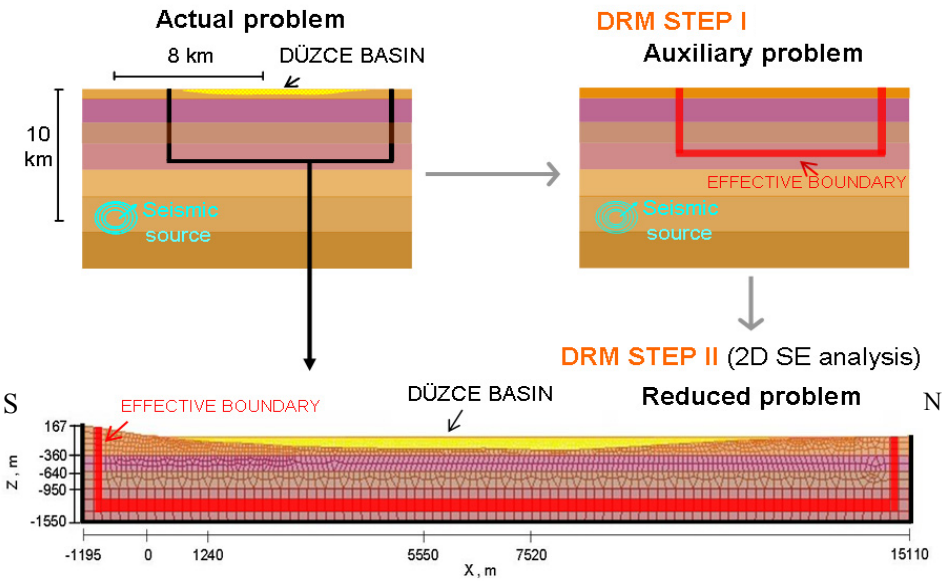

Figure 2.49: Outline of the DRM approach applied to the case of the Düzce urban area. The real problem is subdivided into two simpler ones analysed in different steps. Step I: 3D analysis of the source and the wave propagation in a layered half-space using the semi-analytical method of Hisada. Step II: 2D wave propagation in the Düzce basin by means of the Spectral Element Method.

The original problem is subdivided into two simpler ones solved in two successive steps: i) an auxiliary problem (Step I) from which the Düzce basin has been removed and replaced by the same material as the surrounding domain; ii) a reduced model (Step II) which contains the Düzce basin, the geological feature of interest, but not the causative fault. The excitation applied to the reduced model is a set of equivalent localized forces derived from the first step. These forces are equivalent to and replace the original seismic forces applied in the first step to reproduce the seismic source. In Figure 2.49 (bottom) the red stripes of elements represents the "effective" boundary where the free field displacements are evaluated in the first step and the equivalent forces are applied in the second step.

2.2.2.3 *DRM: Step I*

Here, a 3D analysis of the source and the wave propagation in a horizontally layered Earth crust profile has been carried out using the semi-analytical method of [Hisada and Bielak, 2003]. This relies on the computation of displacements and stress of static and dynamic Green's functions for viscoelastic horizontally layered half spaces. It uses an analytic form for the asymptotic solutions of the integrands of Green's functions, stemming from the generalized R/T (reflection and transmission) coefficient method and the stress discontinuity representations for boundary and source conditions respectively.

Source model of the November 12, 1999 earthquake

Several studies have been performed to reproduce the rupture process of the November, 1999 Düzce earthquake [Yagi and Kikuchi, 2000, Bürgmann et al, 2002, Birgören et al., 2004]. In this study an extended seismic source with the hypocenter located at 10 km of depth and a slip time-dependence given by a smoothed ramp function, as proposed by Yagi and Kikuchi (2000), has been adopted. The source parameters are listed in Table 2.14.

Table 2.14 Source parameters of the rupture model for the November 12, 1999 earthquake

Source coord.	Depth	M_o	M_w	Δu_m	W	L	v_R	Rise time	Strike	Dip	Rake
(°)	(km)	(Nm)	-	(m)	(km)	(km)	(km/s)	(s)	(°)	(°)	(°)
40.77°N 31.20°E	10.00	4.9×10^{19}	7.1	5.60	16.50	16.50	2.80	2.80	265	65	-168

Available information to construct a numerical model of the Düzce basin

To construct the numerical model for the simulation of seismic response of Düzce basin, the following information was considered:

a) Geological and geomorphological maps, paleotopography map (before the Quaternary) and N_{SPT} values (see Table 2.15) from shallow boreholes (see Figure 2.50) provided by KOERI, together with several soil profiles from deep borings provided by AUTH [Pitiliakis et al., 2005]

b) The velocity profile by [Kudo et al., 2002], based on array observations of microtremors at Düzce city, 1 km E from the strong-motion observation site. The SPAC method was used to determine the phase velocity of Rayleigh waves

from which the shear wave velocity profile was obtained by an inversion procedure. Since this is only an indirect measure of the V_S profile, the previous information based on cross-hole surveys was preferred. Note also that Kudo's profile stops at nearly 1 km depth where a relatively low shear wave velocity of 1500 m/s is proposed.

c) A standard rock model proposed by [Boore and Joyner, 1997] successfully used [Faccioli at al., 2002] to reproduce the seismic response recorded at Düzce and neighbouring cites during the November 1999 earthquake.

The Düzce municipality lies on an almost flat area, which can be seen as a tectonically generated basin (Düzce basin), characterized by the presence of quaternary geological units. The basin area, surrounded by mountain relief made of older rock materials, is mainly constituted by the following geological units:
- Qal3 (silty clay), originated by lake deposits,
- Qal2 (sands and gravel), having an alluvial origin,

Unit Qal3 deposits are coeval or more recent than the unit Qal2. The depth of the Qal3 deposit has been obtained from the N_{SPT} values measured in shallow boreholes (see Table 2.15 and Figure 2.50). The thickness of the Qal2 deposits with respect to the outcropping bedrock, together with the identification of river deposits and Holocene alluvial fans (located as expected along rivers and not represented in the cross-section), has been obtained from the paleo-topographical map.
Regarding the geomorphology aspects, a strike-slip fault can be recognized on the mountainous area located along the edge of the basin. Other fault systems located within the plane have been interpreted as vertical, but it is not clear from the scarce data available if they reach the bedrock located below the quaternary units, or not.
From the previous data, a SN geological cross-section along the alignment of Figure 2.50 has been obtained, as shown in Figure 2.51, and adopted as a basis for the numerical analyses illustrated in the following paragraphs.

To highlight the problems arising from the merging of the information at points b) and c) listed earlier, the Boore and Joyner rock velocity profile is superimposed to the Kudo profile in Figure 2.52. For the latter case we regularly increased V_S to reach realistic values at about 3 km depth. The shallow layers adopted for the local response of the Düzce basin are not considered. The problems in adopting the Kudo model are apparent, since it provides a relatively high and perhaps unrealistic velocity gradient that deeply affects the ground response at surface. To point out this effect, we show in Figure 2.53 and Figure 2.54 the comparison of strong ground motion recorded at two stiff soil sites, namely Karadere and Bolu, and the simulated response. The location of these accelerograph sites is reported in [Faccioli et al., 2002]. The numerical results have been obtained using the Hisada method, i.e., the first step of the DRM where the Düzce basin

is excluded. It is clear that using the Kudo model leads to an overestimation of observed ground response, so that in the following we preferred to consider the Boore and Joyner profile at least for the definition of the crustal profile (see Table 2.16 for a detailed list of the adopted dynamic properties). For the detailed model of the Düzce basin considered in the second step, reference will be made to the deep boring profiles.

Note that a detailed simulation of the seismic response at Düzce is not the object of main interest here, but rather the identification of the most critical zones in the basin in terms of peak ground velocities and strains; therefore the agreement achieved in this first step can be considered satisfactory.

Table 2.15: N_{SPT} values obtained from the soil studies (shallow boreholes) performed near the selected NS alignment (see Figure 2.50).

	Boreholes ID along the S-N alignment									
Depth,m	94	93	92	97	95	96	24	33	176	174
2	16	7	32	8	14	7	8	10	18	7
4	34	8	26	8	13	6	2	14	24	12
6	9	11	9	9	9	45	4	6	22	14
8	7	14	11	21	9	41	9	6	28	34
10	17	21	69	47	18	41	7	17	76	31
12	0	0	76	42	0	31	0	0	0	0
14	0	0	62	34	0	36	0	0	0	0
16	0	0	24	47	0	41	0	0	0	0
18	0	0	28	0	0	0	0	0	0	0
20	0	0	13	0	0	0	0	0	0	0

	Boreholes ID along the S-N alignment										
Depth,m	177	175	178	141	139	140	117	138	116	118	119
2	18	18	24	8	32	13	37	18	43	4	27
4	15	14	23	26	61	43	70	19	39	31	0
6	13	14	59	34	73	47	75	34	34	36	0
8	20	17	32	46	46	0	39	55	24	33	63
10	30	32	73	64	73	80	37	59	52	0	49
12	0	0	0	0	0	0	37	0	0	0	0
14	0	0	0	0	0	0	53	0	0	0	0
16	0	0	0	0	0	0	48	0	0	0	0
18	0	0	0	0	0	0	0	0	0	0	0
20	0	0	0	0	0	0	0	0	0	0	0

Nspt < 15 bw/ft ***15 < Nspt < 55 bw/ft*** ***Nspt > 55 bw/ft***

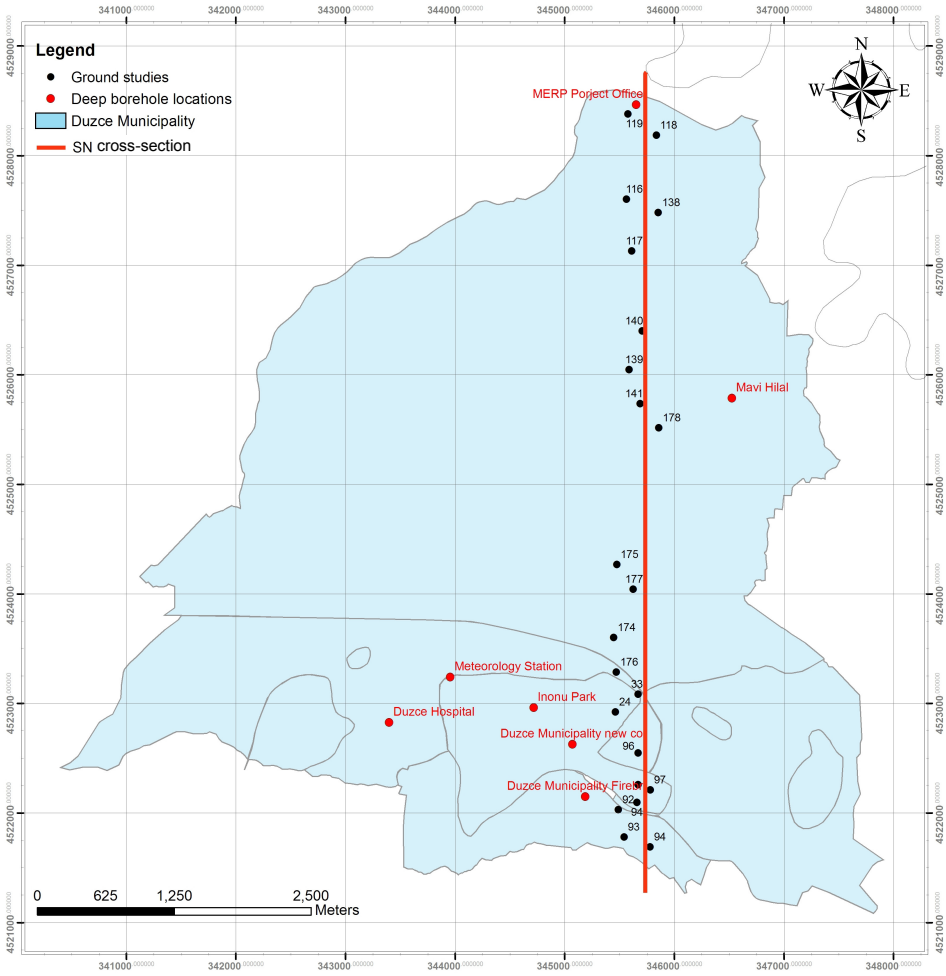

Figure 2.50: **Location of selected deep and shallow boreholes performed within the Düzce Municipality, adopted for the NS cross-section tracing.**

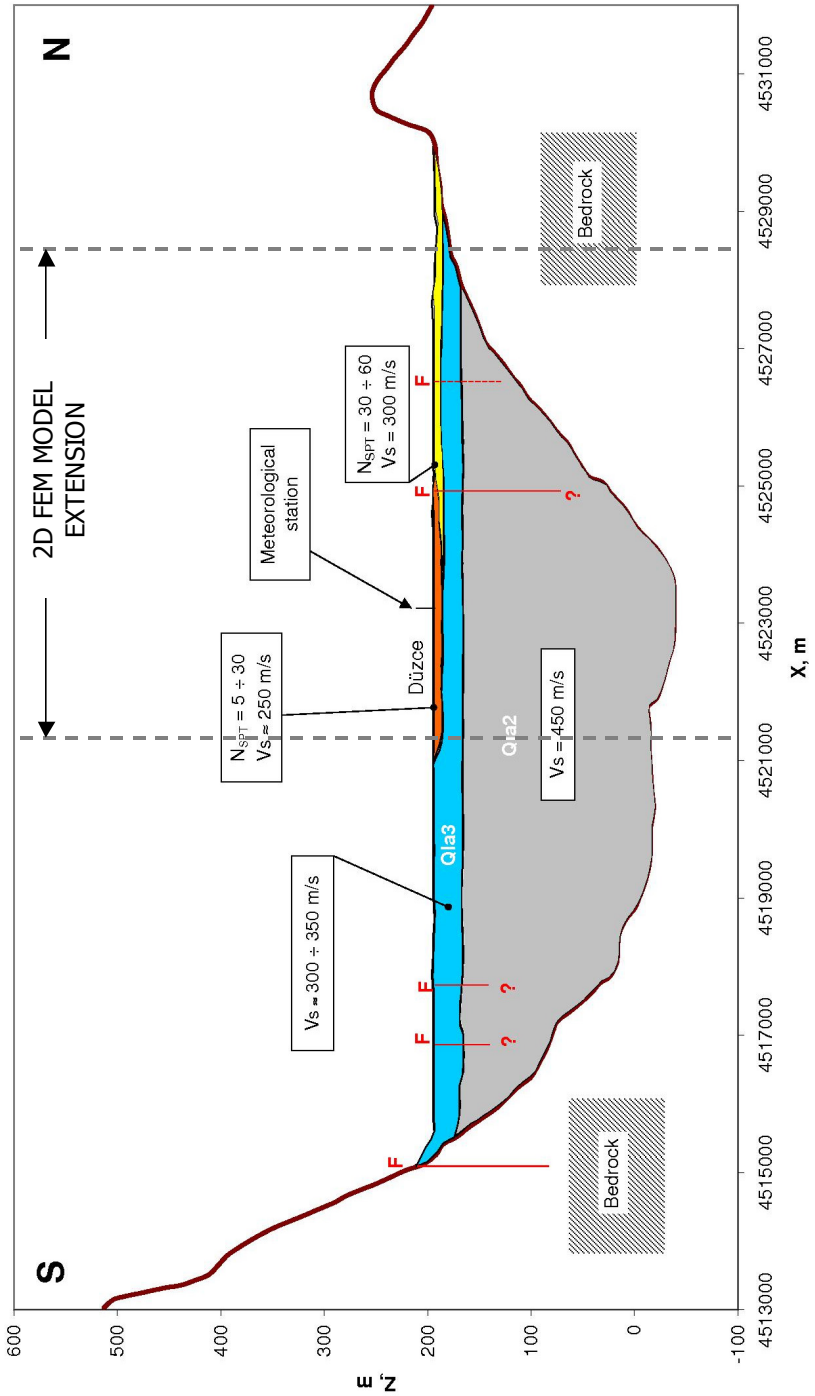

Figure 2.51: Düzce basin. NS cross-section obtained from paleotopography, geology and geotechnical investigations (data provided by KOERI and AUTH)

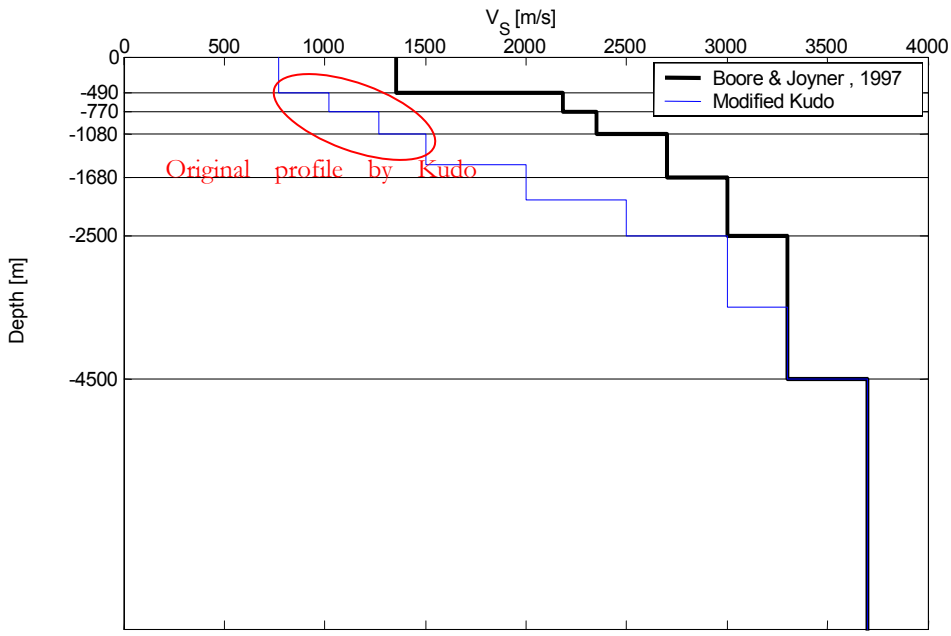

Figure 2.52: V_S profile proposed for the first step analysis: modified Kudo (thin line), Boore and Joyner, 1997. Both profiles adopt average values for the uppermost 490 m.

Table 2.16. Dynamic soil properties of the adopted crustal model based on Boore & Joyner, 1997

Layer No	ρ (t/m³)	V_P (m/s)	V_S (m/s)	Q_P	Q_S	Depth (m)	Thickness (m)
1	2.20	2300	1350	200	100	from 0 to 490	490
2	2.25	3750	2180	250	150	from 490 to 770	280
3	2.30	4000	2350	350	200	from 770 to 1080	310
4	2.30	4600	2700	350	200	from 1080 to 1680	600
5	2.40	5050	3000	350	200	from 1680 to 2500	820
6	2.50	5500	3300	500	300	from 2500 to 4500	2000
7	2.70	6300	3700	800	500	from 4500 to ∞	-

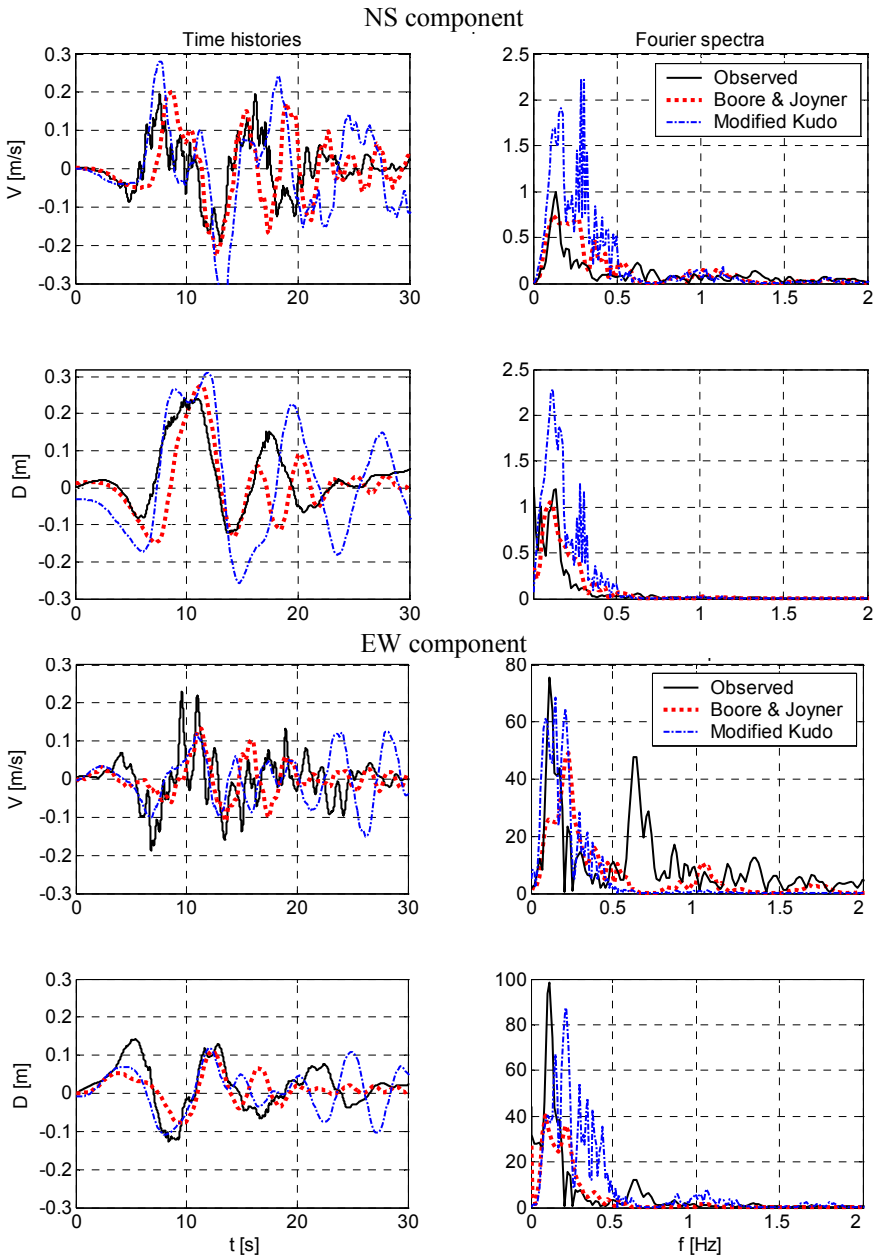

Figure 2.53: Comparison of NS (top 2 graphs) and EW (bottom 2 graphs) components of observed and simulated ground velocities and displacements time histories (left) and Fourier spectra (right) at Karadere accelerographs stations.

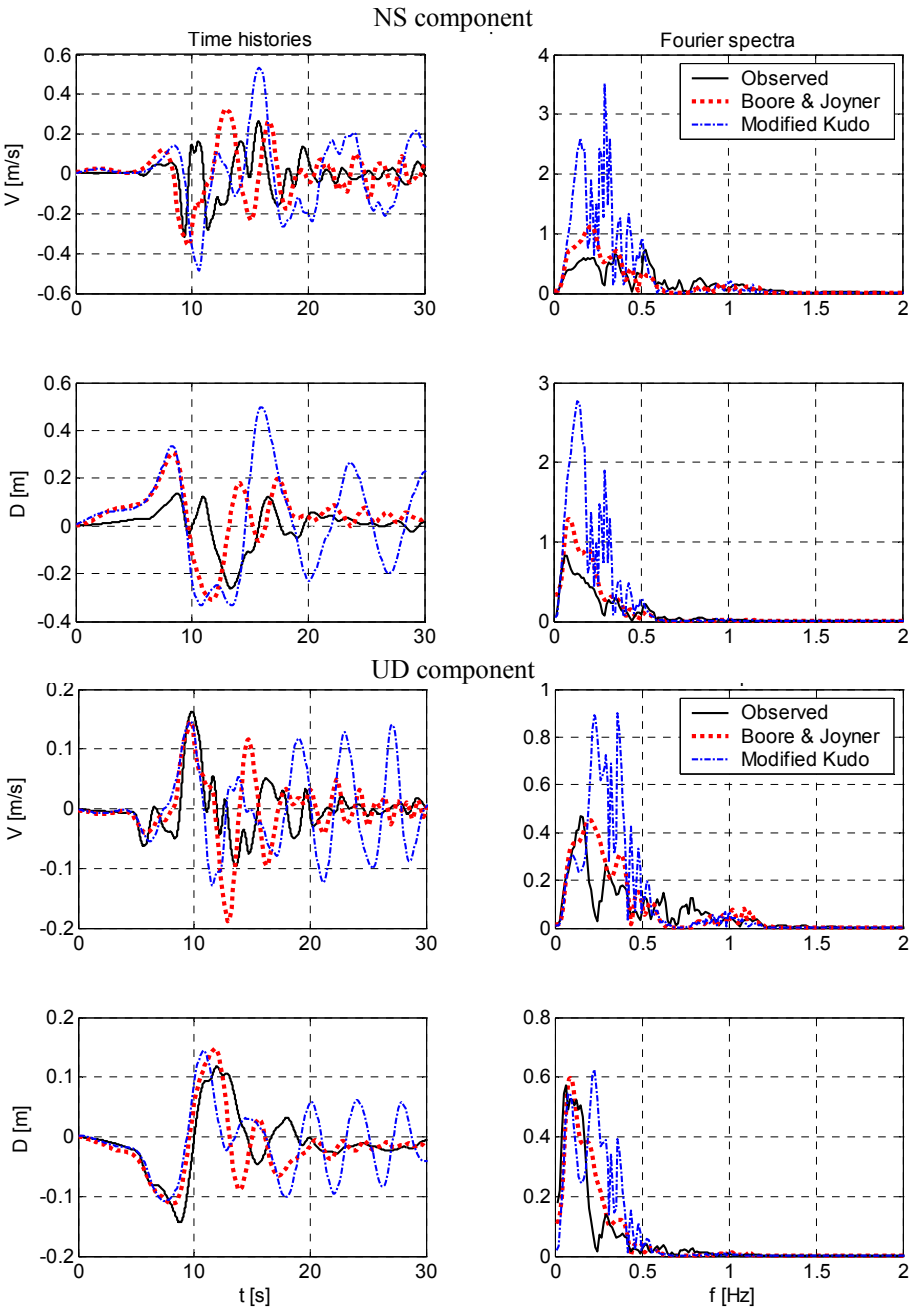

Figure 2.54: Comparison of NS (top 2 graphs) and UD (bottom 2 graphs) components of observed and simulated ground velocities and displacements time histories (left) and Fourier spectra (right) at Bolu accelerographs stations.

2.2.2.4 *DRM: Step II*

In the second step the Spectral Element Method, implemented in the GEO-ELSE numerical code (see LessLoss Deliverable 83) has been used to simulate the 2D ground response in the Düzce basin.
Since the reduced problem is 2D, the effective forces that exactly reproduce at the boundary the wave propagating from the seismic source have been evaluated taking into account only the vertical and horizontal displacements in the SN cross-section plane, shown in Figure 2.51. The cross-section has been discretised by Spectral Elements so as to propagate frequencies up to 5 Hz.
The materials are assumed linear visco-elastic. Internal soil dissipation has been introduced by a frequency dependent quality factor of the form

$$Q = \frac{q_o f}{f_o} \tag{3.1}$$

where q_o is the quality factor at frequency f_o; in the following we will consider $f_o = 0.5\,Hz$, while q_0 is chosen so as to obtain the Q values specified for the different materials.

Soil model

The S-wave profile adopted for the reduced model, referring to the Düzce accelerograph station (Metereological station) location (5500 m from the S end on the NS cross-section in Figure 2.51), is shown in Figure 2.55. The profile in the uppermost 500 m has been refined with respect to the previous numerical simulation based on the Hisada method, including the soft layers of the basin. The adopted dynamic soil properties are listed in Table 2.17. In the numerical model a thin surface layer, about 5 m thick with V_S=250 m/s has been omitted, because its introduction would have required an excessive reduction of the minimum grid size, with a corresponding reduction of the time step and a consequent increase of the computational time. Moreover, this layer would have influenced only the high frequency range of minor relevance for this study.

Comparison of simulated results with available observed data in Düzce

The final results of the two-step simulation procedure have been compared with the instrumental observations at the Düzce accelerograph station (Meteorogical station). Velocity and displacement waveforms obtained from single and double integration of recorded accelerations (Figure 2.56 and Figure 2.57) show that the soft basin slightly influences the response in terms of displacement amplitudes, introducing an amplification that tends to exceed the observed values especially at 0.5 Hz in the NS component. Probably a more regular increase of V_S with depth would decrease such a sharp peak.

In spite of these discrepancies, the overall agreement with the observed response can be considered as satisfactory, at least for the purpose of this study.
Note that the peak at 0.5 Hz can be clearly seen in the 1D soil amplification function of the site (Figure 2.58).
Although the seismic response of the flat Düzce basin is dominated by 1D amplification, it will be shown in the following section that the near field response coupled with the Southern edge of the basin induces surface waves that have some relevant consequences on the earthquake induced ground strains.

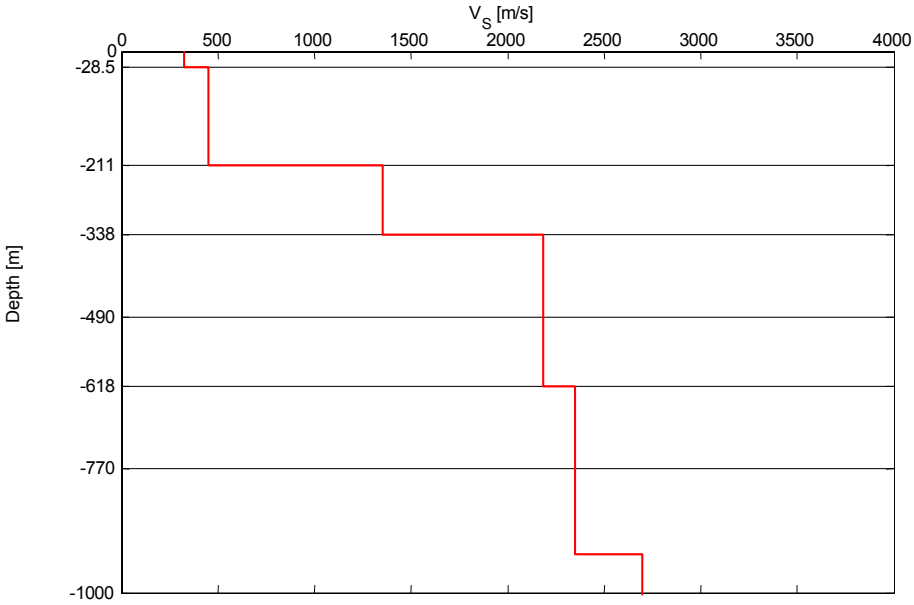

Figure 2.55: V_S profile adopted for the reduced model at the Düzce accelerograph station

Table 2.17. Dynamic soil properties for the reduced 2D model (see Figure 2.55). Layers listed from top to bottom.

Layer No	ρ (t/m³)	V_P (m/s)	V_S (m/s)	Q_S	Depth (m)	Thickness (m)
1	1.80	796	325	30	from -21.8 to -50.4	28
2	2.00	937.	450	50	from -50.4 to -233	183
3	2.20	2300	1350	100	from -233 to -360	126.5
4	2.25	3750	2180	150	from -360 to -640	280
5	2.30	4000	2350	200	from -640 to -950	310
6	2.30	4600	2700	200	from -950 to ∞	-

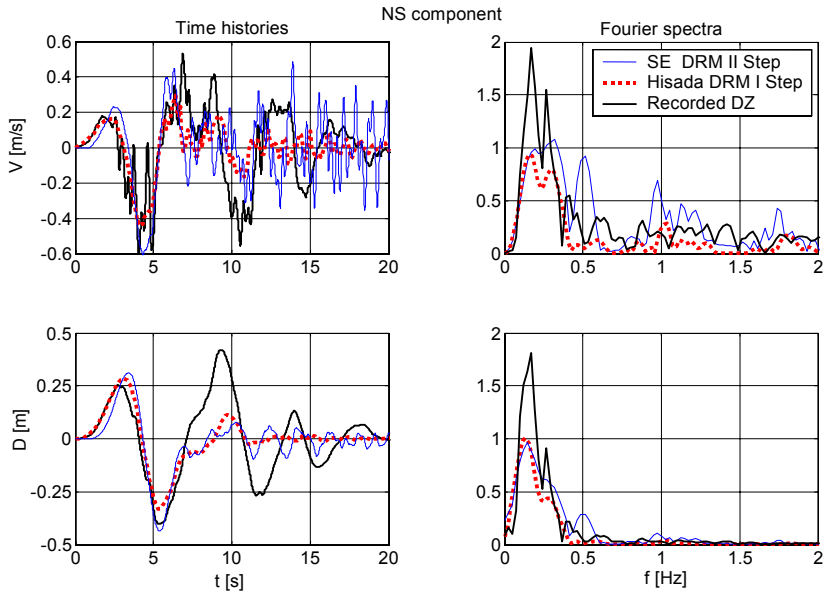

Figure 2.56: Comparison of NS component of observed and simulated displacements and velocities time histories (left) and Fourier spectra (right) at the Düzce accelerograph station site

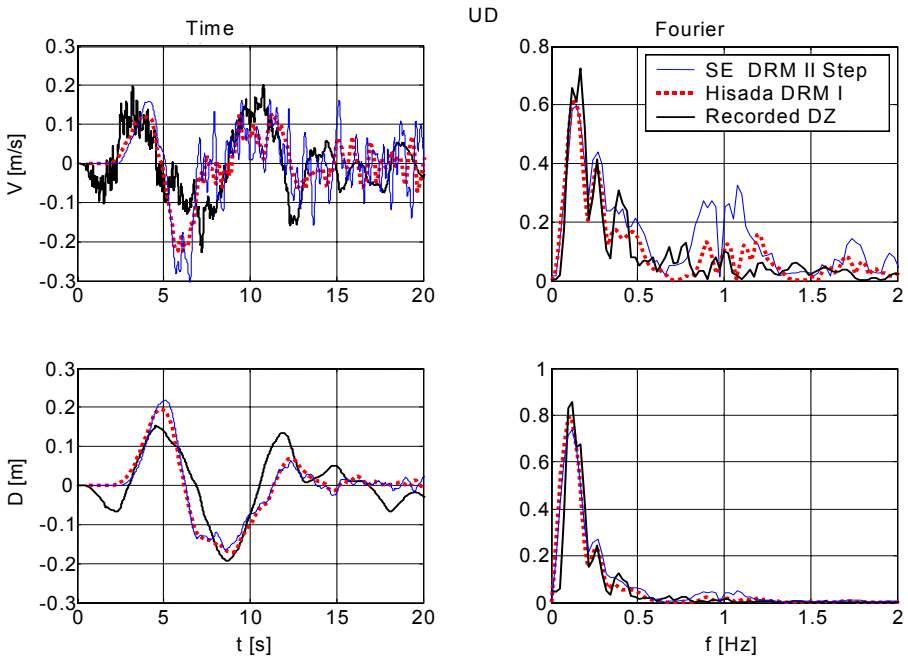

Figure 2.57: Comparison of UD component of observed and simulated displacements and velocities time histories (left) and Fourier spectra (right) at the Düzce accelerograph station site

Surface ground response

The NS cross-section is characterized by a distinct horizontal transition from low to higher velocity values at the basin borders, especially at the Southern side. It is interesting to analyse the spatial variation of peak ground displacement, velocities, accelerations (Figure 2.59) and strains (longitudinal PGS_{xx}, vertical PGS_{yy} and shear PGS_{xy} in Figure 2.60) at the surface and at 3 m depth, at which pipelines are commonly buried. Note that the origin of the x-axis in these figures denotes the Southern basin edge, and the prevailing wave propagation direction is S to N, in agreement with the location of the earthquake epicentre with respect to Düzce. While there is a smooth variation with horizontal distance of peak displacement and velocity, both PGA and PGS are strongly influenced by the lateral discontinuities, which imply a significant increase of values between around 1 km and 3 km from the South edge. The town of Düzce lies between around x = 4500 m and x = 11500 m at the surface of the numerical model.

The variation of PGV with depth, in the proximity of the surface, as well that of longitudinal peak ground strains PGS_{xx}, is not relevant; on the contrary, shear strains PGSxy are negligible near the surface, but they increase rapidly with depth, and should therefore be taken into consideration.

Since the soil dissipation has been introduced by a linearly frequency dependent quality factor Q, function of a q_o fixed at the frequency f_o =0.5 Hz (see equation (3.10), the calculated acceleration time histories are realistic up to a frequency of the order of 2 Hz. Beyond this threshold the values are not correctly damped.. Furthermore, non linearities and liquefaction effects, which contribute to decrease soil response, are not taken into account; for these reasons, acceleration time histories have been filtered by a low pass filter with a cut-off of 2 Hz.

In Figure 2.61 the variation of PGS_{xx} and PGS_{xy} with depth is plotted. As expected, there is a relatively smooth decrease of the horizontal component, while the shear strain attains its maximum between 80 and 200 m depth. The peak PGS is around $6 \div 8 \times 10^{-4}$, so that the influence of non linearity in ground response, not considered in our approach, should be significant.

Focussing on ground response in the horizontal direction, it is interesting to evaluate how peak ground strains are related to peak ground velocities and check the performance of simple formulas, useful in engineering practice. As shown by eq. (3.1), simple solutions for ground strain evaluation relate the peak horizontal strain to the peak horizontal particle velocity PGV by the relationship:

$$PGS = \frac{PGV}{C}, \tag{3.2}$$

where C denotes either the apparent propagation velocity of S-waves in the horizontal direction (V_{Sapp}) or the prevailing phase velocity of Rayleigh waves (V_R).
In Figure 2.62 V_{Sapp} and V_R have been visually evaluated on the basis of the displacement time section, by connecting the peaks of the most relevant phases. Note that we are only interested in rough estimates of the apparent velocities and that a precise evaluation is out of the scope of this work.

Since the propagation velocity contrast between the basin and the underlying bedrock is sharp, S-waves propagate nearly vertically in the basin, yielding a very high value of the apparent velocity C (see equation (3.2)), the use of which would lead to strongly underestimating PGS.

For the purpose of highlighting the possible limitations of use of equation (3.2), it is interesting to compare in Figure 2.62 and Figure 2.63 the waveforms of displacement and longitudinal strain respectively, evaluated along equally spaced receivers at ground surface.

It is evident that the nearly in phase S-arrivals do not give rise to any significant ground strain, while the highest values of strain are associated to the later Rayleigh wave arrivals. This is further confirmed by Figure 2.64 that compares at several selected receivers time histories of horizontal velocity and horizontal strain: there is an evident lack of correlation between the phases that carry the peak values of velocity, associated to S-waves, and those carrying the highest values of strain, associated to surface waves. This proves that the use of equation (3.2) coupled with (3.1) stemming from 1D wave propagation assumptions in a homogeneous soil, should be probably discarded in the presence of strong lateral soil irregularities that may give rise to horizontally propagating waves.

In this case, an alternative approach to ground strain evaluation is equation (3.5); the geometrical meaning of the geometrical parameters L and $\hat{H}=L\tan\alpha$ is illustrated in Figure 2.64.

Note that equation (3.5) has the advantage of not introducing an apparent wave propagation velocity, the evaluation of which is one of the main problems for application of equation (3.1).

To apply (3.7) to the present case, we have considered an average shear velocity for the uppermost 30 m, $\beta = 325$ m/s, an average dip angle of the bedrock $\alpha = 4^o$, $L = 2000$ m and $r = 0.89$. The latter parameter has been evaluated using an impedance contrast of 0.12 between the basin surface layer and the rock layers outside the basin.

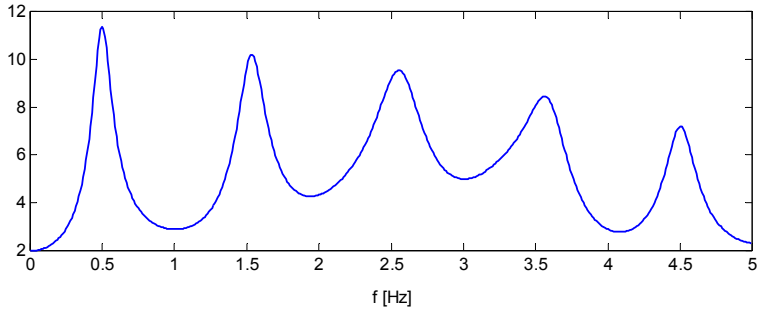

Figure 2.58: 1D soil amplification function at Düzce station (x=5550 m referring to Figure 2.51)

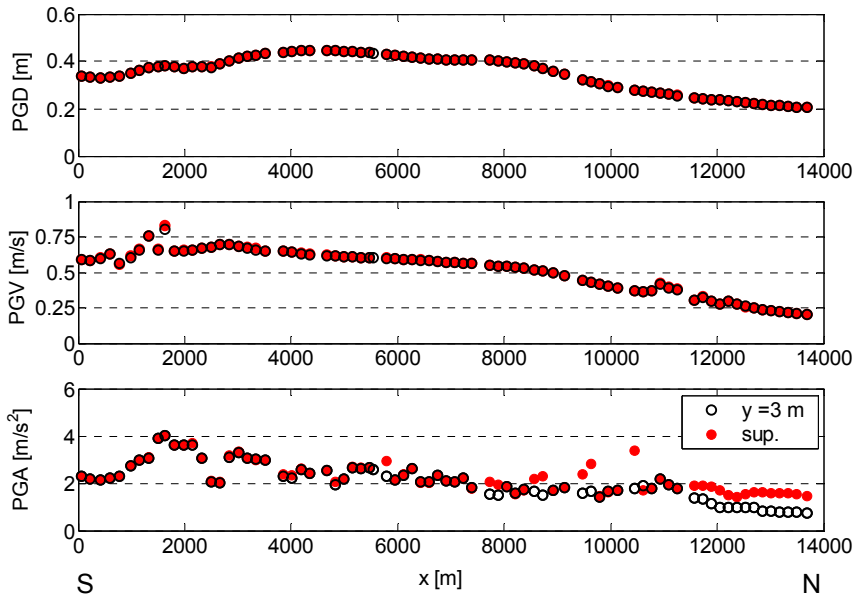

Figure 2.59: Spatial variation of peak ground displacement (PGD), velocity (PGV) and acceleration (PGA) along the NS cross-section at the surface and at 3 m depth.

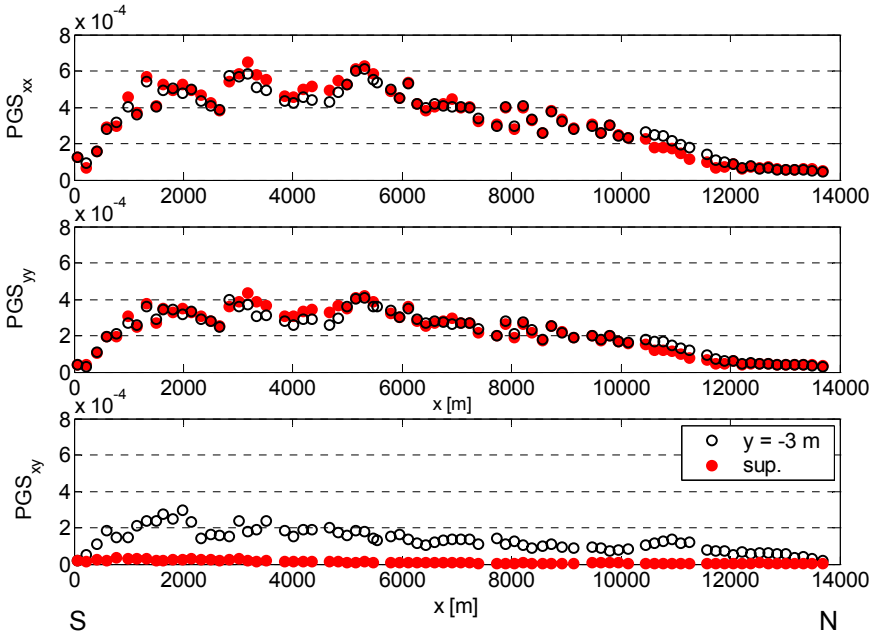

Figure 2.60: Spatial variation of peak ground strains in the horizontal (PGS_{xx}) and vertical (PGS_{yy}) directions along the NS cross-section at the surface and at 3 m depth.

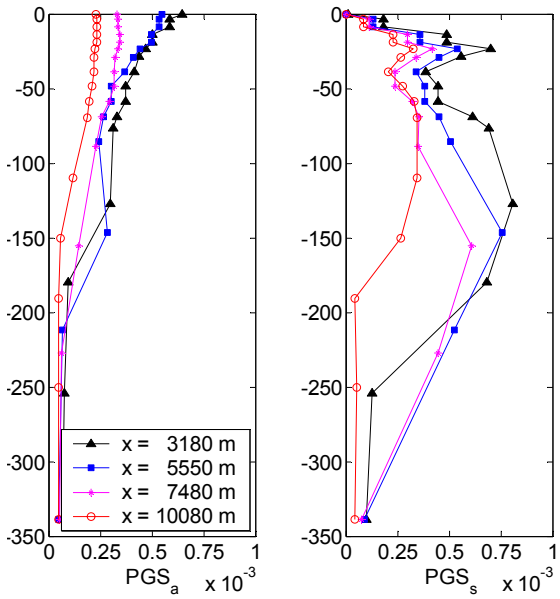

Figure 2.61: Variation of horizontal (PGSa) and shear (PGSs), peak ground strains with depth along some verticals of the NS cross-section of figure .

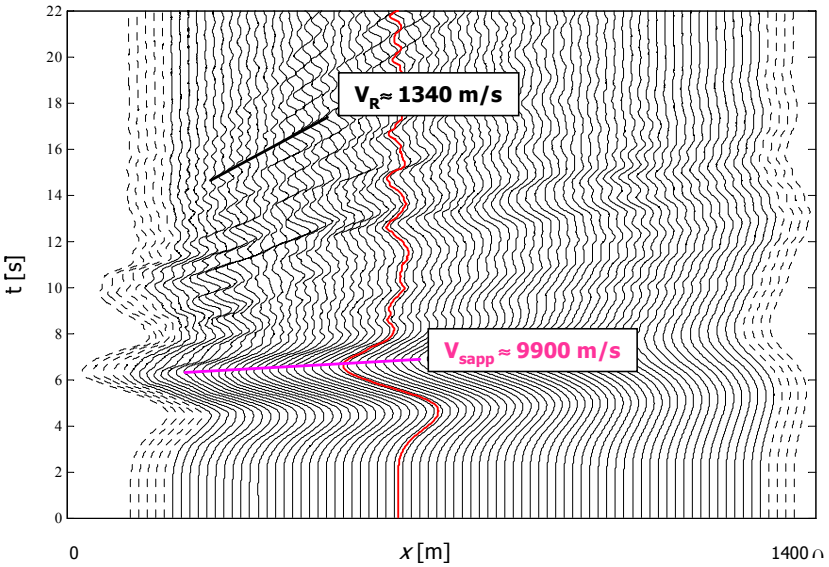

Figure 2.62: Horizontal (in plane) displacement time section with equally spaced receivers, with estimation of wave propagation velocities for S and Rayleigh waves. The abscissa indicates the receiver location on the surface along the NS cross-section. The dotted lines are the displacements at points out of the basin, the thick red line refers to the site of the Düzce accelerograph station

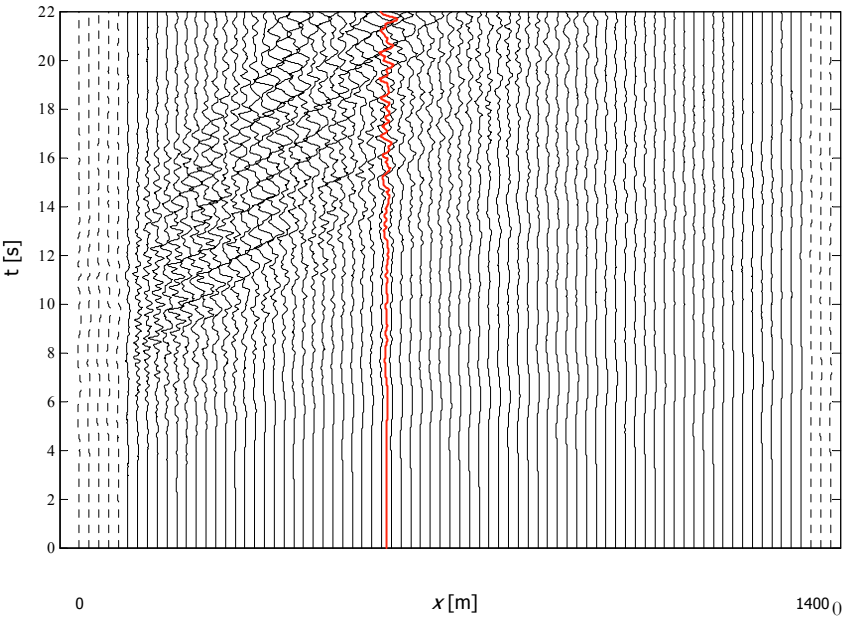

Figure 2.63: Horizontal (in plane) strain time section with equally spaced receivers. The abscissa indicates the receiver location on the surface along the NS cross-section. The dotted lines refer to points out of the basin, the thick red line refers to the site of the Düzce accelerograph station

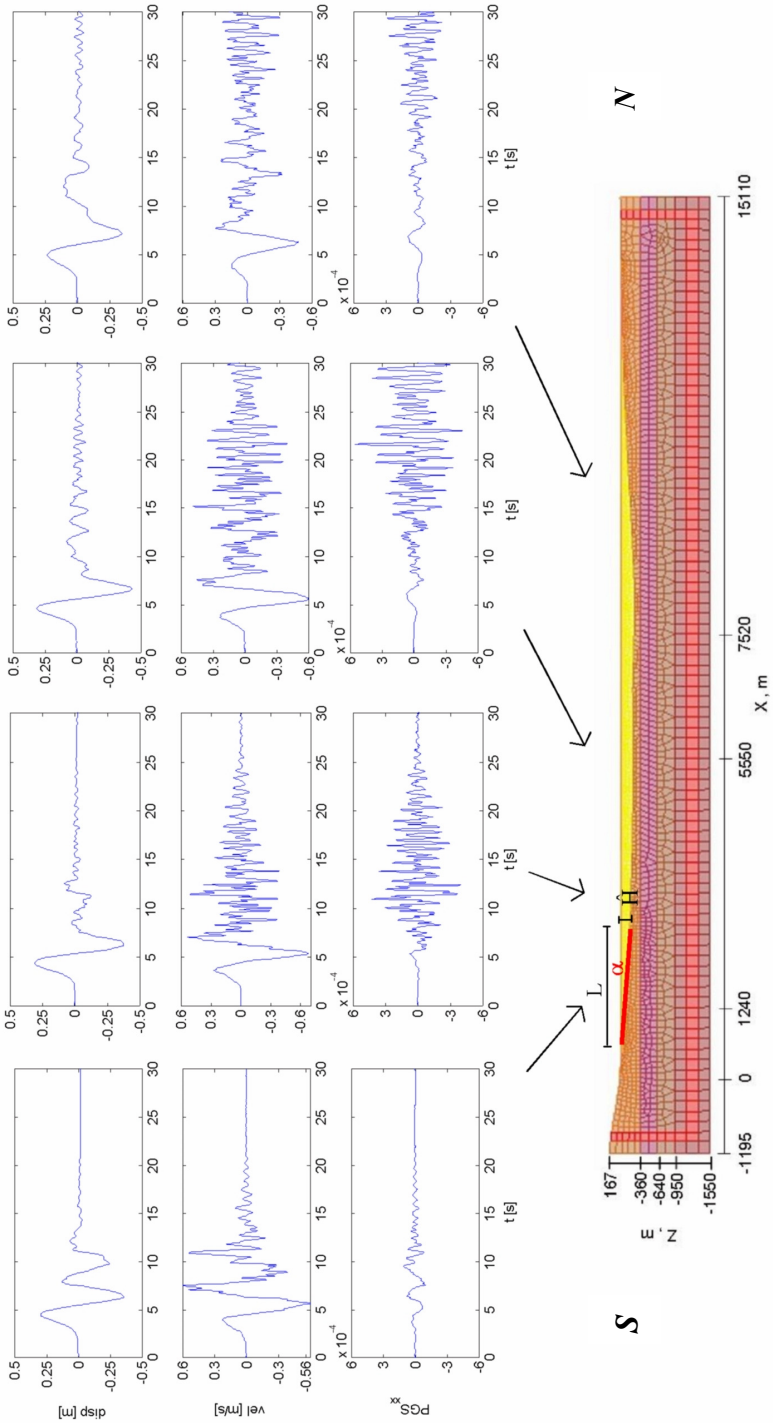

Figure 2.64: Ground response at some surface points of the reduced model (up). SE model of the NS cross-section with the meaning of the geometrical parameters L and α used in the simplified formula (3.5) (model at bottom)

In Figure 2.65 the different PGS evaluations are compared. We have omitted the case where C=V_{Sapp}, leading to unrealistically values of strains. The best agreement with the results of the numerical simulations is obtained using (3.5), if we consider both the PGS-PGV relationship and the position where the maximum value of *PGS* occur. Equation (3.2), with C=V_R, leads to an acceptable agreement with numerical results, but it does not capture the details of the spatial variability of PGS as in the case of application of equation (3.9).

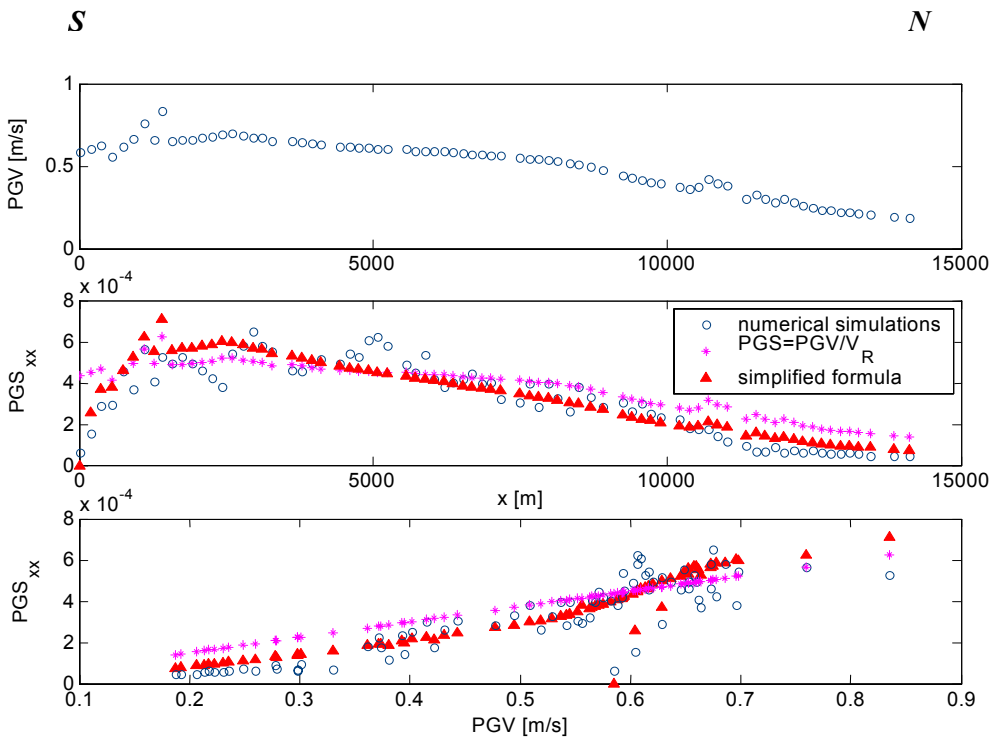

Figure 2.65: Horizontal PGS vs. PGV for the Düzce case, obtained by numerical simulations, application of equation (3.8) with C=V_R, and application of equation (3.9).

It is also useful to compare the 2D results with those evaluated by 1D equivalent wave propagation analyses (Pitilakis et al., 2005) in which the deconvolution of the recorded motion at the Düzce accelerograph station was taken as input motion at seismic bedrock. Figure 2.66 shows the map of computed 1D shear strains in Düzce. Note that, ground strains obtained by 1D analyses of S-wave propagation are purely of shear nature, with a relatively sharp variation with depth, and they cannot be translated straightforwardly in terms of longitudinal strains, which govern the seismic design of pipelines. The peak values of the computed shear strains within the top 15 m range from $5{\cdot}10^{-4}$ to $2{\cdot}10^{-3}$

(figure 2.66) along the NS cross-section in the city of Düzce. Taking an average ratio $PGS_{xy}/PGS_{xx} \approx 1.75$, based on the results of Figure 2.46, the estimated axial strain PGS_{xx} assume values between $2.8 \cdot 10^{-4}$ in the southern part and $1.3 \cdot 10^{-3}$.in the northern part of the city. Considering instead maximum ratio $PGS_{xy}/PGS_{xx} \approx 4$, PGS_{xx} ranges between $1.2 \cdot 10^{-4}$ and $5 \cdot 10^{-4}$.

From the 2D analyses, between around x = 4500 m and x = 11500 m of the 2D model (i.e. the segment occupied by the urban area), the evaluated PGS_{xx} range between $2 \cdot 10^{-4}$ in the northern part and $5 \div 6 \cdot 10^{-4}$ in the southern part. These values are in agreement with those estimated with $PGS_{xy}/PGS_{xx} \approx 4$, and significantly less than those evaluated with the average ratio of 1.75, probably because 2D results represent strains close to the surface, while the 1D ones refer to the top 15 m.

Note that 1D analyses cannot reproduce the decreasing trend of the strain profile from South to North, due to the fault radiation effects simulated by the DRM application, and they neglect the contribution of surface waves generated in the basin, so that they can only provide a rough average estimate.

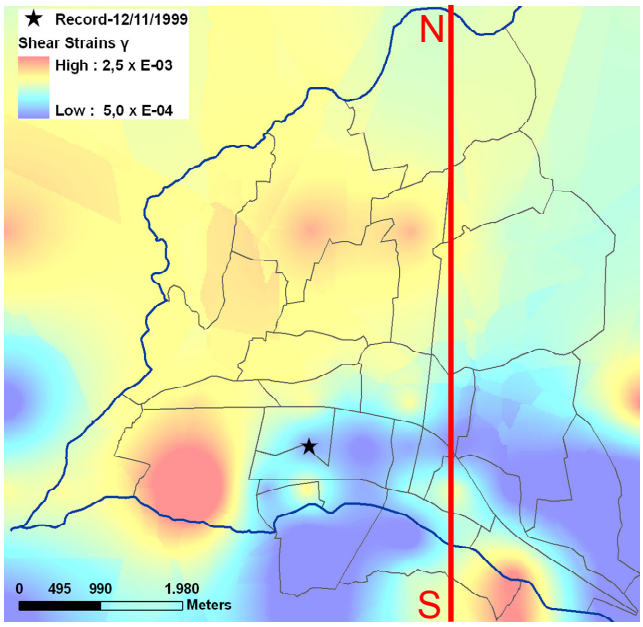

Figure 2.66: Distribution of maximum shear strains in the top 15m across Düzce area. Input motion: deconvolution of Düzce Nov 12, 1999 record, at the Meteorological Station – EW component). The superimposed thick line indicates the 2D NS cross-section analysed (from AUTH).

3.ON THE SEISMIC RESPONSE OF BURIED PIPELINES AND THEIR VERIFICATION

3.1 PIPELINES RESPONSE

Buried pipelines are commonly used to transport water, sewage, fuels, natural gas and other materials. They can be classified as either continuous or segmented. Steel pipelines with welded joints are considered to be continuous while segmented pipelines include cast iron pipe with caulked or rubber gasketed joints, ductile iron pipes with rubber gasketed joints, concrete pipes, asbestos cement pipes etc.

Because pipeline networks cover large areas, they are subjected to a variety of geo-tectonic hazards. Pipes can be damaged either by permanent ground movements, governed by maximum permanent ground displacement (PGD), or by transient seismic wave propagation. Permanent ground movement includes surface faulting, settlements and lateral spreading due to liquefaction and landslides. Although PGD hazards are limited to small regions within the pipeline network, their potential for damage is high since they impose large localised deformation on pipelines. The wave propagation hazards typically affect the whole pipeline network, but with lower damage rates. The correlation between severity of ground shaking at a pipeline location and the associated damage has in recent years been predominantly established in terms of peak ground velocity (PGV) at the surface. The orientation of the pipe relative to the wave field and permanent displacements, the material, the type of joints, the burial depth, the age and the corrosion, the appurtenances and the branches, the connection points [e.g. tanks], the valves or SCADA equipments are important factors that can influence the damage of the pipes.

The basic failure modes of pipelines for wave propagation are illustrated in Table 3.1 while Figure 3.1 depicts the failure modes of segmented pipes. [Shirozu et al., 1996] classify the possible pipeline failures according to material and joint type for the case of wave propagation (Table 3.2)

In case of settlement and lateral spreading caused by soil liquefaction, horizontal and vertical forces are applied on pipelines because of the water flow [O'Rourke T.D. and Palmer, 1996]. In slope failures, the location of the pipe relative to the landslide zone (Figure 3.2) defines the seismic load on the pipe. If the pipe crosses a landslide perpendicular to the direction of sliding, pipe bending is the main failure mode, otherwise the pipe is subjected to tension or/and compression.

The basic pipeline failure modes as a result of fault offset are also shown in Figure 3.3.

Table 3.1 Pipe failure modes due to wave propagation.

Continuous pipes **[O'Rourke & Liu, 1999]**	**Segmented pipes [Singhal, 1984, O'Rourke & Liu, 1999]**	**ALA [2001a]**
Tensile failure, Wrinkling, Beam buckling, Welded slip joint	Axial pull-out, Crushing of bell and spigot joints, Joint rotation, Round flexural cracks	Axial pull-out, Joint rotation, Tensile and bending deformations of the pipe barrel.

Table 3.2 Pipe failure modes for different materials, due to wave propagation [Shirozu et al, 1996].

Material	**Joint type**	**Failure mode**
Ductile iron pipe	General joints [type A, K,T]	weld-joint slip
	Flexible joints [Type S, SII]	No failure
Cast iron pipes	Socket and Spigot	Failure in the main body, or weld-joint slip
	Type A	Failure in the main body or weld-joint slip
Steel pipe	Welding	Failure of welding
	Threaded joints SGP	Failure in the main body or weld-joint slip
PVC	Type TS	Failure in the main body or weld-joint slip
Asbestos-cement pipe	Rubber gasket	Failure in the main body or weld-joint slip

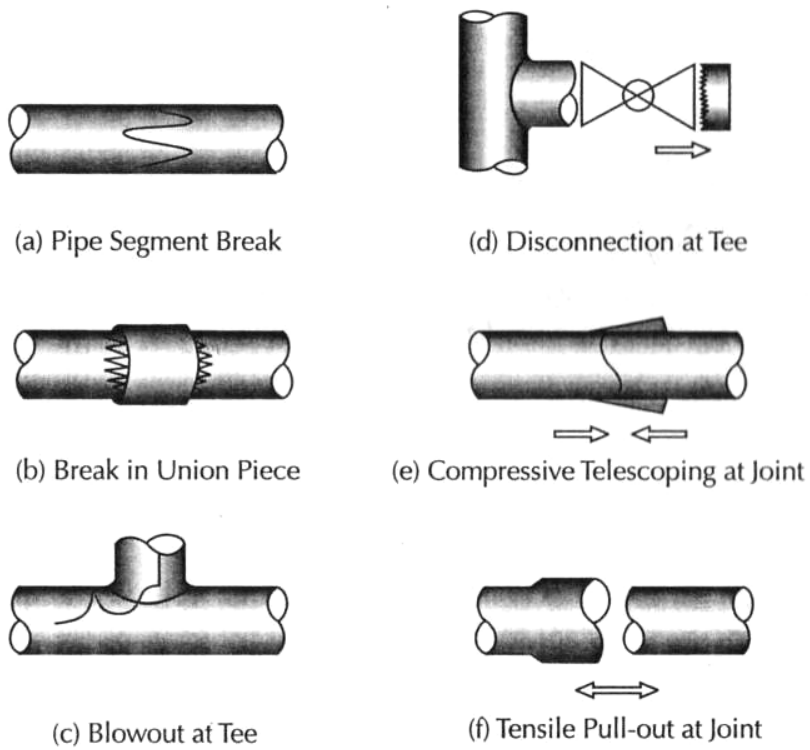

Figure 3.1: Failure modes for segmented pipes [O'Rourke & Liu, 1999].

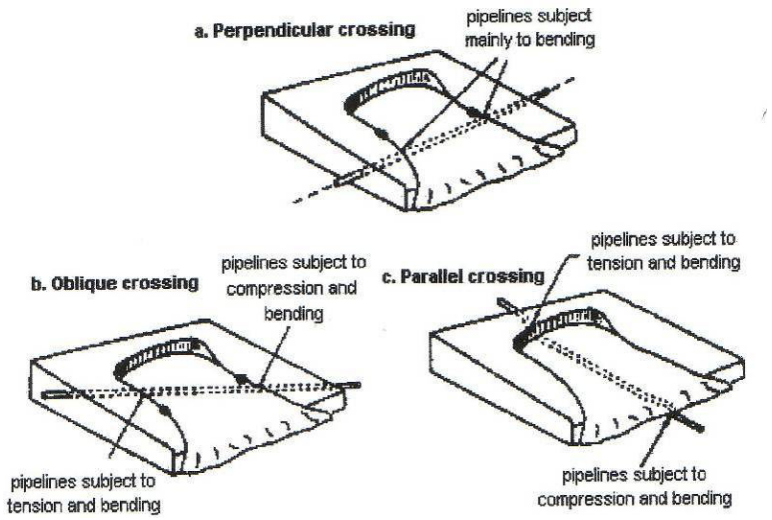

Figure 3.2: Failure modes for pipes as a result of landslides [O'Rourke et al, 1996].

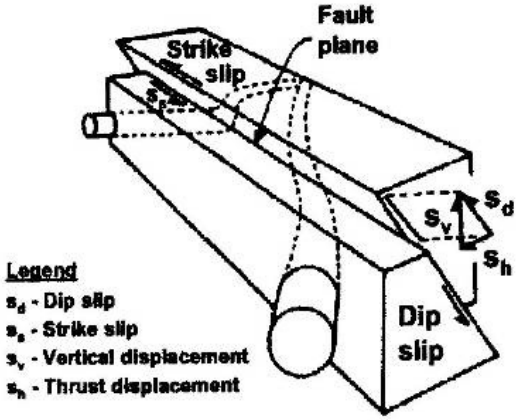

Figure 3.3: Failure mode for pipes as a result of faulting (O'Rourke et al, 1996).

3.2 EUROCODE 8 CONCEPTS ON THE SEISMIC VERIFICATION OF BURIED PIPES

As it has been shown in Sect. 2, seismic scenario analyses for IS are often carried out in a deterministic perspective, although they need not be restricted to this, see [Faccioli 2006]: this means that the response of the system at study is evaluated for a well defined spatial distribution of ground shaking, generated by an earthquake rupture of specified magnitude on a given fault.

Nevertheless, if the results are to be practically meaningful, the scenario ground motions should be checked through comparisons with the design earthquakes of the current seismic codes, in the present case Eurocode 8, Part 4 [CEN 2006], and the associated limit states for the seismic verification of the system structural components should be kept in mind. In Eurocode 8, in particular, the design seismic action with 475 yr return period is to be used for the Ultimate Limit State (ULS) verification, while the action with 95 yr return period is appropriate for the Damage Limitation State (DLS). In practice, in many cases the scenarios will have to be consistent with the need of checking the DLS occurrence. As a matter of fact, to quote Eurocode 8, Part 4: "*Depending the characteristics and the purposes of the structure considered, a DLS that meets one or both of the two following performance levels may need to be satisfied:*

– *'integrity';*

– *'minimum operating level'.*

In order to satisfy the 'integrity' requirement, the considered system, including a specified set of accessory elements integrated with it, shall remain fully serviceable and leak proof under the relevant seismic action.

To satisfy the 'minimum operating level' requirement, the extent and amount of damage of the considered system, including some of its components, shall be limited, so that, after the operations for damage checking and control are carried out, the capacity of the system can be restored up to a predefined level of operation."

In addition, as regards specifically the IS consisting of buried pipelines, it is prescribed that: " Buried pipeline systems shall be designed and constructed in such a way as to maintain their integrity or some of their supplying capacity after the seismic events relevant to the damage limitation state, even with considerable local damage."

4.VULNERABILITY FUNCTIONS FOR INFRASTRUCTURAL SYSTEM COMPONENTS

4.1 INTRODUCTION

The aim of this section is to illustrate and propose fragility curves and improved methods to assess vulnerability: a) for pipelines subjected to earthquake-generated ground shaking and permanent ground deformations [including landslides and fault rupture], and b) for shallow tunnels and waterfront structures subjected to ground shaking. A new method for the seismic verification of pipelines subjected to fault rupture is also presented.

While the illustrated vulnerability functions include, as just mentioned, also those for shallow tunnels and quaywalls, the buried pipelines (including applications to real cases) have been studied in greater detail. This choice stems from the circustamce that buried pipeline networks are, with electricity cables, the most diffusely present IS components in any developed urban area. Thus, in any mid-size western city there are easily many hundreds of km of buried pipes, if one includes water, natural gas and sewage.

4.2 LIFELINE DAMAGE IN RECENT EUROPEAN AND NEAR EAST EARTHQUAKES

As mentioned in Sect. 1, the scanty documented damage to IS in earlier European earthquakes includes failure to some harbour quaywalls during the 1979 Montenegro event and localized ruptures to the main tunnel of the Apulian acqueduct in Italy, during the 1980 Irpinia event.
In more recent years, the August 17 and November 12, 1999, Kocaeli and Düzce (Turkey) earthquakes caused significant damage to pipelines and waterfront structures due to fault rupture, differential soil movements, ground softening, and liquefaction-induced deformations, settlements and lateral spreading. Another recent seismic event that has caused important damage to pipelines, and to waterfront structures mainly due to permanent deformations is the August 14, 2003, Lefkas earthquake. Observed failures modes and seismic response of pipelines, tunnels and waterfront structures in the latter earthquakes are summarized below.

4.2.1 Buried pipelines

Buried pipelines are commonly used to transport water, sewage, fuels, natural gas and other materials. Because pipelines cover large areas, they are subjected to a variety of geotectonic hazards. They can be damaged either by permanent ground movements,

PGD (surface faulting, settlements and lateral spreading due to liquefaction and landslides), or by transient seismic wave propagation. Although PGD hazards are limited to small regions within the pipeline network, their potential for damage is very high since they impose large deformation on pipelines. The wave propagation hazards typically affect the whole pipeline network, but with lower damage rates. The level of ground shaking at a pipeline location and the associated damage can be assessed more accurately in terms of peak ground velocity and, even better, by peak (transient) longitudinal ground strain. The orientation of the pipe relative to the wave field and permanent displacements, the material, the type of joints, the burial depth, the age and the corrosion, the appurtenances and the branches, the connection points [e.g. tanks], the valves or SCADA equipments are important factors that can influence the damage of the pipes.

Damage to water supply systems

During and after the 1999 Kocaeli earthquake, the water supply system in Adapazarı experienced extensive damage mostly due to ground surface faulting and permanent ground deformation associated with soil liquefaction and softening of alluvial sediments, see Figure 4.1 and Figure 4.2. Figure 4.3 depicts one typical asbestos concrete (AC) replacement/repair after the earthquake. In contrast to the widespread damage in the pipeline network, the water treatment and storage facilities at Adapazarı sustained only minor damage that was quickly repaired. During the same earthquake, the fault rupture near Kullar severed the main trunk line leading from the regional water treatment plant to the distribution network circling Izmit Bay area. The November 1999 Düzce earthquake resulted in some pipe damage in the water distribution system of Kaynaşlı village occurred at the fault zone and at the joints.

During the Kocaeli and Düzce earthquakes' of 1999, the Düzce potable water system suffered extensive damage. It comprises of a network of old pipelines, with new segments connected to the old ones with a series of bypasses. After gathering the available information of pipe damage, two damage databases were assembled [Tromans, 2004; Alexoudi, 2005], see Figure 4.4, Figure 4.5 and Figure 4.6.

The Greek experience on damage of potable water systems is limited. No major damage to water distribution network was recorded in Thessaloniki from the 1978 Thessaloniki earthquake [PGA= 0.15g, PGV= 16.7cm/sec, PGD=3.4cm]. In the 1986 Kalamata earthquake [Mw= 6.0, R= 12km, PGA= 0.27g, PGV= 32.3cm/sec, PGD=7.2cm] and in the Kozani earthquake, the recorded damage was limited and localized in small areas. No detailed and well documented data are available. The only well documented case is the recent Lefkas earthquake [Ms=6.4, 14-8-2003]. The main water network of Lefkas city sustained 10 failures in water mains [old city], 5 in Marina of Lefkas and more than 80 failures in service connections in the whole city, see Figure 4.7. From the 10 main water failures, 6 were attributed to permanent ground deformation, while the rest to wave propagation and material failures caused by seawater corrosion [at 1.0m depth from the

surface].

Damage to waste water systems

The Izmit wastewater treatment plant was closed after the 1999 Kocaeli earthquake due to damage to the mechanical equipment, while the intercepting sewer pipes in Golcuk were heavily damaged. In the Düzce earthquake the sewage systems in Düzce and Kaynasli were heavily damaged due to ground deformations [Erdik, 2000]. The collector line along the southern coast of the Izmit bay, located approximately parallel to fault rupture experienced different degrees and types of damage due to different factors such as liquefaction, lateral spreading, fault rupture, and inundation of the shore line.
In the wastewater network of Lefkas some damage was recorded as a result of the Lefkas earthquake mainly due to permanent deformations. No damage was observed in the wastewater treatment plant and the wastewater pumping station, despite an observed settlement of 11cm.
Natural Gas and Oil Pipelines

In the Izmit municipal gas [IZGAS] distribution system (the only urban gas system in the affected area, except Istanbul) no damage was reported to the main distribution network in the Kocaeli earthquake. The system performed exceptionally well during the earthquake and afterward, while no fires were attributed to leaking gas. The damage sustained in the system occurred when buildings collapsed onto service boxes [O'Rourke et al. 2000].

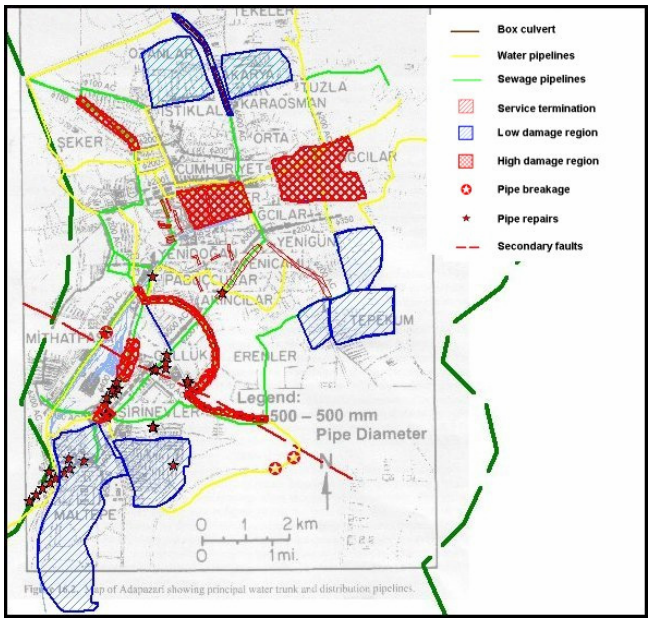

Figure 4.1 Map of damage distribution in Adapazarı [Ansal et. Al, 2000] and pipeline network, with comparison of principal distribution pipelines given by O'Rourke et al. [2000].

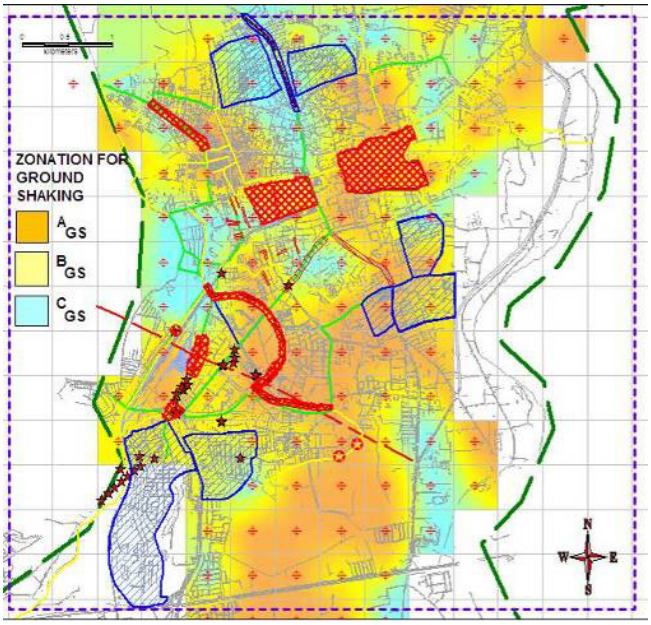

Figure 4.2 Damage distribution map compared with ground shaking zonation [Adapazarı] where Ags, Cgs and Bgs show the zones with high, low and intermediate ground shaking intensities, respectively.

Figure 4.3: Repair and replacement of damaged AC pipeline after the August 1999 earthquake in Adapazari.

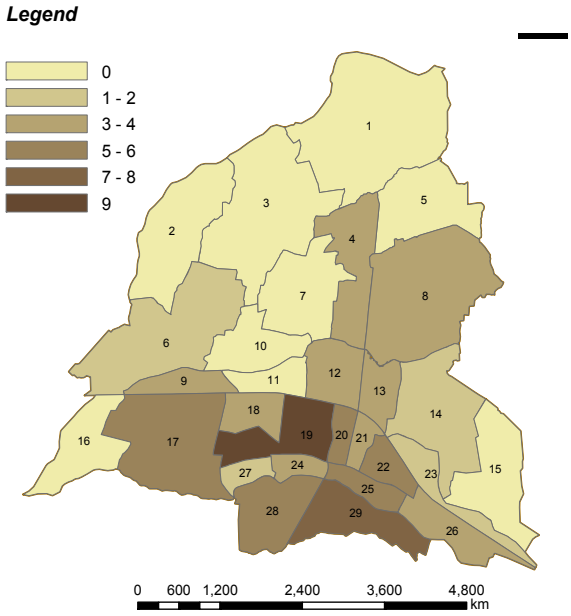

Figure 4.4: Average failure rate of potable water system of Düzce. Düzce earthquake [Period: December 1999- January 2001]- Tromans[2004].

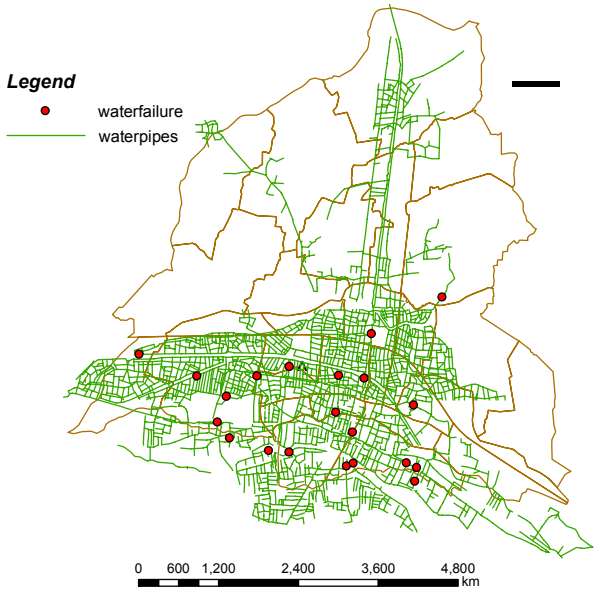

Figure 4.5: Water pipeline failures [red points] in Düzce, from Alexoudi [2005].

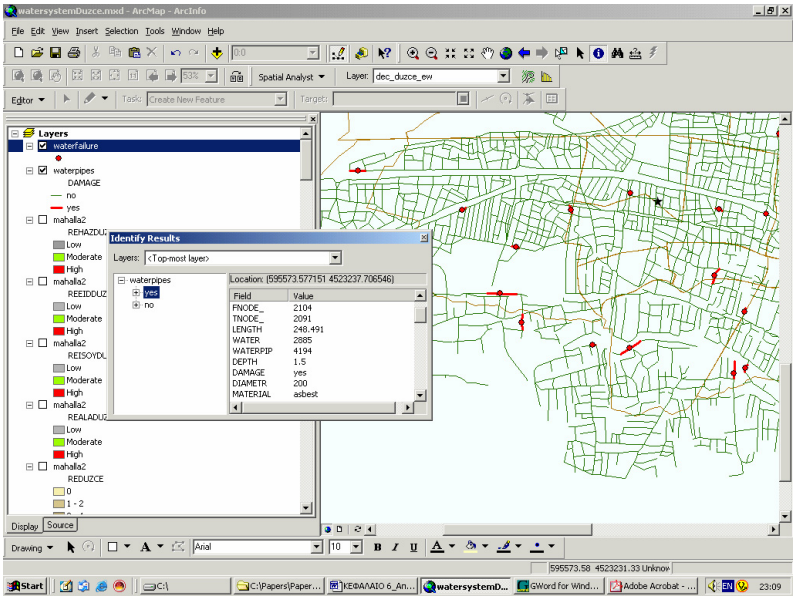

Figure 4.6: The GIS related damage database, from Alexoudi [2005].

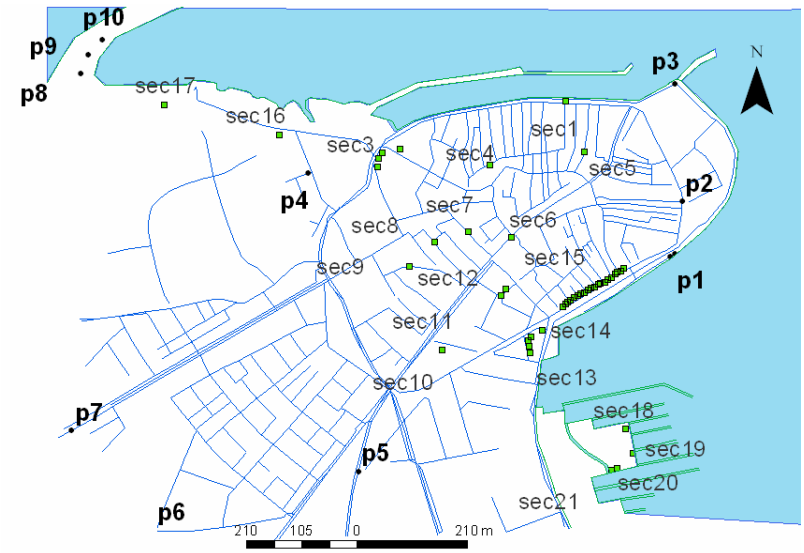

Figure 4.7: Water distribution network of old city section of Lefka*s* and the location of main water system failures and secondary connections [p- primary network, sec- secondary network-connections with customers].

4.2.2 Tunnels

In general, tunnels have performed well during past earthquakes compared to aboveground structures, with the exception of older masonry tunnels in the epicentral region of strong events (e.g. the Pavoncelli Tunnel illustrated in Sect. 1). This can be attributed to the fact that a fully embedded tunnel tends to move with the ground and does not experience a strong inertial response as in the case of aboveground structures. The fact that the amplitude of seismic ground motion tends to decrease with depth below the ground surface also reduces damage. However, tunnels, especially the shallow ones, may still be susceptible to seismic damage, not necessarily complete failures, especially in areas with high seismicity. The seismic performance of tunnels [highway, railway, potable/waste water] in past earthquakes is summarized in various reports [Dowding and Rozen, 1978, Owen and Scholl, 1981, Wang, 1985, Sharma and Judd, 1991, Wang 1993, Power et al., 1998, ALA, 2001a, b, Wang et al., 2001, Hashash et al., 2001]. For ground shaking, an overview of tunnel response is provided in Figure 4.8.

The earthquake effects on tunnel structures can be classified into two categories [Hashash et al. 2001, Wang 1993]: ground failure and ground shaking. The majority of damage records has been associated with permanent ground displacements due to ground failure, i.e., fault rupture through a tunnel, landsliding [especially at tunnel portals], and soil liquefaction.

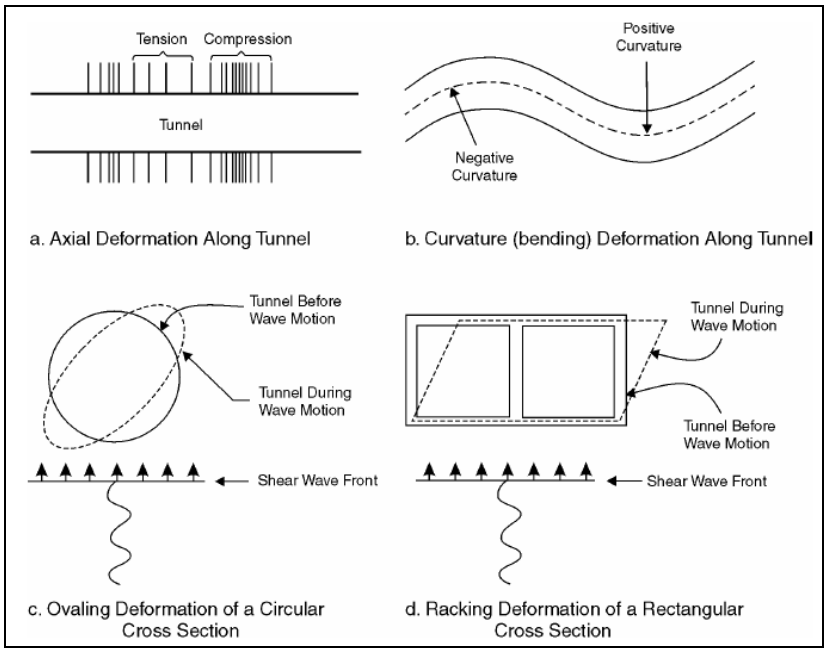

Figure 4.8: Tunnel response to seismic waves [Wang, 1993].

4.2.3 Waterfront structures

By far, the most significant source of earthquake-induced damage to port and harbor facilities is the increase of induced earth pressures caused by inertial forces to the retained ground mass and by hydrodynamic and pore-water pressure buildup in the saturated cohesionless soils that prevail at these facilities. This pressure buildup can lead to excessive lateral pressures to quay walls. Liquefaction and massive submarine sliding are also very important causes for spectacular failures. Other sources are local permanent ground displacements, ground failure and extensive settlement related to ground shaking [Pachakis and Kiremidjian, 2004, Werner, 1998]. Yet, the liquefaction of loose, saturated, sandy soils that often prevail at coastal areas (especially reclaimed land and uncompacted fills) is the most widespread source of seismic damage to port structures. Figure 4.9 and Figure 4.10 illustrate some examples of damage. Past experience has demonstrated that even moderate levels of earthquake intensity can cause liquefaction, resulting in the reduced stiffness and loss of shear strength of the liquefied soils. This can in turn result in induced soil settlements, increased lateral earth pressures against retaining structures and loss of passive resistance against walls and anchors [PIANC, 2001]. Finally, port structures are also subjected to damage due to tsunamis.

Most failures of waterfront structures are associated with outward sliding, deformation and tilting of quay walls and sheet-pile bulkheads. There are a large number of references regarding seismic damage of port structures, mostly during earthquakes in the USA and Japan. On the other hand, records of damage sustained by waterfront structures are quite limited in European earthquakes (e.g. in the Ulcinj harbour, as a result of the destructive Montenegro earthquake of 1979).

Figure 4.9: Damage to waterfront structures and supporting piles during the 1999 Kocaeli earthquake.

Figure 4.10: Damaged quay walls at Golcück navy base during the 1999 Kocaeli earthquake.

4.3 MAIN APPROACHES TO SEISMIC DAMAGE ESTIMATION FOR IS

A fundamental requirement for assessing the seismic performance of an IS is the ability to quantify the potential for component damage as a function of the level of seismic hazard intensity. In general, the vulnerability expresses the behavior of an element at risk subjected to a phenomenon with variable intensity. It is given in terms of a vulnerability relationship, referring to a general deterministic, statistical or probabilistic relationship relating the component's damage state, functionality, economic losses etc, to an appropriate measure of the intensity of the earthquake hazard. The relationship between the probability of the component damage and the level of seismic hazard is normally referred to as a fragility relationship, or fragility curve, or vulnerability curve.

Damage states of lifeline components are usually classified as: No damage - Slight / Minor - Moderate - Extensive - Complete. This qualitative approach requires an agreement about the meaning and the content of each damage state and in general the definition of damage states is rather subjective. Alternative ways expressing losses are also suggested like: functionality (binary decision: Yes or No); possibility of damage (usually between 0 and 1 or 100%); repairs/km (especially for pipes); serviceability; nominal use, reduced use or not usable; usable without repairs, after repairs or not repairable; damage factor or replacement cost (usually between 0 and 1 or 100%).

There are different methods to construct vulnerability or fragility curves and to quantify damage according to the shaking intensity, such as:

- Vulnerability index approaches. These are based on the definition of an index resulting in most cases from an analytical expression that combines the main factors affecting the seismic behavior of the element at risk. A rating system is used to assign a score in each attribute of the selected factors. The scaling values are defined based on expert judgment and the experience of past earthquakes, while the expression usually includes weighting factors in order to account the relative contribution of each attribute to the total vulnerability of the component.
- Expert judgment based models. In many cases, expert opinion is used for the evaluation of the seismic behavior of lifeline components with different typology. These expert evaluations are always useful but for reasons described previously and with the increased number of data after the recent strong earthquakes, they are less used.
- Empirical models. The development of empirical fragility curves is based on statistical analysis of damage data from previous earthquakes. The fragility curves are usually provided as medians and dispersions of lognormal distribution. Several uncertainties are involved in such analysis; however real reported and validated damage data and the derived methods are extremely valuable, even to check the reliability of other more accurate methods.
- Analytical models. Fragility curves can also be constructed analytically using simple or more complicated models according to the type of analysis, the characteristics and the simulation method of the component. Produced analytical curves could be compared with empirical ones derived from actual damage data.

4.4 VULNERABILITY FUNCTIONS FOR PERMANENT GROUND DEFORMATION

4.4.1 Pipelines

Empirical relations have been proposed for pipe damage, which relate peak ground velocity [PGV, due to wave propagation] or permanent ground deformation [PGD] to the Repair Rate/km [RR/km], i.e. the expected number of repairs per km of pipe. Macroseismic intensities were also used as appropriate indicator. After 1990 reliable earthquake damage databases were made available, and more accurate vulnerability functions have been proposed for wave propagation and permanent deformations. In particular, more refined approaches based on the ground strains as appropriate indicator have been proposed [O'Rourke and Deyoe, 2004].

The most commonly used empirical relations for the estimation for pipeline performance related to permanent ground deformation are depicted in Table 4.1 and Figure 4.11.

Table 4.1 Empirical relations for pipelines related to Permanent Ground Deformations (PGD).

Empirical relation	Influence factors	Reference
Bi-linear relation	PGD [inches] Material	Porter et al [1991]
R.R/km. =K[7.821*PGD$^{0.56}$]	PGD [m] K: indicator depending on pipe material	Honegger & Eguchi [1992]
R.R/km = 100*[1-exp[[0.283*PGD]$^{1.33}$]] R.R/km = 100*[1-exp[[0.899*PGD]$^{1.11}$]] R.R/km = 100*[1-exp[[0.578*PGD]$^{1.55}$]] R.R/km = 100*[1-exp[[1.120*PGD]$^{1.69}$]] R.R/km = 100*[1-exp[[0.743*PGD]$^{0.71}$]] R.R/km=100*[1-exp[-[1.120*PGD]$^{0.761}$]] R.R/km = 100*[1-exp[-[0.644*PGD]$^{1.37}$]] R.R/km = 100*[1-exp[-[1.530*PGD]$^{1.62}$]] R.R/km = 100*[1-exp[-[0.961*PGD]$^{1.64}$]] R.R/km = 100*[1-exp[-[1.830*PGD]$^{1.83}$]]	PGD [m] Material Joint type	Heubach [1995]
R.R/km. = K2*23.674*[PGD]$^{0.53}$	PGD [m] K2: indicator depending on pipe material and joint type	Eidinger & Avila [1999]
R.R/km. = K2*11.223*PGD$^{0.319}$	PGD [m] K2: indicator depending on pipe material and joint type	ALA [2001a,b]

R.R/km. = Repair Rate (average number of pipe repairs per km)

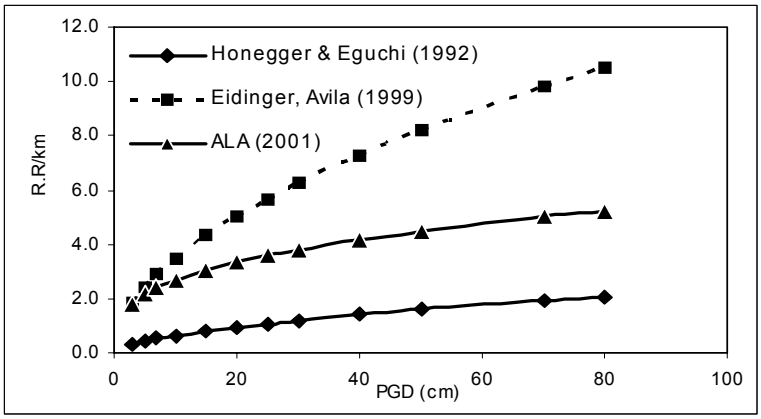

Figure 4.11 Comparison between different empirical relations for pipeline failures for the case of PGDs [brittle pipes].

The previous relations were validated with the observed damage (pipeline failures) of Lefkas earthquake. The relation of Honegger & Eguchi, 1992, gives the best estimated results compared with the field observations. The relations by Eidinger & Avila E [1999] and ALA [2001] overestimate the damage.

O'Rourke & Deyoe [2004] proposed a fragility curve that correlates the RR with ground strains (Figure 4.12). 9 field observations from the Northridge, 1994 earthquake [Sano et al, 1999] and from a Japan earthquake [Hamada & Akioka, 1997] were used. The ground strains used by Sano et al [1999] were back-calculated from pre-and post- event photogrammetric analysis. As described by Hamada & Akioka, 1997 the damage mechanism for the second data set was tensile ground strains due to longitudinal PGD.

Moreover, O'Rourke & Deyoe E [2004] proposed a fragility relation [Equation (4-1)] that correlates both the wave propagation and the PGD repairs rates to the longitudinal ground strain ε:

$$R.R. = k_1 * 513 * \varepsilon^{0.89} \quad (4.1)$$

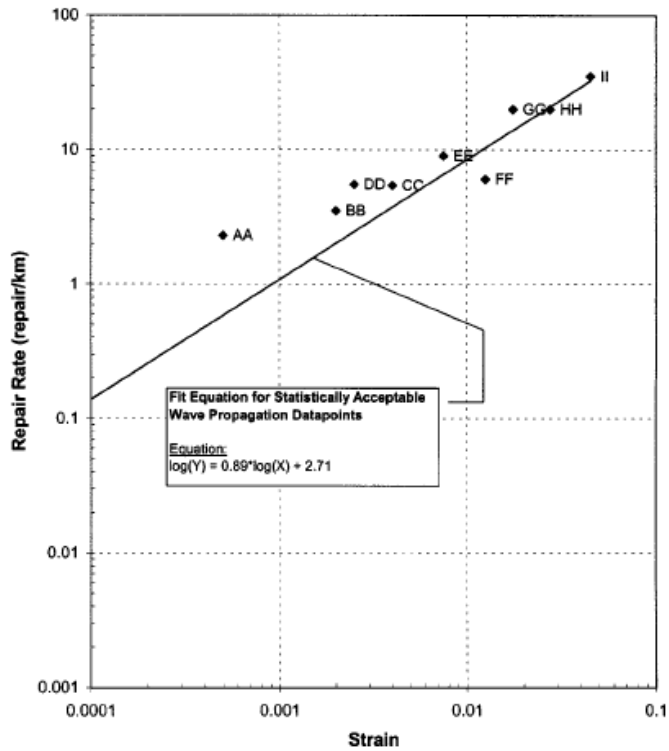

Figure 4.12 Pipe repair ratio vs ground strains [O'Rourke & Deyoe, 2004].

It was already noted in previous Sub-Sect. 4.3 that the definition of damage state is an important element in estimating the pipeline performance. Heubach [1995] considers as "break" the failure which results in the complete interruption of liquid/ solid/ gas transfer through the pipeline, while "failure" is considered to be any malfunction leading to a pipe leakage without complete interruption of liquid/ solid/ gas transfer. The circular failures as result of corrosion or the pin-holes according to Ballantyne et al [1990] can be described as leaks while longitudinal pipe ruptures can be accounted as breaks. ATC 13/ FEMA 226 [1985] define 7 damage as a function of the Repair Rate (see Table 4.2).

Table 4.2: Pipeline damage states [ATC-13].

Description of damage state	Pipes	
	Breaks/ km	% Failures
None	0	0
Slight	0.25	0.6
Light	0.75	2
Moderate	5.5	14
Heavy	15	38
Major	30	75
Destroyed	40	100

Ballantyne & Heubach [1996] propose a different categorization of the damage state shown in Table 4.3.

Eurocode 8 (EC8) distinguishes pipes into single lines [their behavior during and after the earthquake is not influenced by other pipes] and redundant networks. For the failure of the pipes in a redundant network, EC8 assumes that pipelines should be constructed in such way as to maintain the supply capacity as a global serving system. A global deformation of the pipe not greater than 1.5 times its yield deformation is acceptable. EC8 proposes specific computation analysis for above ground and buried pipelines. The code does not mention the use of empirical methods for the estimation of the performance of the network. Moreover, it gives allowable tensile & compressive strains for welded steel pipes while the strains in concrete pipes must follow EN-1992-1-1 (Eurocode 2). For the other pipe types, no mention is made. However, the proposed allowable stresses and strains should be used for the estimation of the damage states. No specific work has been done so far on this issue.

Table 4.3 Damage state according to Repair Rate.

Description of damage state	Repair Rate
No-damage	0 ≤R.R≤ 0.001
Low	0.001<R.R ≤ 0.01
Low- Moderate	0.01< R.R ≤ 0.1
Moderate	0.1< R.R ≤ 0.7
Moderate- High	0.7< R.R ≤ 1.4
High	1.4< R.R

4.4.2 Waterfront structures

Existing methods for the seismic damage analysis of quay walls

Empirical fragility curves that describe earthquake induced damage to waterfront structures are proposed in HAZUS [NIBS, 2004]. The latter are log-normal cumulative distributions which give the probability of reaching or exceeding certain damage states for a given degree of permanent ground displacement [PGD]. The description of the damage states and the corresponding vulnerability curves are provided in Table 4.4 and Figure 4.13.

Analytical methods are also often used for the vulnerability assessment of quay walls. The standard "structural-engineering approach" to wharf design relies on soil-structure-interaction [SSI] models [Roth et al., 2003]. Alternatively, dynamic analysis can be performed [Roth and Dawson, 2003]. Ichii [2003 & 2004] proposed several analytical fragility curves for the assessment of direct earthquake-induced damage to gravity-type quay walls using simplified dynamic finite element analysis. Different vulnerability curves are given in the form of log-normal probability distributions for peak ground acceleration [PGA].

Damage states for waterfront structures

Different parameters defining damage states of waterfront structures are summarized in Table 4.5.

According to EC8 – Part 5, possible failure modes of earth retaining structures are considered to be bending for flexible structures and sliding and/or rotation for gravity structures. The design of earth retaining structures should ensure the following requirements:

• Stability of foundation soil [overall stability, local soil failure by sliding and/or bearing capacity failure].

• Resistance of anchorage.
• Structural strength.

Table 4.4: Description of damage states and corresponding vulnerability curves for waterfront structures HAZUS [NIBS, 2004].

Damage state	Description	Serviceability		Permanent Ground Displacement [PGD]	
				Median [m]	β (log-standard deviation)
Minor	Minor ground settlement resulting in few piles [for piers/seawalls] getting broken and damaged. Cracks are formed on the surface of the wharf. Repair may be needed.	Reduced use	Operational without repair	0.13	0.50
Moderate	Considerable ground settlement with several piles [for piers/seawalls] getting broken and damaged.	Not usable	Operational after repairs	0.30	0.50
Extensive	Failure of many piles, extensive sliding of piers, and significant ground settlement causing extensive cracking of pavements.		Not repairable	0.43	0.50
Complete	Failure of most piles due to significant ground settlement. Extensive damage is widespread at the port facility.			1.09	0.50

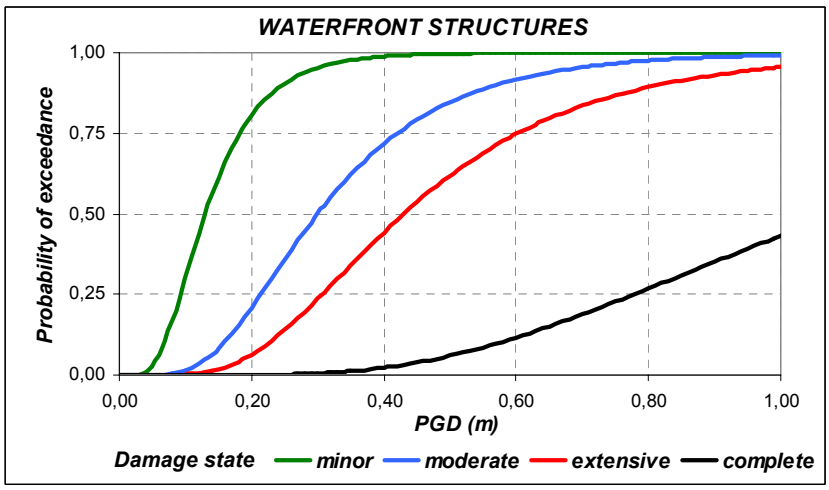

Figure 4.13: Fragility curves for waterfront structures subject to ground failure HAZUS [NIBS, 2004].

Table 4.5: **Parameters defining damage states of waterfront structures.**

Element	Parameters defining damage states	Reference
Quay walls	Level of structural damage Serviceability Normalized seaward displacement/sliding Residual tilting towards the sea Level of apron damage [differential settlement, residual tilting] Permanent / residual displacement at top of wall Horizontal displacement of quay wall	HAZUS, '04 HAZUS, '04, OCDI, 2002 Ichii, 2003, PIANC, 2001 PIANC, 2001 PIANC, 2001 Uwabe, 1983 OCDI, 2002
Caisson-type quay walls	Residual displacements of the caisson and apron Peak response stresses / strains of cell and cell joint	PIANC, 2001
Sheet-pile walls	Normalized seaward displacement / sliding of sheet-pile wall and apron Peak response stresses / strains of sheet-pile wall mad tie-rod [Maximum] residual displacement at top of sheet pile Horizontal displacement Serviceability	PIANC, 2001 PIANC, 2001 Uwabe, 1983, Gazetas et al., 1990 OCDI, 2002 OCDI, 2002
Pile-supported wharves	Residual displacements [differential settlement between deck and land behind, residual tilting towards the sea] Peak response of piles	PIANC, 2001

Validation of vulnerability models for quay walls

The evaluation and examination of the reliability of existing fragility curves has been performed based on the actual seismic performance of the quaywalls of the city of Lefkas, which sustained significant deformations during the 2003 earthquake. This study was primarily aiming at developing fragility curves for small quaywalls based on Greek typology and construction practice [Kakderi et al., 2006]. One of the main input parameters were the results of a site-specific ground motion analysis performed for the old city of Lefkas and the Marina area and for the specific scenario earthquake. The latter aimed at the estimation of site effects necessary for the vulnerability assessment of spatially distributed IS, taking also into consideration the effects of liquefaction phenomena on ground motion characteristics. The spatial distribution of liquefaction induced permanent ground displacements was also estimated.

Based on estimated values of peak ground acceleration and permanent ground displacements, the vulnerability assessment of the Lefkas quay walls was performed using HAZUS [NIBS, 2004] and Ichii, 2003 vulnerability functions. It was concluded that:

- The vulnerability assessment and damage state distribution using the HAZUS '04 relationships is rather compatible with the observed damage.
- Damage from the vulnerability curves proposed by [Ichii, 2003] seems to be slightly overestimated.
- The application of [Ichii, 2003] vulnerability curves requires the knowledge of geotechnical and construction data. Their application is possible in case of lack of specific studies for the estimation of permanent ground displacements.

Finally, it is pointed out that the collection of more damage data should continue in order to improve the current knowledge and produce site and case specific fragilities curves accounting for the European distinctive features. Based on the aforementioned observations, the HAZUS '04 fragility curves are proposed for the vulnerability assessment of quay walls.

4.4.3 Simplified Modelling of Continuous Buried Pipelines Subject to Earthquake Fault Rupture

4.4.3.1 *Introduction*

The seismic analysis of buried pipelines crossing seismically active faults is a task involving a complicated soil-structure interaction problem with several major numerical difficulties, such as: i] 3D geometry; ii] large deformations; iii] local cross-sectional buckling; iv] Eulerian buckling under compressional fault movement; v] pipe sliding with respect to the surrounding soil; vi] non-linear soil behaviour. Furthermore, unless the fault breakage occurs within a narrow zone, as for relatively rigid ground materials, the

longitudinal extension of the pipe affected by large deformations may be large, in some cases of the order of several tens of meters. Due to the aforementioned reasons, the numerical simulation of such a case may be very difficult, even with suitable finite element codes [Liu et al., 2004], so that simplified engineering approaches are still the most feasible way for tackling this problem in practice.
Most of the available engineering approaches stem from the pioneering work of [Newmark and Hall, 1975], who devised a simple method where the pipe was modelled as a cable, connected to the soil by nonlinear springs, and elongating in the axial direction within a region the extension of which was determined based on geometrical and material compatibility conditions. The Newmark and Hall approach was subsequently improved by [Kennedy et al., 1977] to take simply into account flexural deformations and the transversal soil resistance as well. Subsequent contributions to the problem were mainly based on the results of numerical finite element approaches; the most recent ones, such as [Liu et al., 2004], clearly highlight the role of large flexural strain localization and local buckling occurring at few cross-sections along the pipe, the remaining parts being nearly unaffected.

A simple approach is proposed here, that may be helpful for overcoming the previously mentioned drawbacks of the available engineering approaches, and take into account in an approximate way the loss of flexural stiffness of the pipe in few selected cross-sections.

4.4.3.2 *Method*

In the proposed method, a failure mechanism for the pipe is assumed, consisting of the formation of two plastic hinges, on both sides of the pipe relative to the fault trace. In the simplest case, i.e., strike-slip fault with homogeneous soil conditions, the plastic hinges are symmetric with respect to the fault-pipe crossing. In the region within the two plastic hinges, the pipe elongates [or shrinks] plastically. Therefore, the flexural deformation of the pipe is concentrated in the plastic hinges. Due to the complex 3D nature of the problem, it would be practically unfeasible to devise a corresponding failure mechanism for the surrounding soil, in order to introduce the method in the framework of the kinematic approach of the yield design theory. Rather, the soil-structure interaction is taken into account with the assumption that the pipe movement is constrained, both in the axial and transverse direction, by a distribution of forces determined according to empirical formulas available from the literature (see e.g. [O'Rourke and Liu, 1999]) for a comprehensive review of such formulas]. The sketch of the proposed failure mechanism for the pipe is shown in Figure 4.14. Although this figure and the following examples for validation and application, are based on the strike-slip fault and homogeneous soil assumptions, so that symmetry considerations are allowed, the approach can easily be extended to account for normal and reverse fault movement, and inhomogeneous soil conditions as well.
Analytical details on the proposed procedure, as well as the comparison with other

published solutions, are given in [Paolucci, 2006].

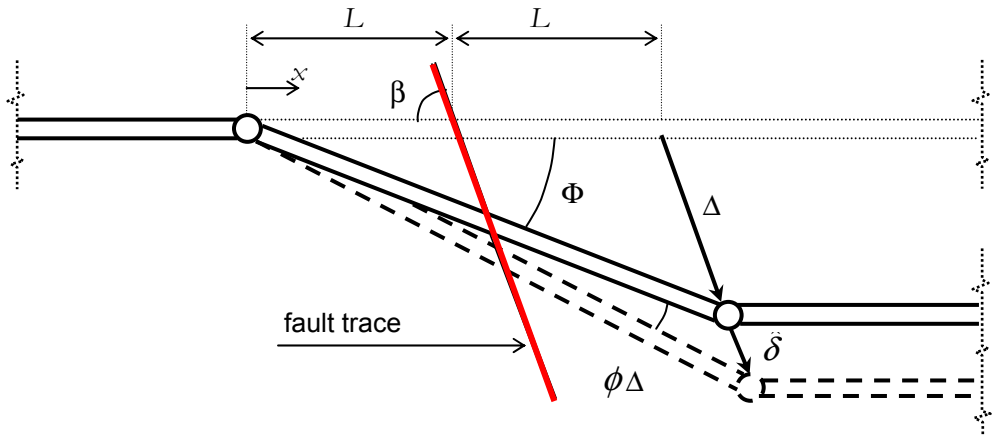

Figure 4.14: Assumed failure mechanism for the continuous pipeline crossed by a strike-slip fault (plan view).

4.4.3.3 *Results of parametric analyses*

The advantage of the proposed approach is that it can easily deal both with extensional and compressional deformation fields, and can be extended with no major difficulties both to normal and reverse faults. Referring to the strike-slip fault case, a set of parametric analyses has bee carried out to check the relative influence on the pipeline behaviour of different parameters affecting its response, namely: i] the angle β between the pipe axis and the fault surface trace; ii] the soil friction angle; iii] the embedment depth z of the centre of the cross-section, normalized by its external diameter D; iv] the cross-sectional thickness t, normalized by the external radius $R = D/2$. The results of these analyses are plotted in Figure 4.15 , and show the predicted fault offset required to induce in the pipeline the allowable strain values for welded steel pipelines according to Eurocode 8, Part 4 [CEN, 2006], namely: allowable tensile strain: 0.03 and allowable compressive strain: min [0.01; 0.2 t/R], where the latter values account for the reduced resistance in compression, due to local or global buckling.

All results plotted in Figure 4.15 are in agreement, at least from a qualitative point of view, with the design measures suggested by the technical guidelines for buried pipelines at fault crossing [see, e.g., section 6.6 of Eurocode 8, Part 4], namely:

- the key role played by the intersection angle of the pipe axis with respect to the fault trace in minimizing the compressive strains;
- the reduction of the angle of interface friction between pipe and soil, that improves the pipeline behaviour since it induces the formation of plastic hinges far away from the fault intersection: in this way the flexural deformations are strongly reduced;

- the role of the embedment depth, that should be kept to a minimum in crossing fault zones;
- the improved pipe behaviour for increasing cross-sectional thickness: it is to be noted that, according to the EC8 prescription, the allowable compressive strain is always attained due to the local buckling limit [0.2 t/R] for t/R < 0.05.

4.5 VULNERABILITY FUNCTIONS FOR EMBEDDED PIPELINES AND SHALLOW TUNNELS SUBJECTED TO TRANSIENT GROUND MOTIONS

4.5.1 Pipelines

The basic empirical fragility relations for the estimation of pipeline damage are summarized for the case of wave propagation in Table 4.6, where RR is the repair rate referred to 1 Km length of the pipeline. A comparison between the different fragility relations is given in Figure 4.16 and Figure 4.17.
A validation of the most commonly used fragility curves was made on the observed damage to the Düzce potable water network as result of Düzce earthquake [Alexoudi M, 2005]. The O'Rourke & Ayala correlation [1993] gives the most reliable results both in amount of damage and in spatial distribution. The same pattern was also observed in Lefkas potable water network. ALA [2001a,b] underestimates the failures as result of wave propagation while Isoyama [1998], gives failure rate in the average of ALA [2001a,b] & O'Rourke & Ayala [1993].

O'Rourke & Deyoe E [2004] proposed fragility curves that correlate PGV with RR/km. They distinguish the damage caused by R and S waves (see Table 4.7).

Moreover, as repeatedly mentioned, O'Rourke & Deyoe E [2004] propose a fragility curve that linearly connects ground strains with R.R. in the case of wave propagation (Table 4.8).

For the calculation of the ground strains, O'Rourke & Deyoe E [2004] suggested to use Newmark [1967] & Yeh [1974] simplified procedures, see the previous discussion in par. 2.1.2. The pipe damage is directly connected with the wave type on the wave propagation. The authors in question use a simple criterion to establish the wave type and the ground strains:

$$\text{If } \frac{epicentral\_distance}{focal\_depth} \geq 5 \Rightarrow \varepsilon_R = \frac{V_{\max}}{C_R} \text{ [R waves]} \tag{4.2}$$

Where: $V_{\max}$: maximum horizontal particle velocity due to surface R waves, C_R: phase velocity of the *R* waves. According to O'Rourke & Deyoe a reasonable assumption of C_R=500m/s can be made.

$$\text{If } \frac{epicentral\_distance}{focal\_depth} < 5 \Rightarrow \varepsilon_S = \frac{V_{\max}}{2 * C_S} \text{ [S waves]} \tag{4.3}$$

Where: V_{max}: peak horizontal particle velocity due to S waves, C_S: apparent propagation velocity of S waves with respect to the ground surface, ε_s: ground strain in the horizontal plane, along a 45° line with respect to the direction of propagation. According to O'Rourke & Deyoe a reasonable assumption of C_R=3000m/s can be made.

A very recent comprehensive analysis of both observed and numerically simulated data [Paolucci, 2007] shows that an overall satisfactory fit is provided by the expression:

$$\varepsilon_S\,(=PGS)=\frac{PGV}{1300} \tag{4.4}$$

4.5.2 Shallow tunnels: improved vulnerability curves

So far the vulnerability assessment of tunnels has been mainly based on empirical fragility curves [NIBS, 2004, ALA, 2002], derived from actual damage in past earthquakes all over the world. A simplified approach for the development of improved analytical vulnerability functions due to ground shaking is presented, considering the distinctive features of the geometry and strength capacity of the tunnel, the local soil conditions and the input ground motion characteristics. The obtained fragility curves are compared with corresponding empirical ones.

4.5.2.1 *Tunnel and soil model*

The proposed numerical approach is applied to two typical shallow tunnel cross sections, a circular one [bored] with diameter equal to 10m and a rectangular one [cut & cover], with dimensions 16 x 12m. The geometrical and technical characteristics are selected based on similar cross sections of the Athens Metro. The upper surface of both tunnels is considered to be at a depth of 10m. Three typical ground profiles are selected, corresponding to categories B, C and D according to Eurocode 8 [EC8].

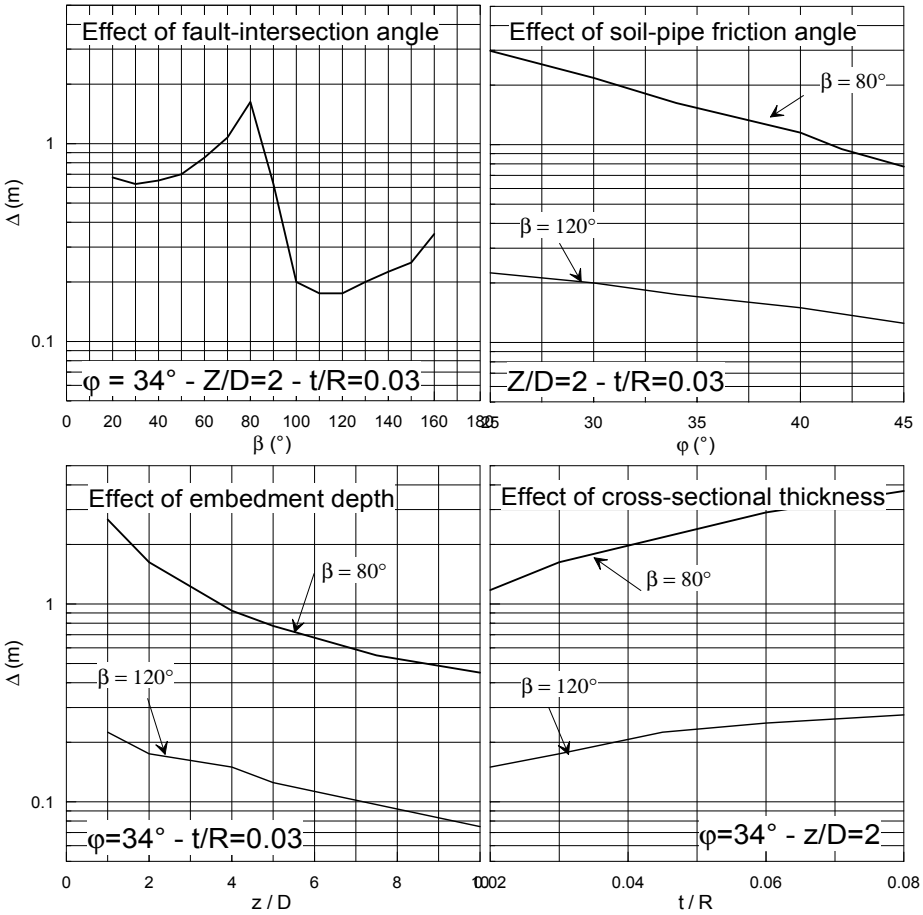

Figure 4.15: Results of parametric analyses on a continuous pipeline subject to fault rupture, as a function of a] the angle β between the pipe axis and the fault surface trace; b] the pipe-soil interface friction angle; c] the embedment depth z of the center of the cross-section, normalized by its external diameter D; d] the cross-sectional thickness t, normalized by the external radius R = D/2.

Table 4.6: Empirical relations for seismic damage [R.R/km] of pipelines related to wave propagation

Empirical relation	Influence parameters	Reference
R.R/km.= $1.698*10^{-16}*PGA^{6.06}$	PGA [g] Cast iron	Isoyama & Katayama [1982]
R.R/km. =K [$0.0001*PGV^{2.25}$]	PGV [cm/s] K: indicator depending on pipe material [ductile, brittle]	O' Rourke & Ayala [1993]
R.R/km =$0.0012*PGV^{0.7677}$ R.R/km =$0.0006*PGV^{1.5542}$ R.R/km =$6*10^{-5} * PGV^{2.2949}$	PGV [cm/s] Material: asbestos-cement, cast-iron, welded steel.	Eidinger [et al. 1995], Eidinger [1998]
R.R/km.= $Cp*Cd*3.11*10^{-3}*$ [PGV-15]$^{1.3}$	PGV [cm/s], Cp & Cd: indicators depending on pipe material and diameter	Isoyama [1998]
R.R/km. = $101.25\log_{10}$[PGA-0.63]	PGA [cm/s^2]	O'Rourke et al [1998]
R.R/km= $0.050*[v_{scaled}]^{0.865}$, v_{scaled} = PGV/ $Do^{1.138}$	PGV [cm/s]: Do[cm]: diameter	O'Rourke & Jeon [1999]
R.R/km. = K1*1.512*[$PGV^{1.98}$]	PGV [m/s] K1: indicator depending on pipe material and joint type, diameter and soil conditions	Eidinger, Avila E [1999]
R.R[X] = Bp*Bd*Bg*BL*Ro[X], Ro[X] = a*[X-Xmin]^b R.R[X] = 2.88*10-6*[PGA-100]$^{1.97}$ & R.R[X] = 3.11*10-3*[PGV-15]$^{1.3}$ Cast iron pipes	R.R[X]: RR/km Bd, Bg, BL: indicators diameter , soil conditions Ro: RR for cast-iron pipes in no liquefied soils a, b: indicators Xmin: PGA or PGV	Isoyama et al [2000]
R.R/km. =K1* 0.241*PGV	PGV [m/s] K1: indicator depending on pipe material and joint type, diameter and soil conditions	ALA [2001]

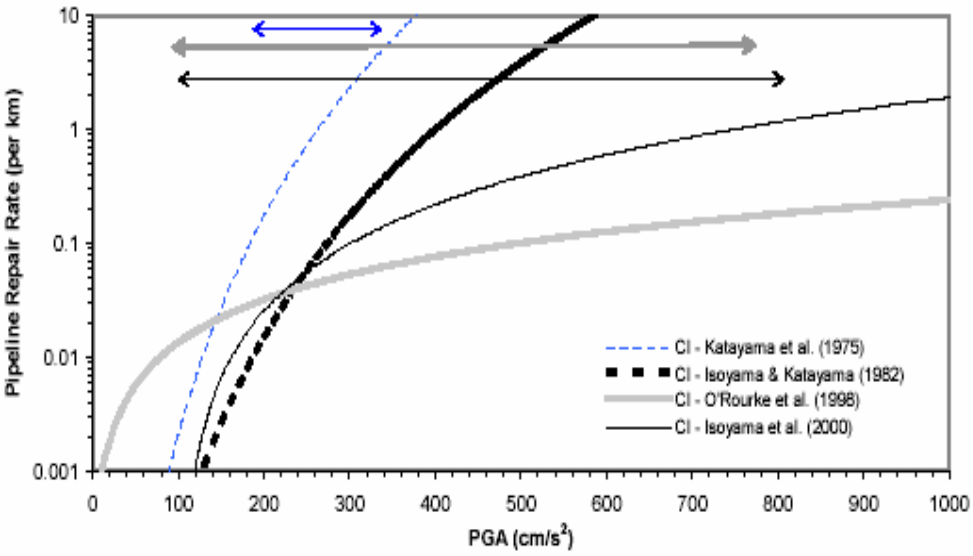

Figure 4.16: Comparison of empirical fragility relations for pipes in terms of PGA [cm/s²]- [Tromans J, 2004]

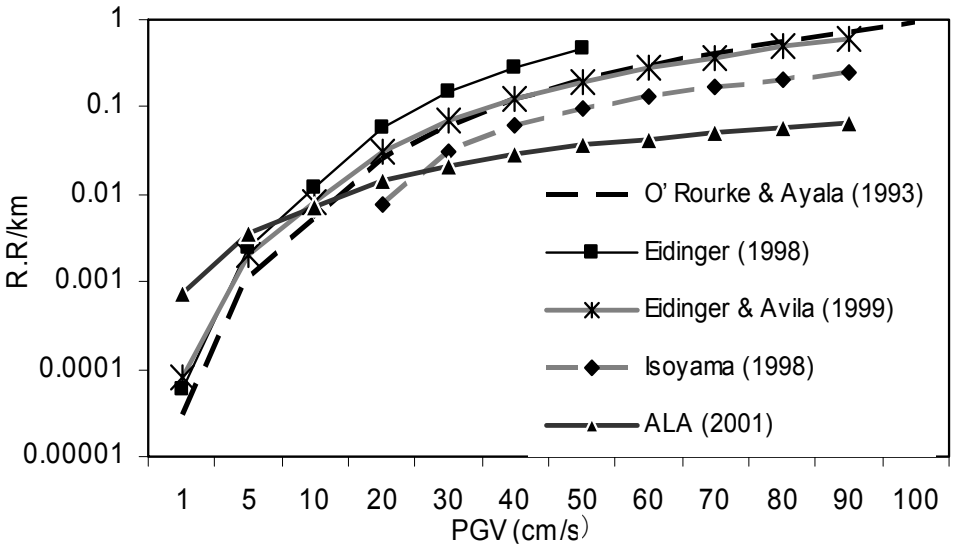

Figure 4.17: Comparison of empirical fragility relations for pipes in terms of PGV [cm/s]- ductile pipes [Pitilakis et al, 2003].

Table 4.7: Fragility curves for pipes [wave propagation- O'Rourke & Deyoe E, 2004].

Empirical relation	Influence factors	Reference
$R.R._R = k1*0.034*PGV^{0.92}$ (Rayleigh waves)	PGV [cm/s] Brittle pipes, k1=1.0, RR_R:surface wave repair rate waves/km	O'Rourke & Deyoe E [2004]
$R.R._S = k1*0.0035*PGV^{0.92}$ (S-waves)	PGV [cm/s] Brittle pipes, k1=1.0, RR_S: body wave repair rate waves	O'Rourke & Deyoe E [2004]

Table 4.8: Fragility curves for pipes in the case of wave propagation - RR/km versus strains- [O'Rourke & Deyoe E, 2004].

Empirical relation	Influence factors	Reference
$R.R. = k1*513*\varepsilon^{0.89}$	ε: (longitudinal) ground strain k1 = 1 for brittle pipes 0.3 for ductile pipes	O'Rourke & Deyoe E [2004]

4.5.2.2 *Ground motion characteristics and soil response analysis*

Real records from five different earthquakes were used as input motion in outcrop conditions: [a] Kozani [T], Greece, Mw=6.6, 1995, [b] Athens [Kypseli-L], Greece, Mw=5.9, 1999, [c] Montenegro -[TRA (EW)], former Yugoslavia, Mw =6.9, 1979 [d] Palm Springs [wwt], USA, Mw=6.0, 1986, [e] Kocaeli [Gebze-NS], Turkey, Mw=7.4, 1999. The selection was based on the facts that the soil conditions of the recording stations are similar to soil class A of EC8 and the shape of the acceleration response spectra is close to the one of EC8 for soil class A. The selected time histories are scaled to 0.1, 0.2, 0.3, 0.4, 0.5 and 0.6g in order to calculate at next step the stresses in the tunnel due to an increasing level of seismic intensity.

The earthquake response of the soil profile is calculated using the code CyberQuake [2000] taking into account the inelastic behavior of the soil. For each analysis the time that the shear strain in tunnel takes the maximum value [top-base of tunnel] is defined. At this time, the displacements of each soil layer are estimated from the corresponding displacement time histories of each analysis. These seismic ground deformations versus the depth will be imposed at the boundaries of a plane strain ground model including the tunnel structure. Moreover, the peak ground acceleration values on the surface are defined as they will be the main index to correlate the tunnel damage and define accordingly the fragility curves.

4.5.2.3 *Tunnel response analysis*

A plane strain ground model and the tunnel cross section are analysed using the Plaxis finite element code [Plaxis, 2002]. The analysis starts with the definition of the initial conditions and continuous with the staged construction of the tunnel and the calculation of the stresses under static loading. The shear deformations that were calculated in the previous step are imposed on the boundaries of the plain strain model. Therefore, stresses and deformations of tunnel lining can be calculated due to the shear distortion of the surrounding ground.

4.5.2.4 *Development of fragility curves*

In this application the fragility curves are represented as a two-parameter [median and log-standard deviation] lognormal distribution functions.

A damage index [DI] is introduced as the ratio of the developing moment [M] to the moment resistance [MRd] of the tunnel lining. In this way it is possible to establish a relationship between the damage index [M/MRd] and PGA at the surface for each model. Based on previous experience of damage and in engineering judgment three different damage states are considered concerning minor, moderate and extensive damage in tunnel lining, which are defined according to the variation of the damage index. It is noted that the limits of the damage index dot not represent the exact values of the appearance of damage as there are many parameters that are involved in the concrete and reinforcement of the lining, however the present assumption could give a representative and qualitative view for the expected damage states.

The median values of peak ground acceleration that correspond to each damage state can be defined as the value that corresponds to the mean damage index based on the mean curve of the damage index-PGA relationship. The standard deviation values [β] describe the total variability associated with each fragility curve. Three primary sources contribute to the total variability for any given damage state [NIBS, 2004], namely the variability associated with the discrete threshold of each damage state, the capacity of each structural type and the earthquake ground motion. The uncertainty in the definition of damage state is assumed to be equal to 0.4 [similar to HAZUS for buildings] and the variability of the capacity is assumed to be equal to 0.3 [BART system for bored tunnels, Salmon et al., 2003]. The last source of uncertainty associated with seismic demand, is taken into consideration by calculating the variability in the results of inelastic dynamic analyses carried out for the 30 input motions at each level of PGA in bedrock. The total uncertainty is estimated as the root of the sum of the squares of the component dispersions. Figures 4.18 – 4.21 illustrate the fragility curves that have been derived in this study for minor and moderate damage for the three soil types, together with the respective empirical curves of HAZUS [NIBS, 2004] and ALA [2001].

It may be seen that the level of damage probability with respect to PGA varies between the analytical fragility curves of this study and the empirical ones. The empirical curves were derived based on data from past observations [ALA] and expert judgement [HAZUS], without taking into account the soil conditions. However, the results of the analyses show that the role of the soil type is very important for the estimation of tunnel's response under seismic loading and subsequently for the derivation of the appropriate fragility curves. The comparison between the available empirical curves and the proposed ones shows a trend that the analytical ones "envelop" the empirical curves, which means that the later express an average performance of the tunnels. Nevertheless, the empirical curves are referring to all possible type of tunnel damage that may occur during a strong earthquake, including for example damage in the longitudinal axis and not only in the transversal direction.

Of course with the parametric analysis of the specific problem is impossible to take into account all the factors that are involved and to quantify through the fragility curves their contribution to the seismic vulnerability with the most reliable way. In the framework of the present study it is attempted to study the role of the most important parameters to the vulnerability of shallow tunnels, such as the soil type [B, C, D /EC8], the tunnel section type [circular/bored, rectangular/cut & cover] and the seismic motion [5 different accelerograms scaled in 6 levels of PGA]. In addition, the uncertainties that are associated with this kind of approach are taken into account for the construction of the fragility curves. The proposed approach includes several considerations concerning the soil profile, the method of analysis and the input motion. Moreover, reasonable hypotheses were made in the definition of damage index, damage states and beta values, minor modification of which can alter the results. These assumptions are made due to the complex nature of the seismic fragility problem. Besides, the purpose of the fragility curves is to make a preliminary assessment of the structure response for different seismic scenarios in order to define the seismic risk of the transportation components and the entire network.

4.6 IS RELIABILITY ANALYSIS

Not treated herein are methods for seismic reliability analysis of IS, notably the water distribution system, because they are still mainly used in the research domain. In the general approach assumed in this report, the seismic impact on spatially distributed networks is evaluated site by site trough superposition of shaking and vulnerability (exposure) maps, as in the HAZUS [National Institute of Building Sciences, 2004] methodology. On the other hand, in a network the damage occurring at a point can significantly affect the operation of the balance of the system, in a way that strongly depends on the system architecture. In the latter perspective, in the past both connectivity and capacity approaches have been used; a very recent method of the network capacity type for water distribution systems has been proposed by [Rasulo et al., 2007] with an application to the city of Düzce.

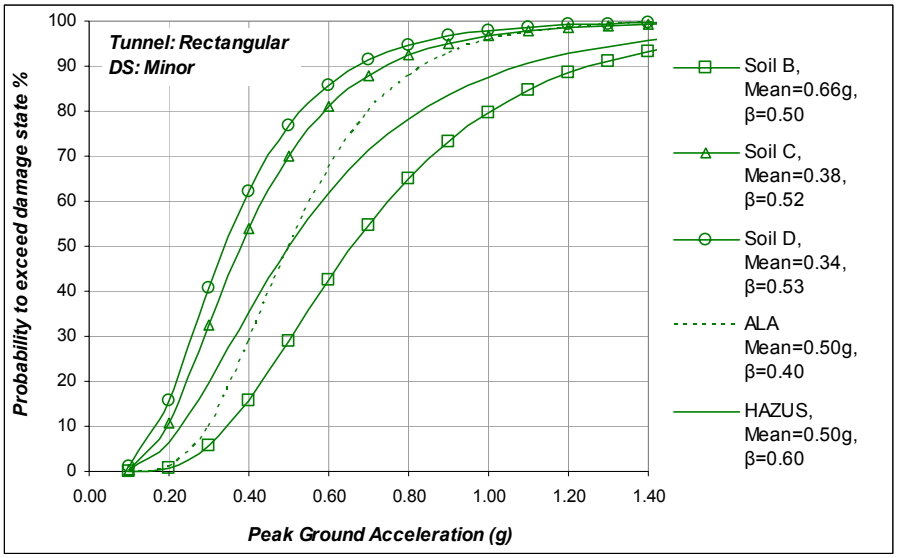

Figure 4.18: Fragility curves of rectangular cross-section for minor damage and for three soil classes.

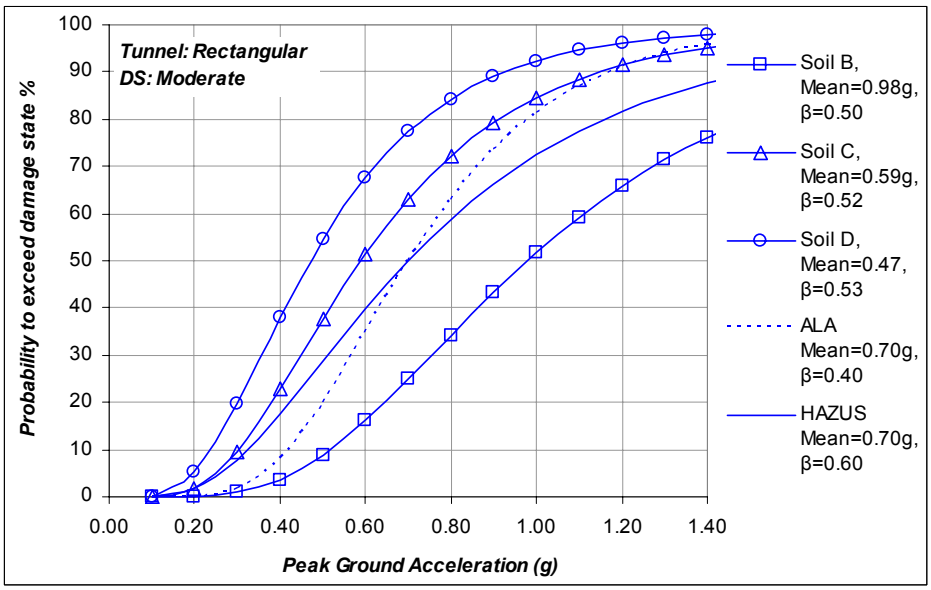

Figure 4.19: Fragility curves of rectangular cross-section for moderate damage and for three soil classes.

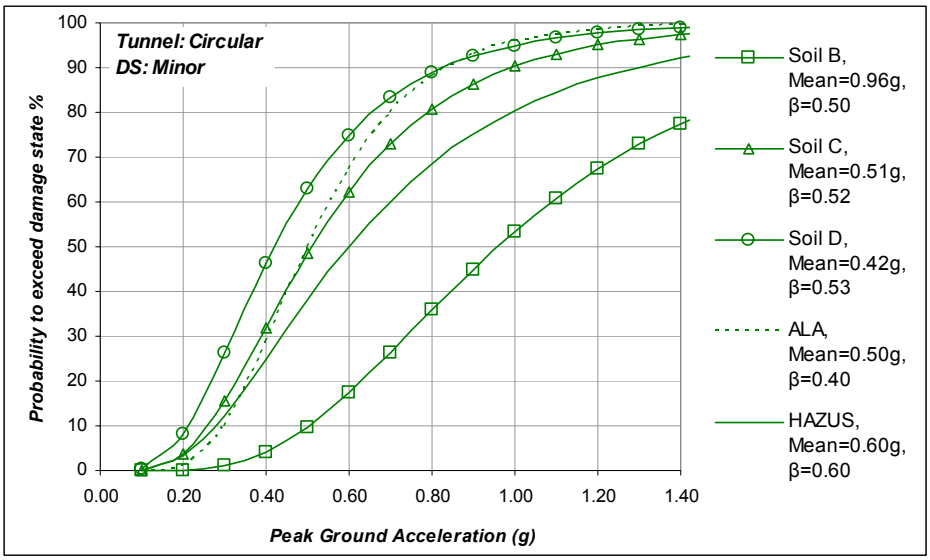

Figure 4.20: Fragility curves of circular cross-section for minor damage and for three soil classes.

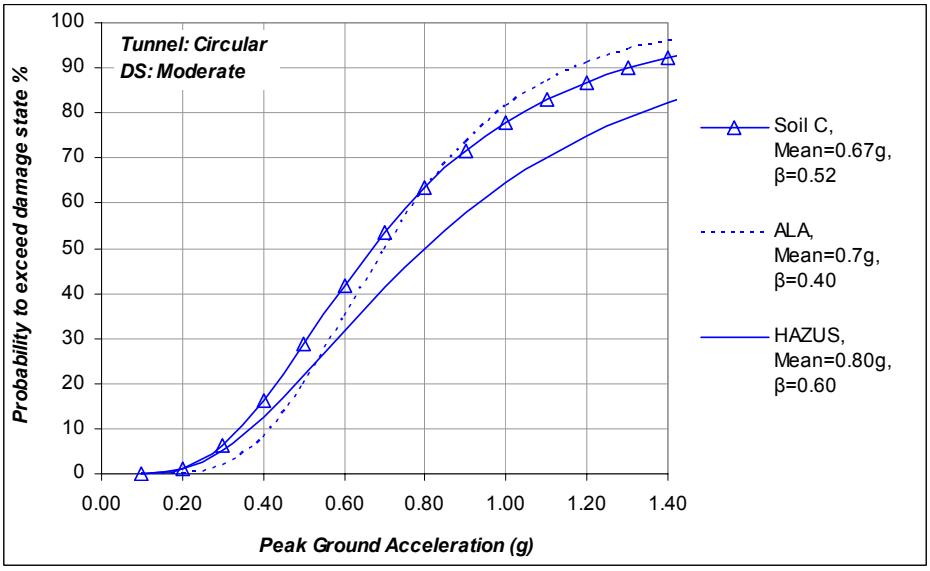

Figure 4.21: Fragility curves of circular cross-section for moderate damage in soil class

5.EXAMPLES OF INFRASTRUCTURAL SYSTEMS (IS) INVENTORIES AND REPRESENTATIONS

5.1 INTRODUCTION

The description and inventory of various ISs considered in LessLoss SP11, using a reasonably uniform format, may be found in Deliverable D88 [2006]. There were significant differences in the amount and quality of the data available for each city and even for the different lifeline systems for the same city. These differences are widespread in Europe, and are bound to have a bearing on the quality and approximation of the seismic damage scenarios. Some of these differences arise from the different limitations imposed in different cities for obtaining the data from the agency in charge of the IS of interest. There seems to be a significant effort in many cities to establish GIS databases for all the infrastructural networks.

This section presents examples of the inventory of selected ISs in Thessaloniki, and Düzce, the ISs in question include the pipeline distribution networks of natural gas, potable water and waste water. An inventory CD including GIS based information and data for the ISs of the reference cities (including also Istanbul and Catania) was given as Appendix to D88. The reference city data were provided by the partners involved in SP11.

5.2 FEATURES OF THE ISS IN THESSALONIKI

5.2.1 General

The activities of Thessaloniki expand in Europe, Balkan and East Mediterranean countries. The urban area of Thessaloniki (Area of the city = 13130Ha, 1991) consists of 17 districts (Figure 5.1, Figure 5.2), the most important being the municipality of Thessaloniki (Density: 216 people/ Ha), which includes the historical city centre, the old town, the International Trade Fair, and the two University campuses. The whole urban area lies on three main large-scale geology structures, oriented in NW-SE direction. The first formation includes the metamorphic substratum consisting of gneiss, epigneiss, and green schists, which reach the surface at the NE border of the urban area. These crystalline rocks constitute the bedrock basement beneath the city reaching a depth of 150-300m near the coastline in W-WS direction. The second formation consists of alluvium deposits, mainly of the Neogene period. In this geological formation the red silty clay series is dominant, covering the bedrock basement beneath the city. Finally,

recent deposits of Holocene clays-sands-pebbles compose the third surface formation. The geotechnical map (Figure 5.3) describes the spatial distribution and the thickness of each soil formation; nine (9) different soil formations are needed to fully describe the subsoil conditions in the city (Table 5.1).

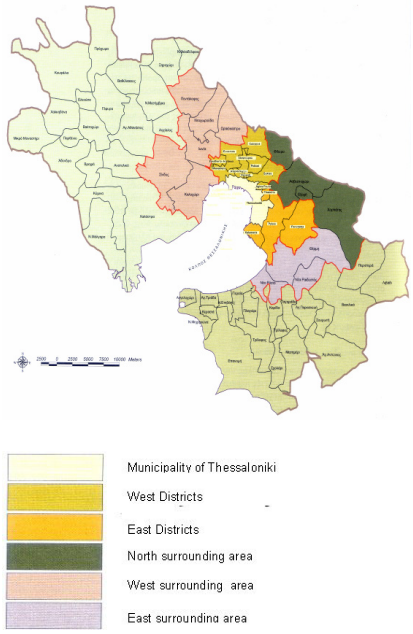

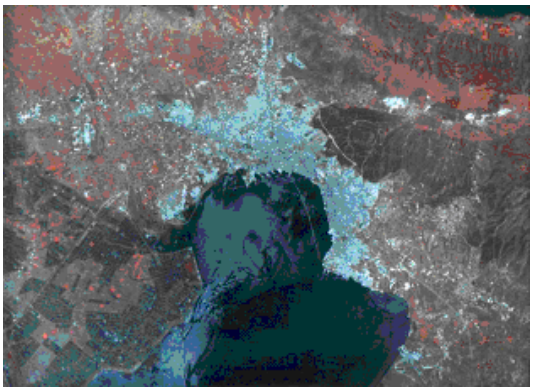

Figure 5.1: ***Urban area of Thessaloniki*** **Figure 5.2*: Satellite photo of Thessaloniki (1987)***

Table 5.1 Dynamic properties of the main soil formations in the Thessaloniki urban area. The values in brackets are the mean of Vs velocities and quality factors Qs.

Formation	Description		V_S (m/s)	V_P (m/s)	Q_S
(1)	(2)		(5)	(6)	(7)
A	*Surficial*	Artificial Fills, demolition materials & debris parts	200-350 (250)	400-1700	8-20 (15)
B1		Very Stiff sandy-silty clays to clayey sands, low plasticity	300-400 (350)	1900	15-20 (20)
B2		Soft sandy-silty clays to clayey sands, low to medium plasticity	200-300 (250)	1800	20-25 (20)
B3		Stiff to hard high plasticity clays	300-400 (350)	1800	20-40 (30)
C		Very soft buy mud and silty sands	120-220 (180)	1800	20-25 (25)
D		Alluvium deposits, sandy-silty clays to clayey sands-silts, low strength and high compressibility	150-250 (200)	1800	15-25 (20)
E	*Subbase*	Stiff to hard sandy-silty clays to clayey sands	350-700 (600)	2000	6-30 (30)
F		Very stiff to hard low to medium plasticity clays to sandy clays,overconsolidated with rubbles and thin layers of gravels	700-850 (750)	3200	50-60 (60)
G		GreenSchists & Gneiss	1750-2200 (2000)	4500	180-200 (200)

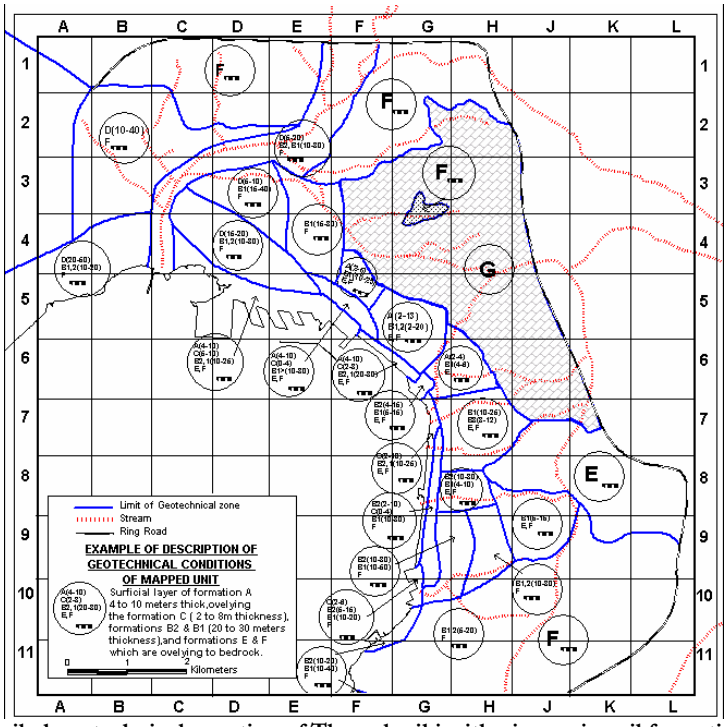

Figure 5.3: detailed geotechnical zonation of Thessaloniki with nine main soil formations (A, B, C, D, E, F, G) and respective ground layering [Anastasiadis et. al., 2001].

Gas distribution system. The Thessaloniki natural gas distribution system includes transmission pipes (19bar), 2 City Gate Stations, and a distribution network of 4bar. In the city there are several Metering and Regulation Stations (M/R stations) and M/Rs for providing gas in large industrial units. Each station reduces the pressure of gas from 19 to 4bar and it interrupts its operation in case of emergency (SCADA system). The urban transmission and distribution networks include steel pipes for 19bar maximum supply pressure (90km length) and PVC gas pipes for 4bar supply pressure (210km). The architecture of the network is designed to be separated into sectors through the closure of valves. Isolation valves are located along distances smaller than 3km, while their diameter has been calculated in order to allow for the system's decompression in less than 15min. At least 2 regional M/R stations are located in each sector for the reduction of pressure from 19 to 4 bars. They ensure the flow and quality of gas and permit the regular maintenance services to take place. M/R stations have a capacity of 5000Nm^3/h and include 2 lines (main and emergency), detonation and shut-off valves. The design of urban transmission and distribution natural gas systems has been made for district category 4 (areas with high-rise buildings, heavy traffic and numerous underground lifeline systems). Gas pipelines, according to the guidelines, are located 0.40m from telecommunication wires and non-metallic conduits for fuel products, 0.50m from

electric power wires and metallic conduits for non-fuel products and 0.60m from conduits for fuel products. Pipes' connections are made through welding. The pipes are buried at 1.10m depth, over a thick layer of sand. An appropriate system of cathodic protection is also used to avoid erosion. The pipe diameters are calculated so as to allow the supply of gas to at least 75% of domestic consumption and 100% of industrial consumption (except from the ones with capacity > 500Nm^3/h) in case of inoperability of one of the two M/Rs (Ricciardi, 2002).

Sewage network. The first systematic construction of sewage facilities in Thessaloniki started after the destructive fire of 1917. Several expansions of the system followed in the decade of 1928-1938. The recent interventions in the sewage system started in 1977, the most important being the construction of the Central Sewage Tunnel (CST or KKA). Between 1976 and 1996, 497 Km of wastewater pipelines were constructed.

The major components of Thessaloniki sewage system are:

- The Central Sewage Tunnel (CST or KKA). Its total length is 15800m and it is connected with the city's sewage network since December 1990. The CST's mean diameter is 2700mm while its depth varies between 10m and 30m. It has been expanded to the Municipality of Thermi.
- The coastline connectors to the CST. The system of coastline connectors comprises the conduits of the 4 coastline zones, which include the main collection sewers, the manholes and 5 pumping stations. Interceptors and a spillover conduit, which flows underwater, have also been constructed.
- The sewage network of low-lying areas of Thessaloniki's west districts. It includes 10866m conduits and 4 pumping stations that are connected with the CST.
- The waste-pressure conduit of Axios-Gallikos. It consists of a "twin" pipe from the wastewater treatment station to the exit manhole to Axios River, with a total length of 12297m. From the exit manhole to the Axios River and for a 1000m length, it is an open dike.
- The flood-preventing facilities in the area of Dendropotamos.
- The wastewater treatment facilities of Thessaloniki's industrial zone. They have a treatment capacity of 40000 m^3 of disposals per day (almost the 1/3 of Thessaloniki's urban disposals). Their daily flow is 160000-180000m^3 (equal to the 95% of Thessaloniki's urban disposals).
- The collection sewer of touristic districts (CST of the municipality of Peraia).
- The wastewater treatment facilities of tourist districts with a treatment capacity during the first stage equal to 29000m^3/day.

The Thessaloniki wastewater system includes a network of rainstorm water, mixed water and waste disposals. The major part of the system includes gravity pipes with an exception of the pressure pipes that start from the pumping stations in the coastline of Thessaloniki to the Central Sewage Tunnel (CST or KKA). It is comprised of open

conduits, dikes, small pipes, large pipes, pumping stations, wastewater treatment plants, stream projects, antilittering facilities and oxygen infusion facilities. Almost 200000 consumers are served from 33000 connections, while the wastewater pipes length is about 1250km. The size of the area served is 80km^2.

The sewage network area operated from Thessaloniki Water and Waste-Water Company (EYATH) is illustrated in Figure 5.4. The digitized sewage network has gaps in several points due to lack of information concerning the existence and geographic location of pipes. Information like material, diameters and age are missing in many cases as well. The components of the wastewater network are given in Figure 5.5.

Figure 5.4 Area of the sewage network operated from Thessaloniki's Water and Waste-Water Company (EYATH).

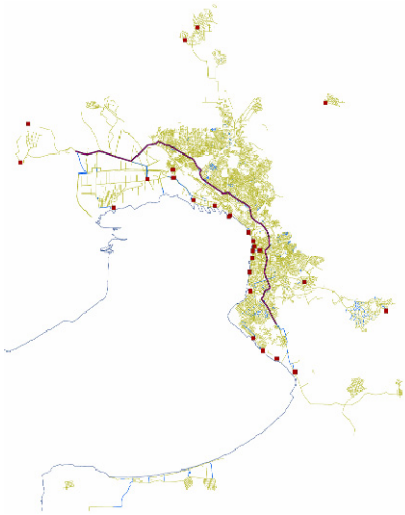

Figure 5.5. The Thessaloniki sewage system.

Wastewater treatment plants in the sanitary sewer system are complex facilities, which include a number of buildings and underground or on ground reinforced concrete tank and basins.

Potable water distribution system. The Thessaloniki main water sources include underground springs, wells and rivers, with total flow varying between 156000 – 285000 m^3/day. Water treatment facilities are located in three central pumping stations. There are also pre-chlorination units in one sedimentation tank and the wells of Narres. The potable water system (including the one serving the industrial area of the city) includes 20 tanks in use nowadays, with a total capacity of 91900m^3. There is also one sedimentation tank with a capacity of 8000m^3 as well as tanks used for fire-fighting purposes with a total capacity of 2100m^3. The larger tank in use has a capacity of 10000m^3. The distribution system is about 300km long. Through pumping stations, the water is supplied to consumption using steel pressure pipes. The latter have a total length of 71Km. The distribution network has a total length of 1284km. It has a supply capacity varying between 280000m^3 and 240000m^3/day. The water connections in urban area of Thessaloniki are about 420.000 (99% common customers), while the served population is 1.000.000people. The needs for water consumption are about 250.000m^3/day. The size of the area served is 55km^2 and the elevation ranging between 0 and 380m. The pressure in the internal network varies between 2-5bar. The potable water network area operated from Thessaloniki's Water and Waste-Water Company (EYATH) is illustrated in Figure 5.6.

Figure 5.6. Area of the potable water network operated from Thessaloniki Water and Waste-Water Company (EYATH).

Two municipalities of Thessaloniki's greater urban area (Themri and Thermaikos) are served by independent networks. They have separate water sources, tanks and pumping stations to cover the needs for water pressure and fire-fighting. The pipelines are mostly PVC.
The water sources, pumping stations, tanks, conduits and buildings facilities are incorporated into the GIS database.

5.2.2 Specific properties and descriptions

The description of the database fields is provided for each system and subcomponent. The database has been developed in the Greek Grid '1987 geodetic co-ordinate system (GGRS 1987) using the software ArcGIS 9 (of ESRI).

5.2.2.1 *Natural Gas Network*

The Thessaloniki gas system, transmission and distribution, includes: City gate stations, M/R stations 19/4 bar, steel pipes with pressure of 19bar and PE pipes with pressure of 4bar. Nowadays, the gas network is in progress and it has 90km of steel pipes for the constant supply (19bar), 2-City gate stations and 210km of PE pipes (4bar).
High-pressure steel pipes (19bar) have welded-type connections. Their diameters vary from 100-250mm and their thickness from 4.37mm-5.56mm respectively. Pipes' yield strength is 241MPa, tensile strength is 414MPa and their elongation is 0.02. The 19bar gas system has been constructed in year 1996.
Pipes with pressure of 4bar have arc-welded connections. Their diameters are 160 and 125mm and their thickness 14.6mm and 11.4mm respectively. Pipes' yield strength is 8MPa, tensile strength is 34MPa and their elongation is 0.02. The distribution gas system has been constructed in year 1999.
The database of the natural gas system is not provided herein due to restrictions by the gas company for public availability.

5.2.2.2 *Sewage Network*

Large Diameter Pipes / Tunnels

The description of the fields in the GIS database for the Central Sewage Tunnel (CST), see Figure 5.7, the pressure pipes and the gravity pipes are available in Deliverable D88 and will not be repeated herein.
The Central Sewage Tunnel (CST) has a total length of 19.7km and it is made exclusively of concrete. The CST's diameters vary from 1800 to 2700mm and its depth from 3 to 30m. Its cross section type is generally circular.
Collection sewers (gravity or pressure pipes) are connected to the CST. Distribution conduits are exclusively gravity pipes. In the most cases, there is no information about the year of construction of sewage gravity pipes. About 97% of the sewage pipeline network consists of wastewater pipes while the rest 2% are Rainstorm and Mixed pipes

(1%). The larger percentage, as expected, are secondary waste-pipes (70%) while the rest are primary pipes.
The Thessaloniki's sewage network includes 28 pumping stations, 27 from which are waste stations and 1 is rainstorm station.

5.2.2.3 *Water Supply Network*

Pumping Stations and Tanks

The GIS database for Tanks is illustrated in Figure 5.11.
Tanks in Thessaloniki are made of concrete with concrete roofs with the exception of one masonry tank. Their year of construction generally varies. Tanks are usually 50-70% full, while the distribution of their capacity, shape is illustrated in the following figures. Their height alter between 2.5 – 35m.

Buried conduits
The field database for water distribution pipes is illustrated in Figure 5.14. A significant percentage of water pipes has unknown year of construction (70%), thus preventing the assessment of the existence or not of specific design provisions regarding their material or construction techniques. Besides, a substantial part of water pipes has unknown material of construction and quite significant is the percentage of water pipes of unknown diameter. This situation is rather common in European cities of the Mediterranean region.

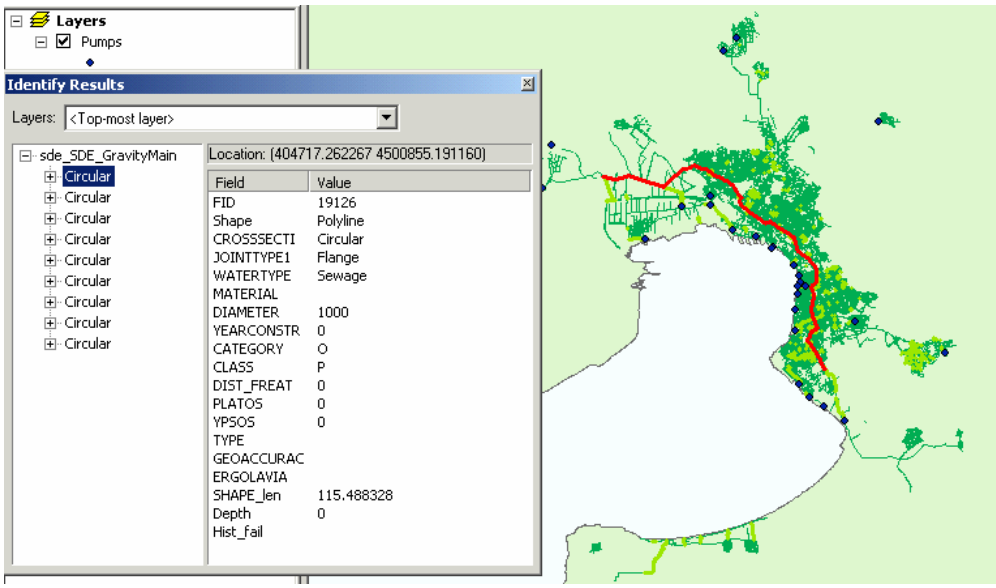

Figure 5.7: Thessaloniki sewage network (Elements: CST, pressure pipes, gravity pipes, pumping

stations). Database for gravity pipes

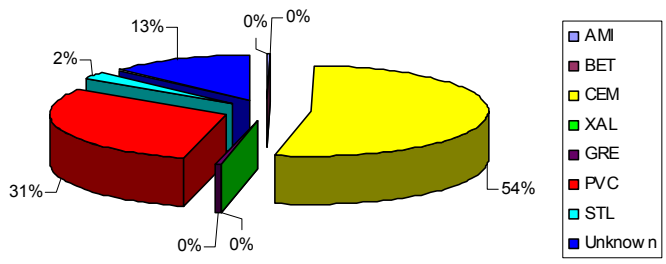

Figure 5.8 Percentage distribution of Thessaloniki's sewage gravity pipes based on their material

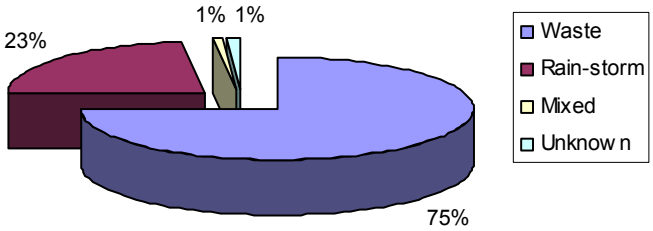

Figure 5.9. Percentage distribution of Thessaloniki's sewage gravity pipes based on their type

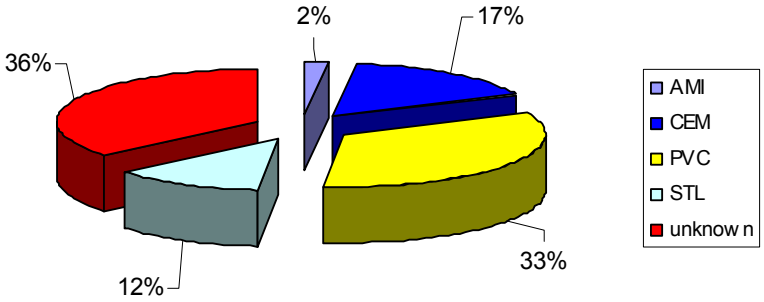

Figure 5.10. Percentage distribution of Thessaloniki's sewage pressure pipes based on their material

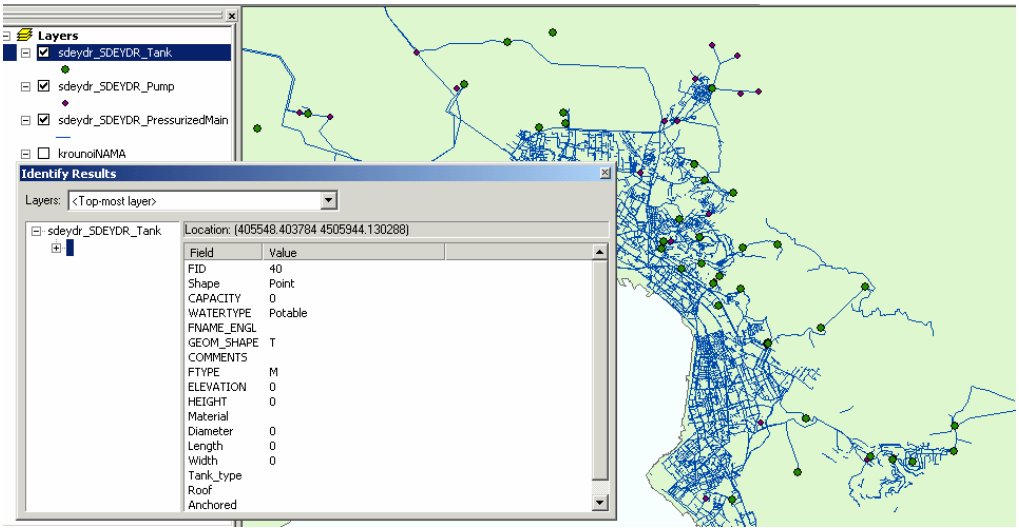

Figure 5.11: Thessaloniki's potable water system (Elements: pressure pipes, pumping stations, tanks). Database for tanks

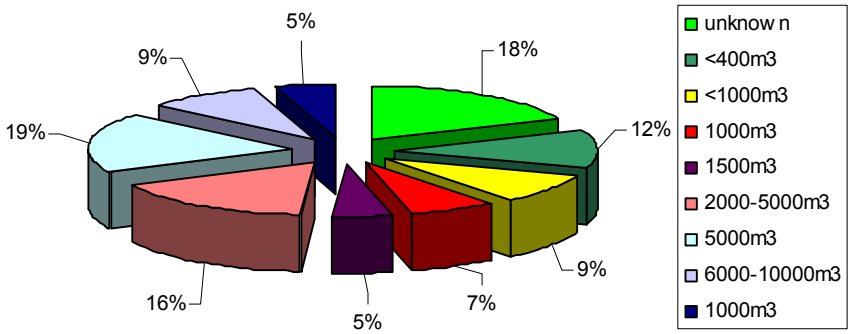

Figure 5.12. Percentage distribution of Thessaloniki's potable water tanks based on their capacity

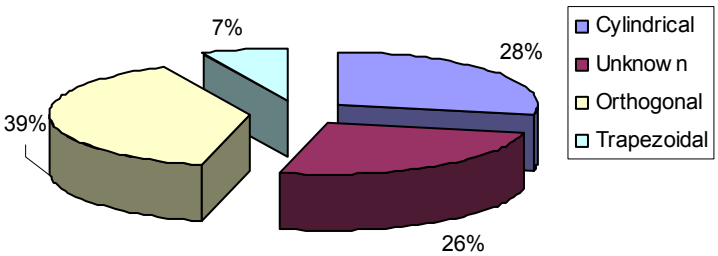

Figure 5.13. Percentage distribution of Thessaloniki's potable water tanks based on their shape

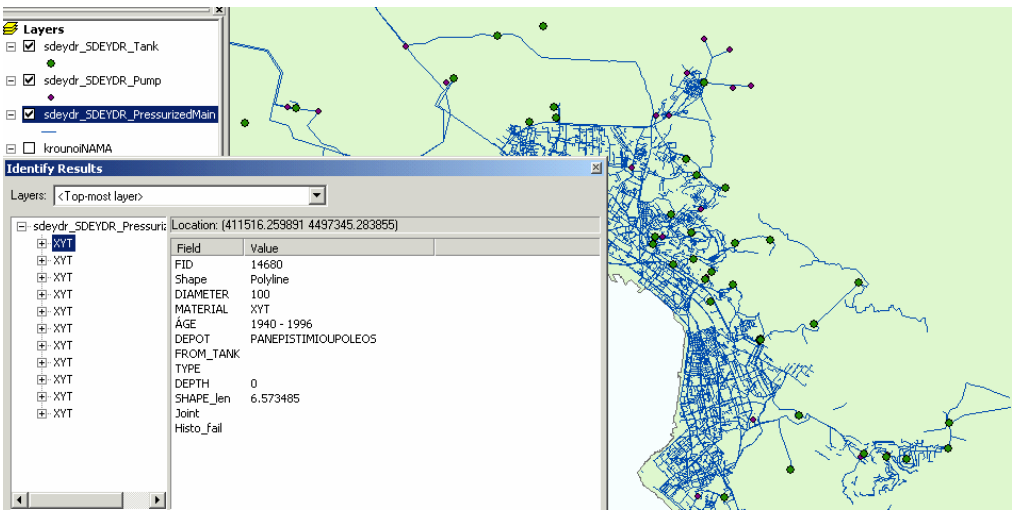

Figure 5.14: Thessaloniki's potable water system (Elements: pressure pipes, pumping stations, tanks). Database for water pipes

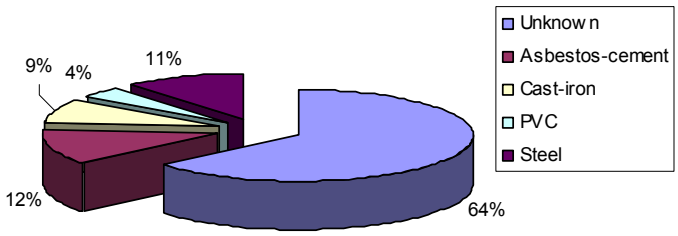

Figure 5.15 Percentage distribution of Thessaloniki's potable water pipes based on their material

5.3 OUTLINE OF FEATURES AND DESCRIPTIONS OF THE ISS IN DÜZCE

5.3.1 Sewage network

The sewage network of the city of Düzce is illustrated in Figure 5.16. Apart from the general layout, no information is available regarding pipe materials, diameters or depth.

5.3.2 Water distribution network.

The Düzce water distribution system is shown in Figure 5.17 where the red segments indicate the pipe sections where damage occurred during the Kocaeli and Düzce (August and November 1999) earthquakes. Reference is made to par. 4.2.1 for further damage description.

The data available for each network segment in a geodatabase (GIS) format include:

- Pipe diameter, mm
- Material (i.e. asbestos, pvc, steel)
- Length of the segment between connections or endings
- Burial depth in m.
- Damage flag (yes/no info).

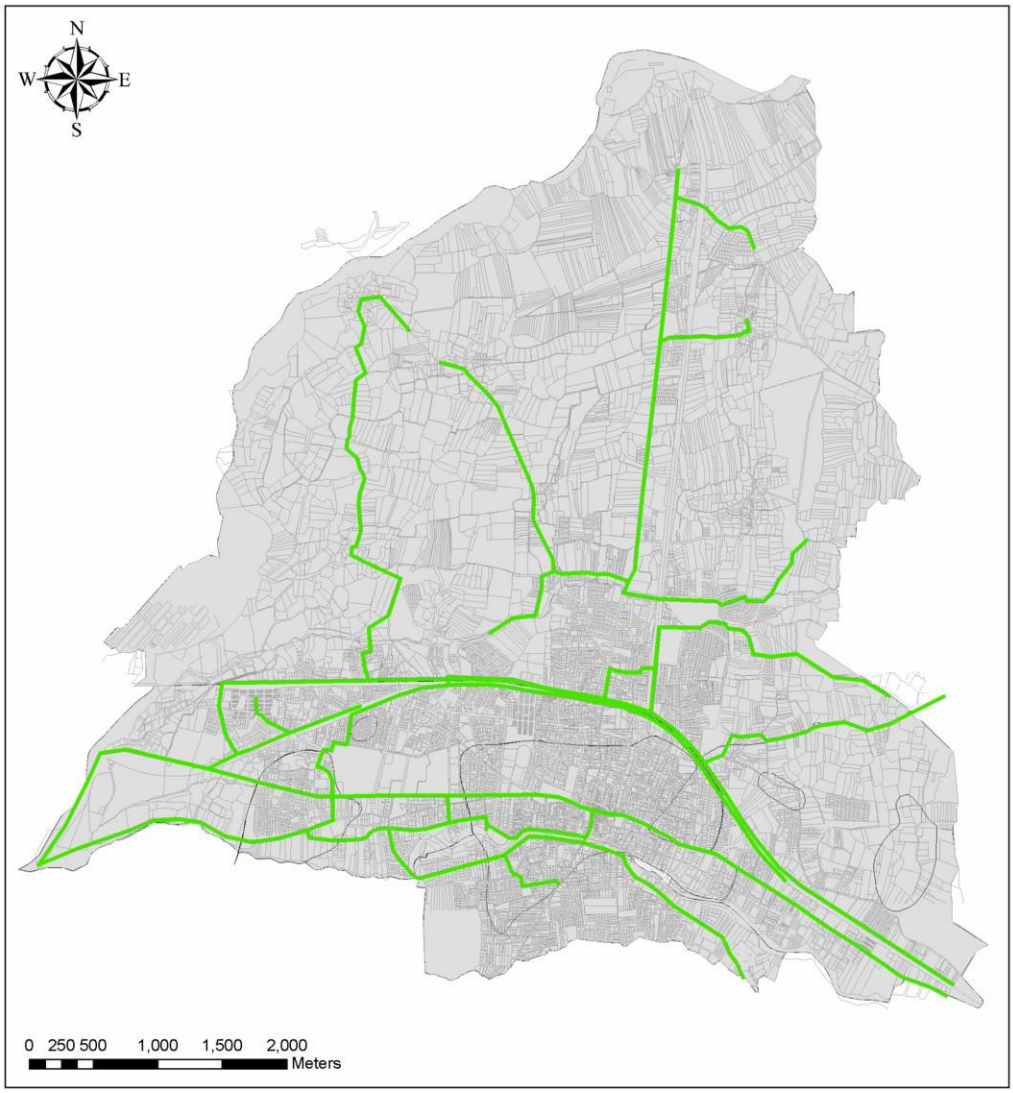

Figure 5.16: Düzce waste water system. The elements represented in green are pipes. No database is available.

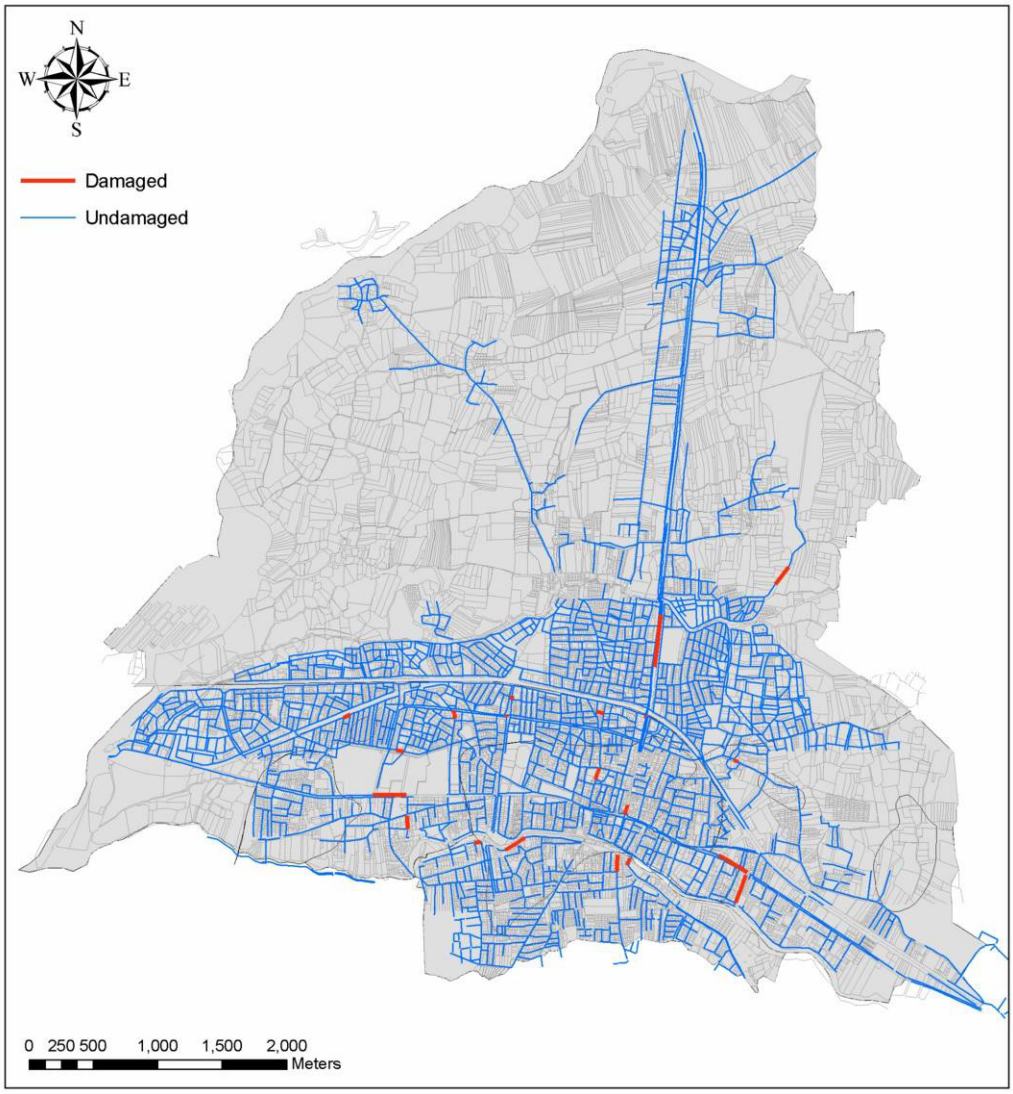

Figure 5.17: Düzce potable water distribution system (blue lines). In red the damaged elements during the Kocaeli 1999 earthquake.

6.SOFTWARE TOOLS FOR PIPE RESPONSE AND ANALYSIS: Seismipipe and Koeripipe

6.1 INTRODUCTION

In the present section two computational tools devoted to the evaluation of the seismic response of buried pipes are presented, i.e.:

- Seismipipe: a computer code which performs a FE analysis of a single pipeline supported by springs that simulate the reaction of the surrounding soil.
- Koeripipe: a software tool developed for evaluating damage scenarios for pipeline networks, based on the approach adopted by the software KoeriLoss2 that operates through Geo-cell systems over GIS layers for evaluating the urban building damage scenario.

6.2 SEISMIPIPE

Seismipipe is a computer code that performs a stress analysis of a single buried pipeline modelled as a beam supported by a system of springs which account for the reaction of the surrounding soil (modelled as a non-linear Winkler foundation, see Figure 6.1). The ground displacement field, as obtained from 2D or 3D wave propagation analyses, is applied to the base of the springs which are characterized by an elastic perfectly plastic behaviour. The approach implemented in Seismipipe is well established in the literature and in particular it follows the recommendations of the American Waterworks Alliance guidelines for the design of buried pipelines [ALA, 2001c], to which reference is made in the following for the definition of the soil spring behaviour.

The analysis performed by Seismipipe procedure is:

a) Elastic as regards the pipe behaviour;

b) Elastic perfectly plastic as regards the soil behaviour;

c) Static, i.e. not taking into account the inertia terms (which are in any case small for a buried flexible pipe).

The stress analysis is carried with the free FEM code Tochnog (source downloadable

directly from the site http://tochnog.sourceforge.net), modified and further improved at SGI-MI. All the geometry pre-processing (Prepipe) and post-processing routines (Pospipe) are coded in Fortran 95. In particular, the pre-processing phase is required to produce the input file for the Tochnog program with a simple definition of the pipeline geometry and surrounding soil properties.

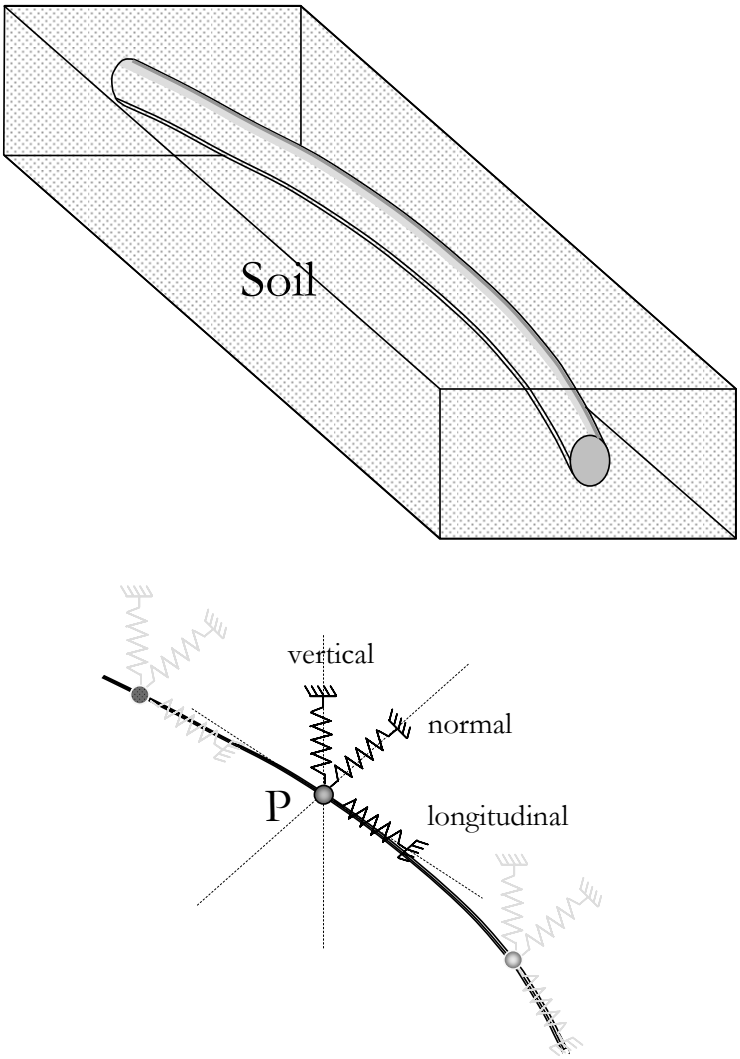

Figure 6.1: Seismipipe: idealised representation of the soil surrounding the pipe as a system of springs oriented along 3 orthogonal directions: vertical (global direction), normal and longitudinal (with respect to the pipe longitudinal axis).

6.2.1 Definition of the pipe geometry

The pipeline must be divided first by the user into segments which are homogeneous in terms of:

a) Pipe cross-section properties (diameter, thickness);

b) Pipe material defined by the elastic characteristics i.e. Young modulus E, Poisson coefficient υ;

c) Soil parameters (Unit weight γ, undrained shear strength (cohesion c_U), internal angle of friction ϕ, etc.)

For each of pipe segment, the following data must be given:

a) End coordinates of the segment. The starting point of each pipe segment is defined as the end point of the previous one, starting from local coordinates $(0;0;z_I)$ with z_I representing the depth of the pipe centreline at the pipeline starting point. The coordinates can be gathered directly from a GIS project by the user, having the pipeline layer loaded, although no direct export routines are provided.

b) Pipe cross-section geometry: outside diameter and thickness.

c) Elastic parameters: Young modulus, Poisson coefficient.

d) Preferred length of the characteristic element for automatic discretization (the suggested length range from 2 to 5 m, depending on the overall length of the pipeline investigated and of the accuracy pursued in the description of both the pipe geometry and displacement field).

e) Soil characteristics and parameters, i.e.:

   - Soil type: cohesive (clayey material) or incoherent (sandy material).
   - Internal angle of friction ϕ and shear strength.
   - Effective and total unit weight of soil γ.

f) Imposed displacement field (typically spatial snapshot when displacement attains its peak), calculated by means of a 2D (or 3D) wave propagation analysis performed in the vertical cross-section (vertical and horizontal-longitudinal components) defined as the X-Z plane. While the pipe analysis is fully 3D, the displacement field obtained from a 2D site analysis is considered to be an invariant with respect to Y global coordinate. At this stage of the Seismipipe development, the displacement values must be defined as a function of the horizontal coordinate in the 2D analysis plane, at a depth equal to the average depth of the pipeline identified by the user.

From the previous input parameters, compiled by the user into a txt file, a Fortran routine called **Prepipe** produces an intermediate file (suitable also for plotting of the geometry), which contains:

a) Nodal coordinates and beam element connectivity (2 nodes beams).

b) Boundary conditions for each pipe and spring node (free displacement for pipe nodes, imposed displacement at the base of the springs)

c) Soil spring limit load and relative displacement as defined in the following.

d) Imposed displacement at the base of each node located at the base of the soil springs.

The global *x* axis is aligned along the plane of 2D seismic propagation analysis (see Figure 6.2). Due to the cited invariance of the displacement field, it is considered that the displacement values given along the pipe length, in terms of in-plane horizontal and vertical components, are unchanged along the global y axis. Then, the *z* axis is aligned along the vertical direction.

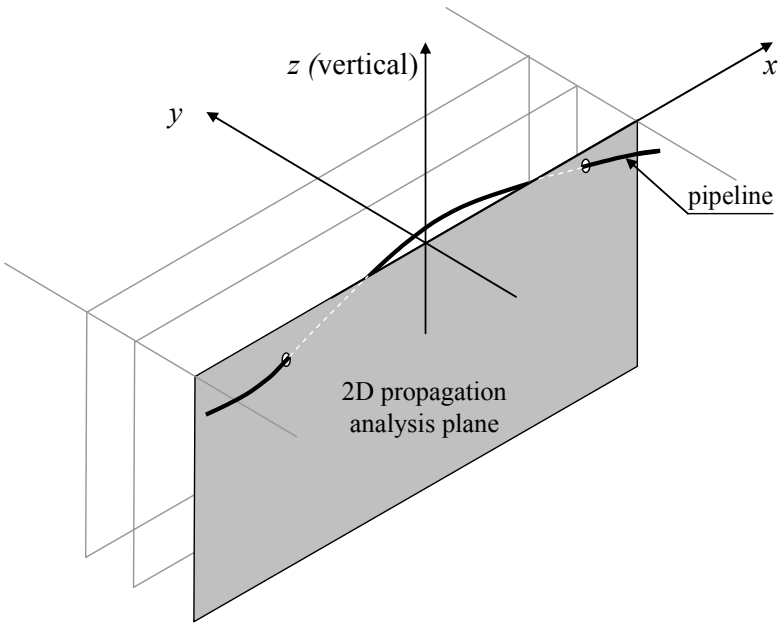

Figure 6.2: 2D propagation plane and pipeline layout

6.2.2 Soil and springs constitutive model

The definition of the soil spring characteristic follows the indications of the ALA Guidelines [ALA, 2001c]. The soil is modelled by means of the system of 3 springs shown in Figure 6.1, defined in each pipe node.

Longitudinal spring

The limit force per unit length, $F_{u,l}$ exerted by the soil on the pipe along its axial (longitudinal) direction (shown in Figure 6.3), is obtained as:

$$F_{u,l} = \pi D \alpha c + \pi D H \bar{\gamma} \frac{1+K_0}{2} \tan\delta$$

Where:

D : pipe outside diameter

$\bar{\gamma}$: effective unit weight of soil

c : soil cohesion

H : depth of pipe centerline

K_0 : coefficient of soil pressure at rest

δ : angle of friction of the interface between pipe and surrounding soil defined as a fraction f of the internal friction angle of the material ϕ ($\delta = f\phi$). The representative values of f suggested by the ALA guidelines [ALA, 2001c] for f, which depends on the pipe coating material, are:

Pipe coating	***f***
Concrete	1.0
Coal Tar	0.9
Rough Steel	0.8
Smooth Steel	0.7
Fusion Bonded Epoxy	0.6
PolyEthylene	0.6

α : adhesion factor defined as a function of the soil cohesion

$$\alpha = 0.608 - 0.123c - \frac{0.274}{c^2+1} + \frac{0.695}{c^3+1} \quad (c \text{ is in KPa/100})$$

The displacement which corresponds to the limit force $F_{u,l}$, $u_{Fu,l}$, depends on the soil stiffness, ranging from 3mm for dense sands, to 10 mm for soft clays.

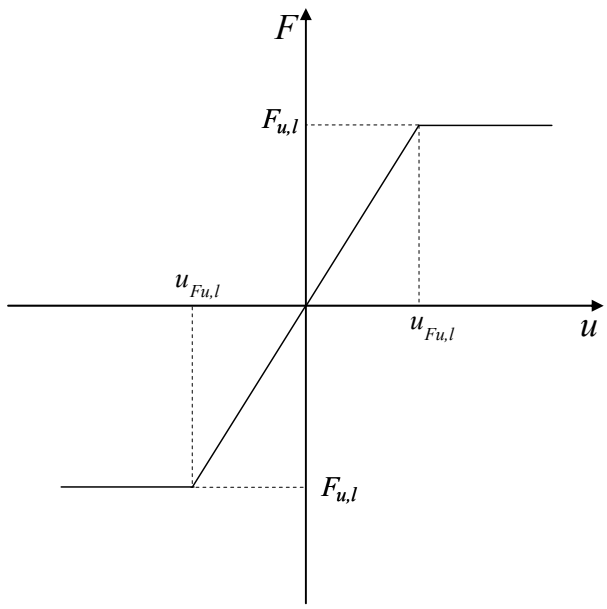

Figure 6.3: elastic perfectly plastic constitutive model for the springs directed along the pipe axis.

Normal spring

The limit force $F_{u,n}$ transmitted by the soil to the pipe along the direction normal to the pipe longitudinal axis is defined as:

$$F_{u,n} = N_{ch}\, c\, D + N_{qh}\ \bar{\gamma}\, H\, D$$

The horizontal bearing capacity factors N_{ch} and N_{qh} are defined respectively for clayey and sandy soils as a function of the non-dimensional bury parameter $x=H/D$ as:

$$N_{ch} = a + bx + \frac{c}{(x+1)^2} + \frac{d}{(x+1)^3} \leq 9 \qquad \text{for clayey soils (= 0 for sand)}$$

$$N_{qh} = a + b(x) + c(x^2) + d(x^3) + e(x^4) \qquad \text{for sandy soils (= 0 for clay)}$$

The parameters *a, b, c, d* and *e* are defined in the following table:

Factor	ϕ	a	b	c	d	e
N_{ch}		6.752	0.065	-11.063	7.119	-
N_{qh}	20°	2.399	0.439	-0.03	1.059E-3	-1.754E-5
	25°	3.332	0.839	-0.090	5.606E-3	-1.319E-4
	30°	4.565	1.234	-0.089	4.275E-3	-9.159E-5
	35°	6.816	2.019	-0.146	7.651E-3	-1.683-4
	40°	10.959	1.784	0.045	-5.425E-3	-1.153E-4
	45°	17.658	3.309	0048	-6.443E-3	-1.299E-4

The displacement $u_{Fu,n}$ which corresponds to the limit force $F_{u,n}$ depends on the pipe depth and diameter, shown in Figure 6.4, as:

$$u_{F,n} = 0.04\left(H + \frac{D}{2}\right) \leq (0.10 \div 0.15)D$$

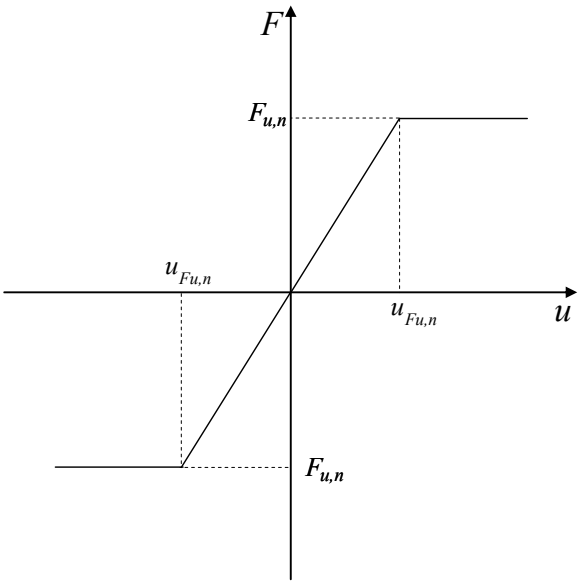

Figure 6.4: elastic perfectly plastic constitutive model for the springs normal to the pipe axis.

Vertical spring

In the case of shallow buried pipelines as the in the case of water distribution and sewer networks (H/D ≤ 10), the behaviour of the vertical spring is different with respect to the uplift and the bearing direction of pipe movement (as represented in Figure 6.5). In terms of limit force e relative displacement one has:

Uplift	Bearing
$F_{u,v}^{up} = N_{cv}\, c\, D + N_{qv}\, \bar{\gamma}\, HD$	$F_{u,v}^{down} = N_c\, c\, D + N_q\, \bar{\gamma}\, HD + N_\gamma\, \gamma \frac{D^2}{2}$
$u_{Fu,v}^{up} = 0.01H \div 0.02H$ (sand; <0.01D)	$u_{Fu,v}^{down} = 0.1\text{D}$ (granular soils)
$u_{Fu,v}^{up} = 0.1H \div 0.2H$ (clay < 0.2D)	$u_{Fu,v}^{up} = 0.2\text{D}$ (cohesive soils)

where:

$$N_{cv} = 2\left(\frac{H}{D}\right) \leq 10$$

$$N_{qv} = \left(\frac{\phi H}{44D}\right) \leq N_q$$

$$N_c = [\cot(\phi + 0.001)]\{\exp[\pi \tan(\phi + 0.001)] \cdot \cdot \tan^2\left(45 + \frac{\phi + 0.001}{2}\right) - 1\}$$

$$N_q = \exp(\pi \tan\phi) \tan^2\left(45 + \frac{\phi}{2}\right)$$

$$N_\gamma = e^{(0.18\phi - 2.5)}$$

and γ the natural weight of soil.

For each spring defined along the pipeline, the previous defined values of $F_{u,d,i}$ (where the subscripts d means one of the 3 directions l, n and v, and i indicates the i-node) shall be multiplied by the influence length $L_{S,i}$ of each spring S_i as defined in Figure 6.6, in order to obtain the effective parameters of the springs defined for each node.

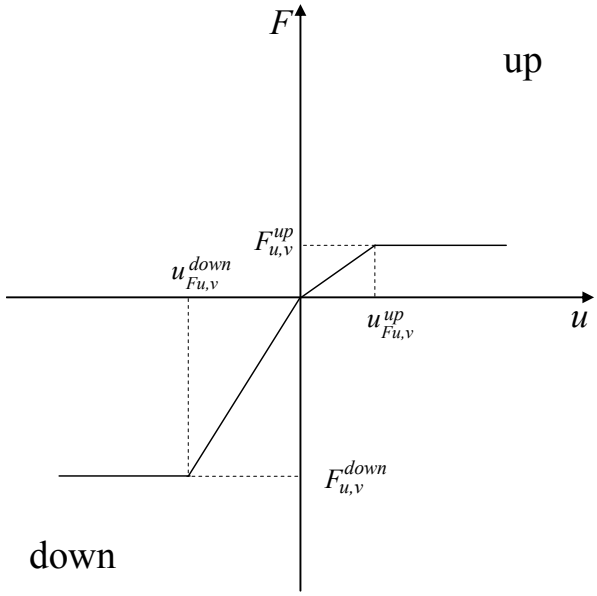

Figure 6.5: elastic perfectly plastic constitutive model for the springs directed vertically.

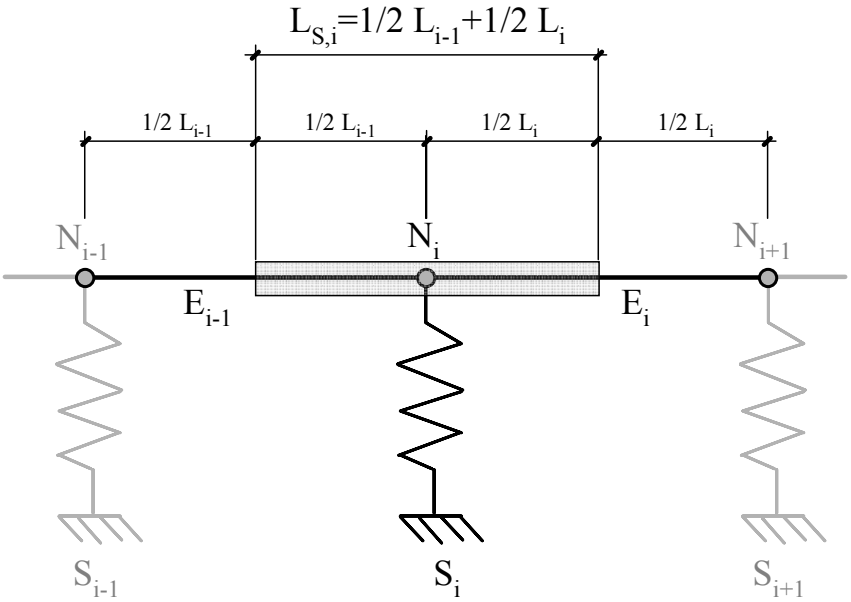

Figure 6.6: definition of the reference length $L_{S,i}$ *in the calculation of effective spring stiffness bounded at each node* N_i of *the discretized pipe.*

6.2.3 Modelling of the pipe as a beam

The pipeline is modelled by means of 3D linear beams. The material constitutive behaviour is linear elastic, having the degrees of freedom represented in Figure 6.7).

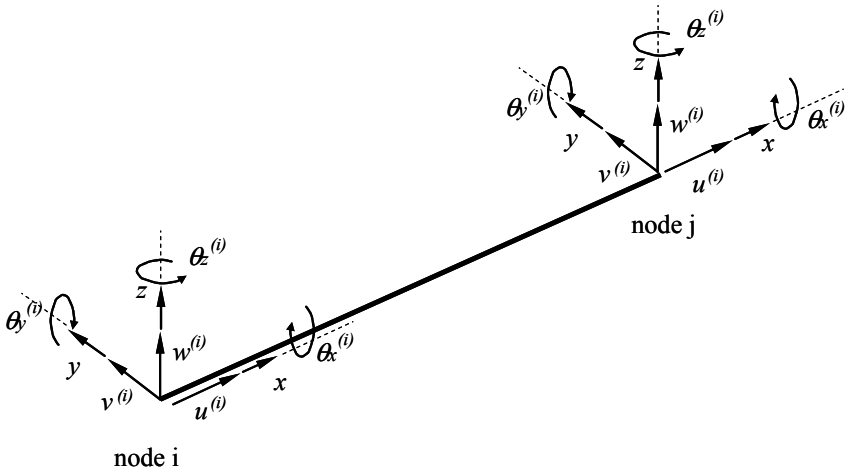

Figure 6.7: Seismipipe. Degrees of freedom of each pipe (beam) element.

6.2.4 Application of the displacement field to the pipeline

The imposed displacement generated by the 2D propagation analyses in both the vertical and horizontal in-plane component) is applied at the base of each soil spring. First of all, the values of both displacement components (vertical and horizontal) are evaluated at each pipe node as a function of the horizontal coordinate x of the node. The vertical component is applied to the base of the vertical spring while the horizontal value is firstly projected along the normal and longitudinal direction of the pipe (see Figure 6.8). Prior to being applied to the longitudinal and normal spring, the calculated projections $D_{h,l}$ and $D_{h,n}$ are decomposed along their cardinal components respectively ($D_{h,lx}$; $D_{h,ly}$) and ($D_{h,nx}$; $D_{h,ny}$) as shown in Figure 6.9.

6.2.5 Calculation phase

The pipe and soil weight, together with the inertia terms are neglected. A static analysis is performed by means of the FEM code Tochnog at increasing levels of displacement, applied by means of an overall displacement multiplier which ranges from 0 to 1. The calculation steps are adjusted by the program as a function of the reached convergence in terms both of displacement and unbalanced force.

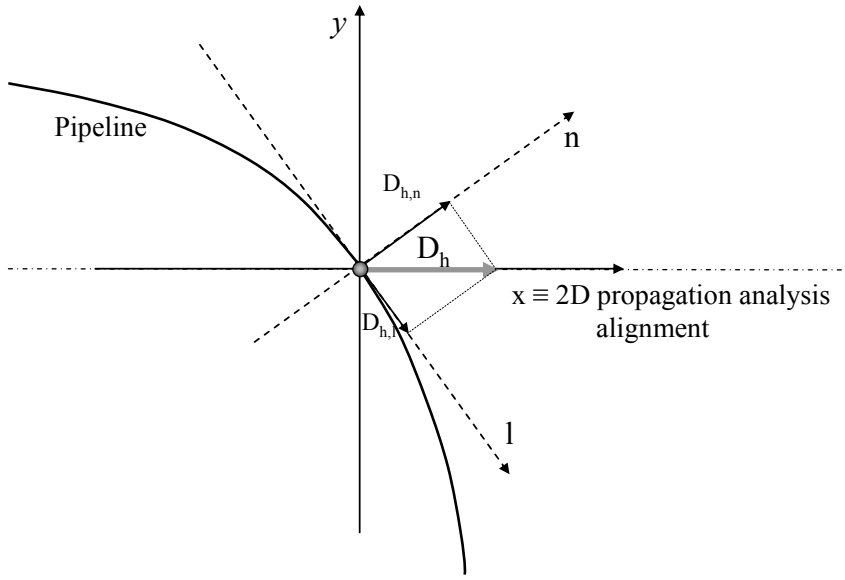

Figure 6.8: decomposition of the horizontal component of displacement (D), calculated in the 2D site analysis, along the normal and longitudinal directions (the D vertical component is applied directly to the base of the vertical springs).

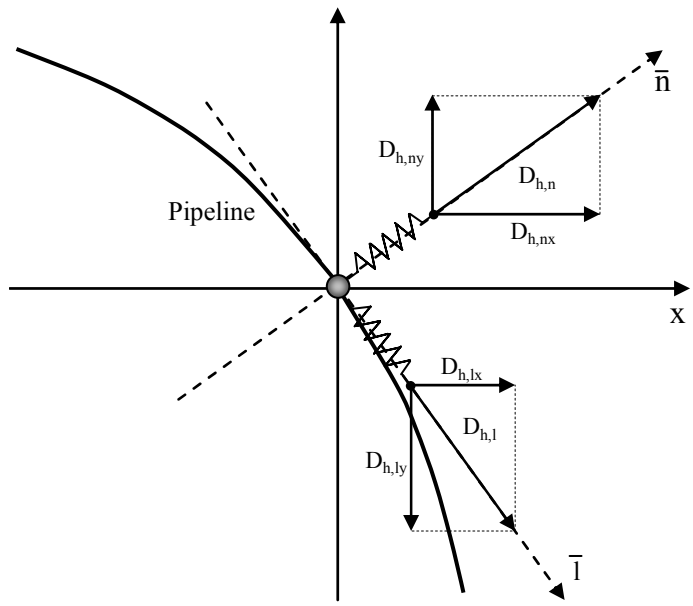

Figure 6.9: decomposition of the Dh,l and Dh,n into their components defined along the x and y axis, applied at the base of the horizontal soil springs.

6.2.6 Post-processing of the results

The procedure Pospipe performs a post-processing of the Tochnog analysis results, obtaining the following data to be plotted:

- Horizontal (2 components) and vertical displacements of the pipe along the global axes system.
- Axial and Bending moment (2 components) values as a function of the position of the pipe cross-section considered.
- Top and bottom fiber axial strain and stress values;
- Pipe curvature in both the horizontal and vertical plane, along the pipeline.
- Force and elongation in horizontal (longitudinal and normal) and vertical springs.

The plotting of the results can be performed by means of the opens source plotting program Gnuplot (for further info and direct download please refer to http://www.gnuplot.info/).

6.3 KOERIPIPE

KoeriPipe is a software tool developed for evaluating seismic damage scenarios for pipeline networks, based on KoeriLoss2 that operates through Geo-cell systems for evaluating urban building damage scenarios. KoeriLoss2 [Ansal et al., 2007] is developed at the Earthquake Engineering Department of Bogazici University, Kandilli Observatory and Earthquake Research Institute within the framework of LessLoss SP10 as the second version of KoeriLoss [Erdik et al., 2002]. The earthquake hazard is separately calculated and used as input to the software package. Thus it is possible to estimate losses either under probabilistic earthquake motions or under a "scenario earthquake". The program package calculates the earthquake characteristics on the ground surface using 1D site response analyses based on equivalent linear model Shake91 [Idriss and Sun, 1992], see previous §2.1.1.2. Shake91 code is slightly modified to simplify input data and to obtain compatible output files to be used in estimating the damage to pipeline systems with respect to wave propagation.
The basic steps of the KoeriPipe for estimation of pipeline seismic damage consist of:

1. Specification of the scenario earthquake or regional probabilistic seismic hazard.
2. Collection/compilation of information for delineating local soil conditions.

3. Collection/compilation of information of pipeline inventory.
4. Computation of site-specific earthquake characteristics on the ground surface.
5. Using vulnerability relationships embedded in the software, evaluation of damage to pipeline network.

The KoeriPipe software package computes site specific earthquake characteristics on the ground surface to be used for microzonation (Step 4) and damage distribution with respect to repair rate (repairs/km) and number of repairs in the pipeline system (Step 5) using the input data given with respect to input earthquake hazard (Step 1), site characterisation (Step 2) and pipeline inventory (Step 3). The output files are in terms of microzonation parameters (i.e. PGV) and pipe damage (i.e. repair rate) that are in Excel Worksheet format and can be used as input to a GIS software (i.e. MapInfo, ArcInfo) to obtain the microzonation and pipeline damage distribution maps in the investigated area.

6.3.1 Overview of software procedure

6.3.1.1 *Method*

The adopted method consists of two main phases. The first one involves generation of microzonation maps displaying the earthquake ground shaking parameters for the selected regional earthquake hazard scenario [Ansal et al., 2006a; 2005a]. In the second phase, the vulnerability of the pipelines is estimated based on the calculated earthquake ground shaking parameters and a damage distribution map for pipeline system is generated.

The approach was based on a grid system composed of cells according to the availability of geological, geophysical and geotechnical data. In the first step of the first phase, the variation of earthquake shaking parameters for bedrock outcrop within the investigated area are externally determined for a specified level of exceedance probability [Erdik et al. 2004, 2005] or based on deterministic simulations [Cultrera et al., 2006], see also Sub-Sect 2.1 above. The regional earthquake hazard description can be of probabilistic or deterministic nature.

In the second step, a site characterization is performed [Ansal et al., 2005b; 2004] based on available borings and other relevant information by defining one representative soil profile for each cell with shear wave velocities extending down to the engineering bedrock (Vs ≥ 750m/s).

The third step involves site response analyses to obtain site specific earthquake characteristics on the ground surface calculated using equivalent linear 1D site response analyses, for each representative soil profile. Hazard compatible acceleration time histories (in terms of expected fault type, fault distance, and earthquake magnitude) are selected from the databases of available real earthquake acceleration records. It is also possible to use acceleration time histories calculated by different simulation models. In

case of using recorded acceleration histories, PGA scaling is adopted [Ansal et al., 2006b; Durukal et al., 2006] and site response analyses are performed for the selected number of acceleration histories. Variations of peak ground acceleration (PGA) and peak ground velocity (PGV) at the ground surface are determined. PGA and PGV values are used to generate microzonation maps for the investigated area.
In the second phase, site-specific PGV values and pipeline inventory of the study area are used to assess the vulnerability of pipeline system with respect to wave propagation. Pipeline inventory includes various details of the system including material type, pipe diameter and length, as illustrated in Sect. 5. Empirical correlations for damage rate due to wave propagation with respect to PGV proposed in LessLoss SP11 Deliverable 89 [Pitilakis et al., 2006a, 2006b] are used to assess the vulnerability of pipeline systems, see the previous Sect. 0.

6.3.1.2 *Flowchart and Components*

The methodology is automated into a Visual Basic application where pipeline vulnerability is computed and displayed in maps. The application utilises Excel and Fortran codes for calculations and uses GIS based software (MapInfo) to map the estimated ground shaking and the damage distribution for the investigated area. The flow chart of the software procedure is schematically illustrated in Figure 6.10. Explanations for the steps are given in the following paragraphs.
Site Response Analyses: Given the ground motion scenario at the engineering bedrock outcrop (in terms of PGA and a suite of hazard compatible acceleration histories or acceleration histories simulated in a deterministic scenarios) and the local soil conditions (in terms of *Vs* profile down to engineering bedrock, soil layering, groundwater level and dynamic soil properties), acceleration time histories are calculated on the ground surface for each cell by 1D linear equivalent analysis. PGV values are determined from integration of acceleration time histories obtained at the ground surface.

Vulnerability Analyses: Using the ground shaking parameter PGV (computed from site response analyses) and the pipeline inventory in the investigated area (material type, joint type, diameter and length of pipelines), the vulnerability of pipelines is computed in terms of expected repair rate and number of repairs for each cell in the system.

6.3.2 Operation of software procedure

6.3.2.1 *Input Files*

The required user input for operation of the software package involves the following input data files:

****.txt:*** Text files each containing a selected input motion (acceleration time history).

These files can have different formats and it is sufficient to specify this format when assigning the selected input motion for the site response analyses. Therefore the user can use all different types of files that may be available from different strong motion data banks (i.e. PEER) or calculated as simulated acceleration time histories.

acc.txt: A text file that includes format information for reading acceleration values (in units of g) from input motion files using Fortran code. This file also includes PGA values at engineering bedrock outcrop for each cell, determined from seismic hazard analyses or by deterministic simulations to be used for input motion scaling.

Figure 6.11 shows an example with the information regarding the three input motion records selected for site response analyses as given in the first three rows of *acc.txt* file. The information contained in these rows is in free Fortran format, separated by commas. The first column is the total number of data points (acceleration values) for the input motion. In accordance with the version of Shake91 used for the site response analysis, the number of acceleration data points should be equal or less than 4096. The second column shows the number of header lines in the input motion text file. The third column specifies the number of data columns to be read from the file, the fourth column gives the time interval; the fifth column gives the filename in which the data is stored and finally the last column gives the Fortran format for acceleration data in the text file. It should be noted that there will be as many descriptive rows as the number of selected input motions. Rows following those describing the input motion records are composed of single column and each row contains PGA value (in units of g) at the bedrock outcrop for each cell in the grid system determined from seismic hazard analyses or based on deterministic earthquake scenario simulations.

soil.xls: An Excel spreadsheet that requires the user to enter information about geotechnical site conditions at each cell in the grid system. The information that should be provided by the user includes soil type, soil layer thickness, ground water level and shear wave velocity profile down to the engineering bedrock ($Vs \geq 750$ m/s) for each cell. Information for each cell is entered in a separate worksheet within *soil.xls*. The number of worksheets can be easily increased to match the number of cells in the investigated area by (edit/copy sheet) option in Excel. A template Excel sheet to prepare *soil.xls* is included in the software package. An example is given in Figure 6.12.

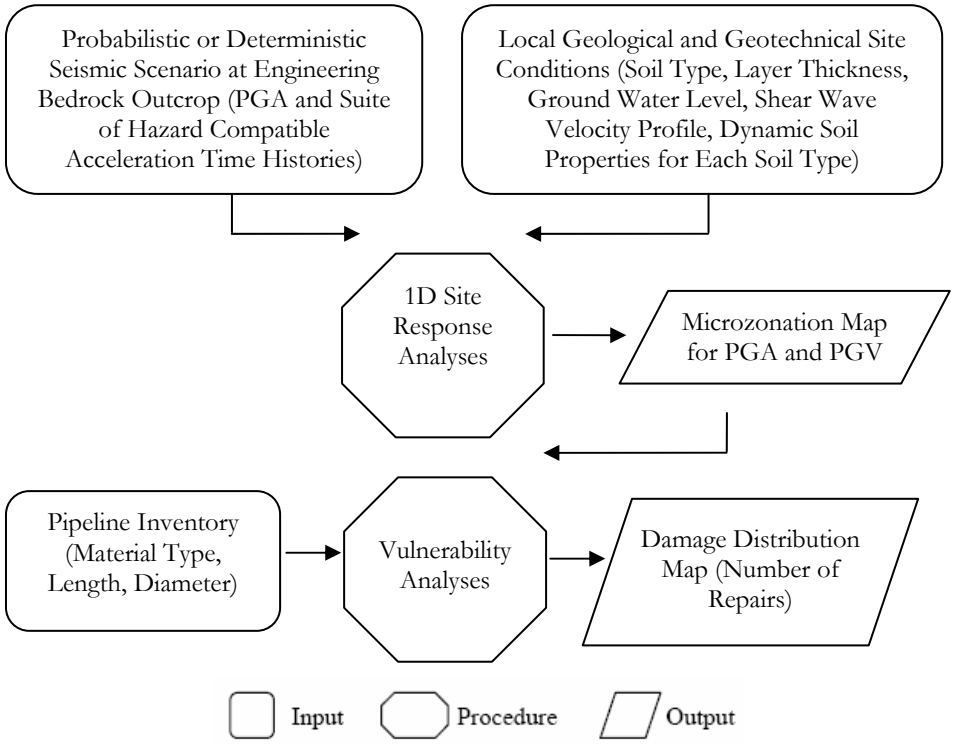

Figure 6.10. Schematic illustration of software package for pipeline loss estimation in urban areas

Figure 6.11. Illustration of an example *acc.txt* file that contains format information for reading input motion files and PGA values on bedrock outcrop determined from seismic hazard analyses for each cell to be used in input motion scaling

In the worksheet illustrated in Figure 6.12, the user is required to enter (blue fonts are user inputs and black fonts are calculated by Excel): cell number, depth (as the midpoint of SPT penetration), corresponding SPT blow counts, corresponding SPT penetration lengths, soil type number, depth of soil layer (in m) if needed, shear wave velocity for soil layer (in m/s) if needed, ground water elevation (in m), and depth of the engineering bedrock (in m).

The Excel worksheet is presently programmed to calculate shear wave velocity based on SPT blow counts utilising the empirical relationship proposed by [Iyisan, 1996]:

$$V_s = 51.5N^{0.516} \leq 500m/s \qquad (6.1)$$

where Vs is shear wave velocity (in m/sec) and N is uncorrected standard penetration blow counts. Eq. (6.1) is used to calculate shear wave velocity values with depth where SPT data is available. In most cases, it is very likely that it will not be possible to establish the engineering bedrock depth based only on SPT tests. Therefore, the user has the option to enter the depths and corresponding shear wave velocities determined by different geophysical seismic wave velocity measurements or estimated based on the local geological information down to the engineering bedrock depth.

Soil type numbers need to be specified in accordance with the soil type numbers given for the modulus reduction and damping ratio properties for different materials. The last row in the input table represents the bedrock layer (engineering bedrock material type is defined as 7) and only shear wave velocity value is entered for this row. The table calculates the thickness of layers, shear wave velocity and unit weight of soil layers based on soil types in suitable units for the site response analysis code. The worksheet also provides a graphical illustration of Vs profile down to the engineering bedrock.

The preparation of the *soil.xls* file requires manual input based on the geotechnical interpretation of the available data. The user has the option to modify the empirical expression to calculate shear wave velocities or to enter the variation of shear wave velocities with depth manually by overriding the provided Vs-SPT relationship.

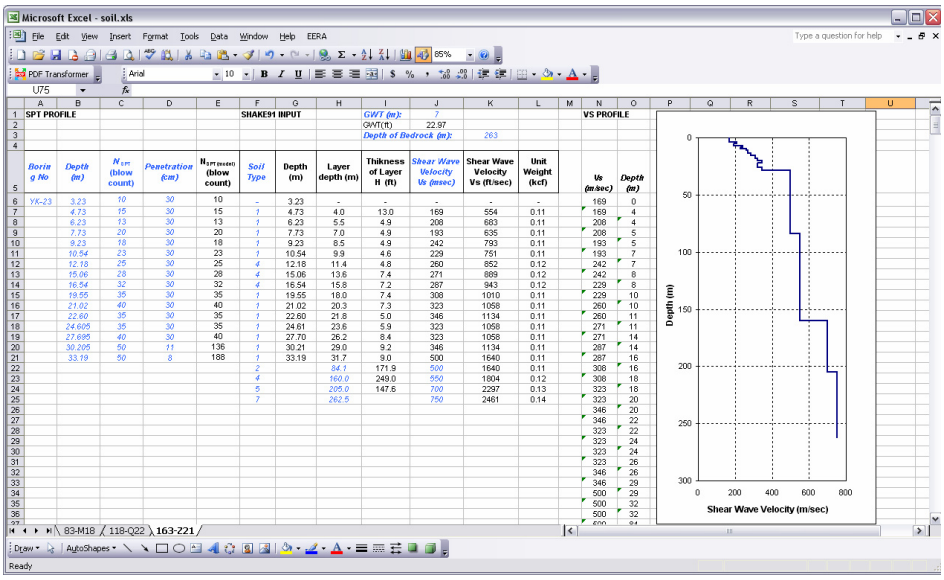

Figure 6.12. Illustration of an example *soil.xls* file that contains representative soil profiles at each cell in the grid system; soil profile for one cell is shown here.

curves.txt: A text file that includes dynamic soil properties (shear modulus reduction and material damping ratio curves) for each soil type. Format of this file is in accordance with the Fortran format as specified in the Shake91 Manual [Idriss and Sun, 1992]. The variation of dynamic properties with shear strain should be defined for each soil type number that is entered in *soil.xls*. An example is shown in Figure 6.13.

The first line is information line. The second line is the option code in (I5) Fortran format and it must be 1. Third line is also in (I5) Fortran format and specifies the number of material types. The maximum number of material types that can be used in this version of Shake91 is 13. In the present version of the KoeriPipe, seven different material types are used. Shear modulus reduction and material damping ratio curves corresponding to these material types are given in *curves.txt* file which is included in the software package. The material types used are summarised in Table 6.1.

Table 6.1. G/Gmax and Damping ratio - shear strain relationships used in site response analysis

Material Type	Soil Type	Reference
Material Type 1	Lean Clay (CL) PI=30%	Vucetic & Dobry (1991)
Material Type 2	Fat clay (CH) PI=45%	Vucetic & Dobry (1991)
Material Type 3	Silt (ML) PI=15%	Vucetic & Dobry (1991)
Material Type 4	Sand (SM-SC)	Darendeli (2001)
Material Type 5	Sand (SP-SW)	Seed et al. (1986)
Material Type 6	Gravel (GM – GC)	Seed et al. (1986)
Material Type 7	Bedrock	Idriss (1990)

The fourth line is in (I5, A30) Fortran format. The first input is the number of data points on the given curve and second is the material type number and material identification. In the following lines, first strain amplitudes (in percent) and then corresponding modulus ratio or damping values are given in (8F9.0) Fortran format.

pipedamage.xls: An excel spreadsheet that requires user to enter information about pipeline inventory. Blue fonts are user inputs and black fonts are calculated by Excel.

In the current version of KoeriPipe, four empirical relations are used for calculating repair rates due to wave propagation. However, users can enter any other correlation that is appropriate for a given inventory. The correlations embedded in *pipedamage.xls* are summarised in Table 6.2, and should be compared with those given in Tables 4.16 to 4.18.

Among those shown in Table 6.2, the [ALA. 2001] relation has the largest database and is affected by significant scatter. As already illustrated in §4.4.1, [O'Rourke and Deyoe, 2004] have shown that the scatter can be significantly reduced if ground strain (instead of PGV) is used as seismic shaking parameter to relate wave propagation and repair rate.

A discussion on values of apparent wave velocities and formulas has been already provided in §2.1.1.3 and §4.1. As to values of apparent velocities to be used to derive the

peak ground strain ε from PGV, eq. (4.4) provides the most satisfactory results.
Once repair rates are computed, the number of expected repairs at each cell location is calculated by multiplying repair rate by total length of pipeline at that location. An example file is shown in Figure 6.14.
The user is required to enter length (in units of km), diameter (in units of mm) and material type of pipeline for each cell in the grid system. The excel spreadsheet computes the damage rate and number of repairs for each cell based on the calculated PGV values.

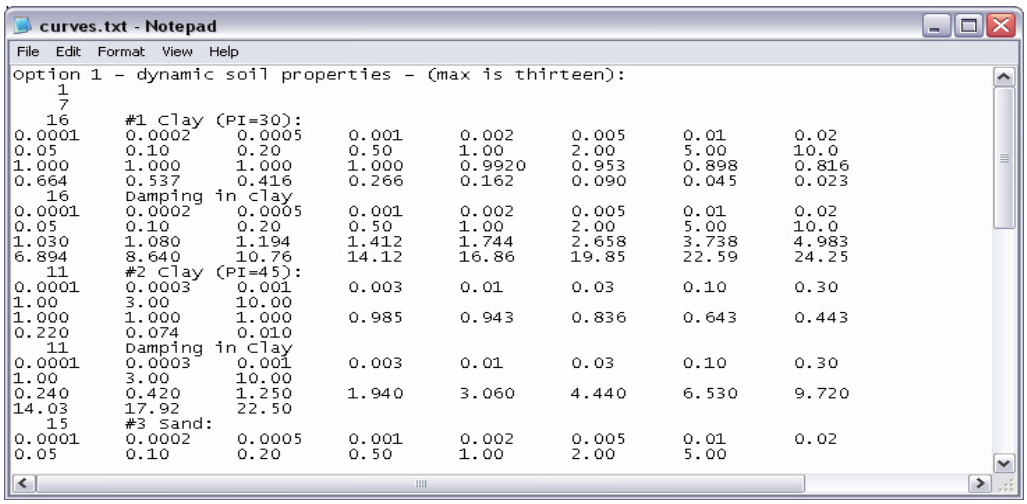

```
curves.txt - Notepad
File  Edit  Format  View  Help
Option 1 - dynamic soil properties - (max is thirteen):
    1
    7
   16      #1 Clay (PI=30):
0.0001     0.0002     0.0005     0.001      0.002      0.005      0.01       0.02
0.05       0.10       0.20       0.50       1.00       2.00       5.00       10.0
1.000      1.000      1.000      1.000      0.9920     0.953      0.898      0.816
0.664      0.537      0.416      0.266      0.162      0.090      0.045      0.023
   16      Damping in clay
0.0001     0.0002     0.0005     0.001      0.002      0.005      0.01       0.02
0.05       0.10       0.20       0.50       1.00       2.00       5.00       10.0
1.030      1.080      1.194      1.412      1.744      2.658      3.738      4.983
6.894      8.640      10.76      14.12      16.86      19.85      22.59      24.25
   11      #2 Clay (PI=45):
0.0001     0.0003     0.001      0.003      0.01       0.03       0.10       0.30
1.00       3.00       10.00
1.000      1.000      1.000      0.985      0.943      0.836      0.643      0.443
0.220      0.074      0.010
   11      Damping in clay
0.0001     0.0003     0.001      0.003      0.01       0.03       0.10       0.30
1.00       3.00       10.00
0.240      0.420      1.250      1.940      3.060      4.440      6.530      9.720
14.03      17.92      22.50
   15      #3 Sand:
0.0001     0.0002     0.0005     0.001      0.002      0.005      0.01       0.02
0.05       0.10       0.20       0.50       1.00       2.00       5.00
```

Figure 6.13. Illustration of *curves.txt* file in which dynamic soil properties for each soil type is defined

Table 6.2. Empirical pipeline vulnerability relations embedded in *pipedamage.xls*.

Empirical Relation	Factors	Number of EQ in Database	Material Type in Database	Reference
RR(repair/km)= $0.0001*K*PGV^{2.25}$	PGV (cm/s) K= 1 if brittle material, K=0.3 if ductile material	6	Brittle	O'Rourke and Ayala (1993)
RR(repair/km)= $0.000166*K*PGV^{1.98}$	PGV (cm/s) K: coefficient depending on material type	1	Mixed	Eidinger (1998)
RR(repair/km)= 0.002415*K*PGV	PGV (cm/s) K: coefficient depending on material type	18	Mixed	ALA (2001)
RR(repair/km)= $K*513*\varepsilon^{0.89}$	PGV (cm/s) ε =ground strain K= 1 if brittle material, K=0.3 if ductile material	8	Brittle	O'Rourke and Deyoe (2004)

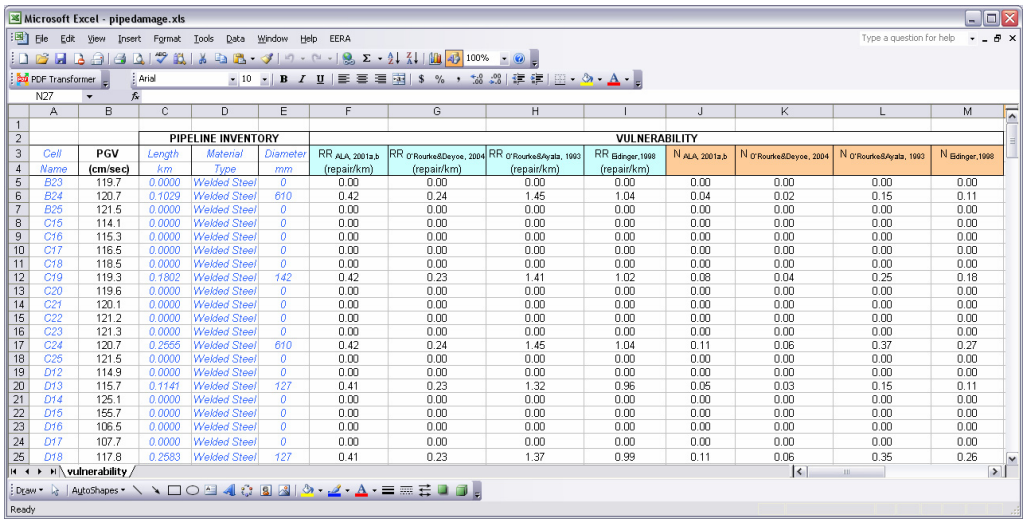

		PIPELINE INVENTORY			VULNERABILITY							
Cell Name	PGV (cm/sec)	Length km	Material Type	Diameter mm	RR ALA, 2001a,b (repair/km)	RR O'Rourke&Deyoe, 2004 (repair/km)	RR O'Rourke&Ayala, 1993 (repair/km)	RR Eidinger,1998 (repair/km)	N ALA, 2001a,b	N O'Rourke&Deyoe, 2004	N O'Rourke&Ayala, 1993	N Eidinger,1998
B23	119.7	0.0000	Welded Steel	0	0.00	0.00	0.00	0.00	0.00	0.00	0.00	0.00
B24	120.7	0.1029	Welded Steel	610	0.42	0.24	1.45	1.04	0.04	0.02	0.15	0.11
B25	121.5	0.0000	Welded Steel	0	0.00	0.00	0.00	0.00	0.00	0.00	0.00	0.00
C15	114.1	0.0000	Welded Steel	0	0.00	0.00	0.00	0.00	0.00	0.00	0.00	0.00
C16	115.3	0.0000	Welded Steel	0	0.00	0.00	0.00	0.00	0.00	0.00	0.00	0.00
C17	116.5	0.0000	Welded Steel	0	0.00	0.00	0.00	0.00	0.00	0.00	0.00	0.00
C18	118.5	0.0000	Welded Steel	0	0.00	0.00	0.00	0.00	0.00	0.00	0.00	0.00
C19	119.3	0.1802	Welded Steel	142	0.42	0.23	1.41	1.02	0.08	0.04	0.25	0.18
C20	119.6	0.0000	Welded Steel	0	0.00	0.00	0.00	0.00	0.00	0.00	0.00	0.00
C21	120.1	0.0000	Welded Steel	0	0.00	0.00	0.00	0.00	0.00	0.00	0.00	0.00
C22	121.2	0.0000	Welded Steel	0	0.00	0.00	0.00	0.00	0.00	0.00	0.00	0.00
C23	121.3	0.0000	Welded Steel	0	0.00	0.00	0.00	0.00	0.00	0.00	0.00	0.00
C24	120.7	0.2555	Welded Steel	610	0.42	0.24	1.45	1.04	0.11	0.06	0.37	0.27
C25	121.5	0.0000	Welded Steel	0	0.00	0.00	0.00	0.00	0.00	0.00	0.00	0.00
D12	114.9	0.0000	Welded Steel	0	0.00	0.00	0.00	0.00	0.00	0.00	0.00	0.00
D13	115.7	0.1141	Welded Steel	127	0.41	0.23	1.32	0.96	0.05	0.03	0.15	0.11
D14	125.1	0.0000	Welded Steel	0	0.00	0.00	0.00	0.00	0.00	0.00	0.00	0.00
D15	155.7	0.0000	Welded Steel	0	0.00	0.00	0.00	0.00	0.00	0.00	0.00	0.00
D16	106.5	0.0000	Welded Steel	0	0.00	0.00	0.00	0.00	0.00	0.00	0.00	0.00
D17	107.7	0.0000	Welded Steel	0	0.00	0.00	0.00	0.00	0.00	0.00	0.00	0.00
D18	117.8	0.2583	Welded Steel	127	0.41	0.23	1.37	0.99	0.11	0.06	0.35	0.26

Figure 6.14. Illustration of an example pipedamage.xls file where pipeline inventory is entered and vulnerability analyses is carried out based on PGV values calculated from site response analyses

6.3.2.2 *Running Software Procedure and Output Files*

The folder in which the software will be executed should include the following files: *soil.xls, table.xls, acc.txt, *.txt* (input motions), *curves.txt, pipedamage.xls, shake5PGV.exe, and PGVavg.exe*. (*These files, as templates, are included with the programme package and the user should start with the same unprocessed set of files for each new case. The user should use the set provided since Visual Basic Macros are embedded in these Excel files.*)

The software package operates within *soil.xls* Excel spreadsheet. In order to execute the software, the user should run a VBA macro called 'MAIN' which is embedded in *soil.xls*. This macro is composed of several modules. Once executed, VBA macro MAIN performs sequence of some actions without interference of the user. The files that will be produced during the operation of software procedure without any input from the user are: *inp.txt, shake.inp, filename.txt, a.bat, temp.txt, shake.acc, shake.out, shake.spc, PGV.txt,* and *PGVavg.xls*.

The peak value (in units of cm/s) from each velocity time history is selected and printed into a text file named *'PGV.txt'*. In this file each PGV value corresponds to one run of Shake. Therefore, the total number of PGV values printed in this file is equal to the number of input motions times the number of soil profiles (or number of cells). *shake.out* is the standard output file as described in Shake91 Manual. *shake.acc* contains acceleration time histories on the ground surface and *shake.spc* contains response spectral accelerations on the ground surface computed. A mean PGV value (in units of cm/s) for each cell by arithmetically averaging PGV values that corresponds to selected input motions are printed in a file named *PGVavg.xls*. *pipedamage.xls* calculates the

repair rate (in units of repair/km) for pipelines based on average PGV values and pipeline inventory information.

6.3.2.3 *Mapping the damage evaluation results*

The results obtained at the end of each stage from the KoeriPipe are given as Excel worksheet outputs. These worksheets can be transferred to any GIS system such as MapInfo to be mapped according to the calculated parameters.
At the end of the first stage, microzonation map with respect to PGV as calculated from site response analyses is plotted using a GIS based software as shown in Figure 6.15 in terms of intervals of calculated peak ground velocities.
At the end of the second stage microzonation maps showing the repair rate and number of pipe damages can be produced as illustrated in Figure 6.16 and Figure 6.17, respectively.

6.3.3 Summary and recommendations

The software package KoeriPipe was developed to estimate pipeline damage based on wave propagation effects distribution within the investigated region. The present version do not account for pipeline damage that may occur due to fault crossing, liquefaction, lateral spreading or landslides. Given the seismic hazard, geotechnical site conditions and pipeline inventory, the procedure estimates the repair rate per km and the number of repairs in each cell in a pipeline system of an urban area based on site-specific response analyses and empirical correlations between ground shaking and damage.
The steps that are performed by the user to operate the software can be summarised as:

1. Prepare input files *soil.xls, acc.txt, *.txt (input motions), curves.txt, pipedamage.xls* as described.
2. Copy files *soil.xls, table.xls, acc.txt, *.txt (input motions), curves.txt, pipedamage.xls, shake5PGV.exe, and PGVavg.exe* into the same folder.
3. Open *soil.xls* and run VBA macro MAIN.
4. Obtain number of repairs corresponding to each cell location from *pipedamage.xls*.
5. Plot damage results using a GIS based software (i.e. MapInfo) to obtain distribution of pipeline damages.

KoeriPipe is being improved continuously within the framework of LessLoss. More options will be added to increase the capabilities of the software with respect to site response analyses as well as for the estimation of the repair rates for pipe damage calculations. In the program package, Excel and Fortran codes were used to give flexibility to the users to make modifications as considered appropriate by them.

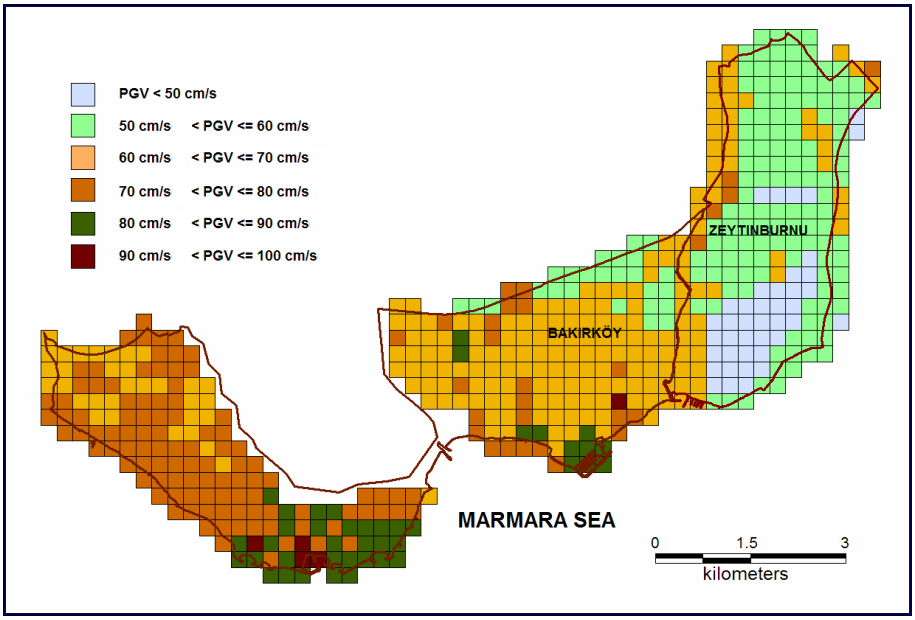

Figure 6.15. Example of microzonation maps (of Istanbul districts) displaying PGV values calculated by the site response analyses

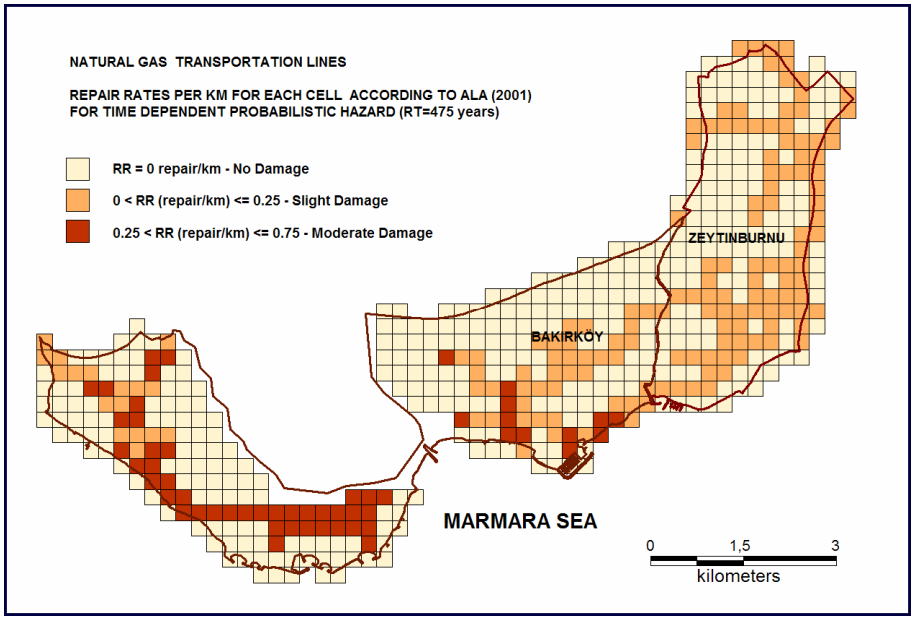

Figure 6.16. Example of microzonation map displaying damage as repair rates per km, for natural gas lines in Istanbul districts.

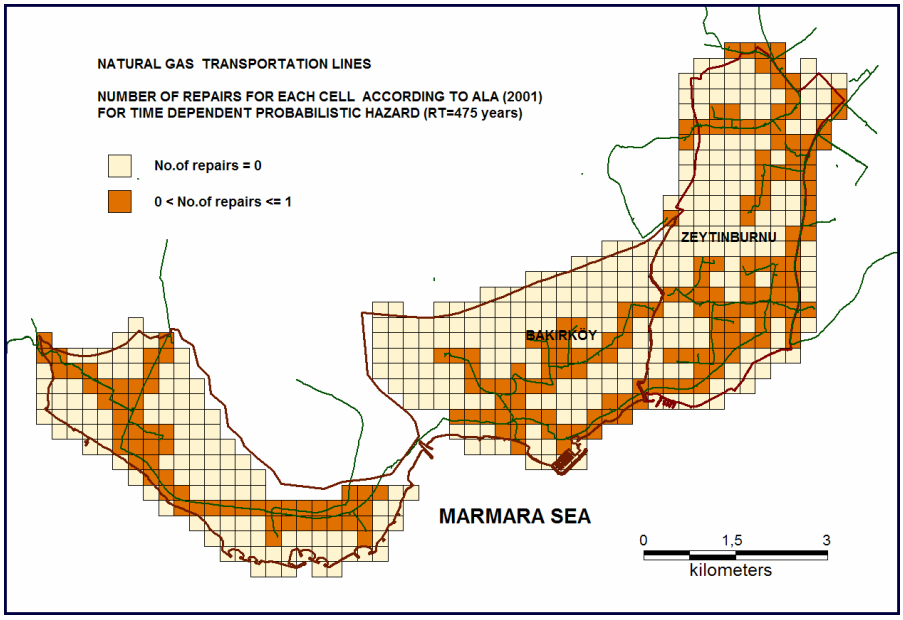

Figure 6.17. As in Figure 6.16, but showing the number of pipe repairs in each cell.

7.SEISMIC DAMAGE AND LOSS SCENARIOS TO INFRASTRUCTURE SYSTEM: TWO APPLICATIONS

This section illustrates how seismic damage to selected IS can be estimated and represented, by making combined use of the ground motion scenarios (discussed in Sect.2) and the available vulnerability functions for the relevant system components. The case of the water distribution systems of Thessaloniki and Düzce are illustrated as applications.

7.1 VULNERABILITY AND DAMAGE EVALUATION FOR THE WATER DISTRIBUTION SYSTEM IN THESSALONIKI (GREECE)

The damage assessment of the water distribution network, including pipelines and buried tanks, in Thessaloniki was performed taking into account both the transient and the permanent contribution on the basis of the ground seismic response from 1D equivalent analyses reported in par. 2.2.1.3. Damage in terms of Repair Rates due to wave propagation only was compared with those based on the 2D wave propagation analyses along the two cross-sections described in detail in paragraph 2.2.1.4, highlighting the estimation differences resulting from these approaches.

7.1.1 Evaluation based on the microzonation study (1D equivalent ground response)

The main characteristics of the drinking water distribution system in Thessaloniki were illustrated in Sect.1. A GIS database contains the construction characteristics of the water pipes in terms of material, diameter and construction year.

As a result of the cited microzonation study of the city, several maps showing the spatial distribution of PGA, PGV, PGD were produced; these provide the input for estimating the seismic damage of the water distribution system (see par. 2.2.1.3).

The fragility functions used for water pipe damage estimation are those of [O'Rourke & Ayala, 1993] for wave propagation, shown in the 2nd row of Table 4.6, and [Honegger & Eguchi, 1992] for permanent deformation, shown in the 2nd row of Table 4.1 [HAZUS methodology NIBS, 2004]. It is recalled here that the [O'Rourke & Ayala, 1993] empirical relationship is based on data collected from actual pipeline damage observed in four USA and two Mexican earthquakes. This relation was validated in Lefkas (Greece) and Düzce

(Turkey) water networks and gave realistic estimations compared with the recorded damage [Alexoudi, 2005]. Two damage states for pipelines were considered, i.e. leaks and breaks, as explained in the sequel in more detail.

Concerning the estimated Repair Rate (RR), according to [Honegger & Eguchi, 1992] for permanent deformation (PGD):

RR [Repairs/Km] $\cong$ K*(7.821*PGD$^{0.56}$)

with PGD (cm) and K: coefficient depending on the type of pipeline (brittle, ductile), it should be noted that for ductile pipelines (steel, ductile iron and PVC), K=0.3, while for brittle pipeline (asbestos cement, concrete and cast iron pipes) K=1.0. Welded steel pipes with arc-welded joints are classified as ductile, while welded steel pipes with gas-welded joints and pre-1935 steel pipes are classified as brittle.

Generally, in Greece most of the tanks are above ground RC tanks. In cases where the components are made of several subcomponents (i.e. pumping plants), fragility curves are based on the probabilistic combination of subcomponents damage functions using Boolean expressions to describe the relationship of subcomponents to the components. For water system facilities (tanks, pumping stations) a total of five damage states are defined (none (ds_1), slight/minor (ds_2), moderate (ds_3), extensive (ds_4) and complete (ds_5)). A pumping station is composed of four subelements: Electric Power, Pump, Building and Electrical/ Mechanical Equipment. Based on Boolean logic a slight/ minor damage for a pumping station was defined by malfunction of plant for a short time (less than three days) due to loss of electric power and backup power if any, or slight damage to building. In Greece, most of water pumping stations does not have electric power generators; there is an anchorage in the electrical/ mechanical equipment without an official code. For the buildings fragility curves a proposal by Kappos et al (2006) was used. It was assumed that the prevailing damage state is the one with the >50% probability of exceeding the respective damage state.
Table 7.1 provides the parameters of the proposed damage functions for pumping plants in Greece (mean values and standard deviations of lognormal distribution functions).

The [HAZUS, 2004] fragility curves were used for wave propagation (Figure 7.1) and for permanent ground deformation (Figure 7.2) for above ground RC tanks. Figure 7.1 and Figure 7.2 also illustrate with the dashed curves the fragility curves proposed by [ALA, 2001a, b].

Table 7.1: Damage Algorithms for Pumping Plants

Peak Ground Acceleration			
Classification	Damage State	Median (g)	σ
Pumping Plants with anchored subcomponents and R/C 1.1.X.X building	slight/minor	0.10	0.55
	moderate	0.15	0.55
	extensive	0.30	0.70
	complete	0.40	0.75
Pumping Plants with anchored subcomponents and R/C 1.1.X.Y building	slight/minor	0.15	0.30
	moderate	0.30	0.35
	extensive	1.10	0.55
	complete	2.10	0.70

(R/C 1.1.X.X: Low- height building, 1- 3 floors, with low level seismic codes; R/C 1.1.X.Y: Low-height building, 1- 3 floors, with advanced seismic codes).

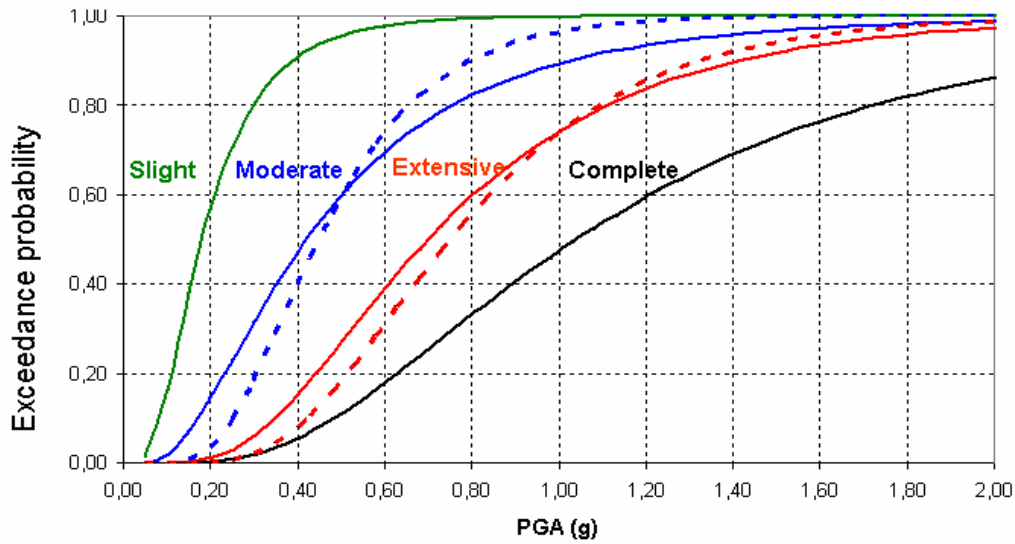

Figure 7.1: Fragility Curves from [HAZUS, 2004] and [ALA, 2001] for above ground RC tanks (wave propagation)

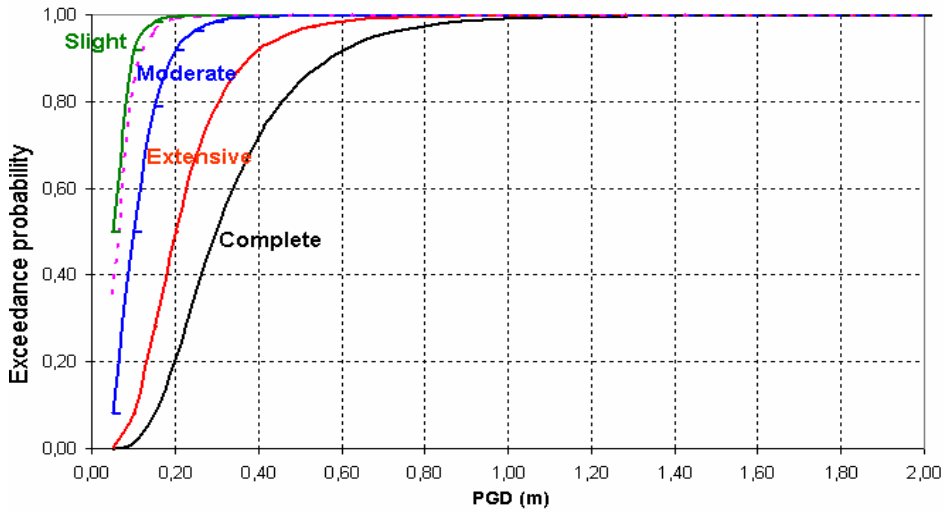

Figure 7.2:. Fragility Curves from [HAZUS, 2004] and [ALA, 2001] for above ground RC tanks (Permanent Ground Deformation)

The spatial distributions of pipe damage due to wave propagation, in terms of RR/km, are illustrated in Figure 7.3 and Figure 7.4 for the 100 and 475 years return period ground motions, respectively. In Thessaloniki a total number of 208 pipes were estimated to experience some type of damage (204 breaks, 4 leaks) for the 100 yr earthquake return period as result of the combined action of permanent ground deformation and wave propagation. For the 475 yr ground motion, about 308 pipes are expected to fail, of which 237 are accounted as breaks and 71 as leaks.

The affected length of damaged pipes, simply considering the actual length between consecutive nodes, is given in the following tables (Table 7.2 and Table 7.3).

The total number of Repairs is obtained, having evaluated RR for each pipeline, multipliying it by the length L_i of each pipe:

$$\text{Repairs} = \sum_i RR_i \cdot L_i$$

Leaks due to permanent ground deformation are assumed to occur on 20% of Repairs, while breaks on the remaining 80%. The position of the first leak (or break) is obtained identifying the pipe that has the highest Repair in the 20% (80%) of Repairs.

Referring to wave propagation, the procedure is the same as for PGD, but now leaks are assumed to occur on 80% of the Repairs and breaks on remaining 20%.

The spatial distribution of estimated damage to water pipes, tanks and pumping stations for the compounded (wave propagation + permanent deformation) 100 and 475 yr ground motions are illustrated in Figures 7.5 and 7.6 respectively.

The distribution of damage in absolute numbers and in percentages for pumping stations and tanks are presented in Table 7.4 and in pie diagrams of Figure 7.7 for 100 and 475 yr return periods.

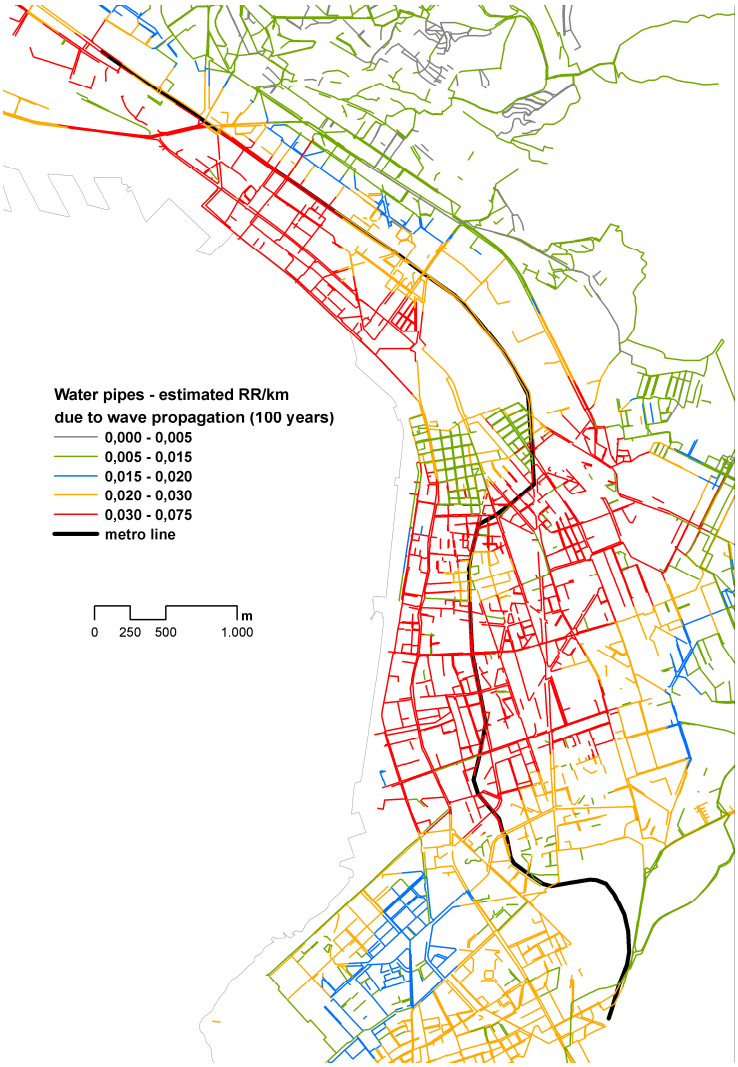

Figure 7.3: Estimated RR/km of water distribution pipes due to wave propagation for the 100 yr ground motions (PGV) calculated in the microzonation study of Thessaloniki.

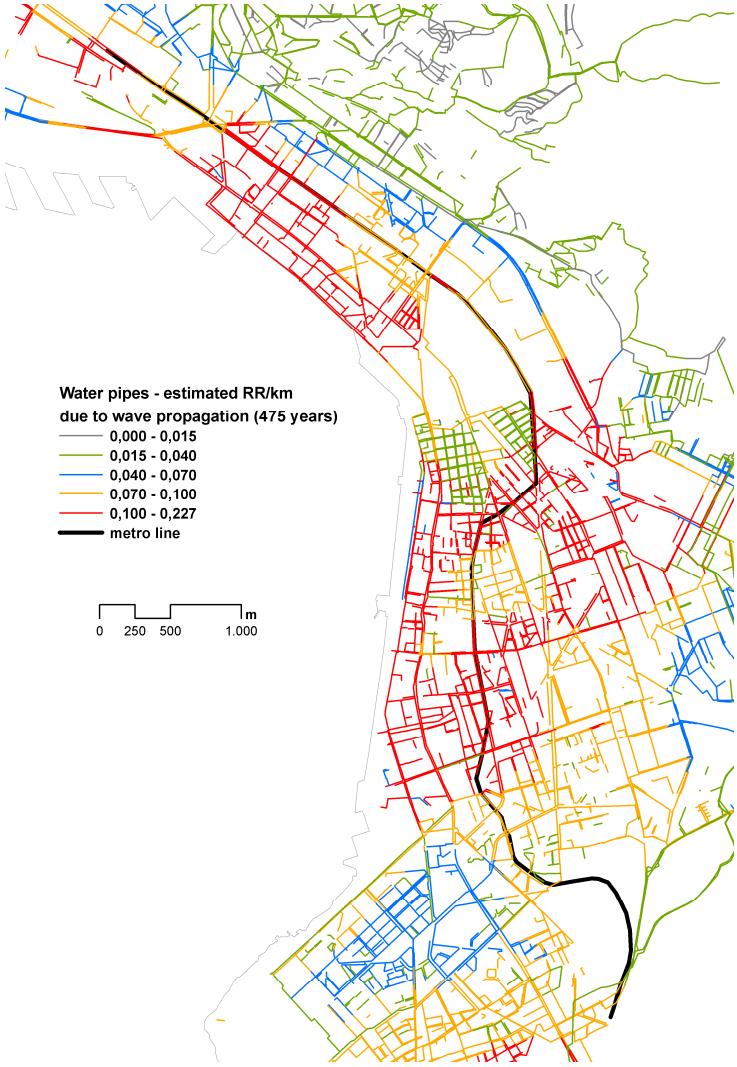

Figure 7.4: Estimated RR/km of water distribution pipes due to wave propagation for the 475 yr ground motions (PGV) calculated in the microzonation study of Thessaloniki.

Table 7.2: Estimated length of damaged water pipes as a result of wave propagation.

	Scenario	
Damage state	**100 years**	**475 years**
Breaks	10 km	28 km
Leaks	24 km	38 km

Table 7.3: Estimated length of damaged water pipes as a result of permanent ground deformation (PGD).

	Scenario	
Damage state	**100 years**	**475 years**
Breaks	71 km	78 km
Leaks	9 km	7 km

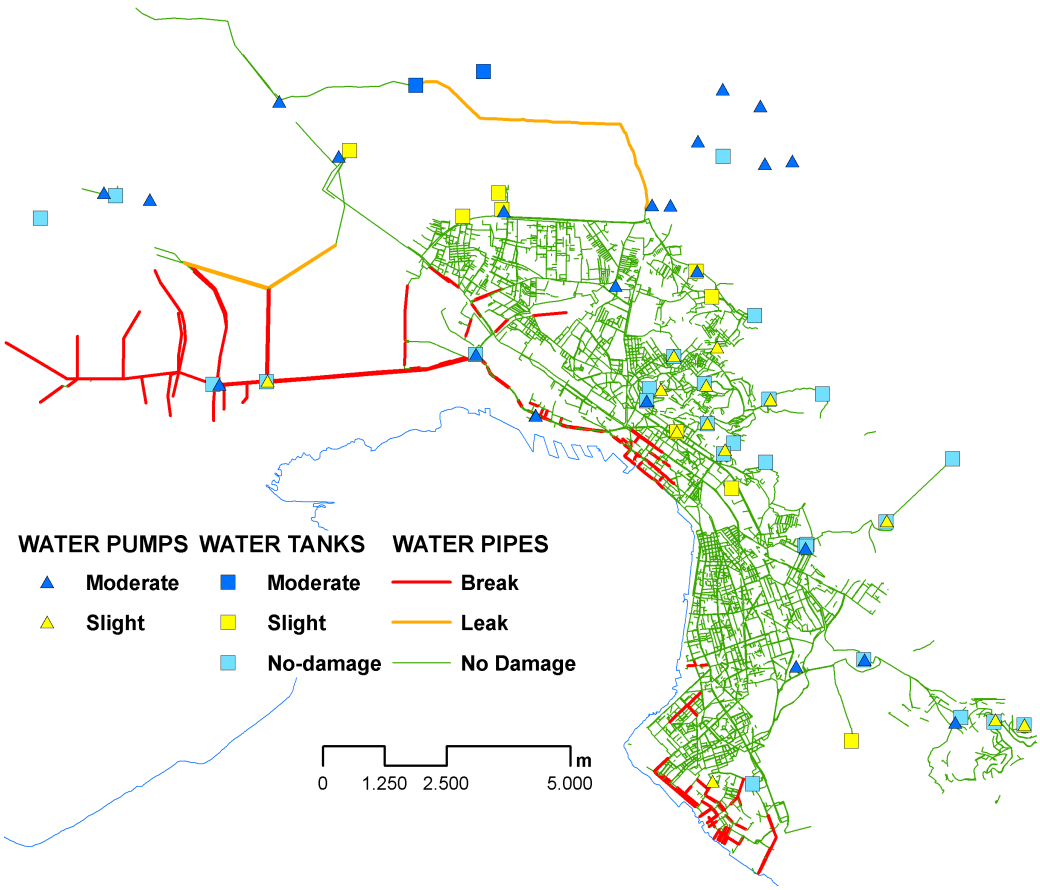

Figure 7.5: Total estimated damage to water system elements in Thessaloniki due to the combination of wave propagation and permanent ground deformations (100 yr return period)

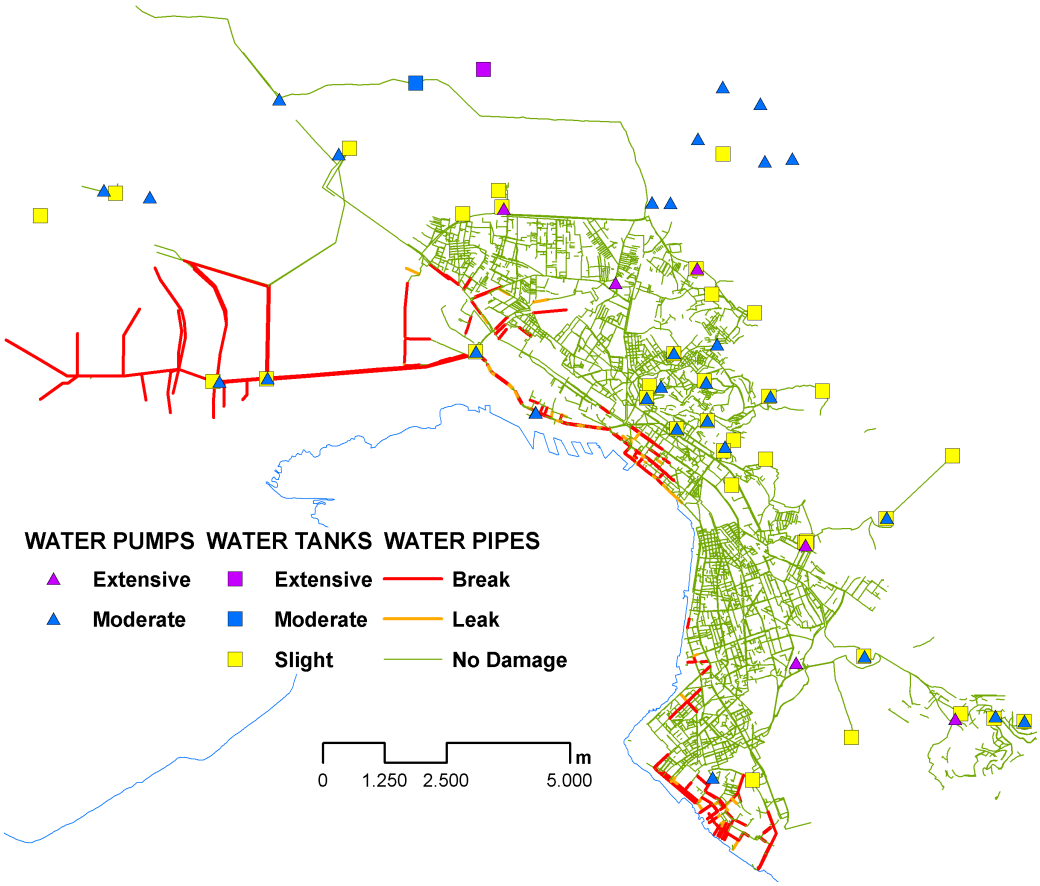

Figure 7.6: Total estimated damage to water system elements in Thessaloniki due to the combination of wave propagation and permanent ground deformations (475 yr return period)

Table 7.4: **Pumping station damages as a result of wave propagation and permanent ground deformation (100 and 475 yr return periods)**

Seismic Scenarios/ Damage state	100 years	475 years
No- damage	-	-
Slight	15	-
Moderate	24	32
Extensive	-	7
Complete	-	-

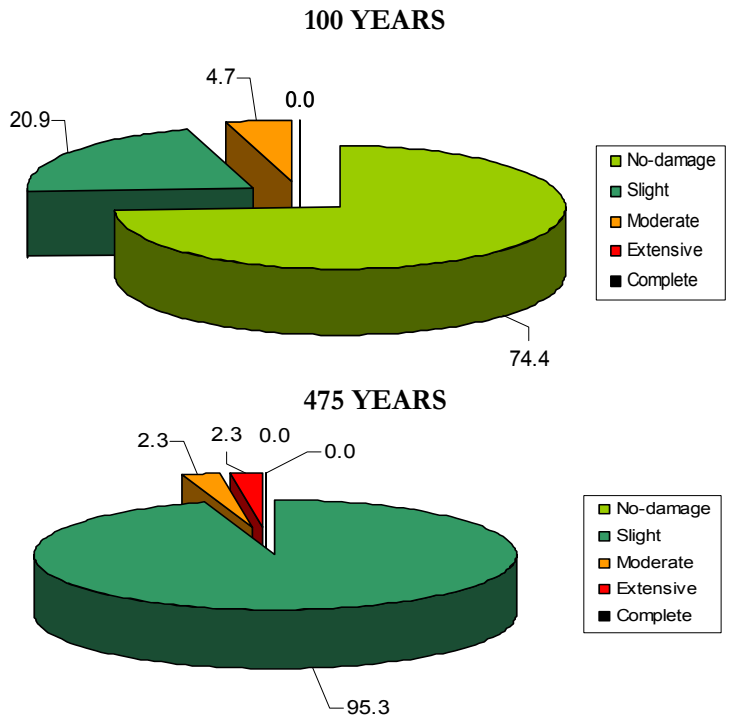

Figure 7.7: Estimated seismic damage to RC tanks in Thessaloniki due to the combined action of wave propagation and permanent ground deformation.

7.1.2 Assessment based on 2D ground response analyses

An independent partial estimation of damage, caused by wave propagation only, has been performed using the ground response values calculated along the 2D cross-sections described in par. 2.2.1.4. The fragility relations are these already introduced (including the one used in 7.1.1), as shown in Figures 7.8 and 7.9.

It turns out that the different fragility functions based on PGV, such as [ALA, 2001] and [O'Rourke and Ayala, 1993], provide quite different predictions of RR, as already noted by [Pitilakis et al., 2005] for other study cases. The [O'Rourke & Ayala, 1993] relation gives similar values as the [O'Rourke & Deyoe, 2004] relation, estimating a high level of damage on soft soils, while the other relations evaluate values smaller by a factor of 2.5, under the threshold of significant damage. These results highlight the uncertainty in the vulnerability assessments; further investigations, possibly based most of all on recorded strain data are required.

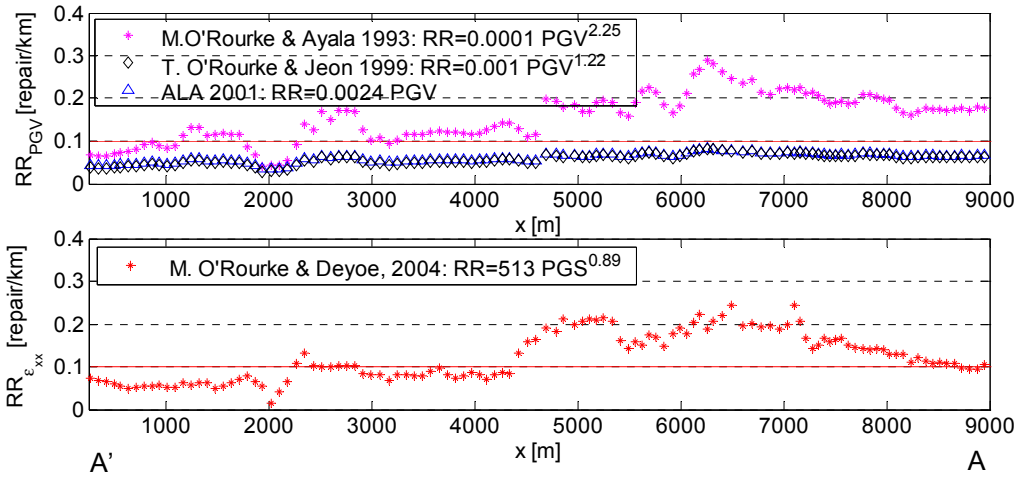

Figure 7.8: Damage response of the "Metro" A'-A cross-section in Thessaloniki (Figure 2.47) to the Mw 6.5 scenario earthquake motion applied as a vertically propagating plane wave: Repair Rate evaluated at 3 m depth on the basis of PGV (RRPGV) and of the peak of longitudinal strain ($RR\varepsilon_{xx}$)

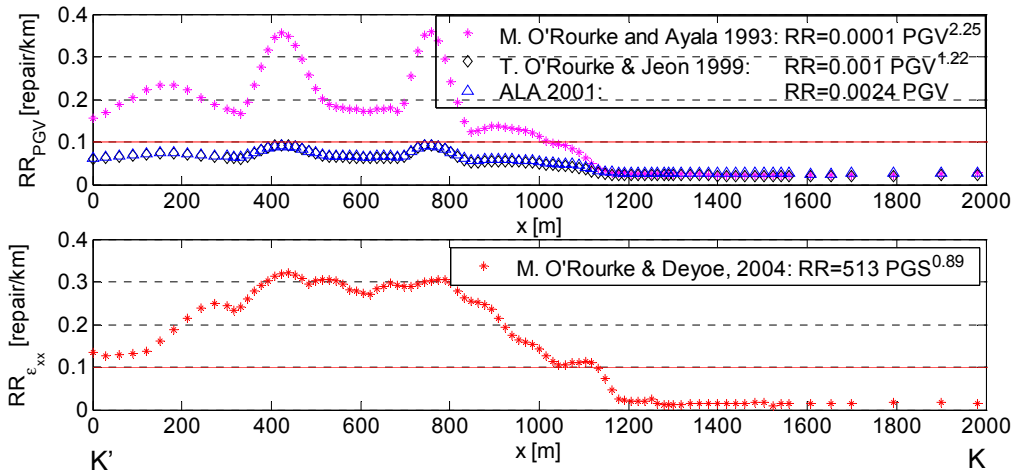

Figure 7.9: Damage response of the "Rotonda" K'-K cross-section in Thessaloniki to the earthquake scenario Mw 6.5 motion applied as a plane wave: Repair Rate evaluated on the basis of the peak ground velocity (RRPGV) and of the peak of longitudinal strain ($RR\varepsilon_{xx}$)

To compare damage estimation from 2D ground response analyses with those based on 1D analyses, evaluated for the return period of 475 years (Figure 7.6), the representation of Figure 7.10 is useful, where RR values are shown at the metro station sites and at the ends of the K-K' cross-sections.

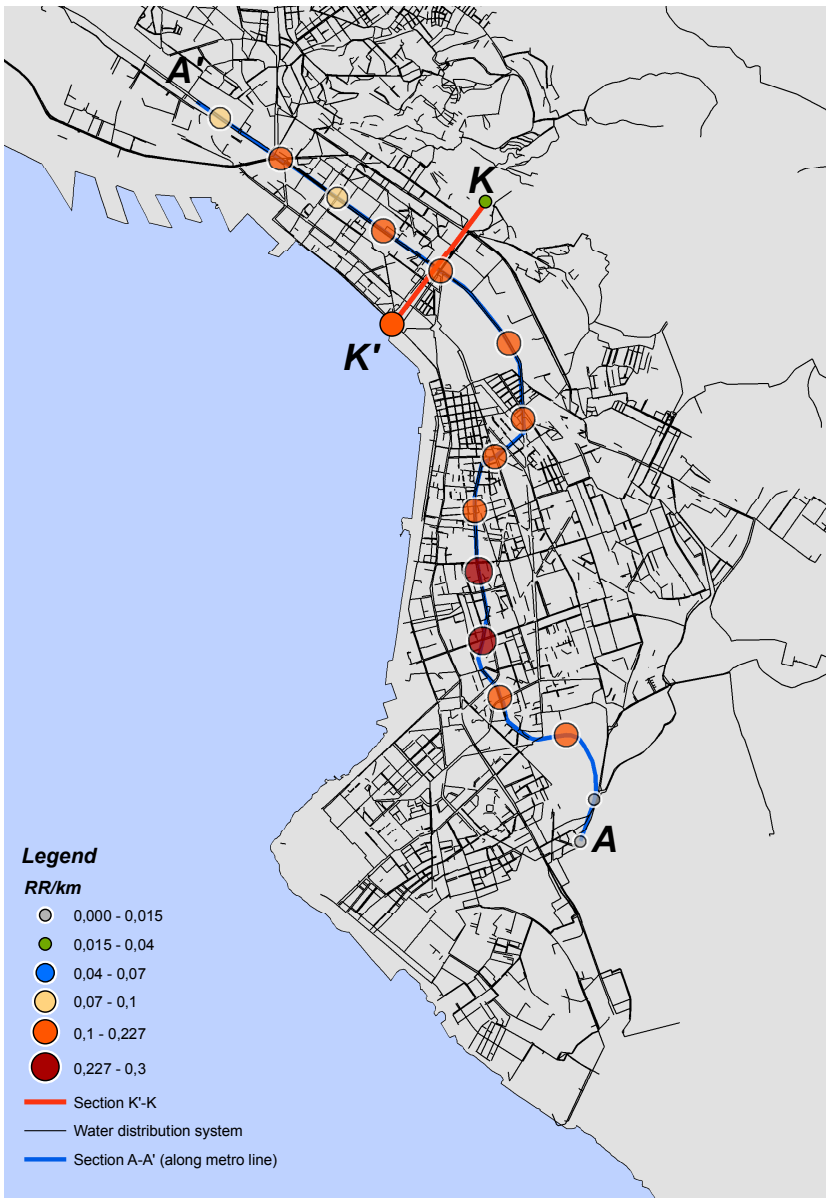

Figure 7.10: Repairs/km estimated by means of the O'Rourke and Ayala (1993) relation on the basis of PGV values calculated by 2D seismic ground response analyses

It appears that an underground pipeline running along the metro line should attain a significant level of damage throughout (RR>0.1). While the results based on 1D analyses attain RR equal to 0.227 as a maximum, the 2D-based evaluations yield a maximum around 0.3. but one should recall that the excitations used in the 1D analyses are more severe than the scenario ground motions used in the 2D simulations.

Along the K'-K cross-section the 1D analyses predict, as expected, higher damage on the soft soil near the sea shore (end K') with respect to rock (end K), similar to the 2D analyses; however, the latter yield damage peaks in correspondence to localised soil amplification zones, as shown in Figure 7.9.

Overall, the 1D analyses seem to underestimate damage by a factor 1.5÷2 with respect to the 2D ones, which take into account the effects of strong lateral heterogeneities and surface wave propagation.

Note that a comparison between 1D and 2D results in terms of damage states (breaks and leaks) is not possible, since the number of Repairs for each pipe of the water network cannot be evaluated from the sole values along a 2D cross-section, without taking into account the pipelines spatial distribution and their length.

7.2 VULNERABILITY AND DAMAGE EVALUATION TO SELECTED PORTIONS OF THE WATER DISTRIBUTION SYSTEM IN DÜZCE (TURKEY)

7.2.1 Repair rate approach

The water pipeline damage in Düzce has been evaluated on the basis of the 2D numerical results illustrated in section 2.2.2 along a NS cross-section. Figure 7.11 shows a comparison between the repair rates evaluated using different vulnerability relations and the PGV – PGS values estimated by the numerical simulations. It turns out that the different vulnerability functions in terms of PGV, such as [ALA, 2001] and [O'Rourke and Ayala, 1993], provide very different predictions of RR, as already noted by [Pitilakis et al., 2005] who estimated, for the area of Düzce, RR varying from 0.117 to 0.884 depending on the relation used. The [O'Rourke and Deyoe, 2004] relationship in terms of PGS (ε_{xx}) provides intermediate values ranging from 0.13 in the Northern part of the town to 0.7 in the Southern one.

If we superimpose in Figure 7.11 the range of RR values observed in different sectors of the city of Düzce reported by e.g. [Tromans, 2004], although the scatter and uncertainty of the evaluation is quite large, we note that both the [O'Rourke and Ayala, 1993] and the [O'Rourke and Deyoe, 2004] relationships result in reasonable agreement with the

observed values, using the simulated range of either PGV or PGS in the most densely built part of the city.

It is important to highlight the difficulty in validating documented data, due to the uncertainties in available reports and, especially in the present case, to the superposition of different causes of damage. This also means that it is difficult to identify which fragility relations yield the most realistic damage scenario.

Comparing the 2D evaluations with the observed failures shown in Figure 4.4 and Figure 4.5 it turns out that the simulated ground motions and the vulnerability relations correctly estimate the concentration of higher damage in the Southern section of the city.

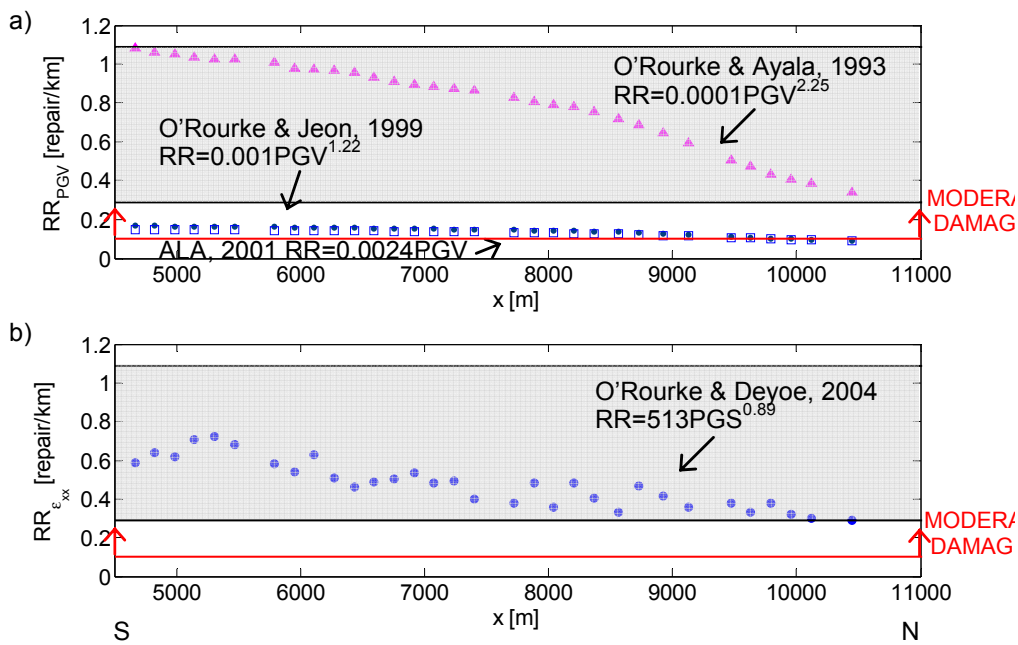

Figure 7.11: Repair Rate evaluation for water pipes in Düzce (meaning of abscissa *x* shown in Figure 2.49) using different vulnerability relations: a) RR based on PGV; b) RR based on PGS. The threshold RR=0.1 Repairs/km associated to moderate damage to pipelines in a large urban area is shown. The shaded strip highlights the range of observed RR [Tromans, 2004]

7.2.2 Detailed analysis of a stretch of water main in Düzce

A further analysis has been performed by means of the programme Seismipipe software described in §6.2 over the stretch of the Düzce water distribution main (oriented SN) shown in Figure 7.12. The pipeline analysed has been considered subjected to the 2D simulated ground displacement field described in par. 3.2.2.

The pipe stretch under investigation, about 2.210 m in length, is described in terms of section properties and material in Table 7.5. The two pipe segments have been considered as fully connected to each other (no deformable joints introduced), and the entire pipeline under examination to be independent from the remaining Duzce water distribution network layout.

As depicted by Figure 2.51, which represent the SN section analysed in the 2D propagation analysis, the pipeline under investigation crosses soils characterized by two different values of average N_{SPT} values, namely:

- From 0 to 630 m (pipe axial local coordinate): $N_{SPT} = 5 \div 30$ (soft soil).
- From 630 to 1800 m: $N_{SPT} = 30 \div 60$ (stiff soil).

In both cases, the soil crossed by the pipeline considered in the analysis to be cohesionless and characterized by the properties listed in Table 7.6.

The characteristic length of the element in the analysis has been taken equal to 5 m, a reasonable value considering the overall length of the pipeline and the very smooth variation of the imposed displacement field along it.

The displacements induced by the propagating waves, as calculated by the 2D site response analysis (see par. 2.2.2), are imposed to the pipeline at the soil-spring supports. Since the Seismipipe analysis should make reference to the worst case in terms of soil displacement configuration, i. e. that characterized by the highest strains (see Figure 2.62 and Figure 2.63), the pipe has been subjected to the spatial ground displacement occurring at t = 14s. At such a time, the pipeline (which in the 2D analysis coordinates covers the range between x = 10520m and x = 12710m) is expected to undergo the highest strain.

The soil-spring characteristics have been defined on the basis of par. 6.2.2 and the analysis performed in 10 steps.

In the diagrams of Figure 7.13 and Figure 7.14, respectively, the results obtained from Seismipipe are given both in terms of bending moments and axial forces. Considering that the yielding moment of the steel pipe section is around 175 KN*m (235 MPa being the yield stress of a reference steel adopted for pipes), the internal action obtained are actually negligible. Such a result should be expected due to the very smooth variation of the displacement field imposed to the pipe by the surrounding soil through the elasto-plastic interaction springs.

It is, however, worth noting how the internal actions in the pipe concentrate around an abscissa x = 550 m (being x in this case aligned along the SN section direction), where the pipeline undergoes a change in direction (see Figure 7.15). This well known behaviour

takes in the literature the name of "cable effect" [ALA, 2001], and is caused by the increase of constraint (and, as a consequence, of the stress) due to a change of the pipe direction.

The application was also meant to demonstrate that when the spatial length of the displacement wave is very long, as in this case, its loading effect on the pipeline is bound to be small, even tough the absolute peak ground displacements are rather large. Only in the presence of strong lateral variations in the surface geology, over distances comparable to the wavelengths at play are likely to induce significantly larger (transient) internal actions.

Table 7.5: Seismipipe application. Pipe characteristics.

Subsection n.	Material	Length m	External Diameter mm	Thickness mm	Burial depth m
1	Asbestos	410	150	15	1.5
2	Steel	1800	500	9	1.5

Table 7.6: Seismipipe application. Properties of soil.

Soil classification	Begin – end (pipeline local coordinates) m		Friction Angle °	Cohesion KPa	Volume weight KN
Soft soil	0	630	30	0	19
Stiff soil	630	1800	35	0	19

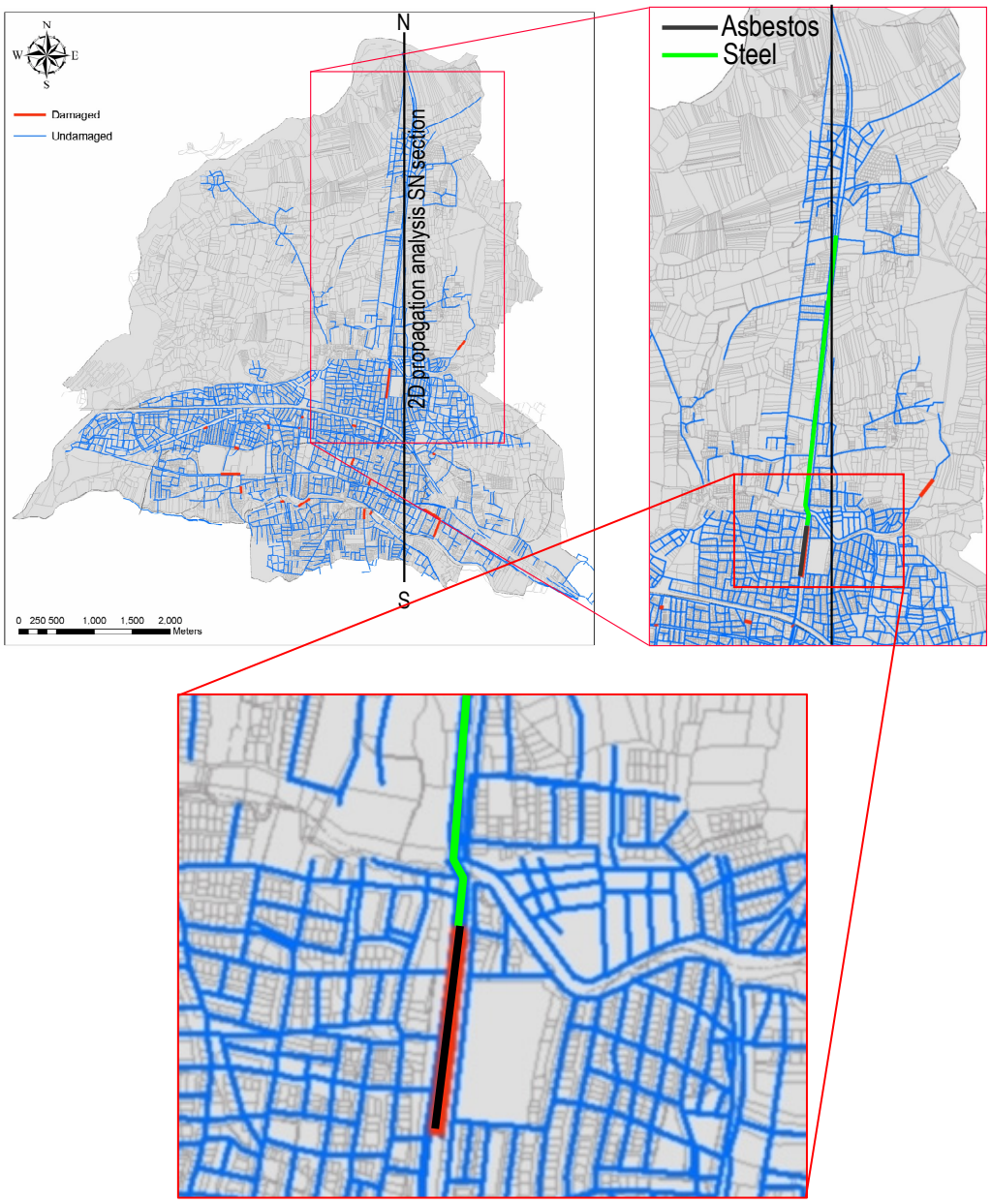

Figure 7.12: Seismipipe application. Stretch of water mainpipe in Düzce analysed by means of the Seismipipe software (see par. 6.2). The lower panel shows the bend in the pipe which generated in the analysis higher local internal actions.

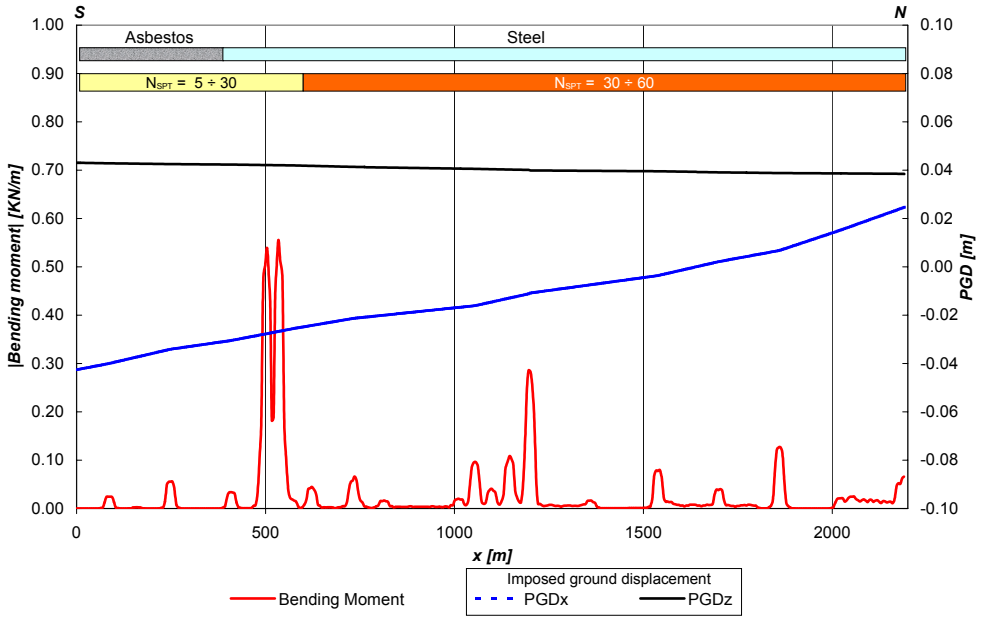

Figure 7.13: Seismipipe application. Bending moment along the pipe, at the end of the analysis.

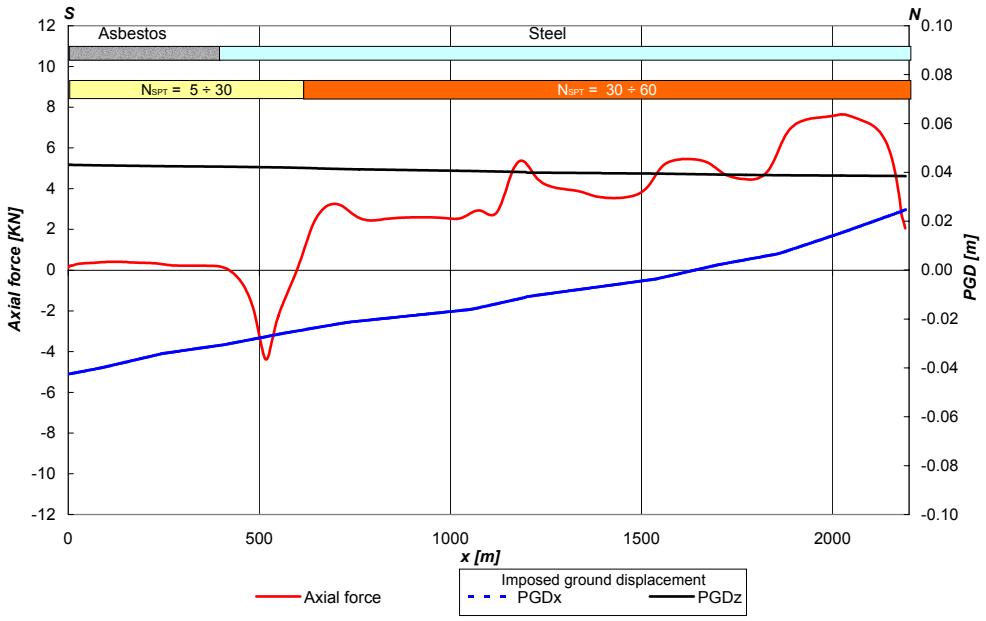

Figure 7.14: Seismipipe application. Axial force along the pipe, at the end of the analysis.

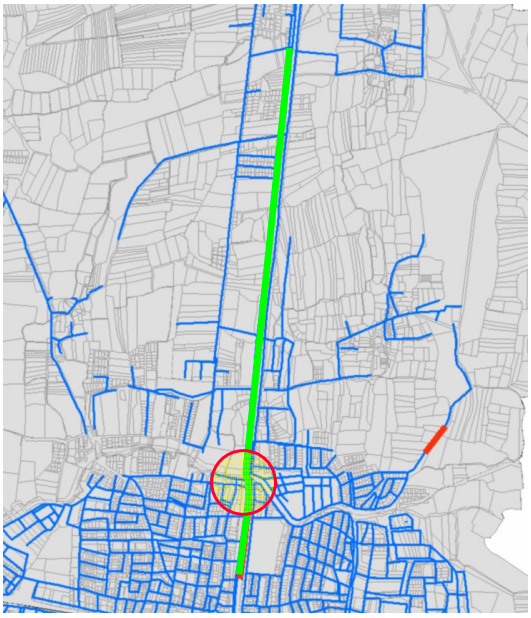

Figure 7.15: Seismipipe application in Düzce. The red circle indicates the location of the pipe segment characterized by higher internal forces induced by the ground displacement.

8.CONCLUSIONS

The following remarks are apt to summarise by way of conclusion the salient indications emerging from the present report:

- The recent historical record in Europe proper indicates that earthquake damage to the most common IS (Infrastructural Systems), including water and gas networks and transportation networks, has been limited and should not be overemphasised; among the main reasons for such moderate impact are the earthquake magnitudes rarely exceeding 7.0, and the uncommon occurrence both of seismically active faults and of extensive soil liquefaction and slope failure phenomena in densely built zones;

- Well documented damage to IS in Europe and neighbouring countries (the 1999 Turkey earthquakes are an exception) is scarce, and in future earthquakes a more dedicated effort by the engineering community is required to progressively fill this gap;

- While a number of European cities have an updated inventory, operated in a GIS environment of the main IS located in their municipal areas, many more don't, and even elementary information on material and diameter of underground pipelines is often not available for some urban sectors;

- While scenario ground motion maps are an indispensable ingredient to perform evaluations of seismic damage to ISs in a city, the type of analysis (and level of sophistication) required to produce such maps should be adjusted to the actual seismic hazard level facing the city, as outlined in the following two items;

    - The simpler approaches for constructing ground motions scenarios are acceptable as long as the seismic hazard is moderate, the near-surface geology exhibits no strong lateral variations, and near field effects from seismic fault ruptures at close range are unlikely; such approaches include those based on propagating in 1D representative recorded accelerograms through local soil profiles to obtain spatial distributions of PGA, PGV and the like, but also producing GIS maps of the same parameters through the use of geological/geotechnical maps and appropriate attenuation relations;

- When, instead, the previous factors (high seismic hazard, irregular surficial geology etc.) are present, the combined influence of earthquake source, propagation path and site effects should be investigated by more advanced tools, including 2D and 3D wave propagation analyses in local geological configurations, as illustrated in different parts of Sect. 3 of this report; in particular the variability of ground motion estimations tied to different possible source scenarios should be carefully considered;

- The main verification of the IS seismic performance should address the Damage Limitation State, in conformity with Eurocode 8 Part 4; hence, the severity of the applicable seismic action should preferably be compatible with the appropriate return period (order of 100 years);
- The RR (Repair Rate), i. e. the expected number of repairs (leaks and breaks) per km of pipe length, is the most convenient simplified indicator of seismic damage for the most commonly impacted ISs, namely water and gas distributions systems; RRs are typically estimated through fragility correlations from PGV, PGA (and permanent ground displacement), or – preferably – from longitudinal ground strain ε;
- In some cases, however, a more accurate verification of a pipeline segment may be required, and this can be performed on structural models of the pipes accounting for interaction with the surrounding ground, as illustrated in Sects. 7 and 8 of this report;
- In the context of simplified damage assessment, emphasis in this report has been placed on the transient, longitudinal peak ground strain as indicator of the local severity of wave propagation effects, in preference to standard parameters such as PGV, because the strain in question is physically more appropriate for representing the seismic action on buried flexible pipelines; however, permanent ground deformations resulting from induced seismic effects (soil liquefaction, landsliding) or fault rupture, tend to be the leading cause of seismic damage to buried pipeline networks;
- RR assessments resting on scenario ground motions based on 1D amplification analyses of local soil profiles, either via PGV or peak ground strains, may underestimate damage because they do not account for important wave propagation effects (e. g. surface waves), as illustrated in this report;
- The spread in IS seismic damage estimations resulting from different fragility correlations is substantial (up to a factor of 5 or so), and much work remains to be done for providing an appropriate conceptual framework to handle this problem.

Acknowledgements

Most of the Düzce geologic and geotechnical data, as well as pertinent GIS layers were provided to Politecnico di Milano and SGI-MI by E. Durukal (KOERI), whose cooperation is gratefully ackowledged. The deeper geotechnical boring data in Düzce were kindly provided to SGI-MI by K. Pitilakis (AUTH).

REFERENCES

Abrahamson, N. A., and Silva, W. J. [1997] "Empirical Response Spectral Attenuation Relations for Shallow Crustal Earthquakes", *Seism. Res. Lett.,* 68, 94–127.

Akinci, A., L. Malagnini, R. B. Herrmann, R. Gok, and M. Sorensen. [2006] "Ground Motion Scaling in the Marmara Region, Turkey". *Geophys. J. Int.*, Volume 166, Page 635 – 651.

Alexoudi, M., [2005] "Contribution to seismic assessment of lifelines in urban areas. Development of a holistic methodology for seismic risk" *PhD Thesis*, Civil Engineering Department, Aristotle University, Thessaloniki, Greece.

Alexoudi, M.,Kakderi K.,Manou D., Batum,E.,Raptakis D., and Pitilakis K. [2005] "Seismic vulnerability analysis of water system. Methodology and application in Lekfas (Greece) and Düzce (Turkey) earthquake, Proc. of the International Symposium on the Geodynamics of Eastern Mediterranean: Active Tectonics of the Aegean Region, Instanbul, Turkey.

Ambraseys, N.N., Douglas, J., Sarma, S.K., and Smit, P.M. [2005]. "Equations for the estimation of strong ground motions from shallow crustal earthquakes using data from Europe and Middle East: Horizontal peak ground acceleration and spectral acceleration", *Bull. of Earthquake Engineering*, 3, 1-53.

Ambraseys, N.N., and Jackson, J. [1998] "Faulting associated with historical and recent earthquakes in the Eastern Mediterranean region", *Geophys. J. Int.,* 133**,** pp.390–406

American Lifelines Alliance [2001a] "Seismic fragility formulations for water systems" *Part 1 – Guideline*. ASCE-FEMA, 104 pp.

American Lifelines Alliance [2001b] "Seismic fragility formulations for water systems" *Part 2 – Appendices*. ASCE-FEMA, 239 pp.

American Lifelines Alliance [2001c] Guidelines for the design of buried steel pipe, www.americanlifelinesalliance.org.

American Lifelines Alliance [2002] "Development of Guidelines to Define Natural Hazards Performance. Objectives for Water Systems". *Volume I*. September, 104 pp.

Anastasiadis, A., Raptakis, D., and Pitilakis, K. [2001] "Thessaloniki's Detailed Microzoning: Subsurface Structure as Basis for Site Response Analysis", *Pure Appl. Geophys.,* Volume 158, Issue 12, pp. 2597-2633.

Anastasiadis, A. [2006] Personal communication, AUTH.

Ansal, A., Laue, J., Buchheister, J., Erdik, M., Springman, S., Studer, J., and Koksal, D. [2004] "Site characterization and site amplification for a seismic microzonation study in Turkey," Proc. of the *11th Int. Conference on Soil Dynamics and Earthquake Engineering and 3rd Earthquake Geotechnical Engineering*, San Francisco.

Ansal, A., Tonuk, G., and Bayraklı, Y. [2005a] "Microzonation for Site Conditions for Bakırköy, Gemlik, Bandırma, Tekirdağ, Eskisehir and Körfez," WB MEER Project -A3 Component, Microzonation and Hazard Vulnerability Studies For Disaster Mitigation in Pilot Municipalities, Bogazici University, Kandilli Observatory and Earthquake Engineering Research Institute, Cengelköy, Istanbul.

Ansal, A., Özaydın, K., Erdik, M., Yıldırım, M., Kılıç, H., Adatepe, S., Özener, P. T., Tonaroglu, M., Sesetyan, K., and Demircioglu, M. [2005b] Seismic Microzonation for Urban Planning and Vulnerability Assessment, Proc. of the *International Symposium of Earthquake Engineering (ISEE2005)*, Geotechnical Session, Awaji Island, Japan.

Ansal, A., Tönük, G., Demircioglu, M., Bayraklı, Y., Sesetyan, K., and Erdik, M. [2006a] "Ground Motion Parameters for Vulnerability Assessment," Proc. of the *First European Conference on Earthquake Engineering and Seismology*, Geneva, Switzerland, Paper Number: 1790.

Ansal, A. Durukal, E., and Tönük, G [2006b] "Selection and Scaling of Real Acceleration Time Histories for Site Response Analyses", Proc. of *ISSMGE, ETC12 Athens Workshop*, Athens Greece.

Ansal, A., Kurtulus, A., and Tönük, G. [2007] "Earthquake Damage Scenario Software For Urban Areas", Proc. of *ECCOMAS Thematic Conference on Computational Methods, in Structural Dynamics and Earthquake Engineering*, Rethymno, Crete, Greece, 13–16 June.

Applied Technology Council [1985] "ATC-13- Earthquake Damage Evaluation Data for California" Redwood City, California, Applied Technology Council.

Applied Technology Council [1991] "Seismic Vulnerability and Impact of Disruption of Lifelines in the Conterminous United States" *ATC-25*, Redwood City, CA.

Ballantyne, D.B, and Heubach W. [1996] "Earthquake Loss Estimation for the City of Everett Washington Lifelines", K/J/C 906014.00, Federal Way, Washington: Kennedy/ Jenks/ Chilton.

Ballantyne, D.B., Berg, E., Kennedy, J., Reneau, R., and Wu, D. [1990] "Earthquake loss estimation modeling for the Seattle water system: report to US Geological Survey under Grant 14-08-0001-G1526", *Technical Report*, Kennedy/Jenks/Chilton, Federal Way, WA.

Bard P.Y., [1999]: "Microtremor measurements: a tool for site effect estimation? State of Art Paper", Proc. of the *2ND International Symposium on the Effects of Surface Geology on Seismic Motion*, eds. K. Irikura, K. Kudo, H. Okada and T. Sasatani (Balkema, Rotterdam).1251-1279.

Bardet J.P., Mace N., Tobita T. and Hu J. [2002] "Regional modeling of Liquefaction-induced ground deformation", *Earthquake Spectra [EERI]*, 18[1].

Bardet J.P., Ichii K., and Lin C.H. [2000] "EERA – A Computer Program for Equivalent-linear Earthquake site Response Analyses of Layered Soil Deposits", UCLA, Department of Civil Engineering.

Bardet J.P., and Tobita T. [2001] NERA – A Computer Program for Non-linear Earthquake site Response Analyses of Layered Soil Deposits, University of South California, Department of Civil Engineering.

Bartlett S.F., and Youd T.L. [1995] "Empirical Prediction of Liquefaction-Induced Lateral Spread", *J. of Geotech. Eng.*, Vol. 121, N°4, pp. 316-329.

Baziar, M. H, Dobry, R, and Elgamal, A.W. "Engineering evaluation of permanent ground deformations due to seismically-induced liquefaction" *National Center for Earthquake Engineering Research (NCEER)* (Technical Report, NCEER-92-0007).

Bernard, P., and Madariaga, R. [1984] "A new asymptotic method for the modeling of near field accelerograms," *Bull. Seismol. Soc. America*, 74, pp. 539-558.

Bielak J., Loukakis K., Hisada Y., and Yoshimura C. [2003] "Domain Reduction Method for Three-Dimensional Earthquake Modeling in Localized Regions, Part I: Theory", *Bull. Seismol. Soc. America*, 817 – 824

Birgören G., Sekiguchi H., and Irikura K., [2004] "Rupture model of the 1999 Düzce, Turkey, earthquake deduced from high and low frequency strong motion data" *Geophysical Research Letters (GRL)*, Vol.31, L05610, 2004.

Bommer, J. J., Elnashai, A. S., Chlimintzas, G. O., and Lee D. [1998] „Review and development of

response spectra for displacement-based design", *ESEE Research Report No. 98-3*, Imperial College, London

Boore, D.M. [2003] "Simulation of ground motion using the stochastic method," *Pure Appl. Geophys*. 160, pp. 635-676.

Boore, D.M., Joyner, W.B., and Fumal, T.E. [1997] "Equations for estimating horizontal response spectra and peak acceleration from Western North American earthquakes: a summary of recent work", *Seismological Research Letters, 68(1),* pp.128-153

BU-KOERI Boğaziçi University, Kandilli Observatory and Earthquake Research Institute [2002] "Earthquake Risk Assessment For Istanbul Metropolitan Area", *American Red Cross Report*

Bürgmann R., Ayhan M.E., Fielding E.J., Wright T.J., McClusky S., Aktuğ B., Demir C., Lenk O., and Türkezer A., [2002], "Deformation during the 12 November 1999 Düzec, Turkey, earthquake from GPS and InSAR data", *Bull. Seismol. Soc. America*, Vol. 92, 161-171.

Byrne, P. [1991] "A Cyclic Shear-Volume Coupling and Pore-Pressure Model for Sand," Proc. *of 2Nd International Conference on Recent Advances in Geotechnical Earthquake Engineering and Soil Dynamics,* St. Louis, Missouri, Paper No. 1.24, 47-55.

CEN [2006], Eurocode 8 – Design of structures for earthquake resistance. Part 4: Silos, tanks and pipelines. prEN 1998-4, Final draft, January 2006, Comité Européen de normalisation, Brussels.

Cotecchia, V., "Effects of the Novembre 23, 1980 earthquake on the lining of Pavoncelli tunnel, Apulian water supply, as related to soils in the area served by the system", Proc. *Interntl. Congress on Large Underground Openings*, Florence (Italy), 8-11 June 1986, Vol. II, p. 86.

Cultrera, G., Pessina, V., Ameri, G., Franceschina, G., Pacor, F., Akinci, A., Cocco, M., Zonno, G., Pitilakis, K., Alexoudi, M., Kakderi, K., Faccioli, E., Paolucci, R., Callerio A., Scandella, L., Ansal, A., Erdik, M., Tönük, G., Demircioglu, M., and Sesetyan, K. (2006), Deliverable 116 – Technical Report on the creation of earthquake ground shaking scenarios, including 2D calculations, appropriate to lifelines systems with examples of application to selected urban areas (Part 2), LESSLOSS Risk Mitigation for Earthquakes and Landslides Integrated Project Deliverable Report

CyberQuake [2000], User's Guide, Version 2.0, BRGM, Orléans.

Day, S.M. 1977. Finite element analysis of seismic scattering problem, PhD Thesis. University of California. San Diego

Dowding, C. H., and Rozen, A. [1978] "Damage to rock tunnels from earthquake shaking", *Journal of the Geotechnical Engineering Division,* 104 [2], 175-191.

Durukal, E., Ansal, A., and Tönük, G. [2006] "Effect of Ground Motion Scaling and Uncertainties in Site Characterisation on Site Response Analyses", Proc. of the *100th Anniversary Earthquake Conference Commemorating the 1906 San Francisco Earthquake*, San Francisco, USA

EC Contract EVK4-CT-2000-00014 "An advanced approach to earthquake risk scenarios with applications to different European towns", RISK-UE [2001-04]

EERI [2000] "Izmit-Kocaeli Earthquake Reconnaissance Report, Chapter 13: Performance of Waterfront Structures", *Earthquake Spectra,* Supplement to Vol. 16, December 2000.

Eidinger J.M., [1998] "Lifelines, Water Distribution System" in the Loma Prieta, California, Earthquake of October 17, 1989, Performance of the Build Environment –Lifelines, US Geological Survey Professional Paper 1552-A, pp. A63-A80, A. Schiff Ed.

Eidinger J.M., Avila E [1999] "Guidelines for the seismic upgrade of Water Transmission Facilities" ASCE, TCLEE, Monograph No. 15.

Eidinger J.M., Maison B, Lee D, and Lau B [1995] "East Bay Municipality Utility District Water Distribution Damage in 1989 Loma Prieta Earthquake", *Proceedings of the Fourth U.S Conference on Lifeline Earthquake Engineering*, ASCE, TCLEE, Monograph 6, ASCE, pp. 240-247.

Elgamal, A., Yang, Z., Parra, E., and Ragheb, A. [2001], CYCLIC 1D, UCSD.

Ellsworth, W. L., Celebi, M., Evans, J. R., Jensen, E. G., Kayen, R., Metz, M. C., Nyman, D. J., Roddick, J.W., Stephens, C. D., and Spudich, P. [2004] "Near-field ground motion of the 2002 Denali fault, Alaska, earthquake recorded at Pump Station 10", *Earthquake Spectra*, 20, (3), 597–615

Erdik, M. Aydınoglu, N. , Barka, A., Yüzügüllü, Ö., Siyahi, B., Durukal, E., Fahjan, Y., Akman, H., Birgören, G., Biro, Y., Demircioğlu, M., Özbey C., and Sesetyan, K. [2002] BU-ARC, Earthquake Risk Assessment for Istanbul Metropolitan Area, Project Report, Bogazici University Publication.

Erdik, M., [2000], Report on 1999 Kocaeli and Düzce [Turkey] Earthquakes, Bogazici University.

Erdik, M., Demircioglu, M., Sesetyan, K., Durukal, E., and Siyahi, B. [2004] "Earthquake Hazard in Marmara Region", *Soil Dynamics and Earthquake Engineering*, Vol.24, pp.605-631

Erdik, M., Demircioglu, M., Sesetyan, K., and Durukal, E. (2005), Assessment of earthquake hazard for Bakırköy, Gemlik, Bandırma, Tekirdağ and Körfez, WB MEER Project -A3 Component, Microzonation and Hazard Vulnerability Studies For Disaster Mitigation in Pilot Municipalities, Bogazici University, Kandilli Observatory and Earthquake Engineering Research Institute.

Faccioli E., Maggio F., Quarteroni A., and Tagliani A. [1996] "Spectral-domain decomposition methods for the solution of acoustic and elastic wave equations", *Geophysics*, Vol. 61, No. 4, pp. 1160-1174

Faccioli E., Maggio F., Paolucci R., and Quarteroni A. [1997] "2d and 3D elastic wave propagation by a pseudo-spectral domain decomposition method", *Journal of seismology*, Volume 1, N.3, 237-251

Faccioli E., Paolucci R., and Pessina V., [2002] "Engineering assessment of seismic hazard and long period ground motions at the Bolu viaduct site following the November 1999 earthquake", *J. of Seismology*, Vol. 6, No. 3, pp. 307 - 327.

Faccioli, E., Paolucci, R., Ameri, G., Akinci, A., Cocco, M., Cultrera, G., Franceschina, G., Pacor, F., Pessina, V., Lombardi, A.M., Zonno, G., Pitilakis, K., Kakderi, K., Alexoudi, M., Ansal, A., Erdik, M., Tönük, G., Demircioglu M., and Scandella, L. [2005] LessLoss Deliverable D83 – Technical report on the creation of earthquake ground shaking scenarios appropriate to lifelines system with examples of application to selected urban areas (Part1).

Faccioli .E. [2006] "Seismic hazard assessment for derivation of earthquake scenarios in Risk-UE, *Bull. Earthquake Engineering*, 4, 341-364.

Faccioli E., Cauzzi C., Villani M., Paolucci R. , Vanini M., and Finazzi D. [2007] **"**Long period strong ground motion and its use as input to displacement based design", Proc. of the *4th International Conference on Earthquake Geotechnical Engineering,* Keynote Lecture Volume Thessaloniki (Greece), June.

FAUST – FAUlts as Seismologists' Tool - Web database of seismogenic sources - http://faust.ingv.it/

FP6 – IP Project LessLoss "Risk mitigation for Earthquake and Landslides" – Deliverable Report D88, Technical report including CD, containing the dataset of the inventory of lifelines in reference cities, Feb. 2006

FP6 – IP Project LessLoss "Risk mitigation for Earthquake and Landslides" – Deliverable Report D116, Technical Report on the creation of earthquake ground shaking scenarios, including

2D calculations, appropriate to lifelines systems, with examples of application to selected urban areas (Part 2), Sept. 2006

FP6 – IP Project LessLoss "Risk mitigation for Earthquake and Landslides" – Report #7:Disaster Scenarios Predictions and Loss Modelling for Urban Areas, Lead editor R.Spence, Reviewer M.Erdik

Gallovič, F., and Brokešová, J. [2007]. "Hybrid k-squared Source Model for Strong Ground Motion Simulations: Introduction", *Phys. Earth Planet. Interiors* 160, 34-50

Gazdag, J., [1981], "Modeling of the acoustic wave equation with transform methods", *Geophysics*, 46,854-859.

Gazetas G., Dakoulas P., and Dennehy K. [1990] "Empirical seismic design method for waterfront anchored sheet pile walls", Proc. *ASCE Specialty Conference on Design and Performance of Earth Retaining Structures*, ASCE Geotechnical Special Publication No. 25, pp. 232-250.

Goldsworthy, M., James J., and Haines, J. [2002] "The continuity of active fault systems in Greece", *Geophys. J. Int.,* 148, pp. 596–618.

Hamada, M., Yasuda, S., Isoyama, R., and Emoto, K. (1986b) "Study on liquefaction-induced permanent ground displacements and earthquake damage", Proc. *JSCE*, No.376/III-6, 221-229

Hamada M., and Akioka Y, [1997] "Liquefaction induced ground strains and damage to buried pipes" Proc. *of Japan Society of Civil Engineers Earthquake Engineering Symposium,* Vol.1, pp.1353-1356 [in Japanese]

Hashash, Y.M.A., Hook, J.J., Schmidt, B., and Yao, J.I-C. [2001] "Seismic design and analysis of underground structures", Tunnelling and Underground Space Technology, 16, 247-293.

Hashash Y.M.A., and Park D. [2005], DEEPSOIL Computer program for 1D non-linear and equivalent linear site response analyses, University of Illinois, U.S.A.

HAZUS Earthquake Loss Estimation Methodology [1999], see National Institute of Building Sciences [2004].

Herrero, A., and Bernard, P. [1994] "A kinematic self-similar rupture process for earthquakes", *Bull. Seismol. Soc. America,* 84, 1216–1228.

Heubach W [1995] "Seismic Damage Estimation for Buried Pipeline Systems" *Proceedings of the*

Fourth US Conference on Lifeline Earthquake Engineering, TCLEE, Monograph No.6, ASCE, pp312-319.

Honegger D. G, and Eguchi R.T. [1992] Determination of the Relative Vulnerabilities to Seismic Damage for Dan Diego Country Water Authority [SDCWA] Water Transmission Pipelines.

Ichii K. [2003] "Application of Performance-Based Seismic Design Concept for Caisson-Type Quay Walls", *Dissertation*, Kyoto University.

Ichii K. [2004] "Fragility Curves for Gravity-Type Quay Walls Based on Effective Stress Analyses", Proc. of the *13th World Conference on Earthquake Engineering*, Vancouver, BC Canada, August 2004.

Idriss, I. M. [1990] "Response of Soft Soil Sites during Earthquakes", Proc. *Memorial Symposium to honor Professor Harry Bolton Seed*, Berkeley, California, Vol. II, May.

Idriss, I. M., and Sun J. I. [1992] Shake91, A Computer Program for Conducting Equivalent Linear Seismic Response Analysis of Horizontally Layered Soil Deposits Modified based on the original SHAKE program Published in December 1972 by Schnabel, Lysmer and Seed.

Isoyama R., and & Katayama, T. [1982] "Reliability Evaluation of Water Supply Systems During Earthquake", *Report of the Institute of Industrial Science*, Univeristy at Tokyo, Vol.30, No.1.

Isoyama, R., E. Ishida, K. Yune, and T. Shirozu [1998] "Seismic Damage Estimation Procedure for Water Supply Pipelines", Proc. *Water & Earthquake '98 Tokyo, IWSA International Workshop, Anti-Seismic Measures on Water Supply, International Water Services Association and Japan Water Works Association,* Tokyo Japan.

Isoyama, R., Ishida, E., Yune, K., and Shirozu, T. [2000] "Seismic damage estimation procedure for water supply pipelines," Proc. of the *Twelfth World Conference on Earthquake Engineering,* CD-ROM Paper No. 1762, 8pp.

Iyisan, R. [1996] "Correlations between Shear Wave Velocity and In-situ Penetration Test Results", *Technical Journal of Turkish Chamber of Civil Engineers*, Vol. 7, No. 2, pp.1187-1199 (in Turkish)

Joyner, W. B., and Boore, D. M. [1988] "Measurement, Characterization, and Prediction of Strong Ground Motion" Proc. *Earthquake Engineering and Soil Dynamics II: Recent Advances in Ground-Motion Evaluation, proceedings of the specialty conference*, June 27-30, 1988, Park City, UT, *Geotechnical Special Publication* No. 20, J. Lawrence Von Thun, ed., ASCE, New York, pp 359-375. pp 43-102.

Kakderi K., Raptakis D., Argyroudis S., Alexoudi M., and Pitilakis K. [2006] "Seismic Response and Vulnerability Assessment of Quaywalls. The Case of Lefkas.", P*roceedings of the 5th National Conference of Geotechnical and Environmental Engineering*, Xanthi, Greece [in Greek]

Kappos, A., Panagopoulos, G., Panagiotopoulos, Ch., and Penelis, Gr. (2006) "A hybrid method for the vulnerability assessment of R/C and URM buildings", *Bulletin of Earthquake Engineering*, Vol. 44, pp. 391-413.

Karagianni, E.E., Papazachos, C.B., Panagiotopoulos, D.G., Suhadolc, P., Vuan, A., and Panza, G. F. [2005] "Shear velocity structure in the Aegean area obtained by inversion of Rayleigh waves", *Geophys. J. Int.*, 160(1), pp. 127-143.

Kayen, R., Thompson, E., Minasian, D., Moss, R. E. S. , Collins, B. D. , Sitar, N. , Dreger, D. and Carver, G. [2004]. "Geotechnical Reconnaissance of the 2002 Denali Fault, Alaska", *Earthquake Spectra*, 20, (3), 639-667.

Kennedy, R.P., Chow, A.W., and Williamson, R.A. [1977] "Fault Movement Effects on Buried Oil Pipeline", *Journal of the Transportation Engineering Division*, ASCE, 103, TE5, 617-633.

Kelly, K.R., Ward, R.W., Treitel, S., and Alford, R.M., [1976] "Synthetic seismograms:A finite-difference approach", *Geophysics*, 41, 2-27.

Klimis, N. S., B. N. Margaris, and P. K. Koliopoulos [1999]. "Site-dependent amplification functions and response spectra in Greece", *J. Earthquake Eng.*, 3, 237–270.

Kosloff, D., Kessler, D., Filho, A.Q., Tessmer, E., and Strahilevitz, R., [1990] "Solution of the Equations of Dynamic Elasticity by a Chebychev Spectral Method".*Geophysics*, Vol. 55, N.6, 734 - 748.

Kosloff, D. D., and Baysal, E., [1982], "Forward modeling by a Fourier method" *Geophysics*, 47, 1402-1412.

Komatitsch D. and Vilotte J.P. [1998] "The spectral element method: An efficient tool to simulate the seismic response of 2D and 3D geological structures", *Bulletin of the Seismological Society of America*; v. 88; no. 2; p. 368-392

Kudo, K., Kanno, T. , Okada, H., Ozel, O., Erdik, M. , Sasatani, T. , Higashi, S., Takahashi, M., and Yoshida, K. [2002], "Site-Specific Issues for Strong Ground Motions during the Kocaeli, Turkey Earthquake of 17 August 1999, as inferred from Array observations of Microtremors and Aftershocks], *Bull. Seismol. Soc. Am.*, 92, 448-465

Liu, A., Takada, S., and Ho, Y. [2004] "A Shell Model with an Equivalent Boundary for Buried Pipelines under the Fault Movement", Proc. of the *13th World Conference on Earthquake Engineering*, Paper n. 613.

Loukakis, K. E. [1988]. "Transient response of shallow layered valleys for inclined incident SV waves calculated by the finite element method", *M.Sc. Thesis*, Carnegie Mellon University, Pittsburgh.

Margaris, B.N., and Boore, D.M. [1998] "Determination of $\Delta\sigma$ and k_0 from response spectra of large earthquakes in Greece", *BSSA*, Vol. 88, No. 1, pp. 170-182.

McClusky, S. *et al.* (28 authors) [2000] "GPS constraints on plate motions and deformations in the eastern Mediterranean: implications for plate dynamics", *J. Geophys. Res.,* 105**,** pp**.** 5695–5719.

Moczo, P., Labak, P., Kristek, J., and Hron, F., [1996] "Amplification and differential motion due to an antiplane 2-D resonance in the sediment valleys embedded in a layer over the halfspace" *Bull. Seism. Soc. Am.*, 86, 1434-1446

Moczo P., Kristek J., and Halada L. [2000] "3D Fourth-order staggered-grid finite-difference schemes: stability and grid dispersion", *Bulletin of the Seismological Society of America*, Vol.90, No.3, pp. 587-603

Monge, O., Alexoudi,M., and Argyroudis,S. [2004] "Vulnerability assessment of linfelines and essential facilities (WP06):basic methodological handbook", RISK-UE, Report n°GTR-RSK 0101-152av7

National Institute of Building Sciences [NIBS] [2004] "Earthquake loss estimation methodology. HAZUS", *Technical manuals*, Federal Emergency Management Agency, Washington, D.C.

Newmark, N.M., and Hall, W.J. [1975] "Pipeline Design to Resist Large Fault Displacement", Proc. of the *U.S. National Conference on Earthquake Engineering*, Ann Arbor, Michigan, 416-425.

Newmark, N.M., [1967] "Problems in WavePropagation in Soil and Rocks", Proc. of the *International Symposium on Wave Propagation and Dynamic Properties of Earth Materials*, Albuquerque, NM, pp. 7-26.

O'Rourke, M.J., and Ayala, G. (1993), "Pipeline damage due to wave propagation", *J. of Geotech. Eng.,* 119 (9), 1490–1498.

O'Rourke, M.J., and Deyoe E [2004] "Seismic Damage to segmented buried pipe", *Earthquake*

Spectra, Vol.20, No.4, pp. 1167-1187

O'Rourke, M.J., and Liu, X. [1999] "Response of buried pipelines subject to earthquake effects" *MCEER. Monograph series n°3.* 249 p.

O'Rourke, T.D., and Palmer, M.C. [1996] "Earthquake performance of gas transmission pipelines", *Earthquake Spectra,* 12 [3], pp. 493- 527

O'Rourke, T.D., and Jeon, S.-S., [1999] "Factors affecting the earthquake damage of water distribution systems," Proc. of the *Fifth US Conference on Lifeline Earthquake Engineering,* Seattle, WA, ASCE, Reston, VA, 379-388.

O'Rourke, T. D., Erdogan, F.H., Savage,W.L., Lund, L.V. , Tang, A, Basoz, N., Edwards,C., Tezel,G., and Wong, F. [2000] "Water, Gas, Electric Power and Telecommunications Performance", *1999 Kocaeli, Turkey, Earthquake Reconnaissance Report, EQ Spectra* Supplement A to Volume 16.

O'Rourke, T.D., Toprak, S., and Sano, Y. [1998] "Factors affecting water supply damage caused by the Northridge earthquake.", Proc. of the *Sixth US National Conference on Earthquake Engineering.* [CD-ROM].

OCDI [2002] "Technical standards and commentaries for port and harbour facilities in Japan", The overseas coastal area development institute of Japan, 600p.

Olson, A.H., Orcutt, J.A., and Frazier, G.A. [1984] "The discrete wavenumber / finite element method for synthetic seismograms", *Geophys. J.R. Astr. Soc.*,v.77, pp. 421-460.

Ohminato T., and Chouet B.A. [1997] "A free-surface boundary condition for including 3D topography in the finite-difference method", *Bulletin of the Seismological Society of America,* v. 87; no. 2; p. 494-515

Ordaz M., Jara, J.M., and Singh, S.K., [1991] "Riesgo sismico y espectros de diseño en el Estado de Guerrero", In forme conjunto del Instituto de Ingeniería, UNAM y el Centro de Investigacíon Sísmica AC de la Fundacíon Javier Barros Sierra, Mexico City.

Owen, G. N., and Scholl, R. E. [1981] "Earthquake engineering of large underground structures, prepared for the Federal Highway Administration", FHWA/RD-80/195, 279p, URS/John A. Blume and Ass.

Pachakis D., and Kiremidjian, A. S. [2004] "Estimation of Downtime-Related Revenue Losses in Seaports Following Scenario Earthquakes", *Earthquake Spectra,* Vol. 20, No. 2, May 2004.

Pacor, F., Cultrera, G., Mendez, A. , and Cocco, M. [2005]. "Finite Fault Modeling of Strong Ground Motion Using a Hybrid Deterministic - Stochastic Method," *Bull. Seism. Soc. Am.*, 95, 225-240.

Paolucci, R. [2006] "Simplified modelling of continous buried pipelines subject to earthquake fault rupture". Proc. *1st European Conference on Earthquake Engineering and Seismology*, Geneva, Switzerland, 2006, Paper n. 559.

Paolucci, R., Faccioli, E., Smerzini, C., Scandella, L., Stephenson, W., Argyroudis, S., Kakderi, K, Pitilakis, K., and Vannoli, P. [2006], LessLoss Deliverable D87 – Technical report on the evaluation of earthquake ground deformations, with applications to representative geological configurations of selected cities.

Paolucci, R., and Pitilakis, K. [2007] "Seismic risk assessment of underground structures under transient ground deformations", *Earthquake Geotechnical Engineering*, K. Pitilakis ed., ch. 18, Springer.

Papazachos, B.C., Comninakis, P.E., Karakaisis, G.F., Karakostas, B.G., Papaioannou, Ch.A., Papazachos, C.B., and Scordilis, E.M. [2000] "A catalogue of earthquakes in Greece and surrounding area for the period 550BC-1999", *Publ. Geoph. Lab.*, Univ. of Thessaloniki, 1, pp. 333

Papazachos, B.C., and Papazachou, C. [1997] The Earthquakes of Greece," Ziti Publications, Thessaloniki.

Papazachos, C., and Nolet, G., [1997] "P and S deep velocity structure of the Hellenic area obtained by robust nonlinear inversion of travel times", *J. Geophys. Res.*, 102, pp. 8349–8367.

Pavlides, S., and Caputo, R. [2004] "Magnitude versus faults' surface parameters: quantitative relationships from the Aegean Region," *Tectonophysics*, 380, 159-188.

PEER Strong Motion Data Bank, http:// peer.berkeley.edu

Pessina, V. [1999] "Empirical prediction of the ground shaking scenario for the Catania area", *J. of Seismology*, Special Issue, Vol.3, N.3, 265-277

PIANC [2001] "Seismic Design Guidelines for Port Structures", International Navigation Association, Balkema, 474p.

Pitilakis K., Alexoudi A., Argyroudis S., Monge O., and Martin C., [2006] "Chapter 9: Vulnerability assessment of lifelines", C.S. Oliveira, A. Roca and X. Goula ed. "*Assessing and Managing*

Earthquake Risk. Geo-Scientific and Engineering Knowledge for Earthquake Risk mitigation: Developments, Tools and Techniques", Springer Publ.

Pitilakis K., [2004] "Chapter 5: Site effects", *Recent Advances in Earthquake Geotechnical Engineering & Microzonation, A. Ansal ed.*, Kluwer Publ.

Pitilakis K., Anastasiadis A., Alexoudi M., and Argyroudis S., [2005]. "An advanced approach to earthquake risk scenarios: The case of Thessaloniki (Greece)". in NATO SfP977231: *Seismic Assessment and Rehabilitation of Existing Buildings, Advances in earthquake Engineering for Urban Risk Reduction*, Istanbul, Turkey, 30 May- 1 June

Pitilakis, K., Alexoudi, M., Kakderi, K., Argyroudis S., Roberto Paolucci, R., Ansal, A., Erdik, M. and Tönük, G. [2006b] Deliverable D89 – Technical Report on the Assessment of Vulnerability Functions for Pipelines, Shallow Tunnels and Waterfront Structures.

Plaxis [2002] "Plaxis finite element code for soil and rock analyses", *User's Manual,* Version 8.0 Dynamic, Plaxis B.V., The Netherlands.

Porter K.A, Scawthorn C, Honegger D.G, O'rourke T.D, and Blackburn F [1991] "Performance of Water Supply Pipelines in Liquefied Soil", Proc. of the *4th US – Japan Workshop on Earthquake Disaster Prevention for Lifeline Systems,* NIST Special Publication 840.

Power M., Rosidi D., Kaneshiro J., Gilstrap S., and Chiou S.J., [1998] "Summary and evaluation of procedures for the seismic design of tunnels", F*inal Report for Task 112-D-5.3[c]*, MCEER Highway Project, Sponsored by US Department of Transportation, Federal Highway Administration, FWHA Contract Number DTFH61-92-C-00112.

Pradel D. [1998] "Procedure to evaluate earthquake-induced settlements in dry sandy soils", *J. Geotech. & Geoenv. Engrg.*, ASCE, 124 (4), 364-368.

Priolo E., Carcione J. M., and Seriani G. [1994] "Numerical simulation of interface waves by high-order spectral modeling techniques", *Journal of Acoustic Society of America,* February 1994, Volume 95, Issue 2, pp. 681-693.

Rasulo, A., Cavalieri, F. and Vanzi, I., [2007] "Affidabilità sismica dei sistemi di distribuzione dell'acqua potabile in ambito urbano: metodologia di Calcolo e Applicazione", Proc. of ANIDIS 2007 – Mem. n.243.

Ricciardi, V. [2002] "Natural gas transmission and distribution system in Thessaliniki", *The natural gas in urban consumption and perspevtives*, Meeting 15-02-2002 (in Greek).

Roth W. H., Dawson E. M., Mehrain M., and Sayegh A. [2003] "Analyzing the seismic

performance of wharves, part 1: Structural-engineering approach", Proc. of the *6th U.S. Conference and Workshop on Lifeline Earthquake Engineering,* TCLEE, Monograph No. 25, August 2003.

Roth, W. H., and Dawson E. M. [2003] "Analyzing the seismic performance of wharves, part 2: SSI analysis with non-linear, effective-stress soil models", Proc. of the *6th U.S. Conference and Workshop on Lifeline Earthquake Engineering,* TCLEE, Monograph No. 25, August 2003.

Sadigh, K., Egan, J. A., and Youngs, R. R. [1986] "Specification of Ground Motion for Seismic Design of Long Period Structures" *Earthquake Notes*, Vol 57, No. 1, p 13.

Salmon M., Wang J., Jones D., Wu Ch. [2003] "Fragility formulations for the BART system", Proc. of the *6th U.S. Conference on Lifeline Earthquake Engineering,* TCLEE, Long Beach, August 10-13.

Sánchez Sesma F.G., Vai R., Dretta E., and Palencia V.J. [1999] "Foundamentals of elastic wave propagation for site amplification studies: The seismic response of alluvial valleys", *Wave in Earthquake Engineering*, WIT Press, Southampton, Boston, pp.7-26

Sano Y, O'Rourke T, and Hamada M [1999] "GIS evaluation of Northridge earthquake ground deformation and water supply damage" Proc. of the *5th US Conference on Lifeline Earthquake Engineering,* TCLEE Monograph #16, ASCE, pp.832-839

Schnabel, P.B., Lysmer, J., and Seed, H.B. [1972] SHAKE – A Computer Program for Earthquake Response Analysis of Horizontally Layered Sites, Report No. EERC 72-12, UC Berkeley

Seed, H. B., Wong, R. T., Idriss, I. M., and Tokimatsu, K. [1986], "Moduli and damping factors for dynamic analysis of cohesionless soils", *J. of Geotech. Eng.*, 112(11), 1016–1032.

Sharma, S., and Judd, W.R. [1991] "Underground opening damage from earthquakes". *Engineering Geology,* 30, 263-276.

Shirozu T, Yune S, Isoyama R, and Iwamoto T [1996] "Report on damage to water distribution pipes caused by the 1995 Hyogoken-Nanbu [Kobe] earthquake" Proc. of the *Sixth Japan-US Workshop on Earthquake Resistant Design of Lifeline Facilities and Countermeasures Against Soil Liquefaction*, Edited by M. Hamada and T.O'Rourke, Technical Report NCEER-96-0012, pp. 93- 110.

Singhal A.C [1984] "Nonlinear Behaviour of Pipeline Joints" Proc. of the *8th World Conference on Earthquake Engineering, San Francisco,* California, Vol. 7, pp. 207-214.

Skarlatoudis, A.A., Papazachos, C.B., Margaris, B.N., Thodulidis, N., Papaioannou, Ch.,

Kalogeras, I., Scordilis, E.M., and Karakostas, V. [2003] "Empirical peak ground-motion predictive relations for shallow earthquakes in Greece", *Bull. Seismol. Soc. America,* 93, 6, pp. 2591-2603.

Spudich, P., and Archuleta, R., [1987] "Techniques for earthquake ground motion calculation with applications to source parameterisation of finite faults," in Bolt, B.A. ed., *Seismic Strong Motion Synthetics: Orlando, Florida*, Academic Press, pp. 205-265.

Spudich, P., and Frazer, N.L. [1984] "Use of ray theory to calculate high-frequency radiation from earthquake sources having spatially variable rupture velocity and stress drop," *Bull. Seismol. Soc. Am.*, 74, pp. 2061-2082.

Spudich, P., and Xu, L. [2002] "Documentation of software package Compsyn sxv3.11: programs for earthquake ground motion calculation using complete 1-d green's functions", *International Handbook of Earthquake and Engineering Seismology CD, Int. Ass. Of Seismology and Physics of Earth's Interior, Academic Press*

Spudich, P.; Joyner, W. B.; Lindh, A. G.; Boore, D. M.; Margaris, B. M., and Fletcher, J. B. [1999] "SEA99 - A Revised Ground Motion Prediction Relation for Use in Extensional Tectonic Regimes", *Bull. Seismol. Soc. Am.*, 89, 1156 - 1170.

St John, C. M., and Zahrah, T. F., [1987] "Aseismic design of underground structures", TUST, Vol. 2, Nr. 2, pp. 165 - 197

Stiros, S.C., and Drakos, A. [2000] "Geodetic constrain on the fault pattern of the 1978 Thessaloniki earthquake", *Geophysical Journ. Int.*, 143, pp. 679-688.

Takada, S., and Takabe, K. [1998] "Estimation of EQ induced settlements for lifeline engineering." Proc. of the *9th World Conference Earthquake Engineering.* August Vol. VII, p.109-114.

Tokimatsu, K., and H. B. Seed. [1987] "Evaluation of Settlements in Sands Due to Earthquake Shaking." *J. of Geotech. Eng.* ASCE 113(8): p.861-878.

Tranos, M.D., Papadimitriou, E.E., and Kilias, A.A. [2003] "Thessaloniki–Gerakarou Fault Zone (TGFZ): the western extension of the 1978 Thessaloniki earthquake fault (Northern Greece) and seismic hazard assessment", *Journal of Structural Geology* 25, pp. 2109–2123.

Travasarou, T., Bray, J.D., and Der Kiureghian, A.D. "A Probabilistic Methodology for Assessing Seismic Slope Displacements," Proc. of the *13th World Conference on Earthquake Engineering,* Vancouver, Canada, Paper No. 2326, Aug 1-6, 2004.

Tromans I.J., and Bommer J.J. [2002]. « The attenuation of strong-motion peaks in Europe", Proc. of the *Twelfth European Conference on Earthquake Engineering*, London, Paper No. 394

Tromans I.J.[2004] "Behaviour of buried water supply pipelines in earthquake zones", *Phd Thesis,* Department of Civil and Environmental Engineering, Imperial College of Science, Technology and Medicine, London.

U.S. Geological Survey, National Earthquake Information Center, 2003.

Uwabe, T. [1983] "Estimation of earthquake damage deformation and cost of quaywalls based on earthquake damage records", *Technical Note of Port and Harbour Research Institute,* No. 473, 197 pp

Vucetic, M., and R. Dobry (1991). "Effect of soil plasticity on cyclic response", *J. of Geotech. Eng.*, ASCE, Vol.117, No.1, pp.89-107.

Wang, J. M. [1985] "The distribution of earthquake damage to underground facilities during the 1976 Tang-Shan earthquake", *Earthquake Spectra,* 1[4], 741-757.

Wang J.N. [1993] "Seismic design of tunnels. A simple state-of-the-art design approach". Published by Parsons Brinckerhoff Inc. One Penn Plaza, New York.

Wang, L.R.L., and Yeh, Y. [1985] "A refined seismic analysis and design of buried pipeline for fault movement", *Earthquake Engineering and Structural Dynamics*, 13, 75-96.

Wang W.L., Wang T.T., Su J.J., Lin C.H., and Seng C.R., [2001] "Assessment of damage in mountain tunnels due to the Taiwan Chi-Chi earthquake", *Tunneling & Underground Space Technology*, Vol. 16[3], p. 133–150, Pergamon.

Wells, D.L., and Coppersmith, K.J. [1994] "Empirical relationships among magnitude, rupture length, rupture width, rupture area, and surface displacement", *Bull. Seism. Soc. Am., 84,* pp. 974-1002.

Werner S. D., [1998] "Seismic Guidelines for Ports", Technical Council on Lifeline Earthquake Engineering, Monograph No. 12, March 1998.

Yagi, Y., and M. Kikuchi, [2000] "Source rupture process of the Kocaeli, Turkey, earthquake of August17, 1999, obtained by joint inversion of near-field data and teleseismic data", *Geophys. Res. Lett.*, Vol. 27, pp1969-1972, 2000.

Yeh, G.C.K. [1974] "Seismic analysis of slender buried beams"; *Bulletin of the Seismological Society of America,* v. 64; no. 5; p. 1551-1562.

Youd T. L., et al. [2001] "Liquefaction Resistance of Soils: Summary Report from the 1996 NCEER and 1998 NCEER/NSF Workshops on Evaluation of Liquefaction Resistance of Soils", *Journal of Geot. and Geoenv. Eng.*, 127[10].

Youd, T. L., Hansen, C. M., and Bartlett, S. F., [1999] "Revised Multilinear Regression Equations for Prediction of Lateral Spread Displacement", *J. of Geotech. Eng.* ASCE, 128[12], 1007-1017.

Youd T. L., and Perkins, D. M., [1987] "Mapping of Liquefaction Severity Index", *J. of Geotech. Eng.*, Vol. 113, No. 11, pp. 1374-1392

APPENDIX

Bases of the Spectral Element Method for 2D and 3D numerical wave propagation

Consider an elastic medium occupying the finite region $\boldsymbol{\Omega} \subset \Re^d$ $d = 2$ or 3 number of space dimension) with boundary $\boldsymbol{\Gamma} = \boldsymbol{\Gamma}_N \cup \boldsymbol{\Gamma}_D \cup \boldsymbol{\Gamma}_{NR}$, where $\boldsymbol{\Gamma}_D$ is the portion where the displacement vector $\boldsymbol{u}$ takes prescribed values, $\boldsymbol{\Gamma}_N$ the portion subject to external forces (*tractions*), and $\boldsymbol{\Gamma}_{NR}$ a "virtual" boundary which should be introduced in order to make the computational domain bounded. On $\boldsymbol{\Gamma}_{NR}$ suitable non reflecting conditions need to be set. Through the principle of virtual work, the dynamic equilibrium problem for the medium can be stated in the following *weak*, or variational, form:

Find $\boldsymbol{u} = \boldsymbol{u}(\boldsymbol{x},t)$ such that $\forall t \in (0,T)$

$$\begin{aligned} \frac{\partial^2}{\partial t^2} \int_{\Omega} \rho \boldsymbol{u} \cdot \boldsymbol{v} \, d\boldsymbol{\Omega} + \int_{\Omega} \sigma_{ij}(\boldsymbol{u}) \varepsilon_{ij}(\boldsymbol{v}) \, d\boldsymbol{\Omega} = \\ = \int_{\Gamma_N} \boldsymbol{t} \cdot \boldsymbol{v} \, d\boldsymbol{\Gamma} + \int_{\Gamma_{NR}} \boldsymbol{t}^* \cdot \boldsymbol{v} \, d\boldsymbol{\Gamma} + \int_{\Omega} \boldsymbol{f} \cdot \boldsymbol{v} \, d\boldsymbol{\Omega}, \quad i, j = 1 \ldots d \end{aligned} \tag{A.1}$$

where t is the time, $\rho = \rho(\boldsymbol{x})$ the material density, σ_{ij} the stress tensor, ε_{ij} the small-strain tensor, $\boldsymbol{f} = \boldsymbol{f}(\boldsymbol{x},t)$ a known body force distribution, $\boldsymbol{t} = \boldsymbol{t}(\boldsymbol{x},t)$ the vector of external traction prescribed on Γ_N, $\boldsymbol{t}^* = \boldsymbol{t}^*(\boldsymbol{x},t)$ a vector of fictitious tractions prescribed on $\boldsymbol{\Gamma}_{NR}$ so as to minimize spurious reflections, and $\boldsymbol{v} = \boldsymbol{v}(\boldsymbol{x})$ is a generic function (candidate to represent admissible displacements) chosen so that all integrals in (A.1) re finite. Summation on repeated indices will be understood, unless otherwise specified.

The previous equation must be supplemented by suitable conditions prescribing the value of both $\boldsymbol{u}$ and $\partial \boldsymbol{u} / \partial t$ for all $\boldsymbol{x} \in \boldsymbol{\Omega}$ at the initial time $t = 0$. Concerning the boundary conditions, for simplicity, but without loss of generality, displacements have been assumed to vanish on $\boldsymbol{\Gamma}_D$. In numerical wave propagation analyses in unbounded earth media, fictitious boundaries with suitable non-reflecting conditions are usually introduced to limit the computations domain. Thus $\boldsymbol{\Gamma}_{NR}$ denotes the non-reflecting portion of the

boundary, and the traction $\boldsymbol{t}^*$ in the corresponding integral of (A.1) can be replaced by a combination of time and space derivatives of the displacement through an appropriate non-reflecting condition specified later.

The Galerkin method stemming from (A.1) is the basis for the spectral element approach as well as for the finite element method.

Bases of the Domain Reduction Method for numerical wave propagation

Making reference to a half-space that contains a geological feature of interest (Figure A.1), a fictitious interface Γ subdivides the total domain into two separated subdomains: Ω containing the localized geological feature, and Ω^+. Γ^+ is the outer boundary that truncates the original semi-infinite region and where are applied absorbing boundary conditions; $\boldsymbol{P}$ is a set of nodal forces equivalent to the seismic source. Assuming linear viscoelastic behaviour for the material, $u_j, \dot{u}_j, \ddot{u}_j$ denote the vector fields of nodal displacement, velocities, and accelerations respectively, with $j = \{i, b, e\}$, subindices for Ω, Γ, Ω^+ respectively.

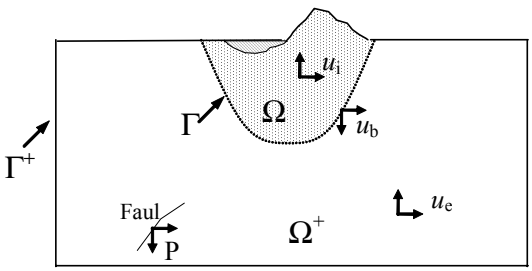

Figure A.1. Idealized seismic region. Outer boundary Γ^+ restricts computation to a finite domain; fictitious interface Γ divides region into two subdomains: Ω^+, which includes the seismic source, represented by nodal forces P, and Ω containing the localized geological features. [Bielak *et al.*, 2003].

Applying the DRM the original problem is subdivided into two simpler ones. The first is an auxiliary problem (see Figure A.2a) that simulates the earthquake source and propagation path effects with a model that encompasses the source and a background structure $\Omega^+ \cup \Omega_0$ from which the localized feature has been removed (Ω_0 denote the interior domain without geological heterogeneities, that contains the same material as Ω^+). This model requires a mesh that is only as fine as dictated by the softness material in the background model. Moreover it needs to be performed only once for a specified

earthquake source and the wave propagation in this external domain can be calculated with numerical or analytical methods suitable for simplified configurations (e.g. a horizontally-layered half-space).

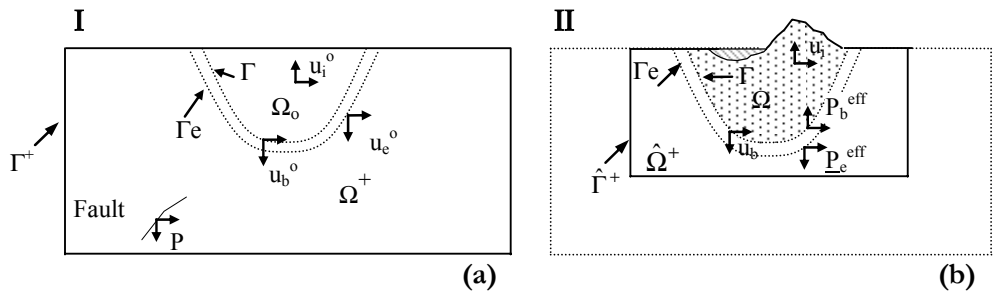

Figure A.2. Two step DRM. (a) Step I defines the auxiliary problem over background geological model. Resulting nodal displacements within Γ, Γ_e, and region between them are used to evaluate effective seismic forces P^{eff} required for step II. (b) Step II defined over reduced region made up of Ω and $\hat{\Omega}^+$. P^{eff} are applied within Γ and Γ_e. [Bielak *et al.*, 2003].

The second problem models with the desired accuracy only a reduced region $\Omega \cup \hat{\Omega}^+$ (a truncate portion of Ω^+) which contains the geological feature of interest, but not the causative fault as in Figureb. Its input is a set of equivalent localized forces P^{eff} derived from the first step. These forces are equivalent to and replace the original seismic forces $\boldsymbol{P}$, which act in the vicinity of the causative fault.

The equivalent forces act only within a single layer of elements adjacent to the interface between the exterior region and the geological feature of interest, (at the nodes that lie on Γ, Γ_e and between them, as shown in Figure A.2b and in detail in Figure A.3, considering spectral elements of degree 4) and depend on the free field displacement.

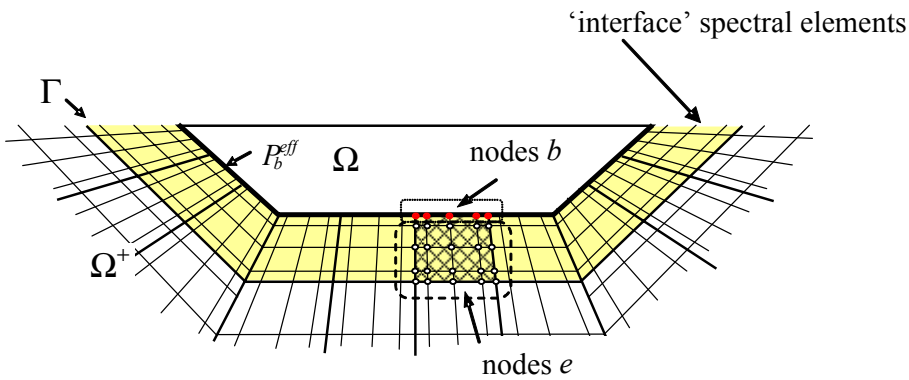

Figure A.3. Interface spectral elements of region Ω^+ where effective forces are applied (between Γ and Γ_e). Boundary nodes *b* and interior nodes *e* of a single spectral element are shown. [Faccioli *et al.*, 2005].

APPENDIX REFERENCES

Bielak J., Loukakis K., Hisada Y. and Yoshimura C. "Domain Reduction Method for Three-Dimensional Earthquake Modeling in Localized Regions, Part I: Theory",*Bulletin of the Seismological Society of America*, 817 – 824, [2003]

Faccioli E., Vanini M., Paolucci R., Stupazzini M., Comment on "*Domain reduction method for three-dimensional earthquake modeling in localized regions*", Part I, by J. Bielak, K. Loukakis, Y. Hisada, and C. Yoshimura, and Part II, by C. Yoshimura, J. Bielak, Y. Hisada, and a. Fernandez", Bull. Seismol. Soc. Amer., Vol. 95(2), pp. 763-769 [2005]